University of Southampton

Faculty of Environmental and Life Sciences

School of Ocean and Earth Science

Ecological characterisation and paleo-evolution of two contrasting cold-water coral mound provinces of the Mediterranean Sea

by

Guillem Corbera Pascual

B.Sc. Universitat de Barcelona, M.Sc. University of Southampton

ORCID ID 0000-0002-0207-1668

Thesis for the degree of Doctor of Philosophy

January 2021

University of Southampton

Abstract

Faculty of Natural And Environmental Sciences
School of Ocean and Earth Sciences

Thesis for the degree of Doctor of Philosophy
by
Guillem Corbera Pascual

Scleractinian cold-water coral reefs are considered to be key hotspots of benthic biodiversity in the deep ocean. Due to their relevant ecological role and susceptibility to anthropogenic disturbances protection and conservation measures have been applied to these habitats, even though they are far from being completely understood. Throughout the last two decades several studies have quantitatively described the biodiversity of Atlantic cold-water coral reefs, finding considerable differences among biogeographic regions. In contrast, and probably owed to the scarcity of these habitats in the Mediterranean Sea, the knowledge related to coral reef biodiversity in this basin remains modest and almost purely qualitative. On a different note, when coral reefs are under persistent suitable environmental conditions and have a sufficient sediment input, they can develop and form large geomorphic structures known as coral mounds. The latter are sensitive to changes in climate and capable of recording such variations in the chemical composition of the coral skeletons. Numerous surveys in the Atlantic have associated coral mound development patterns to environmental variations caused by glacial-interglacial cycles. Within the Mediterranean, coral mound formation studies have been so far limited to the Alboran Sea and to the last 15 kyr, due to the lack of gravity cores encompassing longer periods of time. In this thesis a wide range of techniques, including ROV video-analysis, multivariate statistics, U-series dating, computed tomography and geochemical analyses were applied to acquire a better understanding of the spatiotemporal distribution of Mediterranean cold-water coral reefs and the processes controlling their evolution into mounds during the last 400 kyr. More precisely, the present study aimed to (1) quantify the density of uncommonly thriving coral reefs and accompanying megabenthic species within the Cabliers Coral Mound Province, and describe their distribution along it; and (2) explore which are the main environmental variables and paleoclimatic events that have controlled coral mound formation in Cabliers and in the newly discovered Tunisian Coral Mound Province. The research presented here revealed the densest and most flourishing cold-water coral reefs witnessed so far in the Mediterranean Sea and brought further insight into their distribution along the crests of ridge-like coral mounds. This thesis also contributed to increase our knowledge on the main species associated to Mediterranean coral reefs and their relative abundances, which showed considerable differences to those found in Atlantic reefs. In regards to coral mound formation, this work has expanded the current knowledge outside the Alboran Sea and back to 400 ka BP. Almost opposite development patterns were observed between the Cabliers and Tunisian coral mound provinces, with the former mainly developing throughout deglaciations and temperate interstadial periods and the latter during glacial periods. Nonetheless, both provinces seem to depend on a high surface productivity and an appropriate depth of the interface between Atlantic and Levantine Intermediate Waters for the coral mounds to develop. Lastly, the oceanographic alterations caused in the Eastern Mediterranean Basin during Sapropel events also seem to have had detrimental effects for coral mound formation in the Western basin.

Table of Contents

Table of Tables

Table of Figures

Research Thesis: Declaration of Authorship

Print name: Guillem Corbera Pascual

Title of thesis: Ecological characterisation and paleo-evolution of two contrasting cold-water coral mound provinces of the Mediterranean Sea

I declare that this thesis and the work presented in it is my own and has been generated by me as the result of my own original research.

I confirm that:

1. This work was done wholly or mainly while in candidature for a research degree at this University;
2. Where any part of this thesis has previously been submitted for a degree or any other qualification at this University or any other institution, this has been clearly stated;
3. Where I have consulted the published work of others, this is always clearly attributed;
4. Where I have quoted from the work of others, the source is always given. With the exception of such quotations, this thesis is entirely my own work;
5. I have acknowledged all main sources of help;
6. Where the thesis is based on work done by myself jointly with others, I have made clear exactly what was done by others and what I have contributed myself;
7. Parts of this work have been published as:

Corbera, G., Lo Iacono, C., Gràcia, E., Grinyó, J., Pierdomenico, M., Huvenne, V.A.I., Aguilar, R., Gili, J.M. (2019). Ecological characterisation of a Mediterranean cold-water coral reef: Cabliers Coral Mound Province (Alboran Sea, western Mediterranean). *Progress in Oceanography*, 175, 245–262. https://doi.org/10.1016/j.pocean.2019.04.010

Corbera, G., Lo Iacono, C., Standish, C.D., Anagnostou, E., Titschack, J., Katsamenis, O., Cacho, I., Van Rooij, D., Huvenne, V.A.I., Foster, G.L. (2021). Glacio-eustatic variations and Sapropel events as main controls on the Middle Pleistocene-Holocene evolution of the Cabliers Coral Mound Province (W Mediterranean). *Quaternary Science Reviews*, 253, 106783 https://doi.org/10.1016/j.quascirev.2020.106783

Signature: Date: January 2021

Acknowledgements

This thesis was funded by the Graduate School, National Oceanography Centre Southampton (GSNOCS) with the collaboration of the NGO OCEANA.

First of all, I would like to thank Dr. Claudio Lo Iacono, Dr. Veerle Huvenne, Dr. Eleni Anagnostou and Prof. Gavin Foster for all their support during these four years of thesis supervision. This thesis would not have been possible without their help. Claudio, thank you very much for all your patience and for showing me a view of cold-water coral ecosystems that goes beyond biology. Veerle thank you for teaching me how to be a more methodical researcher and for all the ideas that have inspired me when I was lost. Eleni thank you for helping me understand a field that was almost completely unknown to me. Gavin thanks a lot for all the advice given during writing, I have learnt a lot from you.

Throughout the duration of this Ph.D., I have had the chance to work with people belonging to different research fields that have taught me new analytical techniques and helped with some of the data analysis. I really appreciate the time that Dr. Christopher Standish has dedicated to train me on how perform U-series to date coral samples and for his supervision during this process. I am also really grateful to Dr. Orestis Katsamenis for introducing me to the field of computed tomography scans and for teaching me the basics of CT scan analysis. Dr. Jordi Grinyó, thanks a lot for all the discussions we had regarding statistical analyses, your knowledge and advice on the subject has been really useful. Dr. Heather Goring-Harford, thank you for helping me with some of the trace element analyses.

I really appreciate all the help provided by Dr. Suzanne MacLachlan and the rest of the British Ocean Sediment Core Research Facility (BOSCORF) Team, while working with the gravity cores. I am extremely grateful to Dr. Jürgen Titschack and the rest of the Marine Sedimentology research group for hosting me during my research placement at MARUM (Bremen, Germany) and for dedicating so much time to teach me how to process and analyse CT-scans of coral mound gravity cores. I would also like to thank Prof. Josep-Maria Gili for introducing me to the world of benthic ecology and for supporting me when I applied for this Ph.D. thesis.

Throughout the duration of this Ph.D. I have made many friendships both at the National Oceanography Centre and at the Institut de Ciències del Mar (Barcelona, Catalonia). I am sincerely thankful to David Price, Tabitha Pearman, Loïc Van Audenhaege, Urska Martincic, Jamie Hudson, Maria De La Fuente, Erik Simón, Matthew Cobain, Michael Faggetter, Patricia Baena, Andreu Santín, Stefano Ambroso, Marina Biel, Maria Montseny, Janire Salazar, Ariadna Martínez, Claudia Traboni, Arianna Rocchi, Daniel Gómez, Charlie Gaborit, Miguel Cabrera, Ana Trindade, Manuel Olivares, and Elena Martínez for all the laughs and beers shared. This experience would not have been the same without you!

To my parents, I will never be able to repay you for everything you have done in order to enable me to achieve my goals. I hope I have made you proud. Dad, since I was a little kid you have always showed me how amazing nature can be, by taking me on field trips to the countryside and by sharing your wide knowledge with me. If I started to pursue a career in Marine Biology, it is thanks to you. Mum, I do not know what I would do without you. Your jokes and hugs have always put a smile in my face, even during tough moments. Therefore, it is only my duty to follow up with one of our inside jokes here: I am extremely grateful to "Su Gran Florentineza Foundation" and to her president Dolors Pascual for all the grants that I have been awarded during the course of this Ph.D.

Lastly, although she might not remember this, I promised my grandmother that I would once become a doctor and thus, it is to her that I dedicate this thesis.

"Et portaré a la Plaça Catalunya a donar de menjar als coloms com quan erets petitet"

Definitions and Abbreviations

ANOVA: Analysis of Variance
AR: Aggradation Rate
AUV: Automanomous Underwater Vehicle
AW: Atlantic Water
B/A: Bølling-Allerød
CCA: Canonical Correspondence Analysis
CITES: Convention on International Trade in Endangered Species
CMP: Cabliers Coral Mound Province
CPP: Coral Preservation Pattern
CT: Computed Tomography
CWC: Scleractinian Cold-Water Coral
EMM: East Melilla Mounds
FAO: Food and Agriculture Organisation
GFCM: General Fisheries Commission for the Mediterranean
LIW: Levantine Intermediate Water
MC-ICP-MS: Multi-collector Inductively Coupled Plasma Mass Spectrometry
MIS: Marine Isotopic Stage
MOW: Mediterranean Outflow Water
MSFD: Marine Strategy Framework Directive
ORL1: Organic Rich Layer 1
RFMO: Regional Fishery Management Organisation
RSL: Relative Sea-level
SAC: Special Areas of Conservation
SWT: Sea Water Temperature
TMP: Tunisian Coral Mound Province
WDMA: Average Water Depth During Mound Aggradation
WMDW: West Mediterranean Deep Water
WMM: West Melilla Mounds
YD: Younger Dryas

Chapter 1
Introduction

1.1. Cold-water corals

The bathyal depths of the ocean seafloor are home to the azooxanthellate cold-water corals (i.e. missing the symbiotic dinoflagellate *Symbiodinium* sp.). They are sessile organisms that feed on dissolved and particulate organic matter such as phytoplankton, zooplankton and remains from organisms living in the water column (Roberts et al., 2006; Mueller et al., 2014). The term "cold-water corals" encompasses a wide variety of soft coral (Subclass Octocorallia), black coral (Order Antipatharia) and stony coral (Order Scleractinia) species that belong to the Class Anthozoa (Phyllum Cnidaria; Roberts et al., 2006). Calcifying lace corals of the Family Stylasteridae (Hydrozoa, Cnidaria) are also comprehended by the term "cold-water corals" (Roberts et al., 2006). Among all these groups, only scleractinian cold-water corals (hereafter referred as CWCs) can form large and complex three-dimensional features consisting of calcium carbonate aragonitic skeletons that persist over long periods of time, even after they die (i.e. thousands to millions of years; Kano et al., 2007). This taxonomic group encompasses >700 CWC species (Cairns, 2007; Roberts et al., 2009a), which can be solitary (i.e. formed by a single polyp), pseudo-colonial or colonial, with structures containing up to several hundreds of polyps. Some colonial species can eventually produce intricate branching frameworks, which over time can grow and build large reefs (Roberts et al., 2006). The main framework-building CWC species are *Goniocorella dumosa*, *Dendrophyllia cornigera* (Le Danois, 1948), *Enallopsammia profunda*, *Enallopsammia rostrata, Oculina varicosa*, *Solenosmilia variabilis*, *Madrepora oculata* and *Desmophyllum pertusum* (=*Lophelia pertusa*; according to Addamo et al., 2016) with the latter two being the most widespread and studied species (Fig. 1.1; Freiwald et al., 2004; Roberts et al., 2006; Davies and Guinotte, 2011; Henry and Roberts, 2017).

The highest density of CWC assemblages is found in the North Atlantic Ocean (including the Caribbean Sea and the Gulf of Mexico) and the Mediterranean Sea, where *D. pertusum* and *M. oculata* are the most abundant species, followed by *S. variabilis*, *O. varicosa* and to a minor extend by some dendrophylliid species such as *Dendrophyllia cornigera* (Fig. 1.1; Wienberg and Titschack, 2017). Wherever they occur, CWCs are found at depths between 39 and 2000 m, mostly in areas that contain hard substrata on which they can settle (Freiwald et al., 2004; Roberts et al., 2006). The types of hard substrata used by CWCs range from outcropping hardgrounds (including cliffs, vertical walls, overhangs and escarpments) to small-sized pebbles or shells (Wheeler et al., 2007). Nevertheless, the spatial distribution of CWCs not only depends on the availability of hard substrata but also on many environmental and biological factors such as temperature, salinity, density, pH, dissolved oxygen, current intensity, sedimentation rates, food supply and larval dispersal. For instance, *D. pertusum* generally grows in waters with a temperature of 4 to 14°C, a salinity of 33–37 ppt, a density envelope of 27.1–27.65 kg m^{-3} and dissolved oxygen concentrations between 2.6 and 6.7 ml l^{-1} (Rogers, 1999; Wisshak et al., 2005; Dodds et al., 2007; Dullo et al., 2008; Davies et al., 2010). However, some excep-

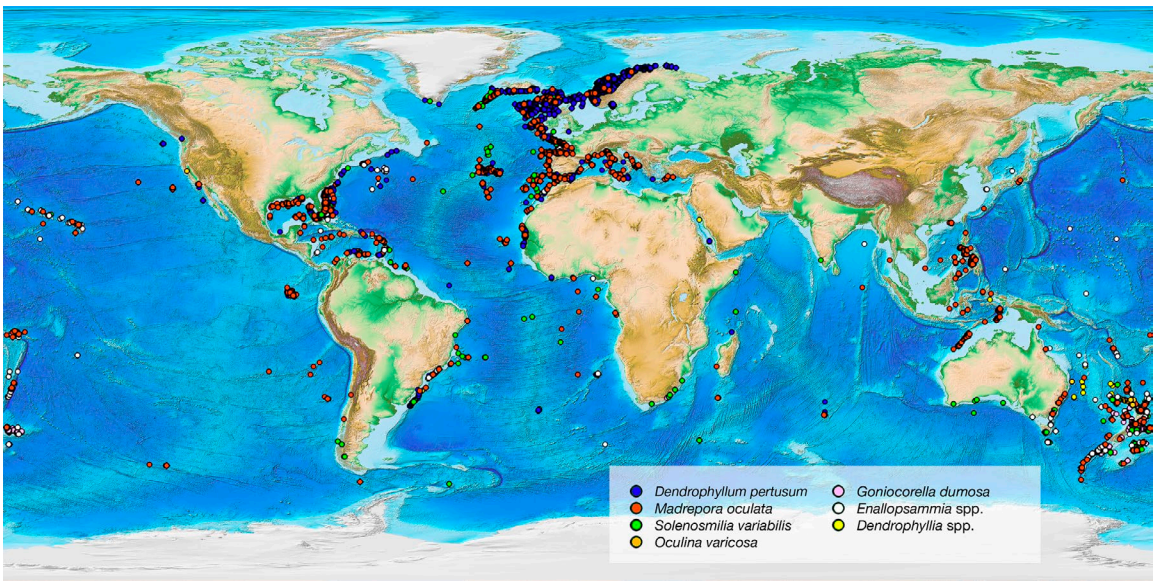

Figure 1.1. Global distribution of the main framework-building CWC species based on data from Freiwald et al. (2017).

tions have been observed, with *D. pertusum* and *M. oculata* colonies living in waters denser than 27.65 kg m^{-3} and warmer than 13 °C in the Mediterranean Sea (Orejas et al., 2009; Taviani et al., 2017; Angeletti et al., 2020a). Similarly, CWC assemblages living in waters with an oxygen content below 2 ml l^{-1} have been reported off the Mauritanian coast (Eisele et al., 2011) and offshore Angola and Namibia (Hanz et al., 2019). Dodds et al. (2007) observed that coral metabolism is doubled after a 1°C increase in temperature and according to Brooke et al. (2013), if temperature increases over 14°C for long periods of time, coral colonies start showing high mortality rates. At the same time, if temperature drops drastically (e.g. from 12 to 6°C), calcification rates can decline down to 58% from their optimal values (Naumann et al., 2014). CWCs also need a high concentration of dissolved carbonate (CO_3^{2-}) to build their own aragonite skeleton and grow. This happens in aragonite-supersaturated waters. In fact, almost 95% of the CWC assemblages are currently located above the aragonite saturation horizon, suggesting this factor is critical for the corals to thrive (Guinotte et al., 2006). This becomes evident in the North Pacific, where the presence of a shallow aragonite saturation horizon (i.e. 50-600 m) translates into a limited distribution of CWC assemblages compared to those reported from the North Atlantic (aragonite saturation horizon > 2000 m; Guinotte et al., 2006).

In regions where the physicochemical conditions of the water masses are favourable for the growth of these organisms, CWCs mainly thrive in advective environments. This occurs due to their need for a constant or periodic flow regime that is responsible for delivering a sufficient food supply and for helping the corals remove any increase in terrigenous draping sediments that might deposit on their tissue and inhibit the growth of reefs (Fosså et al., 2005; Mohn et al., 2014). Therefore, CWCs are generally observed growing on the topographic highs and vertical walls of submarine canyons, ridges and seamounts (Roberts et al., 2006; Orejas et al., 2009; Vertino et al., 2010; Huvenne et al., 2011; Lo Iacono et al. 2018b, 2019), where the corals are subjected to fast flows caused by the action of internal waves, cascading and tidal forcing, with maximum speed values around 0.7 m s^{-1} (Mienis et al., 2009; White and Dorschel, 2010). The average flow speed observed in CWC habitats ranges from 0.08 to 0.15 m s^{-1} (Davies et al., 2010; Mienis et al., 2012a, b), which is close to the threshold for the resuspension of aggregates and fine sediments that can represent a food source for the corals (Thomsen and Gust, 2000). On the other hand, current velocities of 1 m s^{-1} are suggested to be the upper toler-

ance threshold for *D. pertusum* colonies (Frederiksen et al., 1992). Similarly, areas with current speeds below 0.05 m s^{-1} would result in a decreased food supply and enhanced sedimentation rates that in the long term would be detrimental for the corals. In the absence of intense hydrodynamic conditions, high sedimentation rates could cause coral mortality from burial and suffocation (Wesseling et al., 1999; Kelmo et al., 2003). When sedimentation rates are not as intense, corals can remove the sediment through energetically costly processes such as mucus production and ciliary action (Brooke et al., 2009). However, even intermediate sedimentation rates can be fatal for corals if they persist over a long time, as the polyps become energy depleted from shedding all the draping sediments (Brooke et al., 2009). According to Brooke et al. (2009), *D. pertusum* colonies can tolerate high sediment concentrations (i.e. 245 mg l^{-1}) for at least 14 days and a complete burial for 2 days. This implies that *D. pertusum* is quite resilient to extreme environmental conditions such as high sedimentation, although if this setting persists through time survival starts to decline significantly.

In regards to food supply, researchers proposed two main theories that explained possible food sources for CWC assemblages: the Hydraulic theory and the Environmental Control theory (Hovland and Risk, 2003; Roberts et al., 2009a, b). The Hydraulic theory states that the presence of hydrocarbon seepage may provide a food source that increases the biomass along the food chain, ultimately supporting CWC growth (Hovland and Risk, 2003). However, more recent studies point to the Environmental Control theory, which suggests that surface primary productivity and resuspended material are the main food source for CWCs (Duineveld et al., 2004; Roberts et al., 2006; Dodds et al., 2009). In fact, molecular analyses of suspended organic matter and nitrogen isotopic composition of the corals confirmed the presence of lipid-rich organic matter within the corals that originated from surface production (Kiriakoulakis et al., 2007; Carlier et al., 2009). The mechanisms involved in the delivery of food to CWCs generally consist of hydrodynamic processes such as cascading and tidally induced downwelling, which bring fresh and high quality organic matter towards the water depths inhabited by the corals (Thiem et al., 2006; Davies et al., 2009; Soetaert et al., 2016); internal waves/tides and geostrophic currents, which propel the particulate organic matter through the coral framework (Frederiksen et al., 1992; White et al., 2005; Cyr et al., 2016); and the presence of nepheloid layers, which enhance food concentration and its lateral transport (Mienis et al., 2007, 2012a; Fontanier et al., 2013). CWCs appear to be opportunistic with regards to their food sources (Mueller et al., 2014). They have been confirmed to feed on daily migrating zooplankton (e.g. copepods), amphipods, swimming cumaceans and in some aquaria experiments CWCs have even been observed to feed on fish and mussel flesh (Mortensen, 2001; Duineveld et al., 2004; van Oevelen et al., 2009; Dodds et al., 2009). According to isotopic analyses, CWCs are thought to feed on a combination of calanoid copepods and vegetal particulate matter (Roberts et al., 2009b). On the other hand, resuspension of dead organic matter might constitute a major carbon source for CWCs, during periods of low surface productivity (Thiem et al., 2006).

Even if all the environmental requirements needed for the growth of CWCs are met, these organisms still need to reproduce to maintain their populations. Although CWCs can reproduce asexually (e.g. budding and fragmentation), these species depend on sexually produced larvae to maintain genetic diversity and expand to other regions. Larval dispersal is mainly driven by currents, duration of larval life and larval behaviour. Life duration is unknown for most CWC larvae with the exception of *O. varicosa* and *D. pertusum*, which have been observed to present a larval lifespan of 14-21 days and >100 days respectively (Brooke and Young, 2005; Stromberg and Larsson, 2017). In addition, some studies on *D. pertusum* larval behaviour have

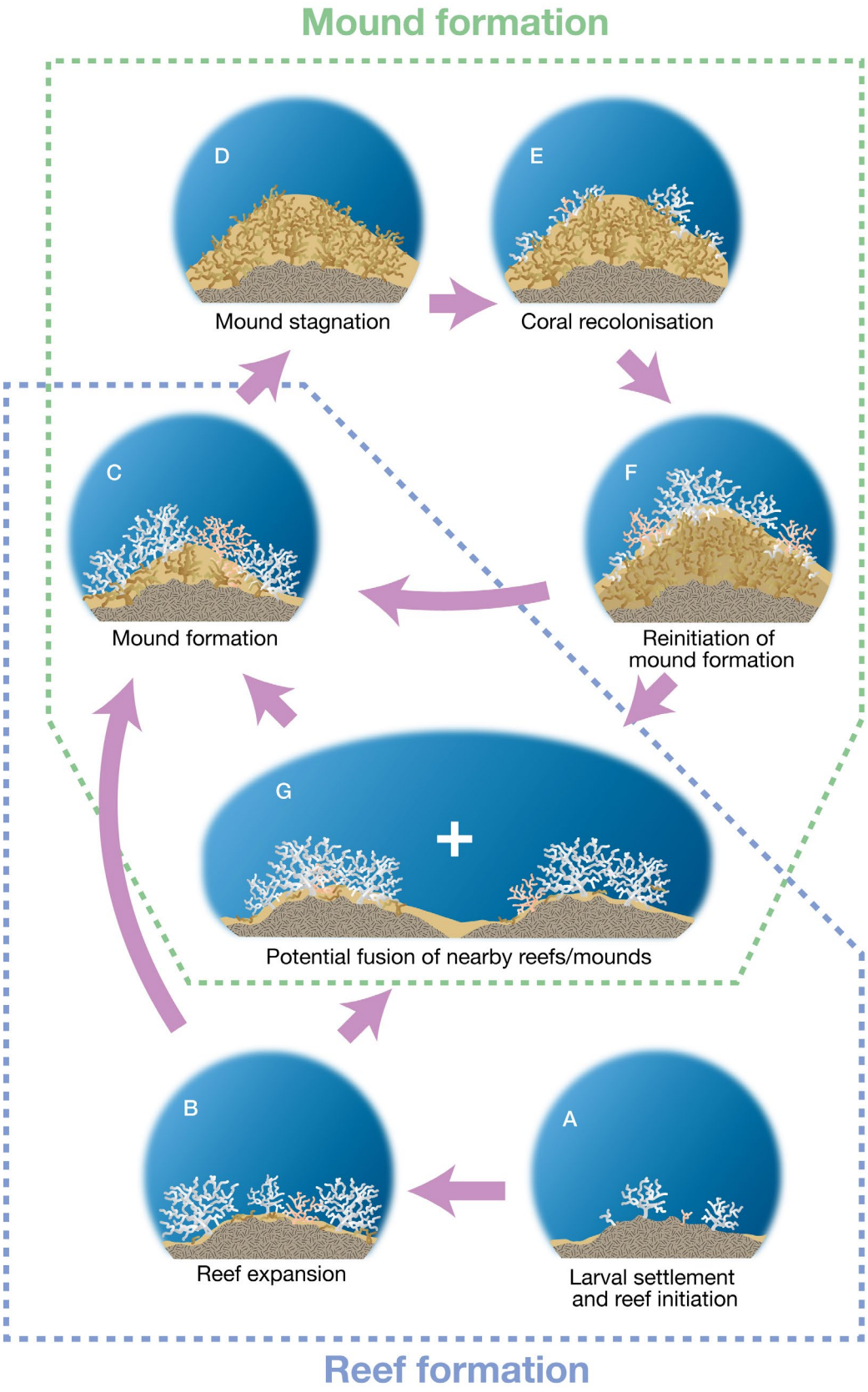

Figure 1.2. Diagram showing the different stages in CWC reef and mound formation. Modified from Roberts et al. (2006) and Douarin et al. (2013). A: Coral larvae settle on an elevated hard substratum and several colonies start to grow; B: Some coral branches break off promoting the development of new colonies and the availability of hard substrata for further larval settlement; C: The coral reef framework entraps hemipelagic sediment that provides structural stability, allowing vertical development and thus the initiation of coral mound formation; D: Unsuitable environmental conditions cause coral demise, thus stopping mound development; E: Suitable environmental conditions allow coral resettlement and a new reef starts to form; F: the new reef generation promotes again the baffling of hemipelagic sediments and the reinitiation of mound formation; G: The expansion of nearby reefs/mounds can produce their coalescence.

detected that larvae migrate upwards to the photic zone in order to feed and increase their dispersal potential (Stromberg and Larsson, 2017). Indeed, larvae from this species have the ability to cross water mass interfaces with considerable density gradients (Larsson et al., 2014; Stromberg and Larsson, 2017). Once on the surface, larvae are subjected to density and wind driven currents, which might transport them for longer distances (Fox et al., 2016). With CWC larvae moving vertically through pycnoclines, the deepest coral assemblages might act as source to repopulate shallower ones, more affected by fishing and other human-induced disturbances (Fox et al., 2016).

1.2. Cold-water coral reefs and mounds

1.2.1. Coral mound formation, morphology and distribution

The potential development of a CWC mound begins with the settlement of several larvae that can grow, forming numerous coral colonies (Fig. 1.2A). During the growing process of coral colonies, their base tends to lose the coral tissue, as the polyps in this lower part of the colony do not receive a sufficient food supply to survive (Wilson, 1979). Physical, chemical and biological (e.g. clionid sponges) degradation eventually causes the collapse and fragmentation of large colonies (Roberts et al., 2006). Living coral fragments can grow as new colonies, while dead fragments, known as coral rubble, can be used as substratum for the settlement of further CWC larvae, thus promoting the initiation of reef formation (Fig. 1.2A, B; Wilson, 1979; De Mol et al., 2005; Douarin et al., 2014). The persistence of coral growth and the recurrent breakage of branches promotes the lateral expansion of the area covered by the coral reef (Fig. 1.2B; Wilson, 1979; Roberts et al., 2006). If suitable environmental conditions for CWC growth persist through time, these organisms can form dense and complex reefs that extend for up to several kilometres and rise a few meters from the seafloor (Fig. 1.2B; Mortensen et al., 2001; Douarin et al., 2014; Lo Iacono et al., 2018a). A CWC reef is defined as a carbonate build-up mostly made of living scleractinian corals and dead coral framework, with a positive three-dimensional expression of a few meters (Roberts et al., 2009a; Lo Iacono et al., 2018a). The largest living reefs discovered so far have been described in the Irish, Scottish and Norwegian margins, with extensions of up to 100 km^2 (i.e. Røst Reef; De Mol et al., 2002; Freiwald et al., 2004; Roberts et al., 2005).

As CWC reefs grow they start baffling by-passing hemipelagic sediments that provide mechanical stability to the reef structure and prevent its physical collapse (Fig. 1.2C; Hebbeln et al., 2016). Over long time-spans (i.e. thousands to millions of years), the combination between coral growth and a contemporaneous sediment supply allows the reefs to grow vertically and form prominent geomorphological features known as CWC mounds (Fig. 1.2C; Hovland et al., 1994; De Mol et al., 2002; Roberts et al., 2006; Lo Iacono et al., 2018a). The formation of these geomorphological structures can last from millennia (e.g. Darwin Mounds; Victorero et al., 2016) to several millions of years (Challenger Mound; Kano et al., 2007). However, coral mound aggradation is not continuous and instead it is the result of several reef development cycles (Fig. 1.2C-F; Dorschel et al., 2005; Kano et al., 2007; Rueggeberg et al., 2007). Through time, nearby single mound features tend to merge and give origin to the development of the so-called giant coral mounds (Fig. 1.2G; Masson et al., 2003; Kenyon et al., 2003). Periods of mound stagnation (i.e. when coral reefs are not growing; Fig. 1.2D) are commonly recorded as temporal hiatuses of mound formation in the mounds' stratigraphy (Dorschel et al., 2005; Wienberg et al., 2018; Wang et al., 2019). The internal structure of coral mounds is characterised by coral fragments embedded in a muddy sediment matrix (> 50%; Titschack et al., 2015) that consists of trapped

hemipelagic sediments and micritic components, derived from eroded coral rubble and calcareous shells of benthic invertebrates (e.g. molluscs, echinoderms, bryozoans and foraminifera; De Mol et al., 2002; Wienberg and Titschack, 2017). On the other hand, the exterior appearance of coral mounds typically grades from small coral sediments and fragments at the base, to coral rubble and patches of dead coral framework at the lower and upper flanks of the mound (Mortensen et al., 1995; Huvenne et al., 2005; Buhl-Mortensen et al., 2010). Depending on their current state, the mounds' summit may consist of thriving coral reefs (i.e. active mound) or dead coral frameworks that are subjected to bio-erosion and sediment burial (i.e. inactive mound; Fig. 1.2D; Hebbeln et al., 2009; Henry and Roberts, 2017; Angeletti et al., 2020a).

CWC mounds present a wide range of sizes and shapes (Lo Iacono et al., 2018a). In terms of size, they can range from mini-mounds that are a few metres tall (e.g. Darwin and Moira Mounds; Bett et al., 2001; Foubert et al., 2011) to giant ridge-like mounds that rise hundreds of meters above the surrounding seafloor (e.g. Challenger Mound and Brittlestar mounds; Kano et al., 2007; Comas and Pinheiro, 2010; Fink et al., 2013). Laterally, coral mounds can expand hundreds of meters for sub-circular shapes and extend for several kilometres in ridge-like morphologies (Huvenne et al., 2005; Mienis et al., 2006; Lo Iacono et al., 2018a). Typically, coral mounds display morphologies that vary among conical, oval, tear-drop and ridge-like shapes (Wheeler et al., 2007; Lo Iacono et al., 2018a; Hebbeln, 2019). Such mound morphologies are commonly associated with the presence of an underlying geological structure on which the corals first settled and started to grow (Lo Iacono et al., 2014, 2018a; Hebbeln, 2019). Nonetheless, persistent current dynamics can also have an effect on the morphology of growing coral mounds (Huvenne et al., 2003; López-Correa et al., 2012; Hebbeln et al., 2014, 2019a; Buhl-Mortensen et al., 2016).

These geomorphic features tend to occur in clusters or provinces consisting of tens to thousands of mounds (Mortensen et al., 2001; Lo Iacono et al., 2014; Hebbeln et al. 2019a; Angeletti et al., 2020a). They are mainly found on the Northeast Atlantic margin, within a depth range of 70–1200 m (Fig. 1.3; Wheeler et al., 2007; Lo Iacono et al 2018a). The spatial distribution of the coral mounds discovered so far resembles that of CWC assemblages but restricted to the continental margins, where sediment supply is constant enough to allow coral mound aggradation. In addition, the bathymetrical distribution of the mounds tends to coincide with water-mass interfaces, reinforcing the role that oceanography has in the development of these features (Wheeler et al., 2007; White and Dorschel, 2010; Lo Iacono et al., 2018a). For instance, the bathymetric range of the coral mounds from the Porcupine Seabight is related to the water mass interface found between the Mediterranean Outflow Water and the Eastern North Atlantic Water (Rüggeberg et al., 2016; Wienberg et al., 2020). The higher concentration of known CWC assemblages and mounds in the Northeast Atlantic is probably the result of a differential sampling effort carried out in this region compared to the rest of the ocean (Freiwald et al., 2004; Wheeler et al., 2007; Wienberg and Titschack, 2017; Lo Iacono et al., 2018a). In the last decade, new coral mound provinces have in fact been discovered off the west-African coast (Eisele et al., 2011, 2014; Vandorpe et al., 2017; Wienberg et al., 2018; Tamborrino et al., 2019), the eastern continental slopes of North and South America (Grasmueck et al., 2006; Mienis et al., 2012b, 2014; Hebbeln et al., 2014; Raddatz et al., 2020; Steinman et al., 2020) and in the Mediterranean Sea (Comas and Pinhero, 2010; Lo Iacono et al., 2014, 2016; Savini and Corselli, 2010). Therefore, further mapping expeditions along the continental margins of the Atlantic Ocean and the Mediterranean Sea would most probably result in the discovery of new CWC coral mound provinces.

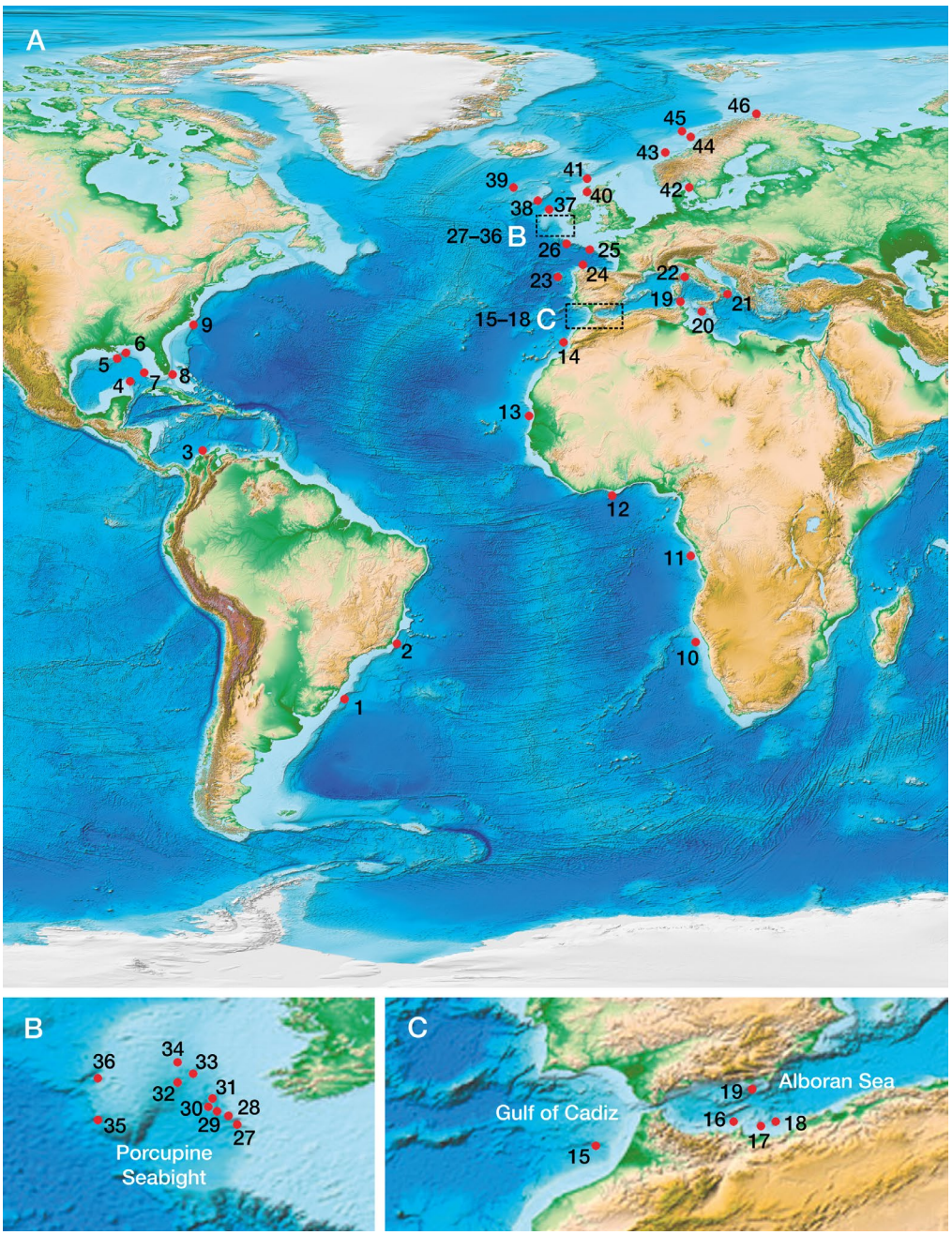

Figure 1.3. Coral mound distribution (red dots) in the Atlantic Ocean, Mediterranean Sea, Gulf of Mexico and Caribbean Sea based on data from Hebbeln and Samankassou (2015), Lo Iacono et al. (2018) and the most recent discoveries. 1, Northern Argentine Mound Province (Steinman et al., 2020); 2, Campos Basin Mounds (Lopes and Hajdu, 2014); 3, Southern Caribbean Coral Reefs/Mounds (Reyes et al., 2005); 4, Campeche Mounds (Hebbeln et al., 2014); 5, Gulf of Mexico Mounds (Georgian et al., 2016); 6, Viosca Knoll Mounds (Brooke and Schroeder, 2007); 7, West Florida Mounds (Neumann et al., 1977); 8, Florida Mounds (Grasmueck et al., 2006); 9, Cape Lookout Mounds (Mienis et al., 2014); 10, Namibia Mounds (Tamborrino et al., 2019); 11, Angola Mini Mounds (Le Guillox et al., 2009); 12, Ghana Mounds (Buhl-Mortensen et al., 2017); 13, Banda Mounds (Eisele et al., 2014); 14, Eugen Seibold Mounds (Glogowski et al., 2015); 15, Pen Duick Mounds (Van Roij et al., 2011); 16, West Melilla Mounds (Lo Iacono et al. 2014); 17, East Melilla Mounds (Fink et al., 2013); 18, Cabliers Mound (Lo Iacono et al. 2016); 19, Chella Mound (Lo Iacono et al., 2018); 20, Tuscan Archipelago Mounds (Remia and Taviani, 2005; Angeletti et al., 2020); 21, Pantelleria Mounds (Martorelli et al., 2011); 22, Santa Maria di Leuca Mounds (Savini and Corselli, 2010); 23, Breoghan Mounds (Somoza et al., 2014); 24, Ferrol and Coruña Canyon Mini Mounds (Lo Iacono et al., 2018); 25, Penmarc'h and Guilvinec mini Mounds (De Mol et al., 2011); 26, Explorer and Dangeard mini Mounds (Stewart et al., 2014); 27, Arc Mounds (Mohn et al., 2014); 28, Porcupine Bank Canyon Mounds (Mazzini et al., 2012); 29, Hovland Mounds (Hovland et al., 1994); 30 Magellan Mounds (Hovland et al., 1994); 31, Viking Mounds (Foubert et al., 2011); 32, Galway Mounds (Dorschel et al., 2007); 33, Therese Mounds (De Mol et al., 2007); 34, Challenger Mound (Kano et al., 2007); 35, Macnas Mounds (Wilson et al., 2007); 36, Enya Mounds (Van Rooij et al., 2009); 37, Pelagia Mounds (Kenyon et al., 2003); 38, Logachev Mounds (Kenyon et al., 2003); 39, Francken Mounds (Wienberg et al., 2008); 40, Mingulay Mounds (Roberts et al., 2005); 41, Darwin Mounds (Masson et al., 2003); 42, Tisler Reef (Wild et al., 2009); 43, Sula Reef (Freiwald et al., 2002); 44, Traena Reef/Mounds (Lindberg, 2004); 45, Røst Reef (Freiwald et al., 2004); 46, Stjernsund Reef/Mounds (Freiwald et al., 1997).

1.2.2. Biodiversity associated with cold-water coral reefs

Besides displaying a broader latitudinal distribution than tropical coral reefs, CWC reefs also host an outstanding species diversity, comparable to that observed in their tropical counterparts (Roberts et al., 2006; Henry et al., 2008; Henry and Roberts, 2017). The capability that CWCs have to create complex three-dimensional frameworks produces an increase in the spatial heterogeneity of the habitat at a local scale (Jones et al. 1994, Buhl-Mortensen et al. 2010; Price et al., 2019). These type of organisms are known as autogenic ecosystem engineers, as they modify the environment through their own physical structure (Jones et al., 1994). The complex frameworks characteristic of a CWC reef provide predator-free spaces that can be used by other species as spawning and nursery grounds (Costello et al., 2005; Quattrini et al., 2009). In fact, abundant juveniles of *Galeus melastomus* and *Etmopterus spinax* have been reported in CWC reefs (D'Onghia et al., 2010, 2012). Furthermore, the exposed dead coral framework of the reefs is a suitable substratum for the settlement and growth of many sessile species (Roberts et al., 2006; Henry and Roberts, 2017). The CWC framework also causes changes in the environmental variables, mainly reducing current speed and enhancing turbulence and sediment deposition, which ultimately increases the amount of food present within the reef (Hebbeln et al., 2016).

Overall, the biologically-generated spatial heterogeneity and complexity causes gradients of biophysical conditions along the reef that promote the creation of a large number of ecological niches, ultimately increasing species diversity (Jones et al., 1994; Buhl-Mortensen et al. 2010; Price et al., 2019). The highest species diversity within CWC reefs is observed in areas that present a mixture between live and dead coral framework, while areas completely covered by living CWCs display fewer associated species (Buhl-Mortensen and Fosså, 2006; Henry et al., 2013). Species richness in *D. pertusum* reefs is probably the highest within CWCs, with more than 1300 associated species reported (Roberts et al., 2006). Excluding the primary producers of the photic zone, the significant functional diversity of the species observed on CWC reefs shows that these habitats encompass a large number of trophic levels of the benthic food web (Buhl-Mortensen et al., 2017).

Sea urchins are generally found in great numbers in CWC reefs as they use corals as a food source and as shelter to protect from predators (Stevenson et al., 2014). Carnivorous cladorhizid sponges have also been found to thrive within the CWC frameworks in the southwest Atlantic and the Mediterranean Sea (Lopes and Hajdu, 2014; Santin et al., 2020). Nevertheless, the most diverse fauna found in CWC reef habitats are the filter and suspension feeders that settle on the dead coral framework sectors of the reef (Henry and Roberts, 2007). These include many octocorals, antipaharians, sponges, crinoids, bryozoans, bivalves, polychaetes and some other species of scleractinians (Buhl-Mortensen et al., 2010; Henry and Roberts, 2017).

Compared to the surrounding seafloor, CWC reefs also display a considerably higher abundance and diversity of demersal fishes, which use these habitats to feed, find refuge and reproduce (Purser et al., 2013; D'Onghia et al., 2019). Among the fish species that occur in CWC reefs, there are several commercially valuable species. The latter include ling (*Molva molva*), blackbelly rosefish (*Helicolenus dactylopterus*), redfish (*Sebastes marinus*), blackspot seabream (*Pagellus bogaravero*) and tusk (*Brosme brosme*) (Husebø et al., 2002; D'Onghia et al., 2011, 2012).

Due to the high species and functional diversity observed in CWC reefs in comparison to the surrounding seafloor, these habitats are considered global biodiversity hotspots. However, not all CWC reefs and mounds share the same fauna. For instance, considerable differences in species composition have been observed between Norwegian and African coral reef assemblages, which are dominated by *D. pertusum*, potentially increasing even more the number of species associated to these remarkable habitats (Henry and Roberts, 2017; Buhl-Mortensen et al., 2017).

1.2.3. Threats for cold-water coral reefs and conservation measures

As a result of the presence of commercially valuable fishes within CWC reefs, these sites have been traditionally exploited by both bottom trawling and long-line fisheries (Rogers, 1999). Indeed, in Joubin (1922) the author already described the "problem" that CWCs supposed for bottom trawlers, as some of them had brought back on deck up to 6 tons of coral in a single trawl haul. Far from being a problem for this type of fishing gear, the detrimental effects of bottom trawling on coral gardens and reefs have been compared to those of forest clear-cutting (Watling and Norse, 1998). According to Fosså et al. (2002), almost 20 years ago, trawling activities in Norwegian deep-waters had already damaged ~30% of their CWC reefs. Stranded nets and trawling marks have also been observed on and around the coral mounds of the Porcupine Seabight (Olu-le Roy et al., 2002). Similarly, extensive trawling damage has been detected in the *O. varicosa* reefs off eastern Florida (Reed et al., 2002, 2005), in the *S. variabilis* reefs of Tasmanian seamounts (Koslow et al., 2001) and in the *D. pertusum* reefs of the Darwin Mounds (Wheeler et al., 2005). In addition to the coral mortality caused by direct physical damage, the sediment resuspension resulting of bottom trawling activities may cause further damage to the remaining living corals. Excessive suspended sediment in bottom waters might clog up the coral polyps, affecting their growth rates and eventually causing their death (Cortes and Risk, 1985; Brooke et al., 2009). Hence, trying to control and limit bottom trawling activities on coral reefs is of utmost importance, as the destruction of these assemblages leads to a considerable loss of biodiversity and spawning areas for some commercially valuable species (Le Danois, 1948; Husebø et al., 2002; Roberts et al., 2006; D'Onghia et al., 2011, 2012). Due to the slow growth rates of these species (i.e. <9 mm y^{-1}; Orejas et al., 2011) CWC reef recovery has proved to be practically inexistent in several regions (e.g. Darwin Mounds and Tasmanian Seamounts) even after 5–10 years of fisheries closure (Althaus et al., 2009; Huvenne et al., 2016). Although long-lines are not as destructive as bottom trawling, several researchers have also pointed out the potential detrimental effects that this type of fishing gear has for CWC reef assemblages (Fosså et al., 2002; Orejas et al., 2009).

With the addition of industrially-derived CO_2 to the atmosphere, the calcium carbonate ($CaCO_3$) saturation state of the ocean is changing (Orr et al., 2005). Indeed, the $CaCO_3$ saturation state is decreasing due to the lower ocean pH caused by the increasing atmospheric CO_2 (Caldeira and Wickett, 2003). While 95% of the present-day CWC assemblages are found above the aragonite saturation horizon, projections suggest that 70% of these locations might be in aragonite undersaturated waters by the end of this century (Guinotte et al., 2006), probably causing a wide-spread CWC habitat degradation.

Due to their high biodiversity, slow growth rate and susceptibility to anthropogenic disturbances, CWC reef ecosystems (EUNIS codes A5.631 and A6.611) have been protected

by several international organisations and agreements (Armstrong et al. 2014). These reefs have been described as "Threatened and/or Declining Habitats" by the OSPAR Commission (OSPAR, 2008) and declared as Vulnerable Marine Ecosystems (VMEs) by the Food and Agriculture Organisation (FAO, 2009) and the General Fisheries Commission for the Mediterranean (GFCM). Within the European Union, the main policies that underlie the protection of CWCs are the Habitats Directive (92/43/EEC, 1992), Natura 2000 and the Marine Strategy Framework Directive (MSFD; 2008/56/EC, 2008). Indeed, several countries have created Special Areas of Conservation (SACs) based on the application of the EU Habitats Directive and the MSFD. Fisheries closures in CWC reef areas that are located in international waters have also been designated by Regional Fishery Management Organisations (RFMOs), following the guidelines of FAO for the application of the UNGA 61/105 and 72/74 resolutions (Auster et al., 2011). Most CWC reef species are also protected by the Barcelona Convention SPA/BD protocol Annex II and the Dark Habitats Action Plan (UNEP-MAP-RAC/SPA, 2015). Lastly, the main reef-building species *D. pertusum* and *M. oculata* are also protected under the Convention on International Trade in Endangered Species (CITES) and included in the IUCN Red List.

1.2.4. Coral mounds as paleoclimatic archives

Due to the baffling effect of CWC framework, during periods of moderate to intense hydrodynamic conditions, coral mounds might still preserve sediment successions that would otherwise be lost owed to the non-deposition or erosion occurring in the areas adjacent to the mounds (Thierens et al., 2013; Hebbeln et al., 2016, 2019b). In addition, given their high stratigraphic resolution during mound formation periods and the dependence of these features on environmental conditions, coral mound deposits have a remarkable potential as archives of paleoclimatic changes (Dorschel et al., 2005; Thierens et al., 2013; Robinson et al., 2014). Even though the paleoenvironmental interpretation of the hemipelagic sediments found within coral mounds may be problematic (Dorschel et al., 2005), some studies have managed to unveil the great potential of these sedimentary records (Thierens et al., 2013; Stalder et al., 2015; Fentimen et al., 2020).

Nonetheless, paleoenvironmental information can also be extracted from the corals themselves, as their aragonitic skeletons can be preserved for hundreds to hundreds of thousands of years within the sedimentary sequences of the coral mounds (Kano et al., 2007; Frank et al., 2011). Such skeletons are suitable to be dated through Uranium series methods, which permit the acquisition of accurate ages as old as ~500 ka BP and their comparison to other records without depending on stratigraphic correlations (Cheng et al., 2000; Robinson et al., 2014). Corals and matrix sediments should, however, be analysed separately as they may display significant age offsets that can complicate the interpretation of the paleoenvironmental information obtained (Dorschel et al., 2005; Hebbeln et al., 2016). Coral skeletons can also record changes in sea water temperature, terrigenous input, water mass circulation, nutrient concentration and pH through the incorporation of certain elements such as Li, Mg, Ba, Nd, P and B dependent on the physicochemical conditions of the water column (Robinson et al., 2014; Montagna et al., 2014; Spooner et al., 2018; Stewart et al., 2020). In fact, considerable research efforts have been dedicated to the creation of coral proxies that give information about changes in the paleoenvironmental setting (Anagnostou et al., 2011, 2012; Montagna et al., 2014; Spooner et al., 2018; Stewart et al., 2020). The main limitation associated with coral-based proxies, is that they evidently cannot grant any infor-

mation during periods of coral absence, making it complicated to clearly determine what caused coral demise and to characterise the physicochemical conditions of the environment during such periods (Robinson et al., 2014; Hebbeln et al., 2019b). Furthermore, the chemical composition of the coral skeletons is not only determined by the environmental conditions but also by the biological activity of the organisms, which is known as "vital effects" (Robinson et al., 2014). For instance, trace metal ratios such as Mg/Ca and Li/Ca, which are used for temperature proxies, display a larger internal variability than that expected from environmental forcing (Case et al., 2010; Robinson et al., 2014). Therefore, it is essential to understand how vital effects work and how they correlate with skeletal structure and chemical composition, in order to develop accurate and robust geochemical proxies (Robinson et al., 2014). Substantial geochemical anomalies involving Mg/Ca and Li/Ca ratios have been reported to occur in the centres of calcification, which are small structural regions located along the central axis of the corals and characterised by the presence of chaotically placed aragonite crystals (Stolarski, 2003; Meibom et al., 2008; Case et al., 2010). In contrast, the content within the coral skeletons of other elements such as Nd does not seem to be affected by vital effects (van de Flierdt et al., 2010). Overall, the higher degree of skeletal chemistry understanding, acquired through the development of geochemical proxies, and the potential that coral mound deposits have as paleoenvironmental archives allows researchers to tackle unresolved questions regarding the environmental controls on coral mound development and the change in the physicochemical conditions of the water column in response to climatic changes.

1.2.5. Temporal patterns of cold-water coral mound development

Although there is not a global pattern for coral mound development, it generally follows glacial-interglacial cycles as main climatic driver, with mound formation occurring either in interglacial (e.g. Irish, Scottish and Norwegian mounds; Kano et al., 2007; de Haas et al., 2009; Thierens et al., 2010; Frank et al., 2011), glacial (Gulf of Cadiz, Mauritanian and Argentinian mounds; Wienberg et al., 2010; Eisele et al., 2011; Steinmann et al., 2020) or deglacials and temperate interstadial periods (Mediterranean mounds: Fink et al., 2013; Wang et al., 2019), depending on the environmental setting of their location. Atlantic coral mounds north of 50° N display a prominent mound aggradation during the Holocene and prior interglacial periods (de Haas et al., 2009; Frank et al., 2011; Kano et al., 2007). During glacial periods the grounding and discharge of ice sheets, together with a surface water temperature decrease of 8°C and reduced productivity might have impeded coral growth (Ottesen et al., 2005; Waelbroeck et al., 2009). Indeed ost of the coral reefs off the Norwegian margin established after the ice sheets retreated, around 11.65 ka BP (Freiwald et al., 1999; López-Correa et al., 2012) causing an abrupt shift in the biogeographic boundary of *D. pertusum*, which moved up to 70° N (Frank et al., 2011). Similarly, the most recent development stages of the coral mounds located on the Irish and Scottish margins started ~11 ka BP and 4.3 ka BP respectively (Frank et al., 2009; Douarin et al., 2013). Contrastingly, coral mounds south of 37°N generally thrived during glacial periods and their growth diminished throughout interglacial periods (Wienberg et al., 2010: Eisele et al., 2011). These cooling periods were associated to enhanced upwelling conditions and nutrient availability in several parts of the Temperate East Atlantic (i.e. off Portugal, Mauritania and the Gulf of Cadiz), causing an important increase in surface productivity (Frank et al., 2011). In fact, Eisele et al. (2011) observed that within glacial stages, Mauritanian coral mounds displayed higher aggradation rates during periods of enhanced productivity conditions.

1.3. Present-day distribution of CWC assemblages and mounds in the Mediterranean Sea

One of the main characteristics of the Mediterranean Sea is its semi-enclosed nature, which allows for the formation of a wind and water-flux driven thermohaline circulation, similar to the one that occurs throughout the world's ocean (Robinson et al., 2001). The basin scale circulation is affected by the entering Atlantic water (AW) and the formation of intermediate and deep-water masses at both the Western and Eastern Mediterranean Basins (Robinson et al., 2001). Both its enclosed nature and circulation pattern promote a high degree of endemism in this sea. This is especially true for benthic communities, as their geographical distribution and larval dispersal is limited by geomorphological barriers (e.g. Strait of Gibraltar), prevailing current patterns and sharp gradients in the physical characteristics of the water column.

CWCs are widespread species in the Mediterranean Sea. Actually, several studies have reported the occurrence of *M. oculata* and, to a lesser extent, *D. pertusum* in a large number of regions of the Mediterranean Sea continental margins, including submarine canyons, seamounts and escarpments (Orejas et al., 2009; De Mol et al., 2012; Fabri et al., 2014; Taviani et al., 2017; Angeletti et al., 2020b). However, extensive coral mound clusters seem to be confined to specific regions of this basin and are generally absent in the northern and eastern sectors of the Mediterranean Sea (Remia and Taviani, 2005; Comas and Pinheiro, 2010; Martorelli et al., 2011; Fink et al., 2013; Lo Iacono et al., 2014, 2016). Although the use of methodologies such as multibeam echosounder mapping and Remotely Operated Vehicle (ROV) surveys have become increasingly popular within benthic researchers, there are still many regions that remain uninvestigated, especially in the Eastern Mediterranean Basin and northern african margin, where only a few studies have been carried out. Instead, most projects dedicated to describing CWC assemblages have been focused on the Western Mediterranean Basin (Fig. 1.4; Mastrototaro et al., 2010; Fabri et al., 2014; Lo Iacono et al., 2014; Gori et al., 2017; Angeletti et al., 2020a). Therefore, an extended exploration and description of the Mediterranean seafloor is needed in order to increase our knowledge on the distribution of the main CWC assemblages and mounds present in this basin, which might also help researchers to gain insights on the main environmental variables driving it. Moreover, only with a broad and robust knowledge of the population dynamics, biodiversity, environmental drivers and threats affecting CWC habitats, we will be able to protect and manage them more thoroughly.

1.3.1. Eastern Mediterranean Basin

In the Adriatic Sea, high abundances of living CWCs are only observed on the walls of the Bari Canyon (Fig. 1.4; Angeletti et al., 2014). In this Canyon *M. oculata* prevails over the other benthic species, especially at depths between 306 and 640 m (Freiwald et al., 2009; Angeletti et al., 2014; D'Onghia et al., 2015), with the largest CWC colonies (i.e. up to 70 cm) occurring on the almost vertical southern wall of the canyon (Freiwald et al., 2009). Indeed, *M. oculata* dominates most of the Mediterranean CWC assemblages, accompanied by other species such as *D. pertusum*, *D. cornigera*, *Desmophyllum dianthus* and *Cariophyllia smithii*. Thriving CWC assemblages are also observed off Santa Maria di Leuca (Ionian Sea; Fig. 1.4; Savini and Corselli, 2010). This CWC province is formed by a highly dense cluster of coral-topped mounds that host abundant living colonies of CWCs in a depth range of 250–650 m (Savini and Corselli, 2010; Savini et al., 2016). These mounds mainly consist of landslide blocks that rise up to 25 m from the seafloor and extent for 500 m laterally (Vertino et al., 2010). Malinverno et al. (2010) determined that

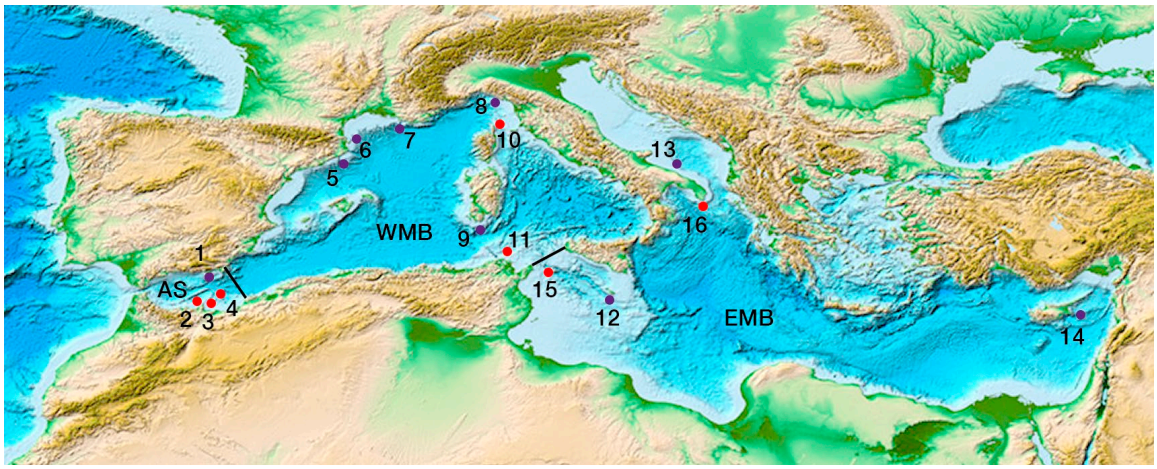

Figure 1.4. Present-day distribution of cold-water coral assemblages (purple dots) and mounds (red dots) in the Mediterranean Sea: 1, North Alboran Seamounts (i.e. Algarrobo, Herradura, Al-Idrissi and Chella seamounts); 2, West Melilla Mounds; 3, East Melilla Mounds; 4, Cabliers Coral Mound Province; 5, Blanes and La Fonera Canyon; 6, Cap de Creus and Lacaze Duthiers canyons; 7, Cassidaigne Canyon; 8, Levante Canyon; 9, Nora Canyon; 10, Corsica Coral Mound Province; 11, Tunisian Coral Mound Province; 12, South Malta; 13, Bari Canyon; 14, East Cyprus; 15, Pantelleria Coral Mounds; 16, Santa Maria di Leuca coral-topped mounds. AS: Alboran Sea; WMB: Western Mediterranean Basin; EMB: Eastern Mediterranean Basin

the blocks were colonised 14 ka BP by assemblages of *M. oculata* and *D. pertusum*, which have created a coral reef up to 1 m thick on top of the sediment blocks (Savini et al., 2016). Vertino et al. (2010) described the coral communities of SML and observed that coral-topped mounds in between 490 and 650 m depth are dominated by populations of *M. oculata*, locally accompanied by *D. pertusum* and hosting a large number of other benthic species (Mastrototaro et al., 2010). In the Levantine Sea, Orejas et al (2017) described assemblages formed by the scleractinian *Dendrophyllia ramea* observed at 120-170 m water depth, off the coast of Cyprus (Fig. 1.4). This species was found with a density of up to 4 col·m^{-2} and a colony size in some cases over 50 cm in height. The fact that outside the Adriatic and Ionian Seas only this study has been carried out in the Eastern Mediterranean, indicates that there is still an important gap of knowledge in this sector of this basin, which might be related to the lower availability of marine infrastructures in the area and its remote location. Although not based on video observations, other descriptions of stony CWCs are available in the Eastern Mediterranean Basin. Schembri et al (2007) recovered, by means of trawling nets, abundant fragments of living *M. oculata* and *D. pertusum* from depths between 390 and 617 m, just south of Malta (Fig. 1.4). Furthermore, just south of Pantelleria (Strait of Sicily) a coral mound cluster was discovered by Martorelli et al. (2011) in a depth range of 300–600 m, through the use of chirp profiles and multibeam backscatter data (Fig. 1.4). This coral mound province is formed by hundreds of mounds up to 10 m high and 20-90 m in diameter (Martorelli et al., 2011).

1.3.2. Western Mediterranean Basin

Scleractinian CWCs in this basin have been observed mainly inhabiting the hard bottoms and steep walls of submarine canyons (Orejas et al., 2009; Gori et al., 2013; Fabri et al., 2014, 2017; Fanelli et al., 2017; Lo Iacono et al., 2018b). De Leo et al. (2019) reported dense *M. oculata* and *D. dianthus* with some *D. pertusum* colonies occurring on the vertical walls of the Blanes Canyon, within a 400–800 m water depth range. Lastras et al. (2016) described the presence of locally dense patches of *M. oculata* occurring on the walls of La Fonera Canyon (Catalan coast) at depths between 180 and 300 m (Fig. 1.4). The walls of this submarine canyon were also colonised by some colonies of *D. cornigera* and the solitary coral *C. smithii*. North of La Fonera Canyon, the Cap de Creus Canyon also hosts dense assemblages of *M. oculata* (156-306 m) with an average

density of 0.44 ± 0.33 col·m^{-2} and maximal values of 10.67 col·m^{-2} (Fig. 1.4; Orejas et al., 2009). Although *M. oculata* represents >90% of the scleractinian colonies observed, *D. pertusum* and *D. cornigera* also sporadically occur on the Cap de Creus Canyon walls (Orejas et al., 2009; Dominguez-Carrio, 2018; Lo Iacono et al., 2018b). Gori et al. (2013) and Fabri et al. (2014) also described dense aggregations of *M.oculata* and *D. pertusum* at depths ranging from 240 to 541 m in Lacaze-Duthiers Canyon, located just north of the adjacent Cap de Creus Canyon (Fig. 1.4). Most of these assemblages were found on the head of the canyon and on the steep walls of its western flank. Together with Lacaze-Duthiers, the Cassidaigne Canyon is the other canyon from the French Mediterranean margin that hosts dense assemblages of *M. oculata* at depths between 200-515 m, with some colonies being bigger than 40 cm in height (Fig. 1.4; Fabri et al., 2017). In the Levante Canyon (Ligurian Sea), Fanelli et al. (2017) discovered the presence of scleractinian assemblages occurring at 525-575 m deep and mainly composed by *M. oculata* (0.6 ± 0.4 col·m^{-2}) and some colonies of *D. dianthus* (Fig. 1.4). Scleractinian assemblages have also been found on the slope areas of the Balearic Islands and Sardinia (Grinyo et al., 2018; Taviani et al., 2017). In the Nora Canyon (South Sardinia) at a depth between 380 and 460 m, *M. oculata* is the dominating species with an average density of 0.2 col·m^{-2} (Fig. 1.4; Taviani et al., 2017). Although the density in this area is lower than in some other regions of the Western Mediterranean Basin, coral colonies here can reach sizes of >1 m in height.

Besides the dense CWC assemblages mainly reported from submarine canyons, the Western Mediterranean Basin also displays thriving CWC reefs growing on several coral mounds, located in the Corsica Channel (Fig. 1.4; Angeletti et al., 2020a). Coral mounds were first reported in this region in a depth range of 355–410 m by Remia and Taviani (2005), through the use of a chirp sonar and the acquisition of seafloor samples containing sub-fossil coral fragments. In addition to the mounds discovered by Remia and Taviani (2005), Angeletti et al. (2020a) reported the presence of 28 more mounds, found in a depth range of 400–430 m, that can extend up to 330 m in length and rise up to 25 m above the surrounding seafloor. The latter are divided in two clusters, the first containing 8 mounds located 20 km south of Gorgona and the second found 12 km east of Capraia and including 20 mounds. Camafort et al. (2020) also described the presence of several coral mounds around the contourite deposits found on the Tunisian Plateau (Fig. 1.4). Nonetheless, the biological assemblages and past development of these mounds have not been described yet.

1.3.3. Alboran Sea

Observations of living stony CWCs have been reported from several seamounts and two coral mound clusters in the Alboran Sea (Fig. 1.4): the Algarrobo, Herradura, Al-Idrissi and Chella seamounts (De Mol et al., 2012; Lo Iacono et al., 2012, 2018b; De la Torriente et al., 2020), the East Melilla Mounds (EMM; Hebbeln et al., 2009; Fink et al., 2013) and the Cabliers Coral Mound Province (CMP; Lo Iacono et al., 2016). These geomorphic features generally harbour isolated colonies of *D. pertusum* or *M. oculata* and they are mostly covered by dense aggregations of soft corals, sponges and echinoderms (Fink et al., 2013, Hebbeln and Weinberg, 2016; Lo Iacono et al., 2019). The Brittlestar Mounds (i.e. EMM; Fig. 1.4) host some colonies of framework-building corals, yet these occurrences are very sparse and generally characterised by small coral colonies (15–20 cm in diameter; Hebbeln and Wienberg, 2016). It is only in the CMP where thriving CWC reefs have been observed to date in this sub-basin of the Mediterranean Sea (Lo Iacono et al., 2016). Furthermore, available studies do not describe and quantify the associated benthic megafauna inhabiting the coral mounds of the Alboran Sea. The same applies

to the most of the Mediterranean Sea, where only Mastrototaro et al. (2010) characterised the fauna associated to Santa Maria di Leuca coral-topped mounds. Thus, there is a gap of knowledge around the megafauna that can be found accompanying CWC reefs in the Mediterranean Sea, limiting the baseline that is needed to protect these sensitive ecosystems from potentially destructive anthropogenic disturbances and support their management.

Besides the living occurrences reported from the Alboran Sea, this sub-basin is characterised by displaying the most impressive coral mound clusters that have been discovered so far in the Mediterranean Sea (Hebbeln, 2019). These are divided into three main provinces: the West Melilla Mounds (WMM; Lo Iacono et al., 2014), the EMM (Comas and Pinheiro, 2010) and the CMP (described in chapters 2 and 3 of this thesis; Lo Iacono et al., 2016). The EMM are characterised by three E-W trending belts of mounds that are located between the Banc de Provençaux and the Moroccan coast. The northernmost belt consists of three steep ridge-like mounds, known as Brittlestar Mounds, that are located between 375 and 475 m water depth (Hebbeln, 2019). These mounds extend from 3 to almost 20 km in length and rise from 50 to 150 m from the seafloor (Hebbeln, 2019). The second coral mound belt, which is located several kilometres southwards in a water depth between 230 and 320 m, is composed by smaller and oval/arcuate shaped mounds. The mounds in this belt only extend for a few hundreds of meters and rise around 20–40 m above the surrounding seafloor (Hebbeln, 2019). The southernmost coral mound belt of the EEM displays branching ridge-like mounds in a depth range between 200 and 240 m. The latter seem to get buried by sediments towards the south but they generally stretch for up to 5 km and rise around 10 m from the seafloor (Hebbeln, 2019). Located to the west of Cape Tres Forcas, the WMM consist of 103 mounds divided in two clusters, found in a depth range of 298–590 m and depleted of living CWCs (Fig. 1.4; Lo Iacono et al., 2014). The main cluster is formed by 81 mounds that display a semi-circular to elongated shape, with a maximum height of 42 m and diameters ranging from 49 to 649 m. The second cluster is composed of 9 mounds that present a maximum height of 48 m and a diameter range of 143–626 m (Lo Iacono et al., 2014). Additional scattered mounds, displaying a maximum height of 35 m occur in the deepest sector of the province (i.e. 450–590 m). The recently discovered CMP consists of a chain of ridge-like mounds that extends NE-SW for ~25 km in a depth range of 260–710 m (Fig. 1.4; Lo Iacono et al., 2016). Nonetheless, the biological assemblages dominating the different regions of the province and its past development are yet to be described.

1.4. Temporal development and paleo-environmental controls on Mediterranean CWC assemblages and mounds

Sub-fossil CWCs are common along the whole Mediterranean basin (McCulloch et al., 2010; Fink et al., 2015). To date, extensive Uranium series dating has been used to obtain coral ages from samples covering a wide range of regions within the Mediterranean Sea (McCulloch et al., 2010; Fink et al., 2013, 2015; Stalder et al., 2015, 2018; Taviani et al., 2019; Wang et al., 2019). However, excluding the Alboran Sea, most of the coral ages acquired through Uranium series dating rely on samples collected from the seafloor surface, which are commonly degraded or present a Fe-Mn crust that appears when the corals are exposed to seawater for a prolonged period of time (McCulloch et al., 2010; Taviani et al., 2011). The ages acquired so far, report that CWCs have grown in this basin from the Middle Pleistocene (i.e. 480 ka BP) to the Holocene, with the latter encompassing most of the coral samples tested (McCulloch et al., 2010; Fink et al., 2013, 2015; Wang et al., 2019). Although isolated seafloor samples have allowed researchers to have a better under-

standing of coral growth periods in the Mediterranean Sea, they cannot parallel the information provided by the prolonged and semi-continuous record of coral mounds.

During the last decade, the discovery of several coral mound fields mainly concentrated in the Alboran Sea encouraged researchers to start using gravity cores to study the past development of these features in the Mediterranean Sea (Fink et al., 2013; Stalder et al., 2015, 2018; Wang et al., 2019). However, since only the upper metres of the mounds have been sampled, the current knowledge on coral mound development in this basin is mostly limited to the last deglacial and the Holocene (Fink et al., 2013; Stalder et al., 2015, 2018; Wang et al., 2019; Fentimen et al., 2020). Therefore, the formation patterns of these structures and their environmental drivers beyond the Holocene are largely unknown.

Several studies have attempted to link coral mound formation patterns in the Mediterranean Sea to different environmental factors, in order to better understand what are the main oceanographic and climatic processes driving coral mound development in this basin (Fink et al., 2013, 2015; Stalder et al., 2015, 2018; Taviani et al., 2019; Wang et al., 2019; Fentimen et al., 2020). McCulloch et al. (2010) observed that corals were abundant almost in the whole basin during the Younger Dryas (YD) cold period, whereas in the Alboran Sea corals seem to be absent during this period (Fink et al., 2013,2015; Wang et al., 2019). Fink et al. (2013) reported fast coral mound formation periods in the EMM during the Bølling-Allerød interstadial (B/A; 13.5–12.8 ka BP) and the Early Holocene (11.4–9.8 ka BP), followed by sporadic coral growth throughout the Middle Holocene (5.4–2.3 ka BP). These mound formation stages were associated to periods of increased productivity in the Alboran Sea caused by enhanced AW inflow into the Mediterranean Sea, which probably promoted gyre circulation, ultimately stimulating upwelling processes (Fink et al., 2013). Stalder et al. (2015, 2018) also showed evidence of *D. pertusum* mound formation stages in the EMM during the B/A and the Early Holocene, associated to enhanced fluxes of labile organic matter and water oxygenation. During the Mid Holocene the coral facies started to be dominated by *M. oculata* coinciding with reduced hydrodynamic conditions, oxygenation and a change from labile to refractory organic matter (Stalder et al., 2015, 2018). Similarly, Wang et al. (2019) described thriving mound formation periods in the WMM during the B/A (14.2–13.0 ka BP) and the Early Holocene (11.6–8.2 ka BP), followed by slow mound development until 3.4 ka BP when the mounds finally entered in a stagnation stage. As in the EMM (Fink et al., 2013; Stalder et al., 2015, 2018), coral proliferation during the B/A and the Early Holocene in the WMM is linked to increased surface productivity and hydrodynamics (Wang et al., 2019). The latter might be driven by the internal waves associated to the interface between the AW and Levantine Intermediate Water (LIW), which changes in depth following the glacio-eustatic cycles (Wang et al., 2019). Throughout the periods of fast mound formation, the interface was closer to the mounds, helping deliver particulate organic matter to the corals through the action of potential internal waves (Wang et al., 2019). Lastly, Fentimen et al. (2020) observed mound formation in the EMM mainly during the B/A (14.7–13.7 ka BP), followed by sporadic coral growth during the Holocene. In this study, the authors associated coral mound formation to enhanced fluvial and nutrient input during the B/A, which probably promoted surface productivity and a sufficient sediment supply for mound aggradation. In addition to all the research carried out in the Alboran Sea, both Fink et al. (2015) and Taviani et al. (2019) suggested that Sapropel deposition events (i.e. dark sediments rich in organic matter) had a detrimental effect for CWC proliferation in the Eastern Mediterranean Basin, as they were linked to reduced LIW formation and dysoxic/anoxic conditions in intermediate and deep water-masses.

1.5. Motivation for this study

CWC reefs and mounds have a remarkable role in the provision of ecosystem services and are valued as biodiversity hotspots and paleoclimatic archives (Freiwald et al., 2004; Roberts et al., 2006; Robinson et al., 2014; Henry and Roberts, 2017; Wienberg and Titschack, 2017). In recent years, a part of the scientific community has performed multidisciplinary studies to acquire a better understanding of the spatio-temporal distribution of CWC mounds and reefs, the environmental drivers that control their development and their associated species diversity. Nonetheless, there are still many aspects related to the species distribution within CWC reefs, their associated biodiversity and the environmental conditions controlling reef/mound development through space and time that have not been resolved by the scientific community.

For instance, CWC reef studies do not commonly report the distribution of associated megabenthic species in relation to the framework-building corals. Furthermore, several studies demonstrate that the number and type of species found living in CWC reefs changes considerably according to the bio-geographical location of the reef (Buhl-Mortensen et al., 2016; Henry and Roberts, 2017). While some studies have quantified the species associated to CWC reefs in the Atlantic Ocean (Henry and Roberts, 2007; Roberts et al., 2008; Van Soest et al., 2015; Buhl-mortensen et al., 2017; De Clippele et al., 2019), only Mastrototaro et al. (2010) has described the species living within Mediterranean CWC reefs.

Climate oscillations experienced since the Middle Pleistocene, which encompass stronger glacio-eustatic cycles, recurrent dysoxic conditions linked to sapropel deposition events and the presence of stadial-interstadial cycles (i.e. Heinrich events and Dansgaard–Oeschger cycles) within glacial periods, most likely had a significant effect on the distribution and development of CWC assemblages and mounds in the Mediterranean Sea. Yet, the current lack of gravity cores comprehending periods of mound formation beyond the last deglacial, has so far prevented researchers from drawing robust hypotheses on how Late Quaternary climate variations affected the development and spatial distribution of these outstanding benthic habitats. Therefore, assessing the distribution of megabenthic species in relation to mound and reef geomorphology, complemented with a comparison of species diversity among Mediterranean and Atlantic coral provinces is needed. Additionally, a description of the main environmental conditions and paleoclimatic events governing the formation of Mediterranean coral mounds from the Middle Pleistocene until the present day would considerably increase the understanding of CWC mound ecology and development patterns.

1.6. Scientific aims and research questions

The main aim of this thesis is to: (1) to quantify the density of living corals and accompanying megabenthic species within a Mediterranean coral mound province and describe their distribution along it; (2) to explore the changes in reef-building species dominance and the main environmental variables driving CWC mound formation in space and time in the Mediterranean Sea. The latter will be assessed in two contrasting coral mound provinces: the Cabliers Coral Mound Province (Alboran Sea, Western Mediterranean) and in the newly discovered Tunisian Coral Mound Province (South Tyrrhenian Sea, Central Mediterranean)

1.6.1. Chapter 2

In the Alboran Sea, north-east of the EMM, the recently surveyed Cabliers Coral Mound Province (CMP) presents thriving CWC assemblages growing on some of their crests (Lo Iacono, 2016). This study aims to quantitatively describe for the first time the megabenthic communities building the CWC reefs found on the CMP, through the analysis of Remoted Operated Vehicle video transects. It attempts to provide a detailed quantification of density and distribution of the main associated species, which contributes to address a basin-wide knowledge gap. Specifically, it will determine the abundance, size and distribution of CWCs and the most prominent associated taxa, determine which are the main megabenthic assemblages occurring on the CMP, reveal which are the most important seafloor features driving their distribution and perform a qualitative comparison between the fauna found on these coral mounds and the ones observed on other Mediterranean and Atlantic coral mounds.

• **Research questions:**

Q1: *What are the main reef-building and associated species occurring on the Cabliers Coral Mound Province? Are these assemblages impacted by fishing activities?*

Q2: *What is the distribution of cold-water corals and associated megabenthic species on the Cabliers Coral Mound Province in relation to mound geomorphology?*

Q3: *Does the size of living cold-water coral patches vary among the different geo-morphic sectors of the mounds?*

Q4: *Are there differences in terms of species composition and abundances between northern and southern Cabliers mounds? What are the main seafloor variables driving species distribution?*

Q5: *Are there differences between the fauna observed in this coral mound province in comparison to other Mediterranean and Atlantic coral mounds?*

1.6.2. Chapter 3

This chapter describes the coral mound development of the recently discovered Cabliers Coral Mound Province (CMP), through the description of the CWC deposits and corresponding Uranium series ages of two on-mound gravity cores collected from opposite ends of the province. With the intention of acquiring a better understanding of coral mound development in the Mediterranean Sea, this study aims to describe the temporal development of the northern and southern sectors of the CMP during the last ~390 kyr, to relate the changes in mound growth patterns to paleo-climatic events that modified the regional and local environmental setting and to compare the paleo-evolution of this province with the mound development patterns of already studied coral mound provinces in the Alboran Sea.

• **Research questions:**

Q6: *When did the mounds in the CMP develop?*

Q7: *What are the main environmental variables driving coral growth on the Cabliers Coral Mound Province?*

Q8: *What environmental variables regulate the differences in mound formation patterns between the northern and southern mounds of this province?*

Q9: *Do fluctuations in the paleoclimatic setting cause changes in the taxonomic composition of the coral deposits?*

Q10: *Is there a difference in mound formation patterns between the Cabliers Coral Mound Province and the rest of coral mound provinces found in the Alboran Sea?*

1.6.3. Chapter 4

This chapter describes the coral mound development of the newly discovered Tunisian Coral Mound Province through the study of 3 on-mound gravity cores by means of U-Th series and trace element analyses. The aim of this chapter is to describe the mound formation patterns of this new province mainly during the last ~80 kyr, to relate the development of the studied mounds to changes in the environmental setting and to compare the mound development patterns of this province with the one observed in the Cabliers Coral Mound Province and the other Alboran Sea coral mound provinces.

• **Research questions:**

Q11: *When did the mounds in the Tunisian Coral Mound Province develop?*

Q12: *What are the main environmental drivers determining cold-water coral mound formation in the Tunisian Coral Mound Province?*

Q13: *Are there differences in mound formation patterns among the three different mounds studied in this region? If yes, what environmental variables regulate these spatio-temporal differences in mound formation?*

Q14: *Do the mound formation periods of the Tunisian Coral Mound Province match with those of the Alboran Sea Coral Mound provinces?*

1.6.4. Chapter 5

This final chapter brings together a synthesised version of the main conclusions acquired in this thesis. The first part of the conclusions includes a description of how CWCs and associated megafaunal species are distributed along a partly thriving CWC mound province in relation to mound geomorphology and seafloor parameters. This is followed by a portrayal of the main environmental drivers that controlled coral mound development in the Mediterranean Sea during the Middle Pleistocene-Holocene. The chapter also presents further sections detailing the contribution of this thesis towards CWC research, as well as its limitations. Finally, some potential scientific lines for future research in the field of coral reef ecology and mound development are proposed.

Chapter 2

Ecological characterisation of a Mediterranean cold-water coral reef: Cabliers Coral Mound Province (Alboran Sea, western Mediterranean)

This chapter is a reproduction of the text published as **Corbera, G.**, Lo Iacono, C., Gràcia, E., Grinyó, J., Pierdomenico, M., Huvenne, V.A.I., Aguilar, R., Gili, J.M. (2019). Ecological characterisation of a Mediterranean cold-water coral reef: Cabliers Coral Mound Province (Alboran Sea, western Mediterranean). Progress in Oceanography, 175, 245–262.
DOI: https://doi.org/10.1016/j.pocean.2019.04.010

Author contributions: Corbera, G., Lo Iacono, C., Gràcia, E. and Huvenne, V.A.I. conceptualised the chapter. Lo Iacono, C., Gràcia, E., Grinyó, J., Pierdomenico, M. and Aguilar, R. acquired the data. Corbera, G. analysed the data and wrote the manuscript. All authors reviewed and commented on the manuscript.

2.1. Abstract

Scleractinian cold-water coral (CWC) reefs are key habitats for benthic fauna as they enhance spatial heterogeneity and biodiversity. Understanding their environmental and ecological dynamics has therefore important implications for biodiversity conservation. This is especially true for the Mediterranean Sea, where living CWC reefs are rare. In this study, we present a quantitative analysis of the CWC assemblages from Cabliers Coral Mound Province (CMP), located in the Alboran Sea (westernmost Mediterranean). The province extends for 25 km, with some mounds rising up to 140 m from the surrounding seafloor and being partly topped by living CWC reefs. The observed megabenthic species were quantified through video analysis of three Remotely Operated Vehicle (ROV) dives (280–485 m water depth) and their distribution was related to mound geomorphic characteristics and seafloor terrain parameters, extracted from a high-resolution Autonomous Underwater Vehicle (AUV) multi-beam bathymetry. The pronounced abundance and size of scleractinian CWCs among the observed assemblages, makes the CMP the only known coral mound province in the Mediterranean Sea with currently growing reefs. Within these reefs, several recruits and juveniles of the sebastid *Helicolenus dactylopterus* were observed, confirming the use of such habitats as nursery grounds by some commercially valuable fish species. The qualitative comparison between the fauna of the CMP and Atlantic coral mounds suggest that the number of species associated with CWC mounds worldwide is even higher than previously thought. This finding has important implications for the conservation and management of CWC habitats in different geographic regions.

2.2. Introduction

Over the last decade, the study of deep-sea benthic communities through Remotely Operated Vehicle (ROV) inspections has constantly expanded, largely due to ongoing technological improvements that have made ROV operating costs more affordable (Marsh et al., 2012; Neves et al., 2014; Gori et al., 2017; Khripounoff et al., 2017). Consequently, marine scientists have been able to describe a vast range of new deep-sea ecosystems and to characterise in more detail those that were already known to science (Roberts et al., 2006; Khripounoff et al., 2017; Bo et al., 2018). However, most of these studies are based on punctual observations, which inhibits to highlight the spatial distribution and ecological role of many benthic habitats and species at a regional scale. In parallel with ROV development, marine acoustics and Autonomous Underwater Vehicles (AUV) have also experienced significant technological advances and currently allow researchers to characterise the seafloor morphology at a metric scale (e.g. 1–2 m^2 pixel size; Huvenne et al., 2011; Wynn et al., 2014; Rona et al., 2015; Fabri et al., 2017). Therefore, combining ROV video-footage and AUV high-resolution multi-beam data allows for a detailed characterisation of benthic communities and helps to understand their spatial correlation with fine-scale seafloor geomorphology.

Among deep-sea benthic assemblages, cold-water corals are generally the focus of the research efforts from the scientific community, as they generate key habitats for benthic fauna (Freiwald et al., 2004; Roberts et al., 2006; Buhl-Mortensen et al., 2010). Several recent studies focused on the distribution of non-scleractinian cold-water corals, such as anthipatarians and octocorals (Fabri and Pedel 2012; Tong et al., 2012; Bullimore et al., 2013; Bo et al., 2014a, b; Grinyó et al., 2016, 2018; Pierdomenico et al., 2018). Nevertheless, stony (i.e. scleractinian) cold-water corals (hereafter mentioned as CWC) such as *Desmophyllum pertu-*

sum and *Madrepora oculata* have become some of the most intensively studied species in the last decade (Freiwald et al., 2004; Roberts et al., 2009a; Huvenne et al., 2011; Mienis et al., 2014; Buhl-Mortensen et al., 2017; Lim et al., 2017; Lo Iacono et al., 2018a). CWC are solitary or colonial organisms that generally occur in areas characterised by hard substrata on which they can settle and that can form dense benthic assemblages across a depth range of 39 m (Norwegian fjords) to 2000 m (NW Mediterranean canyons) (Freiwald et al., 2004; Roberts et al., 2006; Lo Iacono et al., 2018b; Sartoretto and Zibrowius, 2018). Hard substrata are usually located on complex geomorphic features such as submarine canyons, seamounts, shelf edges and landslides, where enhanced food-rich bottom currents provide suitable environmental conditions for CWC settlement and growth (Orejas et al., 2009; Davies et al., 2009; Huvenne et al., 2011; Mienis et al., 2012a; Lo Iacono et al., 2012, 2014, 2018b). CWC have a worldwide distribution, but historically, their assemblages have been more extensively studied along the North Atlantic continental margins (Hovland and Risk, 2003; Kano et al., 2007; De Mol et al., 2011; Mazzini et al., 2012). Among the framework-building CWCs, *D. pertusum* is the most widespread and abundant species, followed by *M. oculata*, which is more abundant in warmer waters such as the Mediterranean Sea (Savini and Corselli 2010; Fabri et al., 2014; Taviani et al., 2017) and *Solenosmilia variablis*, more common in the South Pacific Ocean (Koslow et al., 2001; Tresher et al., 2014).

The spatial distribution of these species is not only controlled by the availability of suitable substrata but also by a complex interplay of many environmental factors such as temperature, salinity, pH, dissolved oxygen, sedimentation rates, current intensity and food supply (Dodds et al 2007; Davies et al., 2009; Maier et al., 2009; Duineveld et al., 2012; Naumann et al., 2014). Framework-building CWC generally grow in waters with temperatures between 3 and 16 °C (Rogers, 1999, Davies and Guinotte, 2011) and salinity of 34-37 psu (Dullo et al., 2008). They are linked to high surface productivity and average bottom current speeds between 8 and 15 cm s^{-1} (Duineveld et al., 2012; Mienis et al., 2012a).

Under persistent suitable environmental conditions, living framework-building CWCs can form dense reefs extending over hundreds of meters and rising up to a few meters above the surrounding seafloor (Mortensen et al., 2001; Lo Iacono et al., 2018a). Over longer timespans and by baffling sediments within the coral framework, these living reefs might develop into three-dimensional geomorphological features, known as coral mounds (Wienberg and Titschack, 2017). These mounds can vary in shape and reach heights of up to 380 m depending on their development stage (Kano et al., 2007; Mienis et al., 2007; Van Rooij et al., 2009; De Mol et al., 2011; Hebbeln et al., 2014; Buhl-Mortensen et al., 2017).

CWC reefs present a higher habitat complexity and heterogeneity than the surrounding seafloor, which allows for an increase in the number of available ecological niches (Jones et al., 1994; Buhl-Mortensen et al., 2010). These habitats may also act as shelter and nursery grounds for many benthic species that use the coral framework to hide from predators (Costello et al., 2005). Because of all the above mentioned ecological benefits provided, CWC reefs are considered biodiversity hotspots, with a biological richness comparable to that of shallow-water tropical reefs (Roberts et al., 2006; Buhl-Mortensen et al., 2010). Species richness in *D. pertusum* reefs is probably the highest within CWC, with more than 1300 associated species (Roberts et al., 2006). However, not all CWC reefs and mounds share the same fauna. Considerable differences in species composition have been observed between Norwegian and African coral mound assemblages, which are dominated by *D. pertusum* (Buhl-Mortensen et al., 2017).

Due to their uniqueness, functional role and susceptibility to anthropogenic disturbances (Fosså et al., 2002; Althaus et al., 2009), framework-building CWC assemblages are considered vulnerable marine ecosystems (FAO, 2009). The OSPAR Commission and the General Fisheries Commission for the Mediterranean (GFCM) also count these assemblages within the lists of sensitive and threatened marine habitats that require protection (OSPAR, 2008; GFCM, 2009). Therefore, understanding the environmental constraints and ecological interactions of these assemblages, has important implications for the determination of their spatial distribution and thus, diversity conservation. This is especially true for the Mediterranean Sea where living CWC reefs are very limited compared to the North Atlantic (Freiwald et al., 2004; Vertino et al., 2010; Lo Iacono et al., 2018b, 2019). Framework-building CWCs in the Mediterranean are generally represented by small populations or scattered colonies, mainly located in submarine canyons and on landslides (Orejas et al., 2009; Savini and Corselli, 2010; Vertino et al., 2010; Gori et al., 2013; Lastras et al., 2016; Fabri et al., 2014; Fanelli et al., 2017; Taviani et al., 2017).

Within the Mediterranean basin, coral mound clusters are mainly located in the Ionian Sea (Savini and Corselli, 2010), Tyrrhenian Sea (Remia and Taviani, 2005) and the Alboran Sea (Comas and Pinheiro, 2010; Lo Iacono et al., 2014). However, they are generally buried beneath meters of sediments or in a stage of decline (Hebbeln et al., 2009; Comas and Pinheiro, 2010; Lo Iacono et al., 2012, 2014). An exception to this general observation are the coral-topped mounds located off Santa Maria di Leuca, Italy, where dense aggregations of *D. pertusum* and *M. oculata* have been observed growing on landslide blocks (Taviani et al., 2005; Vertino et al., 2010; Savini et al., 2016) and supporting a high biodiversity (Mastrototaro et al., 2010). Observations of living CWC have also been reported from two mound clusters in the Alboran Sea: the West Melilla Mounds (WMM; Lo Iacono et al., 2014) and the East Melilla Mounds (EMM; Comas and Pinheiro, 2010; Fink et al., 2013). Nevertheless, they only harbour small isolated colonies of *D. pertusum* or *M. oculata* and they are mostly covered by dense aggregations of non-scleractinian corals, sponges and echinoderms (Fink et al., 2013; Hebbeln and Wienberg, 2016; Lo Iacono et al., 2018a). Furthermore, none of these studies present a quantitative analysis of the megabenthic fauna inhabiting the coral mounds of the Alboran Sea. The same paucity of studies applies to the rest of the Mediterranean Sea, where only Mastrototaro et al. (2010) qualitatively characterised the fauna associated to Santa Maria di Leuca coral-topped mounds. Therefore, there is a knowledge gap regarding the relative abundance of taxa associated to CWC reefs in the Mediterranean Sea. The absence of quantitative data is limiting the creation of solid baselines required to better understand these sensitive ecosystems, which would help towards a more appropriate conservation and management measures.

In the Alboran Sea, north-east of the EMM, the recently surveyed Cabliers Coral Mound Province (CMP present thriving CWC assemblages growing on some of their crests (Lo Iacono et al., 2016; Corbera et al., 2017). The CMP is a coral mound province extending NE-SW for 25 km (Fig. 2.1) and developing on a volcanic outcrop known as Cabliers Bank (Würtz et al., 2015) in a water depth range of 250-710 m. In order to contribute to increase the knowledge of CWC reefs in the Mediterranean Sea, this study aims to quantitatively describe for the first time the assemblages found on the CMP. It also attempts to provide a detailed quantification of density and distribution of the main associated species, addressing a knowledge gap on a regional/basin scale. Specifically, we will:

- Determine the abundance, size and distribution of CWC and the most conspicuous associated taxa.
- Determine which are the main megabenthic assemblages occurring on the CMP

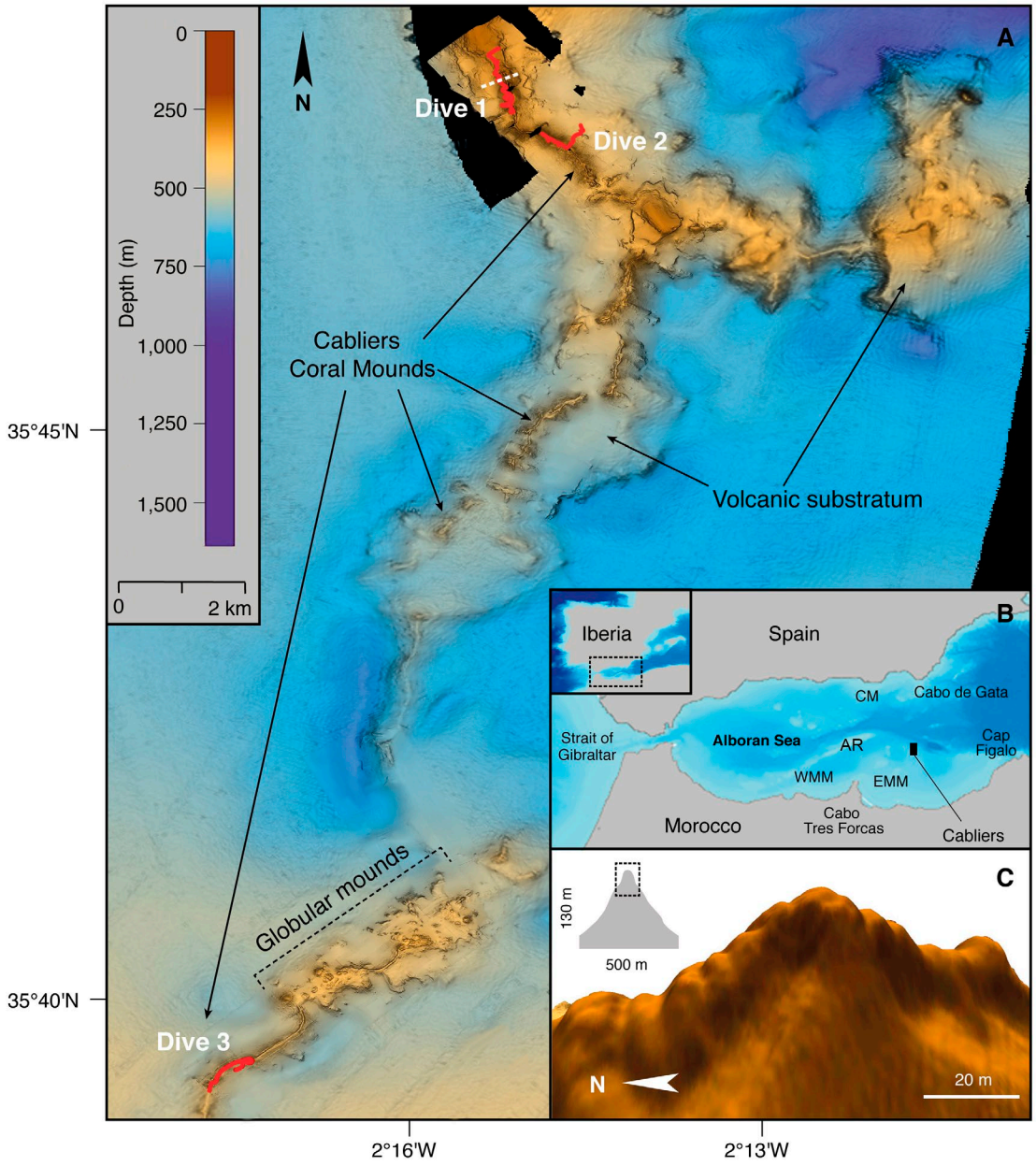

Figure 2.1. Bathymetric map of the IdefX AUV multi-beam bathymetry (2 m resolution) along the Cabliers Coral Mounds overlapped on shipboard bathymetry of the region (20 m resolution) (A). Inset of the Alboran Sea, the black rectangle indicates the location of the Cabliers Coral Mound Province (B). Three-dimensional representation of the mini-mounds occurring on the crest of the Cabliers Coral Mounds (C). The red lines on (A) indicate the path of the three Max-Rover ROV dives; the white dashed line indicates the location of the transversal mound section observed on (C). AR: Alboran Ridge, CM: Chella Mound, WMM: West Melilla Mounds, EMM: East Melilla Mounds.

- Reveal which are the most important seafloor features driving the distribution of the species
- Perform a qualitative comparison between the fauna found on these Mediterranean CWC mounds and the one observed on analogous structures of the Mediterranean Sea and the Atlantic.

2.3. Geological and oceanographic characteristics of the Alboran Sea

The Alboran Sea is a marginal sea located at the westernmost Mediterranean Sea, enclosed between the Iberian Peninsula (South Spain) and North Africa (North Morocco and Algeria) (Fig. 2.1B). This basin is bound by the Strait of Gibraltar to the west, by the Cabo de Gata to

the northeast, and by Cap Figalo to the southeast (Fig. 2. 1). The Alboran Sea includes three main sub-basins (i.e. West, East and South Alboran Basins) separated by the Alboran Ridge (Fig. 2. 1).

The seafloor geomorphology of this basin is relatively complex, displaying long ridges and several seamounts that have been carefully mapped in the frame of successive high-resolution bathymetric cruises (e.g. Gràcia et al., 2006, 2012; Lo Iacono et al., 2008). These features are intrinsically associated to the recent tectonic evolution of the basin and thus, related to the subducting slab located at the West Alboran Basin (Spakman et al., 2018).

The different tectonics domains are defined by large active strike-slip faults, such as the Al-Idrissi Fault System (FS) (Gràcia et al., 2006, 2012); Carboneras FS (Moreno et al., 2016), Averroes-Yusuf FS (Perea et al., 2018), as well as the prominent thrust-fault Alboran Ridge FS (Gómez de la Peña et al., 2018). In consequence, the Alboran Sea is a seismically active area, where moderate to large earthquakes have occurred in the past and recent times (Gràcia et al., 2012; Grevemeyer et al., 2015).

The water mass circulation in this basin is characterised by the interaction between Atlantic and Mediterranean water masses, which create a regional thermohaline circulation (Garcia Lafuente et al., 1998). Atlantic warmer and less saline waters (S~36.2 psu, T~15°C) enter the Alboran Sea through the Strait of Gibraltar and flow within the first 150-200 m of the water column at a velocity of ~50-100 cm s^{-1} (Garcia Lafuente et al., 1998; Oguz et al., 2014). The denser, colder and slower Mediterranean waters (S~38.4 psu, T~13.5°C) flow deeper and head out of the Mediterranean Sea at ~10 cm s^{-1} (Garcia Lafuente et al., 1998). The circulation of the Atlantic waters (AW) is mainly driven by two semi-permanent anticyclonic gyres (western and eastern Alboran Gyres) (Millot, 1999). After entering the Strait of Gibraltar, the AW is dragged towards the Spanish coast by the Western Alboran Gyre and then moves towards the African coast, where it meets the Eastern Alboran Gyre that brings the AW from Melilla to the Cabo de Gata (South Spain) (Millot, 1999). In contrast, the deeper Mediterranean Water, named Levantine Intermediate Water (LIW), flows in the opposite direction but without any effect from the surface gyres. The latter water mass forms in the Eastern Mediterranean basin and travels towards the Alboran Sea, crossing the Western Mediterranean Basin.

Three coral mound clusters have been reported in this basin: the Chella Mound (Lo Iacono et al., 2018a), the WMM (Lo Iacono et al., 2014) and the EMM (Comas and Pinheiro, 2010; Fink et al., 2013). The Chella Mound is located off the Almeria coast, it presents a ridge-like mound that raises 15-70 m from the surrounding seafloor and extends for a maximum of 3.4 km (Lo Iacono et al., 2018a). The WMM and EMM are located off the coast of Cabo Tres Forcas, on the southern margin of the Alboran Sea. The western mounds are smaller (1-48 m tall) and buried by fine sediments (Lo Iacono et al., 2014). On the other hand, the EMM are ridge-like features that can extend for up to 6 km and rise 20-60 m from the seafloor (Comas and Pinheiro, 2010). In this physiographic and oceanographic setting, the CMP is located northeast of the Cape Tres Forcas and the EMM.

2.4. Material and methods

2.4.1. Data acquisition and processing

Three ROV dives and a high-resolution AUV multi-beam bathymetric survey were performed on the CMP during the SHAKE cruise, conducted on board the R/V Sarmiento de Gamboa in April-May 2015. Seafloor video transects were recorded by means of the ROV Max-Rover (Hellenic Centre of Marine Research - Greece), equipped with an HD video camera (1920x1080 pixels), a manipulator arm and two parallel laser beams, 10 cm apart. During the collection of the video transects, ROV positioning was estimated by means of an ultra-short baseline (USBL) transponder mounted on the vehicle, which gave a geographic position every 3 seconds approximately. The ROV tracks were projected to UTM using the Geographic Information System ArcGIS 10.3.1 (ArcGIS Development Team, 2015) and all outlier points of the navigation data were removed to obtain a smooth plot of the geo-referenced transect. Outliers were identified as points located at a distance away from the main path that the ROV could not have reached, even at its maximum speed (0.6 m s^{-1}). These outliers are usually the consequence of signal beam reflections on seafloor features. The total distance covered by the ROV dives across the mounds was 5.2 km. Dive 1 and 2 were recorded at the northern part of the CMP, whereas Dive 3 was performed at the southernmost part. All transects covered sectors of both crest and flanks of the coral mounds (Fig. 2. 1). The three dives were performed in water depths between 280 and 485 m and the length of the video-transects ranged from 1249 to 2516 m (Table 2.1). During the ROV dives, both biological and rock samples were acquired by means of the ROV mechanical arm. These samples were later used to help in faunal identification and bedrock characterisation.

High-resolution multi-beam bathymetric data were acquired by means of an EM2040 Kongsberg Maritime multi-beam echo sounder (300 kHz), installed on the AUV IdefX (IFREMER - France). The AUV was programmed to acquire data 70 m above the seafloor, allowing for a metric-scale bathymetric resolution. The AUV collected the data with inertial navigation. Prior to the start of each survey, a calibration profile across the last 100 m of the water column was acquired on the flattest seafloor sectors. This calibration was used to calibrate the sound velocity during the multi-beam acquisition and in the post-processing phases.

All the multi-beam data obtained was processed on-board. The AUV navigation was corrected in Caraibes 4.3 by means of the RegBat module using both the bathymetric contours and the USBL as a reference for the correction of the inertial navigation. The data was then imported into CARIS HIPS and SIPS 9.1, where a constant zero value of tide was applied. Finally, spikes and noise were reduced through manual cleaning in areas of line overlap, and a bathymetric grid with a 2 m cell size was created as final outcome.

Table 2.1. Geographical coordinates, depth and length for each of the ROV dives analysed in this study.

Dive	Date	Position		Depth range	Length
		Start	End	(m)	(m)
1	21/05/2015	35°48'18" N, 2°15'17" W	35°47'55" N, 2°15'13" W	283-380	2516
2	22/05/2015	35°47'39" N, 2°14'35" W	35°47'34" N, 2°14'55" W	294-444	1250
3	21/05/2015	35°39'19" N, 2°17'47" W	35°39'29" N, 2°17'34" W	418-486	1401

2.4.2. Video analysis

Video transects were analysed using the editing software Adobe Premiere Pro CS6, following the methodology described in Gori et al. (2011). Laser points projected by two parallel beams located on the ROV frame, separated 10 cm from each other, were used to estimate transect width and to measure species size. The field of view slightly varied in relation to the ROV distance from the seafloor, being reduced to 1 m when the vehicle was close to the seabed.

Due to intermittent malfunctioning of the USBL, the location of the organisms along the ROV track had to be acquired by means of the following procedure. Each video transect was divided into over 30 fragments determined by control points. From one control point to the following one, DVL data was used to determine the course and the track of the ROV. This was thoroughly checked combining ROV video images with AUV High-resolution bathymetry. For each fragment, ROV speed was calculated based on the vehicle's travelled distance and the time interval between the corresponding control points. Such velocities were then used to calculate the position of each observed organism by using the following formula:

$$x_t = x_i + v_i \cdot (t - t_i)$$

where x_t is the distance from the start of the track at which the organism was identified, i is the analysed fragment, x_i is the distance covered by the ROV until the start of the current fragment, v_i is velocity of the ROV in the current fragment, t is the time when the organism was identified in the video footage and t_i is the time at the start of the analysed fragment.

All tracks were edited to remove sections of footage where the ROV was stationary (i.e. collecting samples or recording close-up images). Non-valid sequences such as poor visibility footage, caused by sediment resuspension, or parts where organism identification was not possible due to inappropriate altitude of the ROV (i.e. > 4 m) were quantified, isolated and removed from the subsequent statistical analyses.

All megafaunal organisms visible along each transect, within a section of 1 m around the central point of the field of view, were counted and identified to the lowest, practicable taxonomic level (i.e. typically species). Organisms that were not possible to identify to the species level, were classified within higher taxonomic levels or designated as morphospecies (e.g. "white encrusting sponge"). For the species *Phanopathes rigida*, which commonly appeared forming dense aggregations, the quantification of single colonies was not always possible. Therefore, this species' abundance was obtained through the quantification of such aggregations (hereafter named as living-patches). Density of CWC colonies (sensu Oliver, 1968) and associated megafauna were calculated by dividing each ROV transect into 2 m^2 sampling units (i.e. 2 m long × 1 m wide segments). This sampling unit size was chosen in order to quantify the species distribution along the transect at a high resolution. Moreover, the adopted sampling unit already resulted to be adequate for the analysis of deep-sea anthozoan assemblages in the western Mediterranean (Ambroso et al., 2013).

The size of each measurable living colony (sensu Oliver, 1968) of *M. oculata* and *D. pertusum* was calculated by means of still images, extracted from HD video footage when the parallel laser beams crossed the colony base. Still images were processed using the image software Macnification 1.8 (Orbicule, Inc.), which allows measurements of coral colonies by drawing a line

along the largest diameter of the living coral. The same procedure was carried out to measure the total length of the most abundant fish species, the sebastid *Helicolenus dactylopterus*. Substratum type was the only environmental variable determined from the ROV footage and was classified into four classes: fine sands with coral rubble (CRFS), coral rubble (CR), dead coral framework with fine sands (CFFS) and dead coral framework (CF) (Fig. S2.1).

2.4.3. Statistical analyses

The differences in taxonomic composition and diversity amongst the ROV dives were explored via species relative abundance, species richness (S) and Shannon diversity index (H') values. The distribution of the most relevant and abundant taxa observed in the video transects was then plotted, displaying species density against the bathymetric profile and along the transect length of each dive. All 2582 sampling units were used in density plots, 1253 of them corresponding to Dive 1, 626 to Dive 2 and 703 sampling units to Dive 3.

Regarding CWC size structure, descriptive statistical parameters such as skewness and kurtosis were calculated to determine if the population was dominated by small or large colonies. Both *M. oculata* and *D. pertusum* populations, with more than 1000 and 100 colonies respectively, were large enough to perform robust skewness and kurtosis tests. Both tests assume normality as a null hypothesis. Skewness is a measure that gives information about the symmetry of a distribution. A population has an asymmetrical distribution when the skewness is statistically significant ($p<0.05$). If skewness is positive, it indicates a higher percentage of small colonies, whereas negative values of skewness relate to a higher proportion of large ones. If skewness values are close to 0 it indicates that the size structure of the colonies is close to a normal distribution. On the other hand, if the kurtosis test is statistically significant ($p<0.05$) it means that data distribution has shorter or longer tails than expected for a normal distribution. Skewness and kurtosis were calculated using the functions *agostino.test* (Komsta and Novomestky, 2012) and *anscombe.test* (Anscombe and Glynn, 1983) from the *moments* package of the R software (Komsta and Novomestky, 2012; R Core Team, 2017). Colony size of *M. oculata* and *D. pertusum* was plotted using 10 cm size classes. *M. oculata* average size was also plotted against the bathymetric profile and along the transect length in Dive 1, which was the only dive with an abundance high enough to observe size patterns along geomorphologic features. The colony size data from this dive was log-transformed to achieve normality and differences between average size of CWC growing on the flanks and the crest of the mound were assessed by means of a Student's *t*-test. The determination of crest and flank areas was performed through a combination of visual assessment of the footage and the ROV location.

A Spearman rank correlation was used to verify that CWC density increases towards the summit of ridge-like features (hereafter mentioned as mini-mounds) occurring at the crest of the coral mounds. A moving average of period 5 was applied to the CWC density data to exclude small scale variability. This data was then correlated to the values of a fine scale bathymetric position index (BPI) (inner radius: 5 m, outer radius: 10 m), which detected most of the mini-mound features on the AUV multi-beam along the Cabliers mounds crest. The BPI is a measure consisting on a second order derivative of the seafloor surface that determines the elevation of each grid cell in relation to the surrounding landscape of the bathymetry. This derivative produces a new raster where geomorphological features such as crests, slopes, depressions and flat areas are indicated.

To evaluate the relationships between megafaunal abundance and seafloor features (see below) a canonical correspondence analysis (CCA) was performed. CCA is a multivariate constrained ordination test that attempts to explain the effect of each environmental variable on species distribution (Greenacre and Primiceiro, 2013). Taxa that had an abundance lower than five individuals were not considered in the analysis to avoid noise in the final outputs. Furthermore, off-mound areas (i.e. regions of fine sands and outcropping rock), occurring at the beginning of Dive 1 and 2 were not considered for the assemblage analyses. The CCA was carried out for the three Dives, to identify the composition of the main assemblages occurring on the mound and the seafloor physical characteristics influencing their distribution. The CCA was executed using the *cca* function from the *vegan* package (Oksanen et al., 2013) of the R software (R core team, 2017). This was performed together with the function *anova.cca*, which runs an ANOVA-like permutation test. This test was used to assess the significance of each seafloor feature and to determine which was the variable that had a greater effect on the distribution of megafaunal species (Chambers and Hastie, 1992). The CCA was performed for sampling unit sizes of 2, 4, 10 and 20 m^2 in order to assess how spatial scale affects the determination of benthic assemblages and their corresponding environmental setting.

The environmental variables used in the CCA statistical analysis, included depth and seafloor terrain parameters (i.e. slope, terrain roughness, aspect and bathymetric position index) that were derived from the high-resolution bathymetry using the Add-on RSOBIA (Le Bas, 2016) and Benthic Terrain Modeller (Walbridge et al., 2018) within the Geographic Information System software, ArcGIS 10.3.1 (ArcGIS Development Team, 2015). The roughness raster was obtained using the VRM algorithm (Sappington et al., 2007). In this analysis, the BPI was computed at a broad scale (inner radius: 10 m, outer radius: 20 m) to account for large-scale features that can have a greater effect on species distribution. Values of all these seafloor features were obtained from the central point of each sampling unit of the video transects, using the *extract* function from the *raster* package within the R software v 3.4.0 (R Core Team, 2017). Substratum type was also included in the CCA analysis, as four different variables coded for presence absence. The substratum type with the higher cover was assigned to each sampling unit.

2.5. Results

2.5.1. Physiography of the Cabliers Coral Mound Province

The CMP developed over a rocky outcrop, witnessed in the ROV footage and interpreted in the AUV bathymetry. Collected rock samples during Dives one and two helped to determine the substratum as being of volcanic origin. The mounds generally present a ridge-like morphology with an average height of ~77 m and a maximum of 140 m. Flanks are 35° steep on average. Overall, the sections of the mounds with a greater relief exhibited wider bases. The high-resolution AUV multi-beam bathymetry revealed that the crests of the mounds consist of a series of consecutive mini-mounds (Fig. 2.1C). These smaller features, whose internal structure consists of dead coral framework and baffled sediments, can rise up to 7 m on top of the mound's crest and extend for 23 m in width. Towards the southern part of the CMP, a field of complex globular mounds developed (Fig. 2.1A); these mounds have an average diameter of 121 m and rise up to ~40 m from the surrounding seafloor. This field of globular mounds occupies an area of about 3 × 1 km. South of this region, the CMP is again exclusively formed by aligned ridge-like mounds.

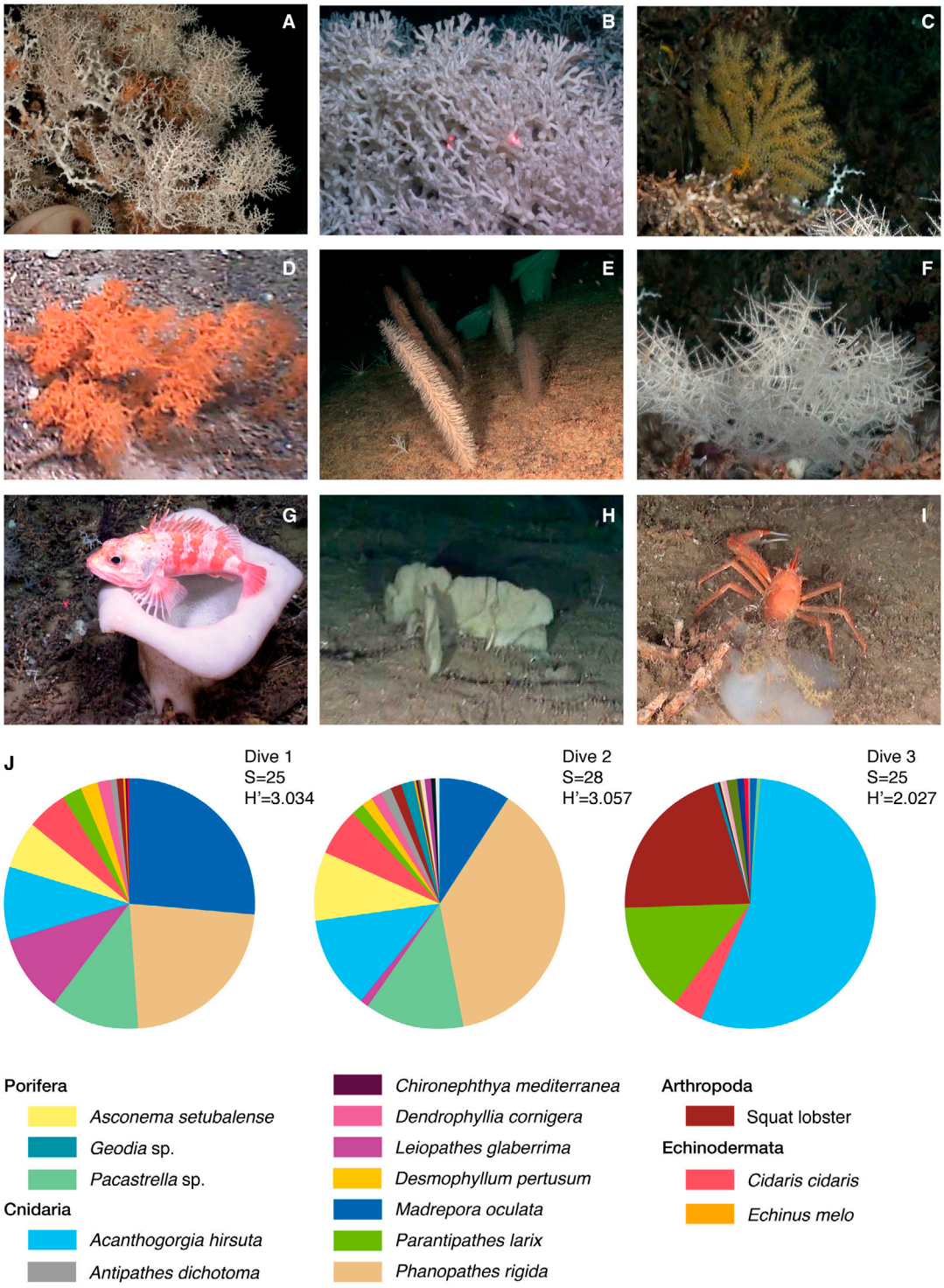

Figure 2.2. Most abundant fauna observed in the ROV footage (A-I), and (J) species relative abundance, richness (S) and diversity (H') of each dive. *Madrepora oculata* (A), *Desmophyllum pertusum* (B), *Acanthogorgia hirsuta* (C), *Leiopathes glaberrima* (D), *Parantipathes larix* (E), *Phanopathes rigida* (F), *Asconema setubalense* (sponge) and *Heliconelus dactylopterus* (fish) (G), sp. (H), Squat lobster (I). Still images A, C, E, F and H, © OCEANA.

2.5.2. General megafaunal characteristics

A total of 2582 sampling units (2 m^2) were obtained from the ROV dives, in which 7737 organisms representing 49 different taxonomic groups were identified (Table S2.1). 64.1% of these organisms, could be identified to species or genus level, whereas 13.1% were included in broader taxonomic categories, and 22.8% were considered as morphospecies. The most abundant species was the antipatharian *Phanopathes rigida* with 1532 colonies, followed by the gorgonian *Acanthogor-*

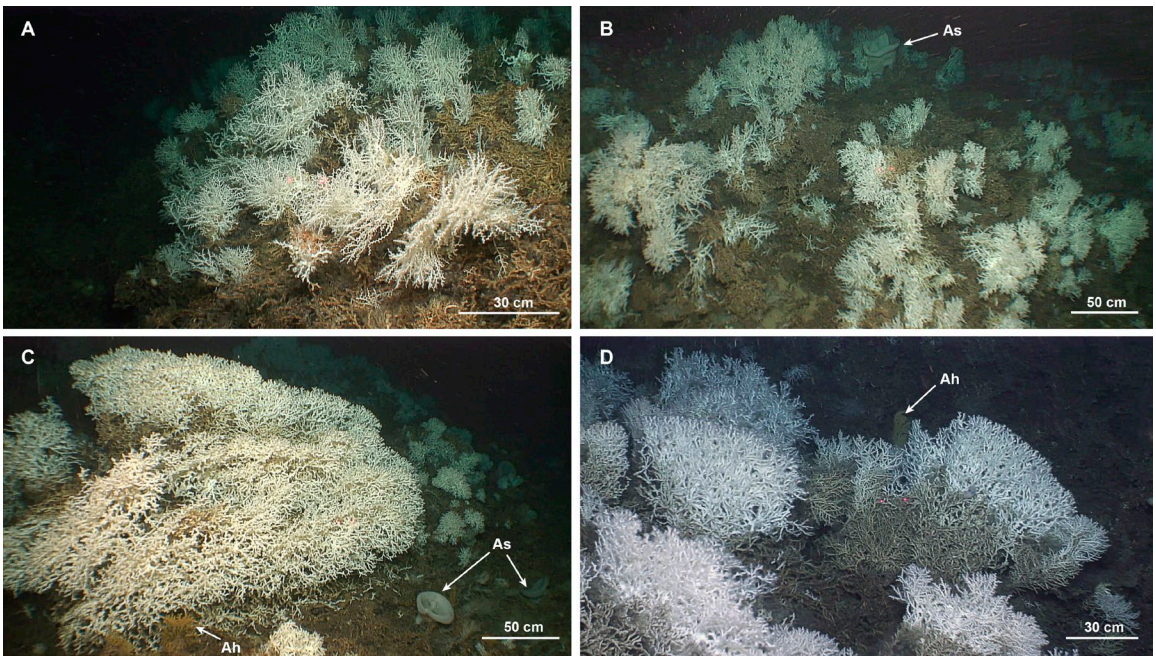

Figure 2.3. Living reefs of *M. oculata* (A, B) and *D. pertusum* (C, D) forming the mini-mounds observed on top of the northern Cabliers Province. The largest *D. pertusum* colony measured in the area is 306 cm wide (C). Arrows indicate some of the accompanying megabenthic species living within and around the reefs. Ah: *A. hirsuta*, As: *A. setubalense*.

gia hirsuta (n = 1491), and *M. oculata* (n = 1160). These species represented respectively the 19.6%, 18.9% and 15.5% of all identified organisms. Other commonly observed species were the sponge *Asconema setubalense* (12% of the total) and the antipatharian *Parantipathes larix* (5%).

2.5.2.1. *Northern sector - Dives 1 and 2*

The seafloor observed on the two northern dives, which were 490 m apart (Fig. 2.1), was characterised by areas of fine sediments mixed with coral rubble at the base of the mounds that changed to coral rubble when approaching the crests. Dives 1 and 2 showed a rather similar taxonomic composition with only a change in the dominant taxa (Fig. 2.2).

Dive 1 was dominated by dense populations of *M. oculata* accompanied by *D. pertusum* (Fig. 2.3), which represents the main constructor building the mini-mound like features located at the crest of the coral mounds. The two species were observed closely cohabiting and even in some cases fusing colony branches (Fig. 2.4). *P. rigida* was the second most abundant species in this dive followed by other megafaunal species such as *L. glaberrima*, *Pachastrella* sp. and *A. hirsuta*. Megafauna in Dive 2 was dominated by *P. rigida* and *Pachastrella* sp., accompanied by other abundant taxa, like *A. hirsuta*, *M. oculata* and *A. setubalense*. Even though there was not a substantial difference in species richness between dives, Dive 2 presented the highest value for this parameter, with 28 taxa compared to the 25 from Dive 1. In regards to species diversity (H'), both dives presented very similar values (Dive 1: H'=3.0/ Dive 2: H'=3.1), regardless of the dramatic decrease in living CWC abundance from Dive 1 to Dive 2 (from 967 colonies in Dive 1 to 178 in Dive 2) (Fig. 2.2).

2.5.2.2. *Southern sector - Dive 3*

In this dive, 15.1 km south of the northern dives (Fig. 2.1), video footage showed that the type of substratum along the mound's flanks was similar to the one observed in the northern region (coral rubble mixed with fine sediments) although with a higher abundance of fine sediments.

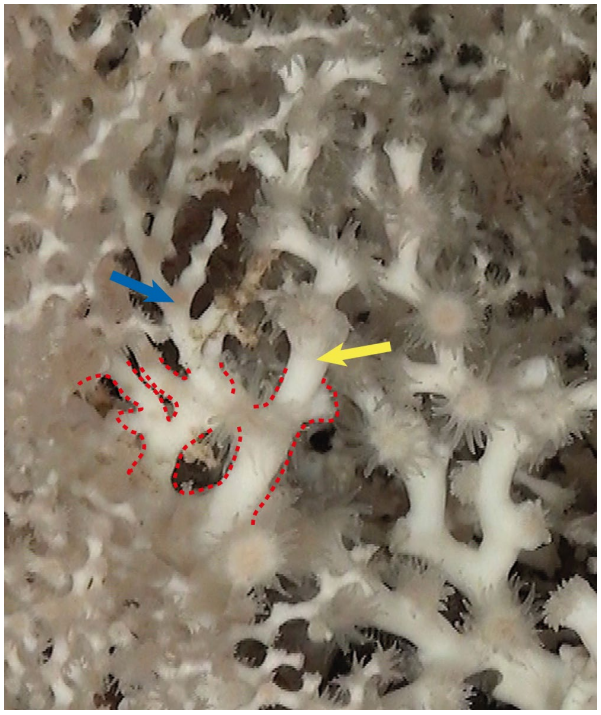

Figure 2.4. *D. pertusum* (yellow arrow) and *M. oculata* (blue arrow) chimaera-like colony. Silhouette of the fusing branches is highlighted by a red dashed line.

The same increase in deposited sediment was observed at the crest, where the dead coral framework was draped by a larger amount of fine sediments than in northern CMP. Video data collected during Dive 3 also showed a different combination of dominant species in comparison to the northern sector (Fig. 2.2). This dive was essentially dominated by the gorgonian species *A. hirsuta* (55%) and characterised by very a few colonies of *M. oculata*. Furthermore, squat lobsters and *P. larix* were also more abundant in this dive in comparison to the northern ones, where they just occurred as accompanying species of *M. oculata* and *D. pertusum* assemblages. Although the number of species observed in Dive 3 was the same as in Dive 1, the diversity of the former was much lower (Dive 3 H'=2.027), probably due to the dominance of three species that represented over 80% of the observed organisms (Fig. 2.2).

2.5.3. Scleractinian cold-water corals

2.5.3.1. *Density and distribution*

M. oculata was the most abundant scleractinian species growing on the CMP, representing 85% of the total (scleractinian) abundance in contrast with the 8% of *D. pertusum* and 6% of *Dendrophyllia cornigera*. As shown in Figure 2.5 and Table 2.2, living CWC density in the northern sector of the province decreases from Dive 1 to Dive 2, with almost a total absence of these species occurring in Dive 3 (i.e. southernmost mound sector). The maximum density values for *M. oculata* and *D. pertusum* were 6 and 5 col. m^{-2}, both of them observed in Dive 1 (Fig. 2. 5). White and orange chromatic morphotypes were found for both species, with the first being the most abundant (>95%). *M. oculata* and *D. pertusum* showed greater densities at the crest of the mounds, especially towards the northernmost part of the province (290-320 m water depth) (Figs. 2.3, 2.5). Conversely, the mounds' flanks, which were mainly covered by coral rubble, were almost completely depleted of CWC (Fig. 2.5). This is particularly evident in Dive 1, where there were no corals growing on the flanks or the densities were comparatively rather low (Fig. 2.5). Dive 2 and 3 presented lower densities of both coral species regardless of the location and thus, for these dives, density differences between mound's crest and flanks were less apparent. Furthermore, in Dive 1, coral density

Table 2.2. Average density of the most abundant and relevant species in each ROV dive performed on the Cabliers Coral Mounds, with scleractinian CWCs also displaying average colony size.

	Madrepora oculata		*Desmophyllum pertusum*		*Acanthogorgia hirsuta*	*Parantipathes larix*	*Phanopathes rigida*	*Leiopathes glaberrima*	*Asconema setubalense*
	Density (patch m^{-2})	Size (cm)	Density (patch m^{-2})	Size (cm)	Density (col. m^{-2})				
Dive 1	0.81±1.87	21.6±11.5	0.14±0.53	49.3±38.3	0.27±0.72	0.08±0.3	0.65±1.6	0.29±0.98	0.17±0.51
Dive 2	0.28±0.7	11.34±6.4	0.04±0.25	31.8±20.6	0.36±0.82	0.05±0.24	1.14±1.89	0.03±0.29	0.27±0.37
Dive 3	0.02±0.17	9.25±2.6	0.002±0.05	–	1.31±2.25	0.33±0.71	–	–	–

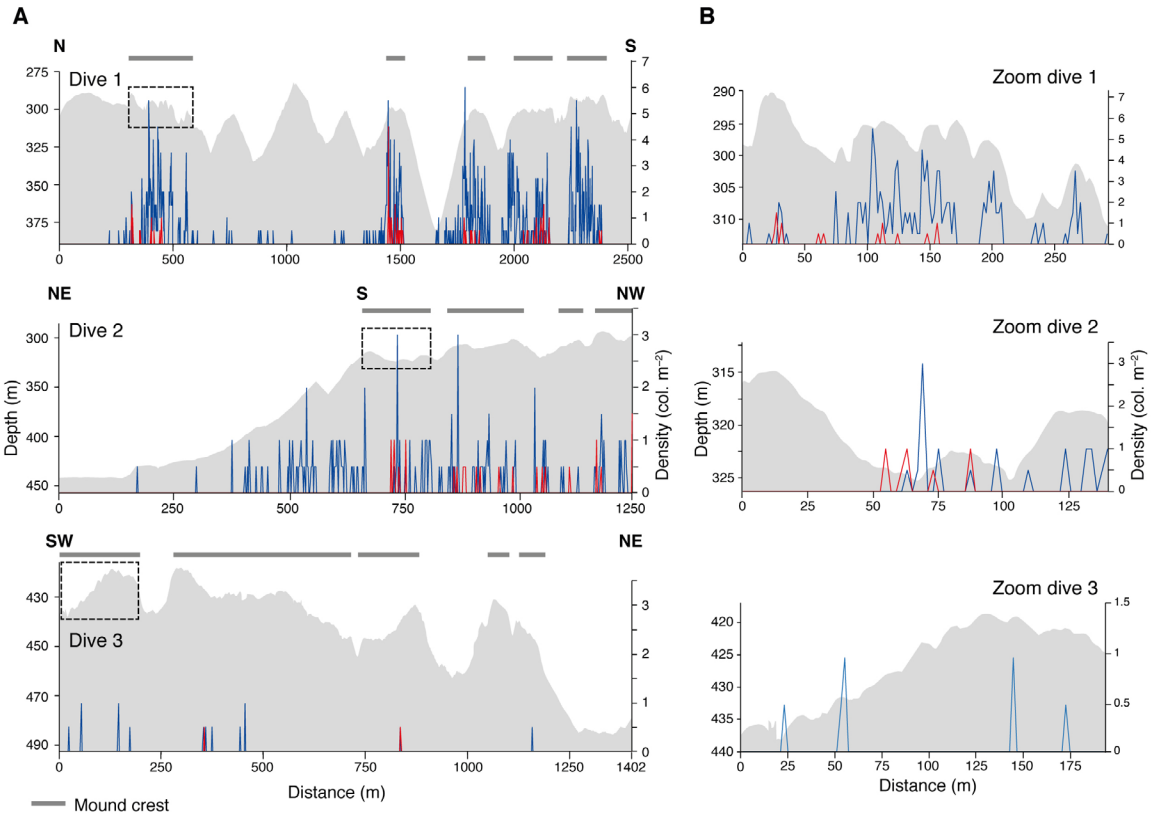

Figure 2.5. Bathymetric profile (grey shading) and density plots of *Madrepora oculata* (blue) and *Desmophyllum pertusum* (red) for each ROV dive (A). Zooms from the black-dotted boxes in graph A, which allow to appreciate the correlation between coral density and mini-mound summits (B). Dark grey lines on top of the graphs indicate the fragments of each dive where the ROV was travelling over the crest of the mounds. Transect orientation is noted at the top of each graph.

on the mound's crest was found to be significantly and positively correlated to the presence of mini-mounds ($p<0.001$, $r = 0.4$), identified by high BPI values (Fig. S2.2). This CWC distribution pattern was apparent in the detailed section of the Dive 1 density plot (Fig. 2.5B), in which the density peaks for both *M. oculata* and *D. pertusum* match with the summits of the mini-mound features observed on the crest of the mound.

2.5.3.2. *Size structure*

In total, 1178 and 139 colonies of *M. oculata* and *D. pertusum* were measured, some of them being out of the video analysis range (1 m) for species density quantification. Similarly to the observed density pattern, the average size of these corals decreased from Dive 1 to Dive 2 (Table 2.2), with *D. pertusum* being almost absent in Dive 3, where only one colony was observed and measured. Colony size ranged from 4 to 130 cm for *M. oculata* and from 7 to 306 cm for *D. pertusum* (Fig. 2.3). The high abundance of *M. oculata* in Dive 1 allowed to observe that colonies found on the flanks of the mound had significantly smaller

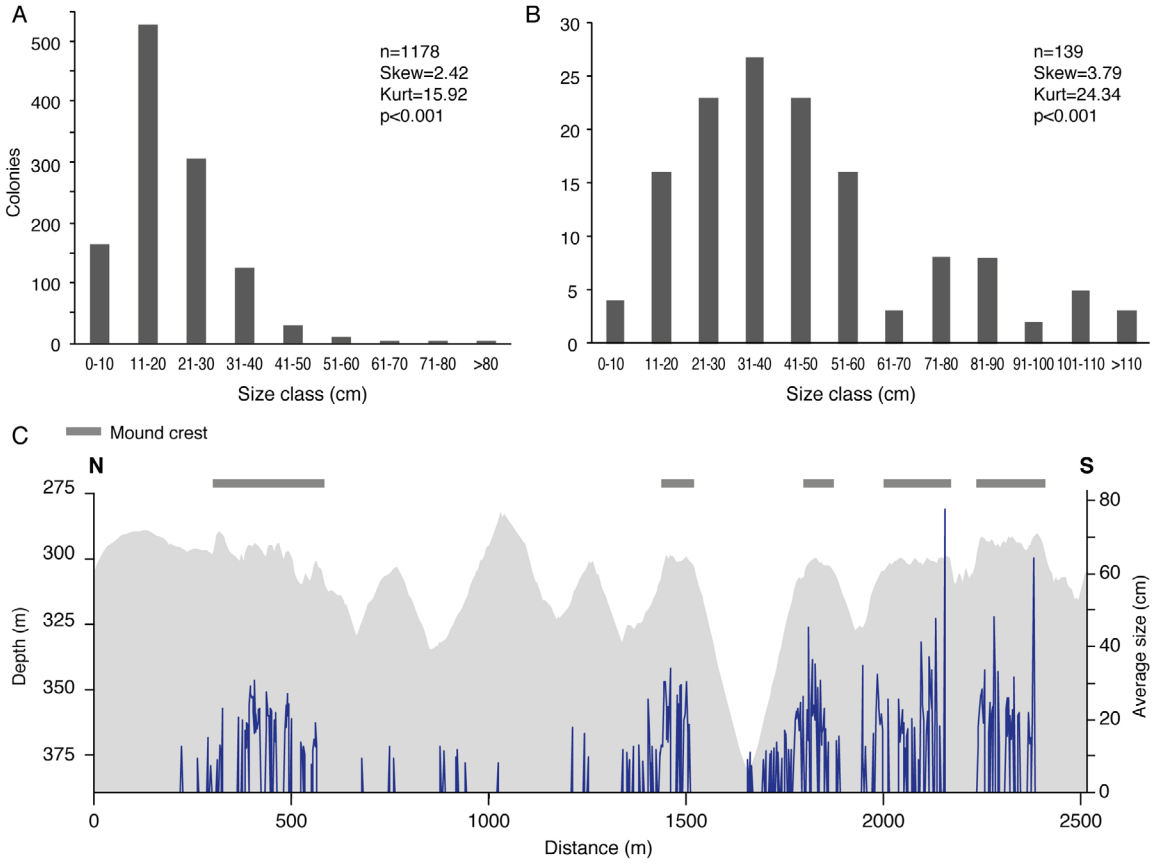

Figure 2.6. Colony size structure of *Madrepora oculata* (A) and *Desmophyllum pertusum* (B), together with the average size of *M. oculata* every 2 m^2 along Dive 1 (C). Grey shading indicates the bathymetric profile of the dive. Dark grey lines denote the fragments of the dive where the ROV operated along the mound's crest. Transect orientation is noted at the top of graph C. n: number of colonies; Skew: skewness; Kurt: kurtosis.

($p<0.001$) average sizes (12 ± 4.6 cm) than the ones at the crest (22.1 ± 8.9 cm) (Fig. 2.6C). Considering the colonies from the whole study area, both *M. oculata* and *D. pertusum* had a higher percentage of smaller size classes than expected in a normal distribution, with significantly positive values of skewness ($p<0.001$, $skew_M = 2.42$ and $skew_L = 3.79$ respectively) and presented a long-tailed distribution ($p<0.001$, $kurt_M = 15.92$ and $kurt_L = 24.34$) with some large colonies (Fig. 2.6).

2.5.4. Main Associated Species

Amongst the most abundant species observed in the CMP, only the gorgonian *A. hirsuta* and the black coral *P. larix* occurred in all dives, with their density increasing towards the south of the mound province (Table 2.2, Fig. 2.7). The maximum density values of *A. hirsuta* and *P. larix* were 11.5 and 3 col. m^{-2} respectively (Fig. 2.7). The distribution of *A. hirsuta* and *P. larix* was widespread across the mounds, although they both presented their highest abundances at the crest (Fig. 2.7). Both *A. hirsuta* and *P. larix* showed greater abundances in Dive 3 (southern CMP), where living framework-building CWCs were absent and these two species could thrive on the exposed dead coral framework that constitutes the mound's crest (Fig. 2.7, see also Fig. 2.9).

The black corals *P. rigida, L. glaberrima* and the sponge *A. setubalense* were only found in Dive 1 and 2, where living CWCs were abundant. Both *P. rigida* and *A. setubalense* presented a higher average density in Dive 2. The highest density value observed for *P. rigida* and *A. setubalense*

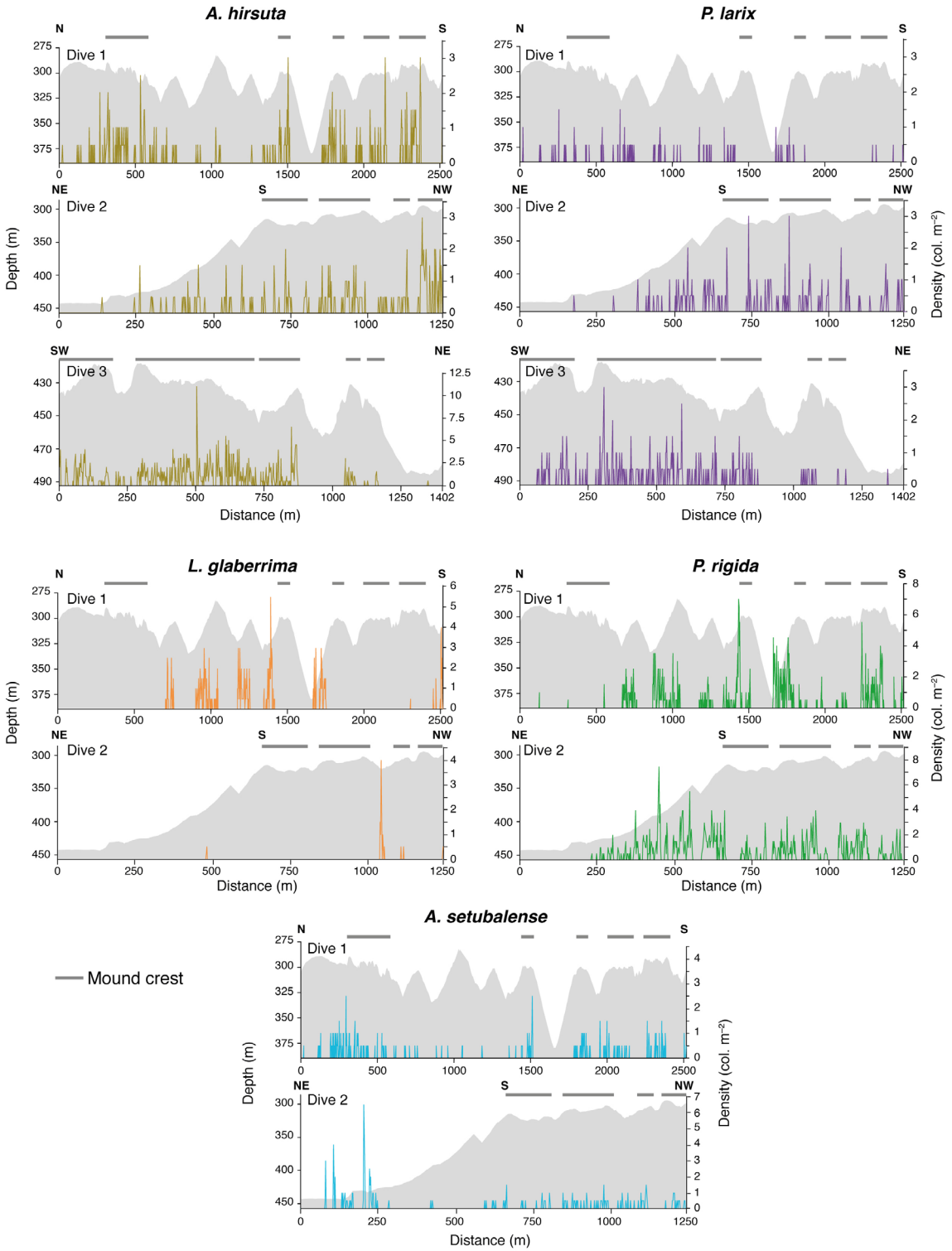

Figure 2.7. Bathymetric profile (grey shading) and density plots of *Acanthogorgia hirsuta*, *Parantipathes larix*, *Leiopathes glaberrima*, *Phanopathes rigida* and *Asconema setubalense*. Dark grey lines denote the fragments of the dive where the ROV operated along the mounds' crest. Transect orientation is noted at the top of each dive.

was 7.5 living-patches m^{-2} and 6.5 col. m^{-2} respectively (Fig. 2.7). *L. glaberrima* had a maximum density of 5.5 col. m^{-2} (Fig. 2.7). *P. rigida* and *L. glaberrima* showed a high density on the coral rubble from the mound's flanks of Dive 1, for water depths ranging from 300 m to 375 m (Fig. 2.7). However, in Dive 2 *L. glaberrima* was nearly absent and the flanks were dominated by *P. rigida*. The latter species was also observed growing on the mounds' crest at the end of Dive 1 and throughout the entire Dive 2. The sponge *A. setubalense* was observed with a greater density on the mound's crest, with up to 2.5 ind. m^{-2}, using the coral framework as substratum

to colonise. However, there was one exception at the beginning of Dive 2, where this species was observed growing on top of a volcanic outcrop at ~425 m water depth, reaching its highest density (6.5 ind. m^{-2}).

Throughout the three ROV dives a total of 519 fish individuals were observed, from which 184 were identified in Dive 1, 195 in Dive 2 and 138 in Dive 3. The most abundant species was *Helicolenus dactylopterus* with 181 individuals, followed by *Hoplostethus mediterraneus* (n = 175) and *Nezumia aequalis* (n = 60). Other species, some of them considered as commercially valuable, such as *Pagellus bogaraveo*, *Conger conger*, *Scorpaena scrofa* and some pleuronectids were also observed along the CMP. 111 individuals of *H. dactylopterus* were measured, showing sizes ranging from 5.1 to 35.6 cm and an average total length of 16.8 ± 7.4 cm. The 20% percent of these individuals have a length under 10 cm, which corresponds to the size of recruit and juvenile stages.

2.5.5. Environmental drivers and assemblages

The set of CCA analyses performed adopting sampling units with different sizes (2, 4, 10 and 20 m^2) showed an increase in the inertia explained by seafloor features with larger sampling units (Table S2.2). However, with increasing sampling unit size, CCA faunal and environmental resolution were reduced due to a decrease in the number of sampling units and a higher variability of environmental factors within each sampling unit. Therefore, the optimal sampling unit size for the CCA analysis was set at 10 m^2, which had the best equilibrium between percentage of inertia explained by seafloor features and CCA resolution.

The ANOVA-like permutation analysis demonstrated that all environmental factors (depth, slope, aspect, substratum type and BPI), apart from terrain roughness, were statistically significant predictors ($p<0.01$) and together explained 19.7% of the variation in species abundance. The first two CCA axes represented 10.3 and 5.6% of the total variance. Regarding predictor performance, the combined explanatory power of the four substratum types was the most relevant in determining species distribution, explaining 9.9% of the variation, followed by depth, which explained a further 7.4% (Fig. 2.8). The CCA ordination together with the ANOVA-like permutation tests, allowed identifying four megabenthic assemblages characterised by different dominant species and controlled by different seafloor features (Fig. 2.8).

Assemblage 1 was mainly characterised by the scleractinians *M. oculata* and *D. pertusum* together with the echinoderm *Cidaris cidaris* and the sponge *A. setubalense* (Fig. 2.3). These species mainly occurred on the northern and shallower parts of the mounds' crests (Dive 1, 2), growing on dead coral framework (CF) (Fig. 2.8).

Assemblage 2 occurred on the deeper and southern parts of the mounds' crests (Dive 3), where dead coral framework with fine sediments (CFFS) was the main substratum type. These areas were covered by aggregations of the gorgonian *A. hirsuta,* squat lobsters and the anthipatharian *P. larix* (Fig. 2.8).

Assemblage 3 occurred on the northern and shallowest parts of the mounds' flanks (Dive 1, 2), where the seafloor is steep and coral rubble (CR) is the most common substratum type. This assemblage is characterised by the presence of *P. rigida*, together with the incrusting sponge *Pachastrella* sp. (Fig. 2.8).

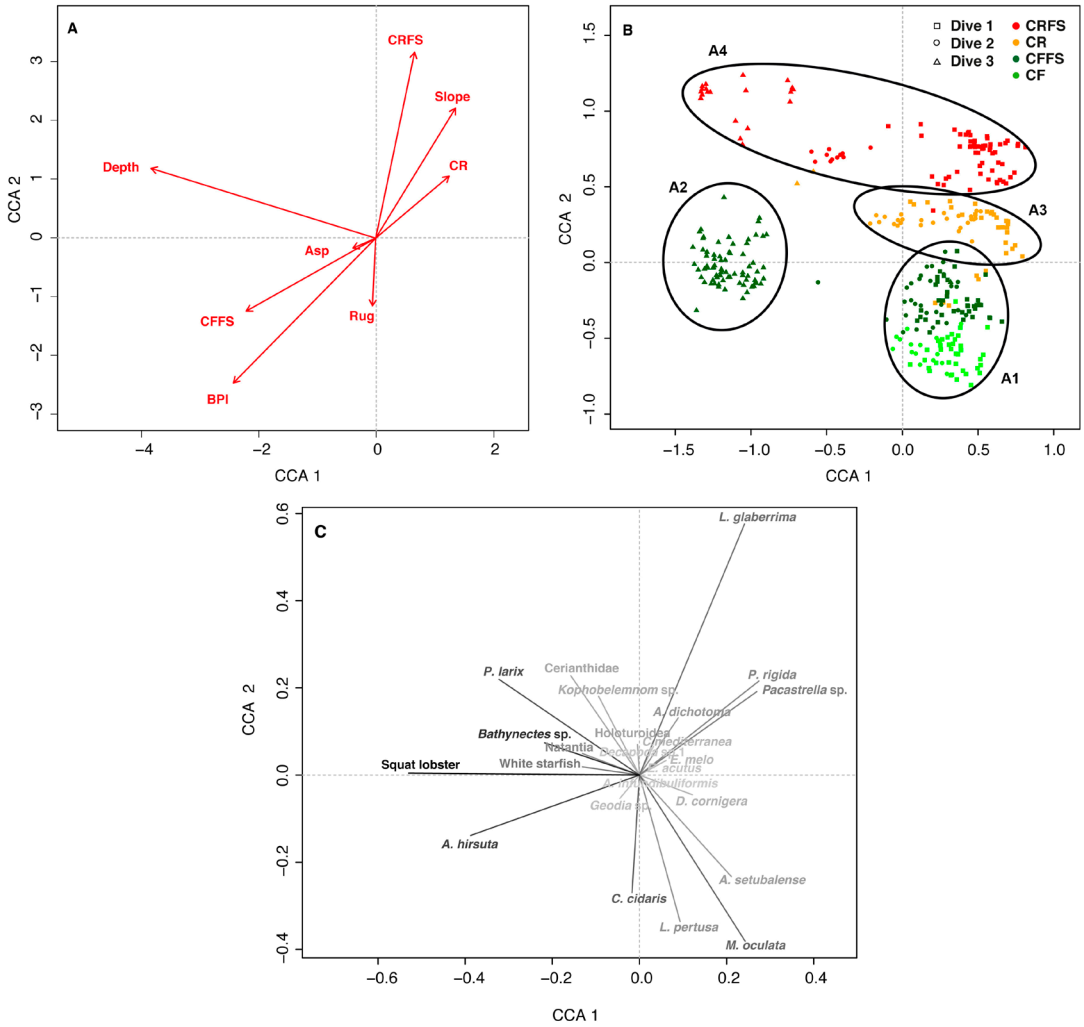

Figure 2.8. Canonical correspondence analysis (CCA) results. The first bi-plot (A) shows all significant seafloor variables considered in the analysis in relation to the axes CCA1 and CCA2. The second bi-plot (B) displays the 10 m^2 sampling units ordination based on species abundance and composition, constrained by the seafloor variables and coloured according to their substratum type. The third bi-plot (C) shows the contribution of each species to the megabenthic assemblages. The grey scale of each species indicates the degree of correlation to the seafloor variables, being black the highest correlation. The length and position of the vectors gives information about their relationship to the axes. Vectors parallel to an axis denote a correlation and their length defines the strength of such correlation. CRFS: coral rubble and fine sediments, CR: coral rubble, CFFS: dead coral framework and fine sediments

Finally, Assemblage 4 comprehended sampling units from all ROV dives and presented a varying taxonomic composition. It was mainly characterised by the presence of *L. glaberrima* and other antozoans such as the pennatulacean *Kophobelemnom* sp., cerianthids and some colonies of *P. larix*. These taxa generally occurred on coral rubble with fine sediments (CRFS) on the deeper parts of the flanks of the mounds (i.e. steep slopes) (Fig. 2.8).

2.6. Discussion

2.6.1. Cabliers Coral Mound Province

The Cabliers coral mounds are among the most extensive coral mound features in the Alboran Sea (Comas and Pinheiro, 2010; Fink et al., 2013; Lo Iacono et al., 2014, 2018a). As other mounds (Hovland and Risk, 2003; Buhl-Mortensen et al., 2010), they developed on a volcanic basement that can be observed at the start of Dive 2 and is well recognisable in the high-resolution AUV bathymetry. This outcrop probably functioned as a substratum for CWC coloniza-

tion and subsequent mound development. As described in Duggen et al. (2004) the outcrop on which the CMP developed, known as Cabliers Bank, probably consists of an andesite basement, dated Middle to Late Miocene.

As with some other giant coral mounds (Buhl-Mortensen et al., 2017), Cabliers ridge-like mounds could be the product of smaller mounds coalescing to form giant elongated coral mounds. This is suggested by the occurrence of numerous mini-mounds aligned along the crest of the northern Cabliers Mounds, where the most thriving CWC assemblages were observed. However, an extensive and more detailed geomorphological study of the CMP is required to prove this hypothesis.

2.6.2. Scleractinian cold-water corals

The incidence of higher density of living CWC at the crest of the mounds agrees with previous observations from other coral mounds and is probably caused by the presence of more favourable environmental conditions (Freiwald et al., 2004; Huvenne et al., 2005; Davies et al., 2009; Lo Iacono et al., 2018a). Furthermore, the dive segments that crossed the crest of the mounds, showed that the peaks in *M. oculata* and *D. pertusum* density generally matched with the presence of the mini-mound like features (Figs. 2.3, 2.5). Considering that the highest CWC density values are observed at the top of these mini-mounds, it could be hypothesised that these features are the engine that drives CWC mound growth (Lo Iacono et al., 2018a). These mini-mound features are comparatively elevated to the rest of the mound's crest, thus their summit is probably exposed to higher current speeds, which might prevent sedimentation on the corals growing there. Additionally, such current speeds might cause a higher amount of food to be advected towards the mini-mounds' summit, providing the most suitable conditions for CWC growth.

Framework-building CWC densities are highly variable in the Mediterranean Sea. The Cap de Creus Canyon, in the NW Mediterranean, presents average densities of both species oscillating between 0.1-0.4 col. m^{-2} for *M. oculata* and 0.004-0.01 col. m^{-2} for *D. pertusum* (Orejas et al., 2009; Gori et al., 2013). In the Lacaze-Duthiers Canyon, Gori et al. (2013) explored with an ROV a distance of 8362 m, where 555 and 97 colonies of *M. oculata* and *D. pertusum* were counted. This would relate to an average density of 0.044 col. m^{-2} and 0.012 col. m^{-2} for each species, comparable to the values observed in other regions of the Mediterranean, where *M. oculata* and especially *D. pertusum* generally occur as small populations or sparse colonies on complex geomorphic features (Savini and Corselli, 2010; Lastras et al., 2016; Fabri et al., 2017; Taviani et al., 2017). Therefore, average densities of *M. oculata* and *D. pertusum* on the northern CMP (0.81 and 0.14 col. m^{-2} respectively) are considerably greater than the ones observed for most of the other CWC assemblages described in the Mediterranean Sea. Only the coral-topped mounds from Santa Maria di Leuca province seem to present an abundance comparable to the CMP reefs, however no quantitative data are yet available for this area (Savini and Corselli, 2010; Vertino et al 2010; Savini et al., 2016; Bargain et al., 2017). In terms of coral mounds, almost the totality of these geomorphologic features discovered to date in the Mediterranean Sea are in a complete stage of decline, with only some sparse living colonies of *M. oculata* and *D. pertusum* (Hebbeln and Wienberg, 2016). The absence of anthropogenic footprint in the ROV footage suggests that the CMP living reefs are in a likely pristine status, which is remarkable considering its proximity to both the coasts of Spain and Morocco, where industrial fishing practices are intense (Aguilar et al., 2017).

The northern mounds of the CMP resemble the characteristics of their thriving Atlantic counterparts, on which a mixture of abundant living coral and exposed dead coral framework is commonly observed (Buhl-Mortensen et al., 2010). The megabenthic assemblages observed in Dive 1 matches with the typical spatial patterns of living CWC reefs, in which the area occupied by dead coral framework is greater than the coverage of living corals (Mortensen et al., 1995; Buhl-Mortensen et al., 2017). The average density of *M. oculata* in the northern CMP (Dive 1: 0.81 col. m^{-2}) presents similar values to those observed in the prolific Atlantic regions such as the Logachev Mounds (1.04 col. m^{-2}) (Arnaud-Haond et al., 2017). In contrast, *D. pertusum* density is much higher in the Logachev Mounds (1.41 col. m^{-2}) in comparison to the CMP (0.14 col. m^{-2}). This makes sense, since Atlantic coral mounds generally present a higher relative abundance of *D. pertusum* contributing to form CWC reefs (Buhl-Mortensen et al., 2017). The reason for this discrepancy could be due to the higher water temperatures of the Mediterranean Sea compared to the north Atlantic. Warmer temperatures in the Mediterranean, which cause a higher oxygen demand by the corals (Dodds et al., 2007), are combined with a lower availability of dissolved oxygen (i.e. from 6-6.2 ml l^{-1} in the North Atlantic to 3.75 ml l^{-1} in the Mediterranean) (Davies et al., 2008; Freiwald et al., 2009). In this setting, *D. pertusum* might be closer to its ecological boundary, which could explain its lower abundances compared to *M. oculata* (Dodds et al., 2007; Freiwald et al., 2009; Davies and Guinotte, 2011). However, this assumption would require further investigation.

Besides the high coral density observed on the northern region of the CMP, 2% of *M. oculata* and 32% of *D. pertusum* coral colonies from these mounds reached sizes over 50 cm in diameter (Figs. 2.3, 2.6). This suggests that CWC have been thriving on this sector during the recent past. On the other hand, there is also an important percentage (58%) of small colonies (<20 cm) of *M. oculata*, which suggests either a high recruitment rate or frequent fragmentation of larger colonies into smaller ones. According to the skewness results, the *D. pertusum* population on the CMP is characterised by medium-sized colonies (20-40 cm = 36%) (Fig. 2.6). This trend could be a consequence of a lower recruitment rate and/or a lower fragmentation of *D. pertusum*, due to its thicker and less fragile skeleton in comparison to *M. oculata*. Gori et al. (2013) observed a similar trend in the Gulf of Lions, where *D. pertusum* also presented larger colony sizes than *M. oculata*. However, in that region, both species generally showed smaller coral colony sizes than the ones observed in the CMP.

Along with CWC density, colony size also increased towards the crest of the Cabliers coral mounds. This is probably caused by a higher substratum stability that allows corals on the sub-horizontal crest to grow larger than the ones on the sloping flanks. Simultaneously a greater food supply might occur across the crest of the mounds, where bottom currents are generally expected to be stronger (Mienis et al., 2012a; Cyr et al., 2016; Lo Iacono et al., 2018a).

Similarly to what has been reported in other studies (Mastrototaro et al., 2010; Mienis et al., 2012a; Duineveld et al., 2012; Oguz et al., 2014), the presence of flourishing CWC assemblages on the CMP is probably linked to suitable oceanographic conditions. In this regard, the Cabliers coral mounds are located within the LIW, a water mass regarded by Taviani et al. (2017) as hosting most of the living CWC assemblages occurring in the Mediterranean Sea. Nevertheless, the CWCs present in the CMP showed a dramatic decrease in abundance towards the southern region of the province (Figs. 2, 5). This pattern could be caused by the presence of slower current speeds in the southern region, which could explain the greater amount of fine sediments observed at the mound's crest. Weaker currents would also bring less amount

of food to the corals and generate lower resuspension of organic material from the seafloor, preventing corals from a sufficient food intake (Duineveld et al., 2004). Furthermore, the crest of the coral mounds from southern Cabliers is found at a greater water depth (Dive 3: ~420-445 m) than the crest of the northern ones (Dive 1 and 2: ~280-325 m). This fits the results from the CCA analysis, where depth was found to be one of the main environmental drivers affecting species distribution (Fig. 2.8). In this sense, the southern, less prolific part of the CMP would be considerably further away from the AW-LIW interface (150-200 m water depth) (Millot, 2009). The global coral mound distribution generally matches with the presence of close sharp thermo- and haloclines, indicating that such water mass interfaces might be relevant for the proliferation of CWC reefs (Dullo et al., 2008; Matos et al., 2017; Lo Iacono et al. 2018a). However, the considerable differences in CWC abundance within the northern sector of the CMP (Dive 1 and Dive 2), suggests that at a local-scale, other variables than depth contribute towards the creation of suitable conditions for the development of such thriving CWC assemblages.

2.6.3. Megabenthic species distribution and environmental variables

The CCA analysis divided the CMP fauna into four main assemblages, which were mainly determined by substratum type and water depth, two environmental variables that have been long regarded as important factors determining species distribution in benthic habitats (Zajac et al., 2000; Santín et al., 2017, 2019). The most common substratum types on a coral mound derive from dead CWCs, which suggests that as some other ecosystem engineers, framework-building corals affect the distribution of the rest of species in the habitat even after they die (Jones et al., 1994).

The megabenthic fauna observed on the CMP mostly features sessile benthic suspension feeders (e.g. octocorals, antipatharians, sponges) that generally grow on the hard substrata provided by dead coral framework and off-mound outcropping volcanic rocks. This is the typical type of fauna found worldwide on coral mounds (Roberts et al., 2006; Mastrototaro et al., 2010; Buhl-Mortensen et al., 2010, 2017). Such geomorphological features are indeed areas with a high hard substrata availability for larval settlement and generally exposed to strong bottom currents, which provide a suitable environment for suspension feeding (Mortensen and Fosså, 2006; Mienis et al., 2012a).

Most of the species associated with CWCs in the CMP are also conspicuous in other areas of the Mediterranean Sea. For instance, *A. hirsuta* has also been observed in other regions of the Alboran Sea (i.e. Al Idrissi Bank and Chella Mound) (Coiras et al., 2011; De la Torriente et al., 2018), as well as on shelf edge and slope settings of the western and central Mediterranean Sea (Bo et al., 2015; Cau et al., 2015; Oceana, 2015; Grinyó et al., 2016). Within the antipatharians, *L. glaberrima* is a very abundant species in areas of the upper slope of the Mediterranean Sea (>130 m water depth) (Vertino et al., 2010; Angeletti et al., 2014; Bo et al., 2015; Ingrassia et al., 2016). The same is true for *P. larix*, which is widespread across the Mediterranean, mostly growing on the upper continental slope (Bo et al., 2014a). On the contrary, the high abundance of *P. rigida* is remarkable, considering this species is Atlantic (Opresko, 2009) and has been observed for the first time in the Mediterranean Sea on the CMP (Bo et al., 2018). The fishes found here have also been observed in other bathyal regions of the Mediterranean Sea (Fabri et al., 2014; Taviani et al., 2017; Deval et al., 2018). Furthermore, *H. dactylopterus* presented individuals covering all the size classes previously described for this species (Deval et al., 2018),

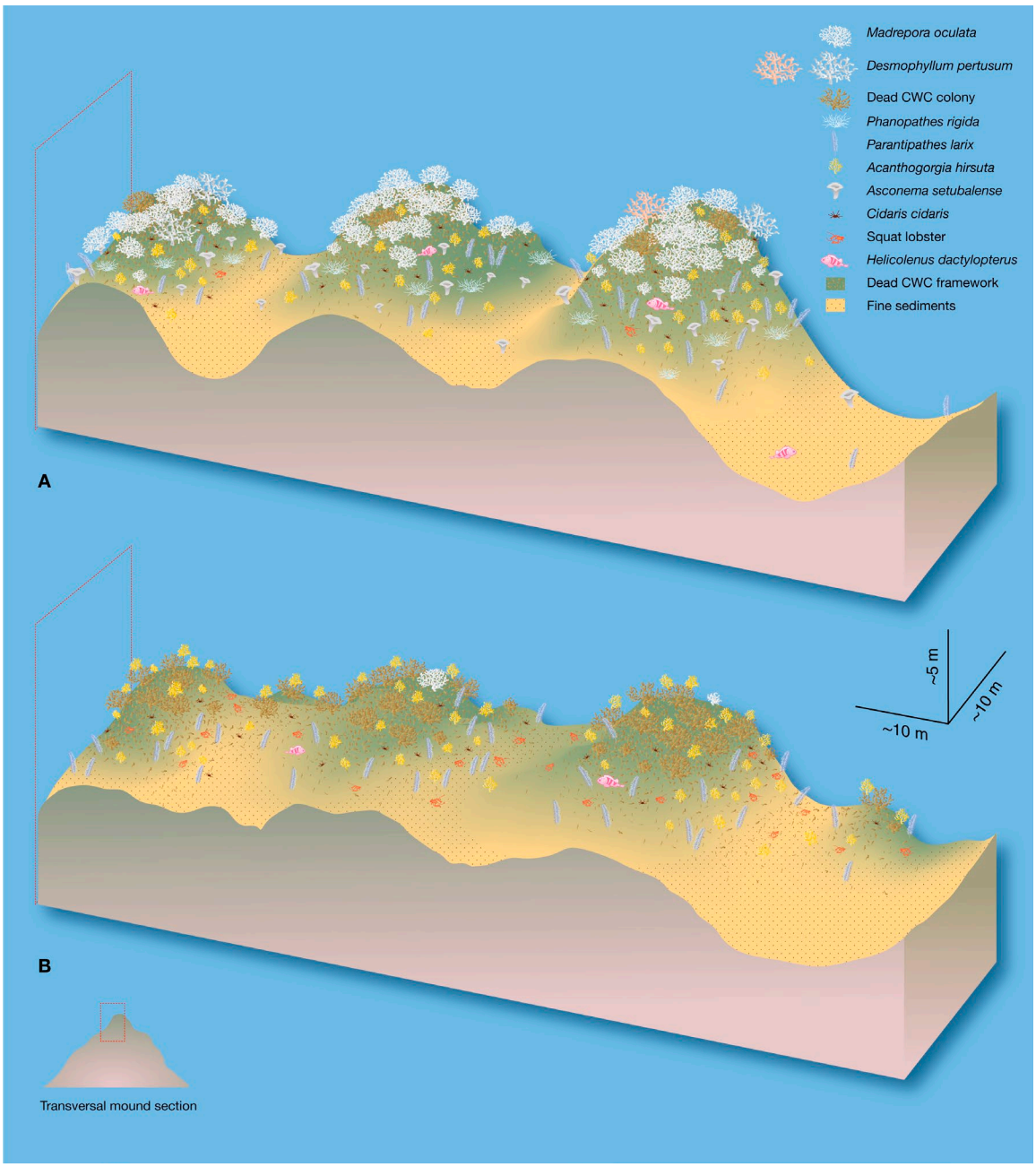

Figure 2.9. Schematic representation of the megabenthic species distribution on the mini-mounds located on the crest of northern (A) and southern (B) Cabliers Coral Mound.

which means that these fishes inhabit CWC reefs during most of their life stages. It is especially important to point out the 20% of juveniles and recruits (<10 cm) of this species observed on the CMP, which confirms the use of CWC assemblages as nursery grounds by a commercially valuable species.

In terms of spatial distribution, some of the sessile species mentioned have been observed to occur on the mini-mounds located at the crest of Cabliers coral mounds. However, when dense aggregations of living CWC cover the summit of these mini-mounds, the associated species are displaced to areas with a higher percentage of exposed dead coral framework (Fig. 2. 9). The availability of this substratum increases towards the mini-mound flanks and there, organisms such as *A. setubalense* and *P. larix* increase in abundance (Fig. 2.9). Nevertheless, smaller species, such as *A. hirsuta* and *C. cidaris*, manage to grow amongst dense *M. oculata* and *D. pertusum* colonies (Figs.

2.7, 2.9). The regions between mini-mounds, where fine sediments drape the dead coral framework or are interspersed with it, seem to have a lower megabenthic abundance (Fig. 2.9). This is probably due to the lack of hard substratum on which benthic sessile organisms could settle.

Although all the mentioned species were observed in the northern CMP, they do not present a homogeneous distribution along the mounds. Similarly to framework-building CWC, some species such as *P. rigida*, *A. setubalense* and *L. glaberrima* decrease in abundance or are completely absent at the southern region of the province (Dive 3; Figs. 2.2, 2.9). This suggests that a marked change in the environmental conditions (e.g. greater depth, weaker current regime or lower food supply) occurs towards the southern part of the mound, which far from only affecting scleractinian corals is also detrimental for the proliferation of the latter taxa.

Some other species, such as *A. hirsuta* and *P. larix* show an increase in abundance towards the southern CMP. This pattern could be related to the absence of living CWCs in that region, which allows other organisms to thrive and dominate the areas of dead coral framework and fine sediments (Figs. 2.7, 2.9). We hypothesise that when environmental conditions are suitable, framework-building corals outcompete these species, which are therefore confined to less suitable sectors of the reef, where dead CWC framework dominates as substratum.

In conclusion, the CMP megabenthic assemblages change from thriving CWC reefs at the north (Dive 1), to dead coral framework mixed with fine sediments and colonised by octocorals, antipatharians and squat lobsters, at the south (Dive 3) (Figs. 2.2, 2.9). The changes in taxonomic composition, abundance and diversity from north to south Cabliers could be a representation of the different ecological succession stages that can occur in a coral mound throughout flourishing and decline periods (Mortensen and Fosså, 2006). However, in order to get a more comprehensive overview of the CMP and confirm these observations, more images or video-transects should be acquired along and across the mounds, and a more detailed study of the environmental conditions should be performed.

2.6.4. Faunal comparison with Mediterranean and Atlantic Mounds

The characterisation of biogeographic provinces has essential implications for understanding the evolutionary and ecological processes that caused the existing large-scale biodiversity patterns (Whittaker et al., 2005; Lomolino et al., 2006). In this sense, they can be of use to predict the areas where certain habitats or species can occur and to foresee the response of such ecosystems to cumulative disturbances (Rice et al., 2011). Biogeographic provinces might also help to detect potentially vulnerable marine ecosystems (VMEs) and to create representative marine protected area networks (Rice et al., 2011). Therefore, comparing the taxonomic composition of the CMP megafauna with the one observed on analogous Mediterranean and Atlantic geomorphologic features might help towards a better understanding of the taxonomic linkages amongst the known CWC mound provinces, which would improve the baseline needed for the designation of sensible marine protected area networks.

The type of megafaunal taxa observed on the CMP showed several similarities with what has been previously described on the thriving Atlantic CWC mounds (Mortensen and Fossa, 2006; Henry and Roberts, 2007; Buhl-Mortensen et al., 2017). Some organisms such as gorgonians, hexactinellid sponges, demosponges, squat lobsters, and sebastid fishes are within the shared fauna between the CMP and its Mediterranean and Atlantic analogues (Roberts et al., 2008,

2009a; Vertino et al., 2010; Purser et al., 2013; Ross et al., 2017). However, as observed in Buhl-Mortensen et al. (2017), the fauna associated to CWC mounds can present considerable taxonomic differences amongst provinces, even though such species belong to the same functional groups.

Within the Mediterranean Basin, the coral mound clusters are in a general stage of decline. Some of them have been reported to be mostly covered by aggregations of gorgonians, sponges and echinoderms (Hebbeln, 2009; Hebbeln and Wienberg, 2016). Probably the coral reefs observed in Santa Maria di Leuca (Central Mediterranean Sea) are the closest ones to the CMP in terms of reef-building coral abundance and megafaunal composition. Both of them present demosponges, antipatharians and gorgonians as the main species accompanying *M. oculata* and *D. pertusum* reefs (Mastrototaro et al., 2010; Vertino et al., 2010). Within these taxonomic groups, *Pachastrella* sp., *A. hirsuta* and *L. glaberrima* dominate the accompanying fauna in both regions (Mastrototaro et al., 2010; Vertino et al., 2010). However, the hexactinellid sponge *A. setubalense* and the antipatharian *P. rigida* are only observed in abundance in the CMP.

Norwegian CWC mounds exhibit gorgonians, demosponges and anemones, within the most conspicuous reef associated fauna. The bivalve *Acesta excavata* is also a common species on these mounds. Although both Norwegian coral mounds and the CMP contain gorgonians, the former are populated by *Paragorgia arborea* and *Primnoa resedaeformis* (Purser et al., 2013; Buhl-Mortensen et al., 2017), while the latter is covered by dense aggregations of *A. hirsuta*. The same occurs with demosponges, which are an important component of the CMP (i.e. *Pachastrella* sp.), yet the dominant species are different from those observed on Norwegian mounds (i.e. *Geodia* sp. and *Mycale lingua*) (Purser et al., 2013; De Clippele et al., 2018). Furthermore, bivalves and anemones are not within the dominant associated fauna observed in the CMP.

The Mingulay Reef Complex, located on the Scottish continental shelf, presents a taxonomic composition similar to the Norwegian mounds, with no hexactinellid sponges and the demosponges *Geodia* sp. and *M. lingua* occurring among the *D. pertusum* colonies (Roberts et al., 2009b; De Clippele et al., 2018). However, dense gorgonian aggregations were not observed on the Mingulay Reef Complex (Roberts et al., 2009b).

Irish and African Atlantic CWC mounds are generally populated by large assemblages of hexactinellid sponges, whose silicic skeleton contributes to the structural formation of the mounds (van Soest et al., 2007; Henry and Roberts, 2007; Buhl-Mortensen et al., 2017). Although this taxonomic group is also present on Mediterranean coral mounds (i.e. CMP), the species do not coincide. *Rosella nodastrella*, *Aphrocallistes bocagei* and *A. beatrix* dominate the associated fauna of Irish and African coral mounds (van Soest et al., 2007; Henry and Roberts, 2007; Buhl-Mortensen et al., 2017), whereas *A. setubalense* is the dominant hexcatinellid sponge in the CMP. Such as in Norwegian Mounds, anemones (i.e. *Phelliactis* sp.), and bivalves (i.e. *Acesta* sp.) thrive on the Irish and the African mounds respectively (Roberts et al., 2008; Buhl-Mortensen et al., 2017).

On the western Atlantic, in the Gulf of Mexico and off North Carolina and Florida's coast, several coral mounds arise (Ross, 2006; Ross and Nizinski, 2007; Hebbeln et al., 2014; Mienis et al., 2014; Ross et al., 2017). In accordance to the African mounds, the hexactinellid sponge *A.*

Beatrix is observed forming aggregations on these American mounds (Ross and Nizinski, 2007). Other suspension feeders such as gorgonians (*Keratoisis* spp.), antipatharians (*L. glaberrima* and *Bathypathes alternata*) and stylasterid corals are also amongst the main associated species to the *D. pertusum* reefs of these mounds.

As already stated, Atlantic coral mounds mostly present *D. pertusum* as the main reef-building species, sometimes accompanied by *M. oculata*, *Enallopsamia profunda* and *Solenosmillia variabilis* (Roberts et al., 2008; Buhl-Mortensen et al., 2017; Ross et al., 2017). On the other hand, The CMP shows a considerably higher proportion of *M. oculata*, accompanied by *D. pertusum* and *D. cornigera*.

This faunistic comparison among coral mound provinces suggests that although most taxonomical groups of organisms observed in the CMP are common to those witnessed on Atlantic coral mounds (Henry and Roberts, 2007; Ross and Nizinski, 2007; Purser et al., 2013; Buhl-Mortensen et al., 2017; Ross et al., 2017), there are considerable differences at the species level. These variations in the megafaunal composition are probably determined by biogeographic factors. Although in most regions the species associated to CWC mounds are probably subjected to similar conditions in terms of current speed and food supply, other environmental variables, such as water temperature and dissolved oxygen might influence their distribution. Another factor that limits species distribution is larval dispersal, which depends on water mass circulation, larval longevity and motility. Therefore, changes in environmental variables due to the incidence of contrasting oceanographic conditions, together with the presence of biogeographical barriers (e.g. Strait of Gibraltar) might prevent some of these species from being found in different CWC mound provinces.

Even though CWCs were already known to host a large diversity of organisms, the taxonomic differences observed between mound provinces suggest that the number of species associated to these habitats is even higher than previously thought (Roberts et al., 2006). As a consequence of the high biodiversity of these ecosystems and their high vulnerability to anthropogenic disturbances (Althaus et al., 2009; Armstrong et al., 2014), many measures have been taken by the United Nations and the Food and Agriculture Organisation (FAO) to protect CWC habitats (Davies et al., 2017). Several international legislations have defined CWC assemblages as vulnerable marine ecosystems (VMEs) and have included them in the list of endangered habitats (EU Habitats Directive, OSPAR, 2008). However, in order to efficiently implement such conservation measures, more detailed information about the distribution, taxonomic composition and ecological state of CWC mounds needs to be provided. This is especially true for the Mediterranean Sea, where to the moment, the Cabliers coral mounds are the only giant CWC mounds hosting living CWC reefs. Therefore, further exploring and research efforts are required in this field to unveil and study new coral mound provinces in order to better constrain the environmental conditions that allow the formation and endurance of these geomorphologically complex bioconstructions.

2.7. Conclusions

- ROV footage integrated with high-resolution AUV bathymetry unveiled thriving CWC reefs with uncommonly high coral densities occurring on the top of some of the Cabliers coral mounds, western Mediterranean Sea.

- Similarly to the Atlantic CWC mounds, coral density and size increase towards the top of the Cabliers coral mounds, probably due to higher food supply and structural stability.

- Statistical analyses showed the presence of four megabenthic assemblages, whose distribution was mainly determined by substratum type and depth.

- The presence of several *H. dactylopterus* individuals under 10 cm confirms that CWC assemblages are used by commercially valuable species as nursery grounds.

- The changes in CWC abundance, taxonomic composition and diversity between the north and south CMP could be a representation of the different succession stages that can occur in a coral mound throughout flourishing and decline stages.

- The taxonomic differences observed between Atlantic and Mediterranean coral mounds, in terms of megabenthic assemblages, indicate that the amount of species associated to CWC reefs is probably higher than previously thought.

- The present study helped to gain insight into the structure of Mediterranean CWC reefs and their associated species. However, a broader quantitative baseline would be required to better understand the environmental constraints of these ecosystems in the Mediterranean Sea and to contribute towards an improved management of CWC assemblages.

2.8. Acknowledgements

Guillem Corbera is funded by the Graduate School of the National Oceanography Centre Southampton (GSNOCS), with the collaboration of the NGO OCEANA. The data for this study was collected during the Spanish national project SHAKE (CGL2011-30005-C02-02, PI: Eulàlia Gràcia). We acknowledge the European Ocean facilities Exchange Group (OPEG) who facilitated the use of the AUV IdefX from IFREMER (France) and the EU Eurofleets-2 Project, which provided the ROV Max Rover from HCMR (Greece) during the SHAKE Cruise. We are indebted with the technical teams of UTM-CSIC, IFREMER and HCMR, for their support provided during the SHAKE cruise. We gratefully acknowledge all the participants on the SHAKE cruise and the crew on board of the R/V Sarmiento de Gamboa for their professional work during the expedition. Finally, we would like to thank the scientific illustrator Jordi Corbera for the design of the schematic representation of the assemblages found on Cabliers.

Chapter 3

Glacio-eustatic variations and Sapropel events as main controls on the Middle Pleistocene-Holocene evolution of the Cabliers Coral Mound Province (W Mediterranean)

This chapter is a reproduction of the text published as **Corbera, G.**, Lo Iacono, C., Standish, C.D., Anagnostou, E., Titschack, J., Katsamenis, O., Cacho, I., Van Rooij, D., Huvenne, V.A.I., Foster, G.L. (2021). Glacio-eustatic variations and Sapropel events as main controls on the Middle Pleistocene-Holocene evolution of the Cabliers Coral Mound Province (W Mediterranean). *Quaternary Science Reviews,* 253: 106783. DOI: https://doi.org/10.1016/j.quascirev.2020.106783

Author contributions: Corbera, G., Lo Iacono, C., Huvenne, V.A.I., Foster, G.L., Anagnostou, E. and Cacho, I. conceptualised the chapter. Lo Iacono, C. and Van Rooij, D. collected the gravity cores. Corbera, G., Standish, C.D., Titschack, J., Anagnostou, E., and Katsamenis, O. acquired and analysed the data. Corbera, G. wrote the manuscript and all authors reviewed and commented on it.

3.1. Abstract

Cold-water coral (CWC) mounds are key hot-spots of deep ocean biodiversity and also important archives of past climatic conditions. Nonetheless, the paleo-oceanographic setting in which coral mounds developed in the Mediterranean Sea during the last 500 kyr still needs to be properly understood. This study describes the coral deposits and corresponding ages of two on-mound gravity cores acquired from opposite sectors of the newly discovered Cabliers Coral Mound Province (CMP, Alboran Sea, W Mediterranean). U-Th data revealed Pleistocene-aged corals covering mound formation periods from >389 to 9.3 ka BP and from 13.7 to 0.3 ka BP in the southern and northern mounds respectively. The coral-rich deposits of the cores were mainly dominated by *Desmophyllum pertusum,* although in some sections concurrent with the Middle Pleistocene and the Holocene, other corals such as *Dendrophyllia cornigera* and *Madrepora oculata* also appeared as dominating species. Coral mound formation stages generally occurred during deglacials and temperate interstadial (3.5–4.1 $\delta^{18}O‰$) periods, whereas during interglacials (<3.5 $\delta^{18}O‰$) coral mound formation only occurred in the northern and shallower mound. We interpret this to indicate that the shoaling of the interface between Atlantic (AW) and Levantine Intermediate Waters (LIW) during interglacial periods prevented the corals in the southern CMP from acquiring sufficient food supply, thus causing periods of coral mound stagnation. Similarly, the interruption in LIW formation throughout sapropel events also coincides with coral mound stagnation phases. This suggests that sapropel-derived processes, which originated in the eastern Mediterranean, likely affected the entire Mediterranean basin and further supports the role of LIW as a conveyor belt facilitating CWC growth in the Mediterranean Sea. Overall, we show that these coral mounds yield important insights into how local changes in oceanographic conditions can influence coral mound development.

3.2. Introduction

With the presence of suitable environmental conditions (e.g. food supply, temperature, salinity, dissolved oxygen, moderate bottom currents) scleractinian cold-water coral (CWC) populations can expand, with new settlement occurring on dead coral framework, and separate coral patches eventually merging to form reefs (Wilson, 1979; De Mol et al., 2005; Roberts el al., 2006; Lo Iacono et al., 2018a). Such reefs consist of a bio-constructed three-dimensional framework composed of living and dead CWCs, which provides a range of ecological niches for the settlement of many species (Roberts et al., 2006; Price et al., 2019). Although most studied CWC reefs are commonly formed by *Desmophyllum pertusum* (synonym = *Lophelia pertusa*; Addamo et al., 2016), other framework-building CWCs such as *Madrepora oculata*, *Enallopsammia profunda, Solenosmilia variabilis* and *Oculina varicosa* can also form reefs on their own (Reed et al., 1980; Roberts et al., 2006; Raddatz et al. 2020). The complex structure of CWC reefs increases turbulence and reduces the current speeds among the corals, thus trapping hemipelagic sediments (Hebbeln et al., 2016). The latter, in turn, help to stabilise the coral framework, preventing its physical collapse when the coral colonies become too large (De Mol et al., 2002; Dorschel et al., 2005; Wienberg and Titschack, 2017). Over geological timescales, if suitable environmental conditions persist, CWC reefs can grow and form prominent geomorphological structures, known as coral mounds (Roberts et al., 2006, 2009a; Wienberg and Titschack, 2017; Lo Iacono et al., 2018a).

Coral mounds generally occur in clusters and they are mainly described from the Northeast Atlantic margin, within a depth range of 70–1200 m (Wheeler et al., 2007; Lo Iacono et al 2018a). However, in the last decade new coral mound provinces have also been discovered off

the west-African coast (Eisele et al., 2011, 2014; Van Dorpe et al., 2017; Wienberg et al., 2018; Tamborrino et al., 2019), the eastern continental slopes of North and South America (Grasmueck et al., 2006; Raddatz et al., 2020) and in the Mediterranean Sea (Comas and Pinhero, 2010; Lo Iacono et al., 2014, 2016; Savini and Corselli, 2010; Corbera et al., 2019). Regardless of where they occur, CWC mounds present a wide range of sizes and shapes (Lo Iacono et al., 2018a). From conical mini-mounds that are a few metres tall (e.g. Darwin and Moira Mounds; Bett et al., 2001; Foubert et al., 2011) to giant ridge-like mounds that rise hundreds of meters above the surrounding seafloor (e.g. Challenger Mound and Brittlestar mounds; Kano et al., 2007; Comas and Pinheiro, 2010; Fink et al., 2013). Such mound morphologies are sometimes associated with the presence of a geological structure on which the corals first settled and started to grow (Lo Iacono et al., 2014, 2018a; Hebbeln, 2019). Nevertheless, persistent current dynamics can also have an effect on the shape of growing coral mounds (Huvenne et al., 2003; López-Correa et al., 2012; Hebbeln et al., 2014; Buhl-Mortensen et al., 2016).

Coral mound development can last from a few thousand up to millions of years (Kano et al., 2007; Frank et al., 2011; Victorero et al., 2016). Over this time, paleo-climatic fluctuations such as glacial-interglacial cycles occurred, involving drastic changes in relative sea-level (RSL), seawater temperature and many other environmental variables, including surface productivity and water oxygenation (Dorschel et al., 2005; Roberts et al., 2006; Thierens et al., 2013). These variations exert a strong control on the increase, reduction and stagnation of coral mound formation, in some cases even producing winnowing and mass-wasting of their exposed portion (López-Correa et al., 2012; Stalder et al., 2015; Tamborrino et al., 2019). Environmental variations experienced during coral mound formation can be recorded in the skeletons of growing corals as the concentration and isotopic composition of certain elements (e.g. Li, Mg, U, Ba, B, Nd) that reflect the local physicochemical parameters of the surrounding water (Montagna et al., 2014; Spooner et al., 2018). As paleoclimatic archives, absolutely dated CWCs combined with the extraction of geochemical proxies and computed tomography (CT) scans can thus give highly relevant information on coral mound development and its paleo-climatic constrains (Fink et al., 2013; Raddatz et al., 2016; Montagna and Taviani, 2019; Wang et al., 2019).

In the Mediterranean basin, CWC mound provinces tend to occur together with contourite deposits (Rebesco and Taviani, 2019) and are concentrated in the Ionian Sea (Savini and Corselli, 2010; Savini et al., 2014), the Thyrrhenian Sea (Remia and Taviani, 2005; Angeletti et al., 2020a) and the Alboran Sea, this last being the only basin where mounds reach sizes of >100 m in height and several kilometres in length (Comas and Pinhero, 2010; Fink et al., 2013; Lo Iacono et al., 2014, 2016; Corbera et al., 2019). Several studies have attempted to link coral mound growth patterns in the Alboran Sea to different environmental factors, in order to better understand what are the main processes driving or limiting CWC mound development in the region (Fink et al., 2013; Lo Iacono et al., 2014; Fink et al., 2015; Stalder et al., 2015; Wang et al., 2019). Fink et al. (2013, 2015) linked coral mound formation in the Alboran Sea to periods of enhanced productivity and increased water mass circulation, while Wang et al. (2019) suggested that mound formation is controlled by a complex interplay between productivity and changes in the RSL, which affected the depth of the interface between Atlantic and Mediterranean water masses. Despite the great amount of knowledge won, none of these studies have been able to investigate CWC mound development beyond the last 15 kyr. Therefore, knowledge on coral mound development prior to the Bølling-Allerød (B/A; i.e. >15 ka BP) is minimal, which impedes a more comprehensive description of Mediterranean coral mound development in response to Late Quaternary paleo-climatic changes in the area.

This study describes the coral deposits and corresponding ages of two on-mound gravity cores collected from opposite ends of the recently discovered Cabliers Coral Mound Province (hereafter as CMP; Fig. 3.1; Lo Iacono et al., 2016). Previous studies have shown that while CWCs thrive on the northernmost sector of the CMP, the corals on its southern end are dead (Corbera et al., 2019). This change in CWC abundance observed between the two ends of the province (15 km apart), most probably reflects differences in the existing local environmental conditions (i.e. hydrodynamics, physicochemical conditions of the water, food supply; Corbera et al., 2019), which makes this mound province an ideal setting for the study of coral mound evolution in response to local and regional environmental changes. Thus, with the general purpose of acquiring a better understanding of coral mound development in the Mediterranean Sea, this study aims to (1) describe the temporal development of the northern and southern sectors of the CMP during the last ~500 kyr, (2) relate the changes in mound growth patterns to paleo-climatic events that modified the regional and local environmental setting and (3) compare the paleo-evolution of the CMP with the mound development patterns of already studied coral mound provinces, specifically in the Alboran Sea.

3.3. Study area

The Alboran Sea is the westernmost basin of the Mediterranean Sea, bound by the Iberian Peninsula to the north and Northern Africa to the south (Fig. 3.1B). To the west, the Strait of Gibraltar connects this basin to the Atlantic Ocean, while to the east the boundary of the Alboran Sea is defined by the area connecting Cabo de Gata (Spain) with Cap Figalo (Algeria) (Fig. 3.1B). The Alboran Sea displays a complex seafloor geomorphology, which exhibits several seamounts, volcanic banks and ridges. (Duggen et al., 2004; Lo Iacono et al., 2008; Palomino et al., 2015).

Ocean circulation patterns within the Alboran Sea are largely driven by the interaction between the Atlantic Water (AW), entering from the west, and the Levantine Intermediate Water (LIW) and West Mediterranean Deep Water (WMDW), flowing in from the east. This creates a small-scale thermohaline circulation (Garcia Lafuente et al., 1998). The AW is the main driver of the surface circulation in the Alboran Sea and consists of warmer and fresher waters (T~15°C, S~36.2, Ba_{SW} ~40 nmol kg^{-1}) that flow towards the east from the surface down to 150-200 m deep (Garcia Lafuente et al., 1998; Vargas-Yañez et al., 2017; Roy-Barman et al., 2019). Below the AW, the colder and more saline waters of the LIW (T~13.2°C, S~38.5, Ba_{SW} ~70 nmol/kg) flow much slower in opposite direction at 200-600 m water depth (Roy-Barman et al., 2019). The LIW is a water mass that originates in the Eastern Mediterranean Basin and spreads across the southern sector of the Western Mediterranean towards the Alboran Sea, where it flows out to the Atlantic Ocean and contributes to the formation of the Mediterranean Outflow Water (MOW) (Millot, 2009). Finally, the WMDW (T~12.9°C, S~38.4, Ba_{SW} ~75 nmol/kg), which is a deep water mass formed in the Gulf of Lions, flows beneath the LIW down to the seafloor, following the same direction and also contributing to the MOW's formation (Vargas-Yañez et al., 2017; Roy-Barman et al., 2019).

The interaction between Atlantic and Mediterranean waters together with the geomorphology of the Alboran Basin sustains a system of two semi-permanent anticyclonic gyres, the stability and intensity of which depend on the amount of AW coming through the Strait of Gibraltar (Vargas-Yáñez et al., 2002). The western quasi-permanent gyre is located between the Strait of Gibraltar and Cabo Tres Forcas, whereas the eastern and more variable gyre is found in be-

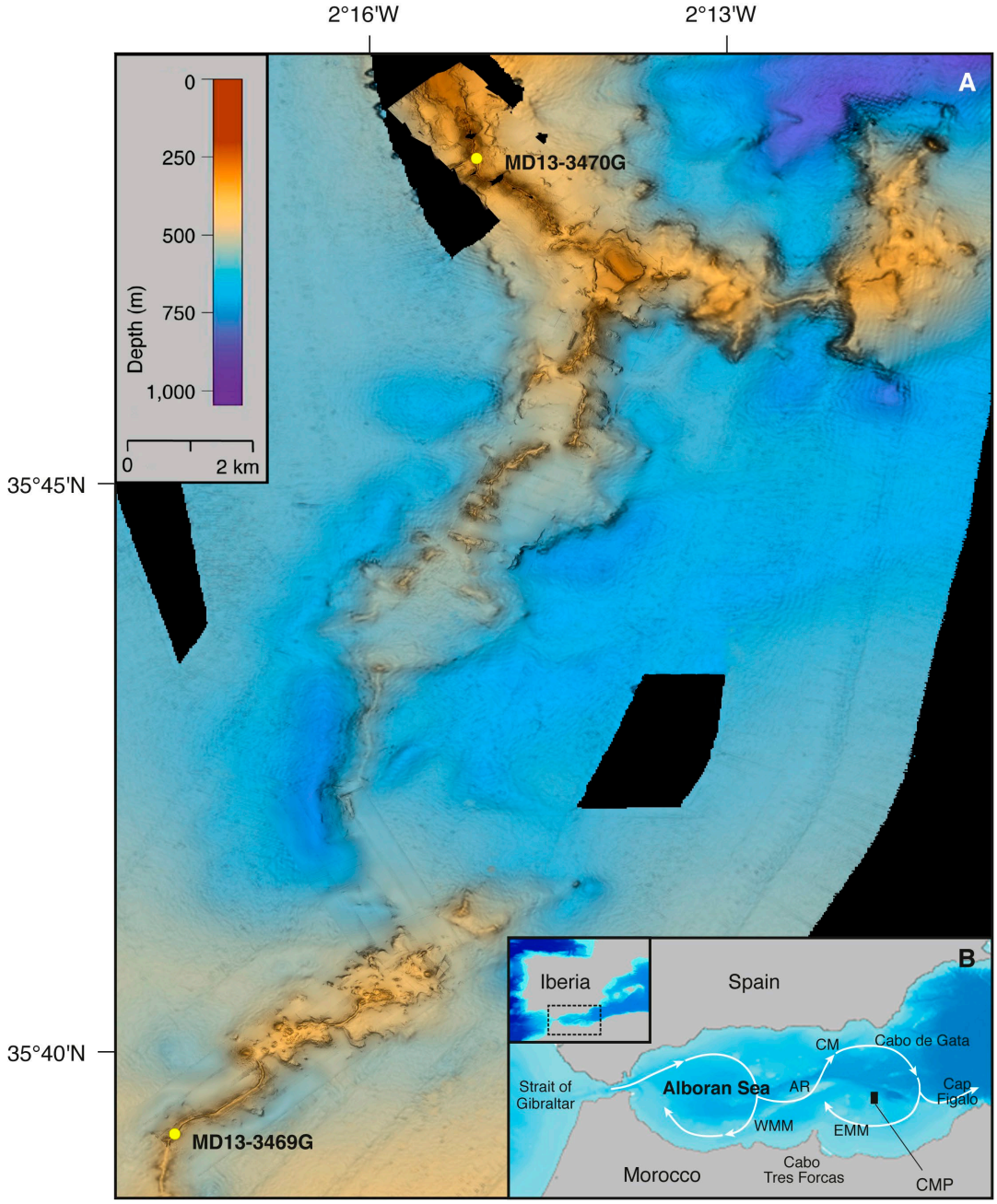

Figure 3.1. Shipboard multi-beam bathymetric model (20 m resolution) of the Cabliers Coral Mound Province (CMP) (A). Inset of the Alboran Sea, with the black rectangle indicating the location of the CMP (B). The yellow dots in (A) show the location of both MD13-3469G and MD13-3470G. AR: Alboran Ridge, CM: Chella Mound (Lo Iacono et al., 2018), WMM: West Melilla Mounds (Lo Iacono et al., 2014), EMM: East Melilla Mounds (Comas and Pinheiro, 2010). White arrows: surface Atlantic Water circulation.

tween Cabo Tres Forcas and Cap Figalo (Fig. 3.1). Both gyres are active during summer, while in winter only the western anticyclonic gyre prevails (Vargas-Yáñez et al., 2002; Macías et al., 2008). Overall, the gyre system stimulates the formation of upwelling areas that bring nutrients up to shallower waters, which increase the primary productivity at the surface and makes the Alboran Sea the most productive region within the Mediterranean Sea, with 200–300 gC m^{-2} a^{-1} (Bosc et al., 2004; Oguz et al., 2014). Such productivity mostly accumulates in a meandering jet of AW that flows into the Alboran Sea following the course of the two anticyclonic gyres (Navarro et al., 2011; Oguz et al., 2014). Moreover, it is known that in the Alboran Sea, around 250 m water depth and close to the interface between AW and LIW, diurnal frequency internal waves occur (Van Haren, 2014).

In this basin, coral mounds are distributed into three main provinces: the West Melilla Mounds (WMM), the East Melilla Mounds (EMM; Fig. 3.1B) and the CMP. The WMM consists of 103 conical-shaped mounds up to 48 m tall and 476 m in diameter, in a depth range of 298–590 m but with no living corals currently occurring on the mounds (Lo Iacono et al., 2014). The EMM are composed of >30 ridge-like mounds that can extend for >15 km and reach 150 m in height, in a depth range of 200–475 m (Hebbeln, 2019). In this province living CWCs are not common and only appear as small scattered colonies at the mounds' crests (Hebbeln et al., 2009). The CMP is located ~40 km northeast of the EMM, it extends NE-SW for 25 km and is mainly formed by ridge-like mounds with an average height of 77 m, in a depth range of 250–710 m (Fig. 3.1). In contrast to what is known for the rest of coral mound provinces in the Mediterranean Sea, ROV footage has revealed large thriving CWC reefs occurring on the summit of the CMP northernmost sector (Corbera et al., 2019).

3.4. Material and methods

3.4.1. Core acquisition and analyses

The two gravity cores (MD13-3469G and MD13-3470G) used for this study were collected from the summit of two coral mounds, located on opposite ends of the CMP, in June 2013 during the Eurofleets "GATEWAY" Cruise MD194, onboard the R/V Marion Dufresne (Table 3.1). Core MD13-3470G was retrieved from 313 m water depth at the northernmost part of the CMP. In contrast, core MD13-3469G was extracted from 417 m water depth, 15 km further to the south-west. The gravity corer managed to recover 8.40 and 10.38 m of core material for MD13-3470G and MD13-3469G respectively, consisting of dense coral framework and coral rubble embedded in hemipelagic sediments. The cores were cut in 1 m sections, scanned through high-resolution computed tomography and frozen before being split. The 1 m long sections were split while frozen using a diamond rock saw, to minimize coral fragmentation during cutting operations. The sections were then defrosted and HD photographed employing the Geotek MSCL-Core Imaging System from the British Ocean Sediment Core Research Facility (BOSCORF). The two cores were visually logged.

3.4.2. Computed tomography scans

Prior to splitting, the ~1m gravity core sections were scanned in sections of 10 cm at the m-Vis facilities of the University of Southampton, using a custom built, dual source 225/450 kV walk-in room CT scanner (Nikon Metrology, UK). To acquire the scans, the microfocus 450 kV source was fitted with a tungsten reflection target together with a Perkin Elmer XRD 1621 CN03 HS detector. Projections were acquired during a full 360° rotation. Images were then reconstructed, resulting in an isotropic voxel-size of 71.4 mm. However, voxel resolution was later down-sampled to 200 mm in order to facilitate a more efficient data handling and analysis. Later, the image processing software Fiji was used to apply an anisotropic dif-

Table 3.1. MD13-3469G and MD13-3470G core location, water depth and recovery. Number of samples for Uranium series and geochemical proxies is indicated, together with the youngest and oldest samples of each core.

Core	Lat	Long	Water depth (m)	Recovery (m)	U-Th samples	Li/Mg and Ba/Ca samples	Age (ka BP) Min.	Age (ka BP) Max.
MD13-3469G	35°39.409'N	2°17.731'W	417	10.38	59	24	9.3	588.9
MD13-3470G	35°47.755'N	2°15.152'W	313	8.4	51	10	0.3	13.7

fusion filter (default settings) to reduce the noise in the scans, while keeping detail in sharp edges. All further processing was performed with the ZIB edition of the Amira software (version 2018.04; Stalling et al., 2005; http://amira.zib.de). The 10 cm volumes were fused into 1 m sections, using the intensity of the core liner to calibrate the variation in intensity of the sediments and the corals between neighbouring volumes. Watershed segmentation was used to segment the macroscopic (>1 mm) carbonate fragments, dominated by CWCs, from the sediment. The volumetric percentage of CWCs in each CT slice was quantified with the *MaterialStatistics* module (Volume per slice). The *ContourTreeSegmentation* module was subsequently employed to achieve an automatic segmentation and separation of neighbouring clasts. The resulting 3D reconstruction of the bigger coral fragments (>20 mm) was used to visually identify the dominating coral species along the core. Finally, coral preservation patterns (CPP) were defined through the quantification of clast size and inclination by means of the *ShapeAnalysis* module. In some cases, the transition section between CPPs is marked by an abrupt variation in different macroscopic parameters (e.g. coral content (vol. %), clast size and inclination, presence of Fe-Mn coated corals and species dominance; hereafter referred to as an unconformity), which suggests that changes in the environmental setting caused a substantive modification in the coral mound development.

3.4.3. Grain size analysis

In total, 53 and 45 sediment samples from the cores MD13-3469G and MD13-3470G were collected every 20 cm and dried at 80°C for 24 hours. The samples where then placed in a solution of H_2O_2 20% for 15 days in order to remove all the organic matter. Subsequently, they were subjected for 24 hours to the action of a dispersant (i.e. sodium polyphosphate 40 ml l^{-1}) to separate the grains. Once the preparation of the samples was finished the coarser fraction was sieved for 6000, 4000 and 2000 mm. Finally, the total sediment fraction finer than 2000 mm was examined using an LA-950V2 laser scattering particle size distribution analyser (HORIBA) at the Institute of Marine Sciences (ICM-CSIC), which detects grains down to 0.031 mm.

3.4.4. Uranium series absolute dating

59 and 51 coral fragments were extracted from the cores MD13-3469G and MD13-3470G respectively to be dated through uranium series techniques at the University of Southampton (Table 3.1). Four coral fragments from each core, were dated via solution multi-collector inductively coupled plasma mass spectrometry (MC-ICP-MS) to provide accurate and precise temporal constraints for both cores. All other samples were dated through laser ablation MC-ICP-MS (Spooner et al. 2016). Four of the samples analysed by solution were split in two pieces before processing to provide internal reference materials for laser ablation MC-ICP-MS.

Given that some samples were analysed by both solution and LA techniques, with LA samples being analysed either singularly or multiple times, ages were prioritised in the following manner when assessing coral growth: 1) solution MC-ICP-MS analyses (Table S3.1); 2) mean (± 2 SD) LA-MC-ICP-MS ages of multiple analyses (Table S3.2); and 3) single LA-MC-ICP-MS analysis (Table S3.2).

The final ages were used to calculate the aggradation rates (ARs) of the different coral mound formation periods. We associated the oldest and youngest ages of each mound formation period to the deepest and shallowest samples of such period respectively. This method provides conservative AR estimations for each mound formation period.

3.4.4.1. *Solution U-Th dating*

Coral fragments were cut into small samples (0.12–0.3 g) using a circular saw. Organic matter and possible Fe-Mn crusts were mechanically and chemically cleaned, following a procedure similar to the one published by Cheng et al. (2000). This protocol consisted of a succession of ultra-sonication steps with 18.2 MΩ cm (ultrapure) H_2O, oxidative and reductive solutions, intercalated with washes of the samples. The samples were then dissolved by stepwise addition of concentrated HNO_3 (~15.5 N). The separation of U and Th from the sample matrix was performed by ion exchange chromatography, employing 0.6 ml columns and 100–150 µm UTEVA Spec (Eichrom) resin (Horwitz et al., 1992) and following the method published in Hoffmann et al. (2018) for the University of Southampton geochemistry facilities. The U and Th isotope measurements were undertaken on a Neptune Plus MC-ICP mass spectrometer (Thermo Fisher Scientific, Waltham, MA, USA) equipped with nine Faraday cup detectors and an energy filter (Retarding Potential Quadrupole lens) on the central ion counter. All analytical procedures and calculations were undertaken following the methods in Hoffman et al. (2007; 2018). For the calculation of activity ratios the following decay constants were used: $\lambda_{230} = (9.1577\pm0.028)\cdot10^{-6}$ a^{-1} (Cheng et al. 2000), $\lambda_{232} = (4.94752\pm0.035)\cdot10^{-11}$ a^{-1} (Holden 1990), $\lambda_{234} = (2.826\pm0.0056)\cdot10^{-6}$ a^{-1} (Cheng et al. 2000), and $\lambda_{238} = (1.55125\pm0.0017)\cdot10^{-10}$ a^{-1} (Jaffey et al. 1971). Ages were calculated iteratively from the activity ratios and using the above half-lives. Following Scholz et al. (2004), corrections for initial Th assume a $(^{232}Th/^{238}U)_A$ value typical of upper crustal silicates (Wedepohl, 1995): 1.250±0.625 (whilst assuming ^{230}Th and U isotopes are in equilibrium).

Long-term accuracy and external reproducibility of solution U-Th dating was demonstrated through repeat analyses of a secular equilibrium standard, uraninite URAN 84.5, over a period of 4 years (detailed in Supplementary Data).

3.4.4.2. *Laser ablation U-Th dating*

Samples and standards for laser ablation analyses were mounted in epoxy resin (2.5 cm diameter disks) and polished until the surface of the resin was flat, and the samples were exposed. The analyses were performed at the University of Southampton, using an Elemental Scientific Lasers (Bozeman, MT, USA) NWR193 excimer laser ablation system with a TwoVol2 ablation chamber coupled to a Thermo Scientific Neptune Plus MC-ICP-MS.

A peak hopping approach between two sub-configurations, based on 'Procedure 2' of Spooner et al. (2016), was employed using VS001/1-A, a fragment of inorganically precipitated aragonite vein (Kampman et al., 2012), as an aragonite standard (detailed in Supplementary Data): ^{230}Th and ^{234}U intensities were measured using the central ion counter whilst ^{238}U intensities were measured using Faraday cups (see Table S3.3). Integration times were 4.194 s and idle times were 1 s for both sub-configurations, giving a total cycle time of 10.388 s. Spooner et al. (2016) demonstrated that measuring ^{232}Th for correction of initial Th was not necessary in most cases when analysing CWCs. Analyses of ^{232}Th was therefore not included in the approach employed here, a decision that is validated by the accuracy of the internal standards discussed below. Typical operating conditions are detailed in Table S3.4. To remove any surface contamination, coral samples were pre-ablated prior to analyses. Rather than ablating a single spot, laser ablation was carried out along a straight line on the sample surface. This method keeps a steadier signal intensity and inter-element fractionation compared to spot analyses (Spooner et al., 2016).

Activity ratios and age calculations were performed in the same way as outlined in section 3.4.1. The number of samples analysed in one run was limited to 40 in order to avoid decreased sensitivity due to carbonate build up on the skimmer and sampler cones. Furthermore, some of the samples found at the initiation or end of an intense coral mound growth period were dated repeatedly (5 measurements) to reach a more precise average age through replication and thus achieve a better constrained picture of mound development.

Accuracy of the laser ablation MC-ICP-MS is demonstrated through analyses of four coral samples also analysed by solution MC-ICP-MS (Table S3.3 and Fig. S3.1). These four samples, alongside a further 12, were analysed multiple times throughout the period of study to demonstrate the external reproducibility of the approach. Expressed as 2 standard deviations (SD) of the mean of the multiple analyses, these range from 20.8 % to 1.2 % for ($^{230}Th/^{238}U$) equal to 0.03 and 1.25 respectively, and are ≤2 % for ($^{234}U/^{238}U$). External reproducibility at 95% confidence of calculated U-Th ages range from ±0.5 kyr for an age of 2.8 ka BP (16.8 %) to ±26.8 kyr for an age of 316.3 ka BP (8.6%); comparable to previous studies using laser ablation MC-ICP-MS (Eggins et al., 2005; McGregor et al., 2011; Spooner et al., 2016). External reproducibility of the $\delta^{234}U_i$ is typically better than 25‰ (2 SD). Spooner et al. (2016) discussed the factors contributing to the external reproducibility of the calculated laser ablation ages in some detail and demonstrated that it is possible to estimate the reproducibility of the age of any sample based on its ($^{230}Th/^{238}U$). This approach is followed here, where age uncertainty is determined based on the relationship between the external reproducibility of those samples analysed multiple (≥3) times and their ($^{230}Th/^{238}U$) (Fig. S3.2). These give calculated uncertainties (at 95% confidence) of ~0.7 kyr for ages of 0–10 ka BP, ~0.9 kyr for ages of ~15 ka BP, ~5 kyr for ages of 100 ka BP, and ~19 kyr for ages of ~350 ka BP. This approach could not characterise uncertainty on samples >400 ka BP, therefore such samples were not considered during dating discussions.

3.4.5. Trace elements analyses

From the dated coral fragments, 24 individuals from core MD13-3469G and 10 from core MD13-3470G were further processed for Li/Mg and Ba/Ca analyses. The Li/Mg ratio in CWCs relates to the seawater temperature in which the corals grew (e.g. Case et al., 2010; Montagna et al., 2014; Stewart et al., 2020). Ba/Ca ratios are linked to seawater Ba concentrations (Ba_{SW}; e.g. Anagnostou et al., 2011; Spooner et al., 2018), which can be used to trace different water masses and changes in terrigenous input (Roy-Barman et al., 2019). The corals were first mechanically cleaned using a circular saw, to remove any Fe-Mn crust and visible borings, and then ultra-sonicated several times to remove any lose sediments trapped within the coral features. Subsequently, the corals were subjected to oxidative and reductive cleaning, to remove the remaining organic and crustal material, and to dissolution through the use of 0.5M HNO_3 (detailed in Chapter 3 Supplementary Materials).

The elemental ratios were then measured on the Thermo Element XR (University of Southampton) following established protocols (e.g. Stewart et al., 2017), with a long-term precision (2s) of consistency standards of 2% for Ba/Ca, and 4% for Li/Mg. To translate elemental ratios into environmental parameters, we used the multispecies calibration of Montagna et al. (2014) on coral Li/Mg ratios to calculate sea water temperatures (SWTs) and the multispecies calibration of Spooner et al. (2018) for reconstructions seawater Ba concentrations. Changes in the Li/Mg ratio in seawater during the last million years are negligible due to the long residence

time of Li and Mg in the ocean (Huh et al., 1998). Therefore, it can be assumed that seawater Li/Mg ratios did not change during the timespan encompassed by this study (i.e. ~600 kyr). Reconstructions and uncertainties for SWTs and Ba_{sw} were calculated by propagating both the analytical uncertainty of our elemental data and the uncertainty associated to the regression fit of each calibration, refitted here using York (2004), with a Monte Carlo approach (n=1000):

$$\text{Li/Mg calibration } (\pm 2\sigma)\text{: Li/Mg} = (5.29\pm0.06)\exp((-0.046\pm0.001)T),$$

$$\text{Ba/Ca calibration } (\pm 2\sigma)\text{: Ba/Ca} = (0.17\pm0.01)Ba_{sw} + (1.9\pm0.7)$$

The values used in all subsequent discussion were the median of the Monte Carlo SWTs and Ba_{sw} realisations for each sample with a 95% confidence derived from the observed 5 and 95% percentiles (Table S3.5). The Li/Mg-temperature calibration on all biogeogenic aragonites in Stewart et al. (2020) provides indistinguishable SWTs to our approach, including for the extreme estimates.

3.5. Results

3.5.1. Cabliers South (Core MD13-3469G)

3.5.1.1. *Visual and CT-based core description*

The core MD13-3469G, collected from the southernmost end of the CMP (Fig. 3.1), consists of 10.38 m of dense CWC framework and coral rubble fragments, within a matrix of fine sediments (Table 3.1, Fig. 3.2). The sediment matrix consists of olive grey muds interspersed with sporadic calcareous fragments that belong to other invertebrates, such as gastropods, bivalves and echinoids. Visual qualitative logging of the core allowed us to estimate that 41% of its length contains high coral fragment abundance (Fig. 3.2), generally observed in the upper 650 cm (Fig. 3.2). Similarly, 40% of the core corresponds to more dispersed but still abundant fragments (medium coral abundance in Fig. 3.2) and 18% to fine sediments with some scattered corals (low coral fragment abundance in Fig. 3.2). Visual characterisation also helped to detect a small section of the core (1% of core length) dominated by a bivalve facies (561–553 cm; Fig. 3.2B) and other short sections where the coral fragments were clearly bio-eroded and covered by a ferromanganese crust (863–854 cm and 575–561 cm; Fig. 3.2B).

The CT-based coral content (vol.%) oscillates along the core between 1 and 35 vol.% and presents an average value of 15±6 vol.% (Fig. 3.2). Generally, the change in coral vol.% values matches with the variations in coral abundance observed through visual description of the core halves (Fig. 3.2). The lowest vol.% values correspond to sections mainly dominated by sediments with scattered corals and to the bivalve facies (Fig. 3.2B). In contrast, the highest

Figure 3.2. Log of the MD13-3469G core (A: 0–483 cm, B: 483–1038 cm core depth). From left to right: core HD photo with location of the coral samples acquired for uranium series dating (blue lines) and the corresponding ages; stratigraphic representation of coral abundance; changes in the dominating species conforming the coral deposits; raw image of the core CT scans; 3D image of the CT scans including all segmented coral clasts; 3D image of the CT scan including coral clasts >2 cm; coral clast size distribution (white line: mean clast size); coral clast inclination (white line: mean clast inclination); coral volume per slice (200 mm) overprinted on the coral preservation pattern (CPP A-dark green: coral frameworks buried in living position; CPP B-light green: slightly collapsed coral framework; CPP C-orange: coral rubble; CPP D-brown: sediments with scattered coral fragments). The black bands indicate areas with bad quality CT scans that could not be included in the analyses. This figure can be found in supplementary material as four high resolution panels.

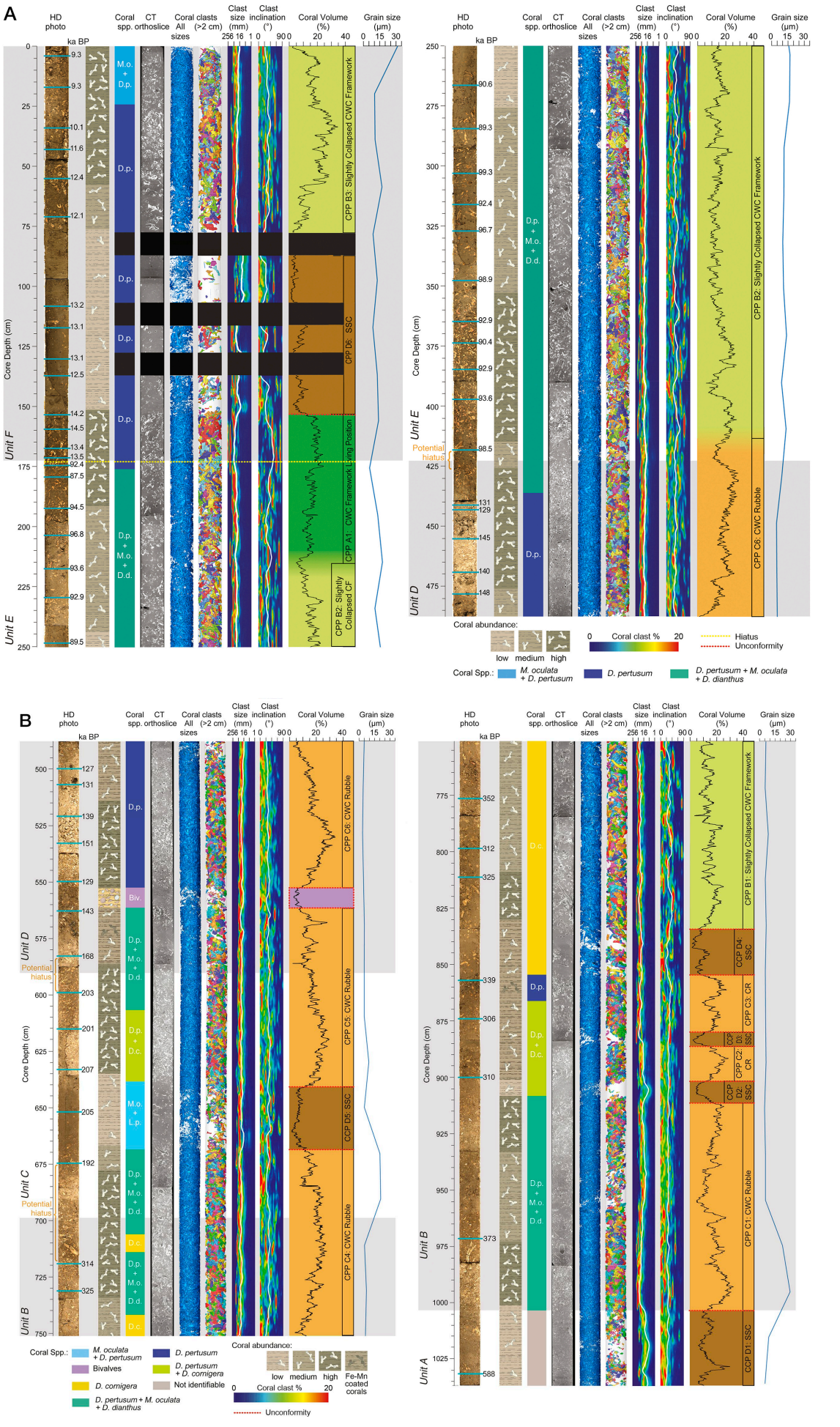
A
B
HD photo
ka BP
Coral spp.
CT orthoslice
Coral clasts All sizes (>2 cm)
Clast size (mm)
Clast inclination (°)
Coral Volume (%)
Grain size (µm)
Core Depth (cm)
Unit F
Unit E
Unit D
Unit C
Unit B
Unit A
Potential hiatus
CPP B3: Slightly Collapsed CWC Framework
CPP B2: Slightly Collapsed CWC Framework
CPP D6: SSC
CPP A1: CWC Framework Living Position
CPP B2: Slightly Collapsed CF
CPP C6: CWC Rubble
CPP C5: CWC Rubble
CCP D5: SSC
CPP C4: CWC Rubble
CPP B1: Slightly Collapsed CWC Framework
CCP D4: SSC
CPP C3: CR
CCP D3: SSC
CPP C2: CR
CCP D2: SSC
CPP C1: CWC Rubble
CCP D1: SSC
M.o. + D.p.
D.p.
D.p. + M.o. + D.d.
D.p. + D.c.
M.o. + L.p.
D.c.
Biv.
Coral abundance:
low
medium
high
Fe-Mn coated corals
Coral clast %
Hiatus
Unconformity
Coral Spp.:
M. oculata + D. pertusum
D. pertusum
D. pertusum + M. oculata + D. dianthus
Bivalves
D. pertusum + D. cornigera
D. cornigera
Not identifiable

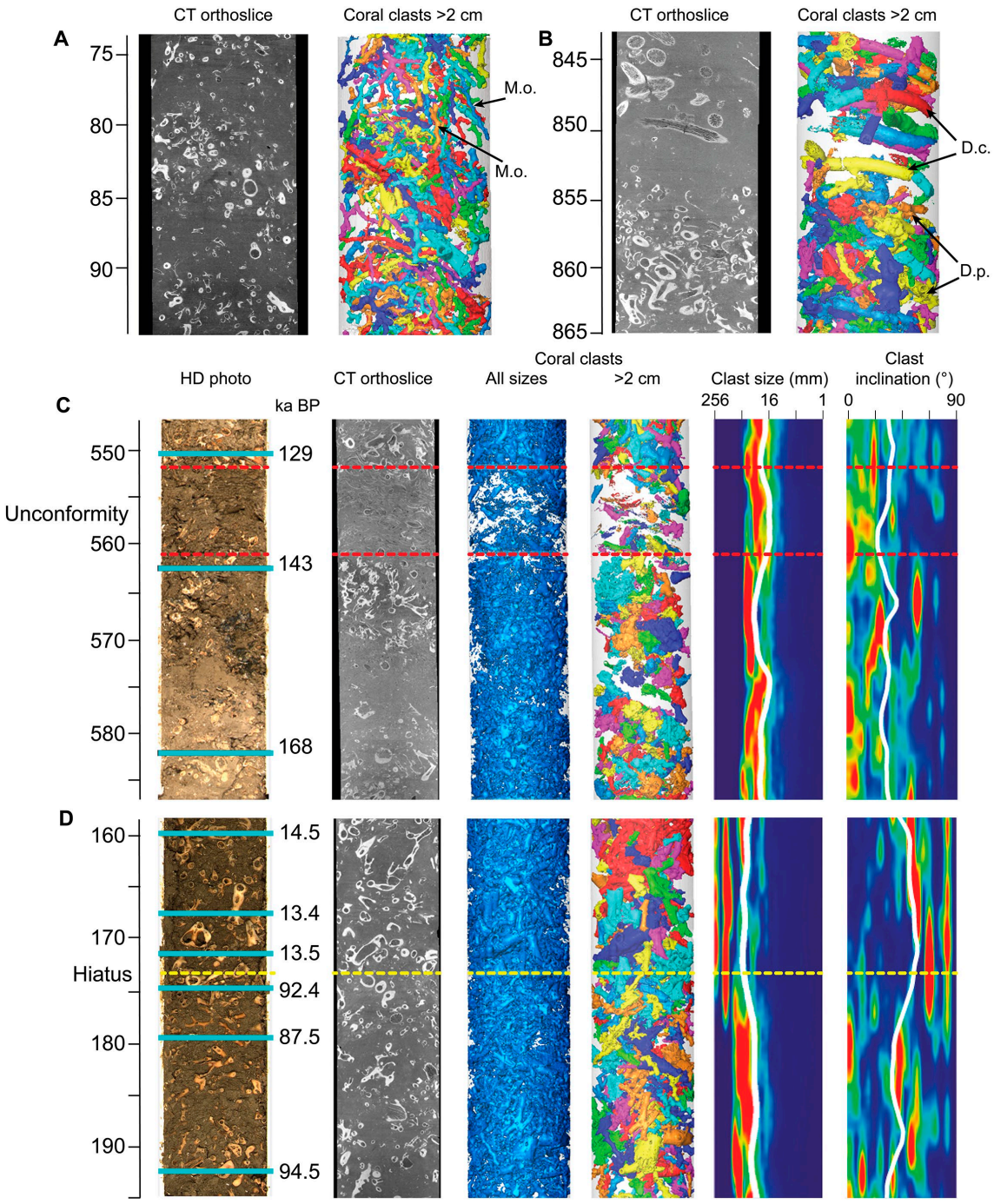

Figure 3.3. Detailed CT raw images and coral clasts >2 cm of (A) the uppermost section of core MD13-3470G, dominated by *M. oculata* facies (MO); (B) a section of core MD13-3469G where the coral facies changes from *D. pertusum* (DP) to *D. cornigera* (DC) fragments; and (C, D) detailed core sections of two possible coral mound growth hiatuses in core MD13-3469G. From left to right: Core HD photo with location of the coral samples acquired for uranium series dating (blue lines) and the corresponding ages; raw image of the core CT scans; 3D image of the CT scans including all segmented coral clasts; 3D image of the CT scan including coral clasts >2 cm; coral clast size distribution (white line: mean clast size); coral clast inclination (white line: mean clast inclination).

vol.% values relate to sections of the core formed by extremely abundant coral fragments, which mainly consist of *D. pertusum*. A combination of visual and CT-based analyses suggests that the predominant species forming the coral deposits is the framework-building coral *D. pertusum*. This species dominates most of the core, accompanied in some cases by *M. oculata*, *Desmophyllum dianthus* and *Dendrophyllia cornigera*. Yet, in certain sections of the core, *D. cornigera* and *M. oculata* dominate the CWC deposits over *D. pertusum* (Figs. 3.2, 3.3B).

The CT scan analyses also allowed the identification of four coral preservation patterns (CPPs), defined by different ranges of mean coral clast size and inclination, similar to those described in Titschack et al. (2015): coral framework in sub-vertical living position, slightly collapsed coral framework, coral rubble and sediments with scattered coral fragments. The deposits containing coral framework buried in living position (CPP A) are characterised by a mean coral clast size of >27 mm and variable inclinations, with clear maxima between 70 and 90° (Figs. 3.2, 3.5). Slightly collapsed coral framework (CPP B) is defined by average clast sizes ranging between 22.6 and 45.3 mm, and inclinations of <60°. Coral rubble (CPP C) is represented by a coral clast size ranging from 16.0 to 32 mm, and inclinations of <45°. Sediments with scattered coral fragments (CPP D) consists of average coral clasts sizes <16 mm, inclinations of <45°, and average coral content values generally under 10%. The lower half of the core displays coral deposits that mainly consist of coral rubble with sections of sediment with scattered coral fragments (Fig. 2B). In contrast the upper half is mainly dominated by slightly collapsed coral framework deposits, with some rubble and coral frameworks buried in living position (Fig. 3.2A). Change of CPPs is generally marked by the presence of unconformities (Fig. 3.2).

Average grain size of the matrix sediment varies from 3.4 mm (clay) to 31.4 mm (medium silt) with a mean value of 10±6.21 mm (Fig. 3.2). Grain size varies gradually along the core, with values of ~5 mm from 1038 to 450 cm, which increase to ~10 mm up to the top. Only three peaks of 30, 21 and 31.4 mm occur at 995, 690 and 0 cm respectively (Fig. 3.2). The coarsest grain size value is thus observed at the shallowest point of the core, corresponding with the demise of the mound (Fig. 3.2A).

To facilitate the description of the change in the species present in the core, the CPPs and the mound formation stages, the core has been divided in six different units according to the phases of mound development and to the most evident sedimentological features (Fig. 3.2A, B):

Unit A (1038–1003 cm) – The base of the core consists of mostly unidentified bioclasts (Fig. 3.2B). This unit is characterised by the dominance of matrix sediments with some scattered coral fragments (CPP D1). Although CPP D1 presents coral volumes over 10% they mainly consist of unidentifiable bioclasts that might not be coral fragments (Fig. 3.2B).

Unit B (1003–699 cm) – This unit mainly consists of coral rubble (CPP C1:1003–911 cm, CPP C2: 902–887 cm, CPP C3: 880–855 cm, CPP C4: 751–699 cm) and slightly collapsed coral framework (CPP B: 1835–751 cm) combined with small sections of sediments with scattered coral fragments (CPP D2: 911–902 cm, CPP D3: 887–880 cm, CPP D4: 855–835 cm). *D. pertusum* combined with *M. oculata* and *D. dianthus* dominates the coral deposits from 1003 to 902 cm. From 902 to 685 cm, *D. cornigera* is present among the coral fragments and it dominates the coral deposits from 855 to 743 cm (Figs. 3.2B, 3.3B). Fe-Mn coated fragments of *D. pertusum* are found at 866–855 cm, whereas at 742–714 cm and at 706–699 cm this species co-occurs with *M. oculata* and *D. dianthus*.

Unit C (699–590 cm) – Unit C is dominated by coral rubble (CPP C4: 699–669 cm, CPP C5: 641–590 cm) and sediments with scattered corals (CPP D5: 669–641 cm). Between 699 and 598 cm, the coral clasts are first composed of a mix of *D. pertusum*, *M. oculata* and *D. dianthus* (699–668 cm), then, set between two unconformities, by *M. oculata* and *D. pertusum* (668–636 cm), and finally by *D. pertusum* and *D. cornigera* (636–606 cm) (Fig. 3.2B).

Unit D (590–423 cm) – This unit is characterised by coral rubble (CPP C5: 590–561 cm, CPP C6: 553–423 cm). From 590 to 436 cm the coral deposits mainly consist of a mix of *D. pertusum*, *M. oculata* and *D. dianthus* (598–561 cm), followed by a section dominated by *D. pertusum* (553–436 cm; Fig. 3.2B). This change in species composition is marked by an unconformity in mound development (561–553 cm) dominated by iso-oriented bivalves and preceded by Fe-Mn coated corals (Figs. 3.2B, 3.3C). The uppermost section of this unit (436–423 cm) contains a mix of *D. pertusum*, *M. oculata* and *D. dianthus*.

Unit E (423–174 cm) – This unit starts with a gradual change from coral rubble (CPP C6: 423–413 cm) to slightly collapsed coral framework (CPP B2: 413–215 cm), followed by another gradual change to coral framework buried in living position (CPP A1: 215–174 cm). Unit E is preceded by the presence of a potential hiatus in coral mound formation and is entirely formed by a mix of *D. pertusum*, *M. oculata* and *D. dianthus* fragments (Fig. 3.2A).

Unit F (174–0 cm) – The coral deposits in this unit change from coral framework buried in living position (CPP A1: 174–153 cm) to sediments with scattered coral fragments (CPP D6: 153–87 cm), followed by slightly collapsed coral framework (CPP B3: 77–0 cm). From 174 to 24 cm, the coral facies consist of *D. pertusum*, while in the uppermost 24 cm the taxonomic composition drastically changes to a mix of *M. oculata* and *D. pertusum* (Fig. 3.2A).

3.5.1.2. *Mound development*

The age model of core MD13-3469G is based on 59 coral samples that were dated by means of U-Th series and whose age ranges from 589^{+248}_{-199} ka BP to 9.30±0.09 ka BP (Fig. 3.4, Tables S3.1, S3.2), indicating that periodic coral growth at this location began during/before ~Marine Isotopic Stage 11 (MIS 11) and ceased during the Early Holocene 9.30 ka BP. From these samples, 47 (80 %) correspond to deglacials and temperate interstadials (i.e. MIS 9c, 7a and 5c) identified as 3.5–4.1 $\delta^{18}O‰$ in the Lisiecki and Raymo $\delta^{18}O$ stack (Lisiecki and Raymo, 2005), 9 (15%) to glacial periods (i.e. MIS 10 and MIS 6; Fig. 3.4A) and 3 of them do not fit in either, due to the large age uncertainty associated to the samples. Due to the considerable error associated with MIS 10 coral ages, their glacial age must therefore be treated with caution.

The age model hints towards the presence of five mound formation periods, covering time intervals between ~5 and ~46 kyr, can be identified (Fig. 3.4A). Four mound stagnation periods are also observed, with durations ranging from ~24 to ~98 kyr (Fig. 3.4A). The first mound formation period, corresponding to Unit B, extends from ~346 to ~305 ka BP, with an AR of 4 cm kyr^{-1} and predominantly matches with the MIS 9 (Fig. 3.4A). However, it must be considered that an age inversion affects one of the samples within this period. This is followed by a potential mound formation hiatus that lasts for ~98 kyr and is coincident with the MIS 8 glacial and the start of MIS 7 (Fig. 3.4A). During MIS 7a-c interglacial, another short mound growth period occurred, going from ~207 to ~192 ka BP and corresponding to Unit C. This mound formation phase is characterised by an AR of 5 cm kyr^{-1} (Fig. 3.4A). Between this mound formation period and the following one, a short potential hiatus of ~24 kyr occurs, corresponding to the start of MIS 6 glacial in Lisiecki and Raymo (2005; Fig. 3.4A). The mound development period equivalent to Unit D, takes place during MIS 6 glacial and the deglacial prior to MIS 5. This period goes from ~168 to 127 ka BP and corresponds to the lowest ARs observed in this study (3.5 cm kyr^{-1}). Within CPP C6 and between 426 and 419 cm core depth, a drastic decrease in coral content (vol.%) and the significantly different coral ages indicate the presence of a potential hi-

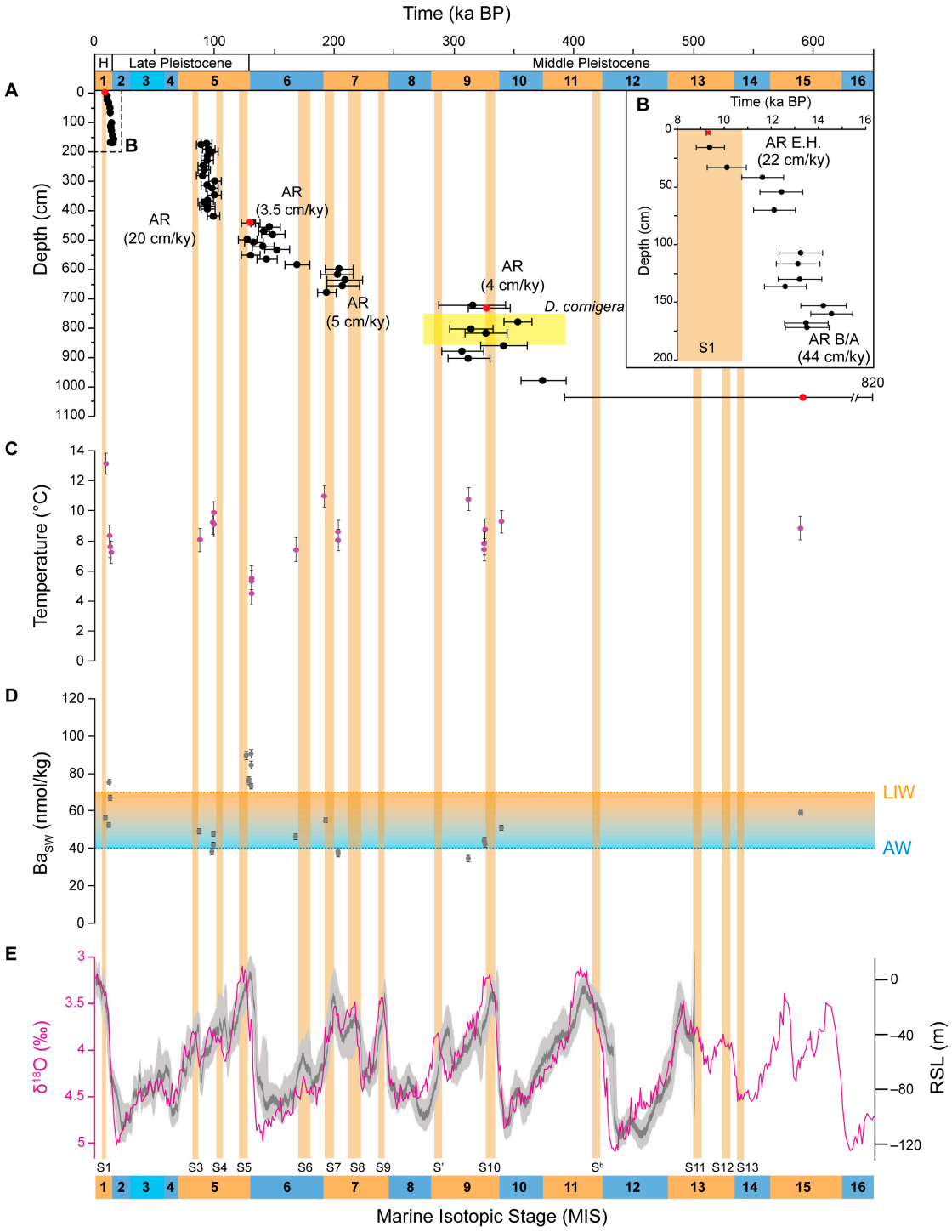

Figure 3.4. (A) MD13-3469G U-Th coral ages (black dots: laser ablation, red dots: solution) with associated 2s uncertainties against core depth and aggradation rates (ARs) of each mound formation phase. The brown bars indicate sapropel events S1–S13 (Ziegler et al., 2010; Konijnendijk et al. 2014); the yellow rectangle indicates a mound evolution phase dominated by *D. cornigera* assemblages. (B) coral mound evolution during the Bølling-Allerød and Holocene, with coral ages against core depth and the ARs of the two mound formation phases. (C) Li/Mg derived Sea Water Temperatures (SWTs), (D) Ba/Ca derived Ba_{SW} values and (E) LR04 $\delta^{18}O$ (‰) stack data for the last 650 ka (Lisiecki and Raymo, 2005) and Relative Sea-level dataset from Grant et al. (2014). The orange and blue shading indicates odd and even numbered Marine Isotopic Stages (MIS). The green and blue dotted lines indicate the present-day Ba_{SW} values of Atlantic (AW) and Levantine Intermediate (LIW) water masses (Jacquet et al. 2016; Roy-Barman et al., 2019).

atus in coral mound formation of ~29 kyr (Figs. 3.2A, 3.4A). The following growth stage, which corresponds with Unit E, extends from 99 to 87 ka BP and is characterised by an AR of 20 cm kyr^{-1}. After this faster mound aggradation phase a long hiatus (i.e. 87 kyr) occurs, encompass-

ing the majority of the last glacial period (MIS 2–4). In Unit F coral mound development starts again at 14.5 ka BP, soon after the onset of the B/A interstadial (14.7–12.7 ka BP), and lasts until 13 ka BP, when the mound enters in a short stagnation stage coincident with the Younger Dryas (YD; 12.8–11.8 ka BP; Fig. 3.4B). This mound formation period displays the highest AR of the whole core with a value of 44 cm kyr^{-1}. After the end of the YD, and corresponding with the start of the Early Holocene, the last mound growth period occurs in core MD13-3469G (i.e. 12.06–9.3 ka BP). This phase exhibits an AR of 22 cm kyr^{-1} and ends soon after the onset of the Sapropel event 1, when the mound enters in a stagnation stage and does not grow anymore until the present day (Fig. 3.4B).

3.5.1.3. *Paleo-environmental proxies*

From the 24 temperature values obtained, two were discarded because they showed negative values, which have most probably been caused by a diagenetic alteration of the samples (Table S3.5). The sample occurring at 129 ka BP also records an unexpected seawater temperature (1.0°C) that is unrealistic for such a shallow depth in any location outside of the polar regions, and below the known range tolerated by CWCs (Table S3.5). Therefore, this sample was not considered when interpreting the results. The remaining Li/Mg ratios for core MD13-3469G range between 2.9 and 4.3 mmol mol^{-1}, equating to SWTs between 4.6±0.7 and 13.1±0.7°C (Fig. 3.4C, Table S3.5). These SWTs reflect the variability following glacial and interglacial cycles. Nonetheless, mound growth in this sector of the CMP generally occurs when the SWTs are between 7 and 10°C (Fig. 3.4A–C). The highest SWT value (i.e. 13.1±0.7°C) coincides with the youngest age of this core (9.3 ka BP), when the mound stopped growing (Fig. 3.4B, C).

Coral Ba/Ca values acquired cover a range of 7.7–16.9 mmol mol^{-1} corresponding to a range of Ba_{sw} from 34.7±1.7 to 89.4±2.2 nmol kg^{-1} (Fig. 3.4D, Table S3.5). From these samples, the majority range between the two present day end-members, AW and LIW (Fig. 3.4D), and 29% is recording higher Ba_{sw}. The highest Ba_{sw} values occur around the onset of the last two deglacials. In contrast, the lowest values occur within MIS 5, 7 and 9 interstadials (Fig. 3.4D).

3.5.2. Cabliers North (Core MD13-3470G)

3.5.2.1. *Visual and CT-based core description*

The core MD13-3470G, acquired from the northernmost end of the CMP, consists of 8.4 m of dense CWC fragments (Fig. 3.5). Such fragments are embedded in an olive grey muddy sediment matrix, mixed with sporadic remains of other invertebrates, such as gastropods, bivalves and echinoids. Visual qualitative assessment indicated that 62% of the core's length is formed by coral deposits with very abundant coral fragments (high coral abundance in Fig. 3.5), mostly located below 450 cm core depth (Fig. 3.5B). In contrast, only 36% of the core's length corresponds to more dispersed but still abundant coral fragments (medium coral abundance in Fig. 3.5) and 2% to sediments with scattered corals (low coral abundance in Fig. 3.5).

CT scanning revealed that coral content in this core varies from 2.9 to 29.3 vol.% with an average value of 14.7±4 vol.% (Fig. 3.5). This core displays a similar range of values to those of MD13-3469G, yet coral vol.% values in MD13-3470G are less variable. When comparing visually characterised coral fragment abundance and CT-derived coral vol.% in this core, there is not such an evident correlation as in MD13-3469G. The combination of visual and CT-based analy-

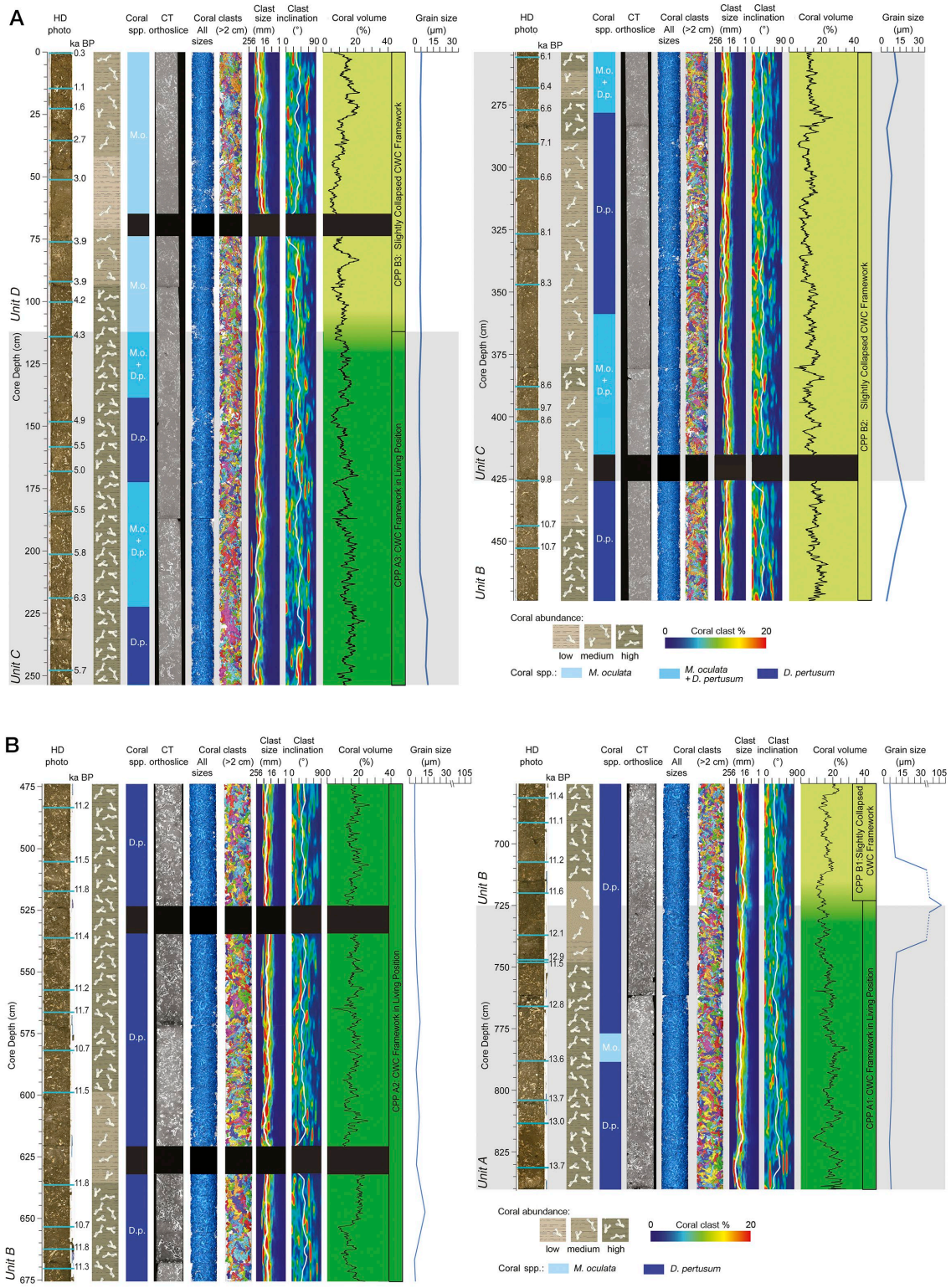

Figure 3.5. Log of the MD13-3470G core (A: 0–474 cm, B: 474–840 cm core depth). From left to right: core HD photo with location of the coral samples acquired for uranium series dating (blue lines) and the corresponding ages; stratigraphic representation of coral abundance; changes in the dominating species conforming the coral deposits; raw image of the core CT scans; 3D image of the CT scans including all segmented coral clasts; 3D image of the CT scan including coral clasts >2 cm; coral clast size distribution (white line: mean clast size); coral clast inclination (white line: mean clast inclination); coral volume per slice (200 mm) overprinted on the coral preservation pattern (CPP A-dark green: coral frameworks buried in living position; CPP B-light green: slightly collapsed coral framework). This figure can be found in supplementary material as four high resolution panels.

ses suggests that the predominant species forming the coral deposits is the framework-building coral *D. pertusum*. This core only contains two coral species that are abundant throughout its length: *D. pertusum* and *M. oculata* (Fig. 3.5). A gradual change from *D. pertusum* to *M. oculata*

dominated facies can be clearly observed towards the top of the core (Figs. 3.3A, 3.5). The CT scan analyses also allowed to identify two CPPs: deposits containing coral framework buried in living position (CPP A), which dominate in the lower part of the core, and slightly collapsed coral framework (CPP B), defined by the same clast size and inclination values as in section 4.1.1, dominating the upper portion of the core. In contrast to MD13-3469G, no unconformities in coral mound evolution are observed throughout this core.

Average sediment grain size along the core oscillates between 3.7 (i.e. clay) and 105 mm (i.e. very fine sand) and displays an average value of 8.8±14.9 mm (i.e. fine silt) (Fig. 3.5). Grain size values are relatively constant throughout the core with only two peaks of 105 mm and 20 mm (i.e. medium silt) occurring at 723 and 435 cm core depth respectively (Fig. 3.5).

As for MD13-3469G, MD13-3470G has been divided into 4 different units according to a combination of coral ages, mound ARs and the main sedimentological features, facilitating the description of the change in coral species, CPPs and mound formation stages (Fig. 3.5):

Unit A (840–723 cm) – The coral deposits in this unit are characterised by the presence of coral frameworks buried in living position (CPP A1: 840–723 cm; Fig. 3.5B). The coral fragments in the lowermost part of the core (840–723 cm) consist predominantly of *D. pertusum*, except for a short section going from 788 to 776 cm, where *M. oculata* dominates (Fig. 3.5B).

Unit B (725–425 cm) – This unit mainly consists of coral framework buried in living position (CPP A2: 675–474 cm) bounded by shorter sections of slightly collapsed coral framework in the lowermost and uppermost parts of the unit (CPP B1:723–675 cm, CPP B2:474–254 cm; Fig. 3.5). Coral fragments in this unit are dominated by *D. pertusum* (Fig. 3.5).

Unit C (425–113 cm) – This unit is characterised by the presence of slightly collapsed coral framework at the base (CPP B2: 474–254 cm) and coral framework buried in living position at the top (CPP A3: 254–113 cm; Fig. 3.5A). Between 415 and 359 cm a mix of *D. pertusum* and *M. oculata* occurs (Fig. 3-5A). Between 359 and 113 cm core depth the coral facies are composed of *D. pertusum* (359–278 cm, 254–223 cm, 173–139 cm) and a mix between *D. pertusum* and *M. oculata* (278–254 cm, 223–173 cm, 139–113 cm).

Unit D (113–0 cm) – The uppermost section of the core (113–0 cm), displays coral facies completely dominated by *M. oculata* (Fig. 3.5A) in the form of slightly collapsed coral framework (CPP B3:113–0 cm; Fig. 3.5A).

3.5.2.2. *Mound development*

The age model of core MD13-3470G is based on 51 coral samples that were U-Th dated, with ages ranging from 14.4 to 0.3 ka BP (Fig. 3.6A, Tables S3.1, S3.2). From these samples, 5 (1%) correspond to the B/A interstadial, 24 (47%) to the Early Holocene, 13 (26%) to the Mid Holocene and 8 (16%) to the Late Holocene (Fig. 3.6A). Although the U-Th dating shows that mound development in this core is almost continuous, four main periods with varying mound formation rates can be identified (Fig. 3.6A).

The first mound formation phase falls within the B/A interstadial and corresponds to Unit A. It extends from 13.69 to 12.8 ka BP and presents an AR of 91 cm kyr^{-1}. At 723 cm, coincident

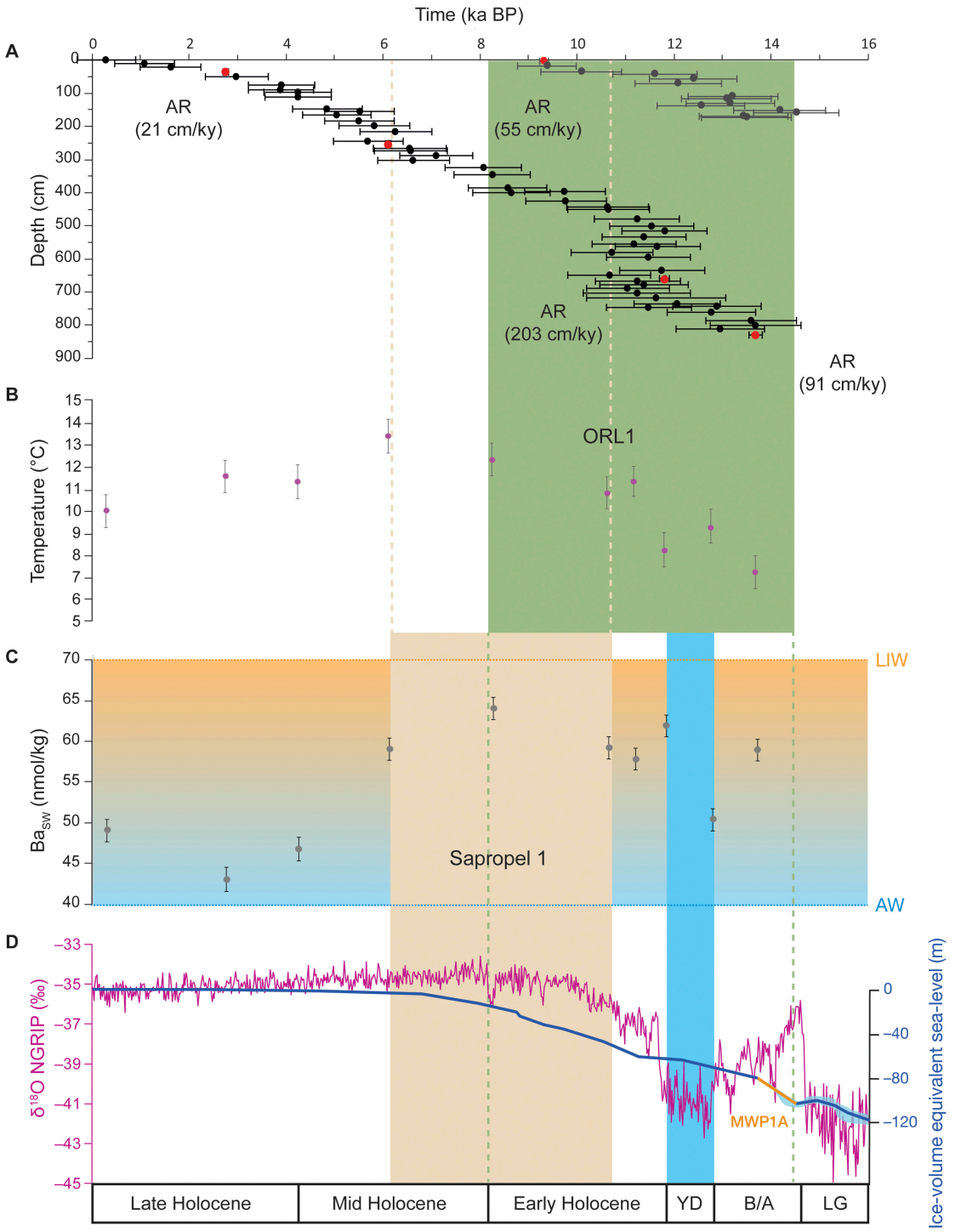

Figure 3.6. (A) MD13-3470G uranium series coral ages (black dots: laser ablation, red dots: solution) against core depth with aggradation rates (ARs) of each coral mound formation period. The blue bar indicates the duration of the Younger Dryas (YD) period; the brown and green rectangles indicate the dates of Sapropel event 1 (S1) and the Organic Rich Layer 1 (ORL1) in the Eastern and Western Mediterranean Sea respectively (Ziegler et al. 2010; Rohling et al., 2015). (B) Li/Mg derived Bottom Water Temperatures (BTWs), (C) Ba/Ca derived Ba_{sw} values and (D) NGRIP $\delta^{18}O$ (‰ SMOW) data for the last 16 ka (North Greenland Ice Core Project members, 2004) and ice-volume equivalent sea-level from Lambeck et al. (2014). B/A: Bølling Allerød; LG: Last Glacial. The green and blue dotted lines indicate the present-day Ba_{sw} values of Atlantic (AW) and Levantine Intermediate (LIW) water masses.

with the grainsize maxima and the change between CPP A1 and CPP B1, a short coral mound stagnation period synchronous with the YD, occurs (Figs. 3.5B, 3.6). With the onset of the Early Holocene, the fastest mound growth period observed in this study occurs (11.8–10.7 ka BP), with an AR of 203 cm kyr^{-1} and corresponding to Unit B (Figs. 3.5, 3.6A). During the rest of

the Early Holocene and until the start of the Late Holocene, which coincides with Unit C, the coral mound keeps growing but at a slower pace (10.7–3.8 ka BP, AR = 55 cm kyr^{-1}). In the Late Holocene, from 3.8 to 0.29 ka BP and corresponding with Unit D, the AR of the mound is even slower (AR = 21 cm kyr^{-1}; Fig. 3.6A). This matches with a change in the coral species forming the CWC deposits, which start to be entirely dominated by *M. oculata*.

3.5.2.3. *Paleo-environmental proxies*

The Li/Mg ratios for the core MD13-3470G range between 2.8 and 3.8 mmol mol^{-1} and the corresponding SWTs show values between 7.2±0.7 and 13.4±0.8°C (Fig. 3.6B; Table S3.5). They exhibit a warming trend from the B/A interstadial until the Mid Holocene (6.1 ka BP), where the SWT reaches 13.4°C. After that age, SWTs start decreasing again until modern times (0.3 ka BP–10±0.7°C). The fastest mound growth in this core occurs when the SWTs are between 8 and 11°C (Fig. 3.6B), a potentially optimal temperature range similar to that observed in the southern CMP (i.e. core MD13-3469G).

Coral Ba/Ca values range from 9.1 to 12.5 mmol mol^{-1}, which results in a range of 43.1±1.4 to 63.6±1.3 nmol kg^{-1} Ba_{SW} (Fig. 3.6C; Table S3.5). All the samples recorded Ba_{SW} within the present range in the Mediterranean (Roy-Barman et al., 2019). Two of the highest Ba_{SW} values correspond with the B/A interstadial (13.69 ka BP) and the end of the YD (11.8 ka BP). Another Ba_{SW} maximum takes place in the transition from the Early Holocene to the Mid Holocene (8.3 ka BP), from which the values show a decreasing trend towards the present (Fig. 3.6C). Finally, the highest ARs observed in this core occur when Ba_{SW} values range between ~58 and 62 nmol kg^{-1}.

3.6. Discussion

Although the present-day distribution of living scleractinian CWCs in the Mediterranean Sea is mainly confined to submarine canyons and cliffs (Orejas et al., 2009; Fabri et al., 2017; Taviani et al., 2017; Titschack, 2019), the occurrence of multiple coral mound structures in the Alboran Sea and, to a minor extent, in the central Mediterranean suggests that there have been periods in the past when favourable environmental conditions supported the long-term formation of CWC reefs (Remia and Taviani, 2005; Martorelli et al., 2011; Fink et al., 2013; Lo Iacono et al., 2014, 2016; Corbera et al., 2019). Nonetheless, not much is known about the evolution of these geological features during the Pleistocene. For instance, even though most of the Alboran Sea coral mounds are considerably tall (i.e. >70 m in height), so far only the uppermost and thus the most recent development of the mounds has been described (Fink et al., 2013, 2015; Stalder et al., 2018; Wang et al., 2019). Particularly, the WMM and EMM have been studied intensively, with ~80 coral ages from ~7 mounds presented so far (Fink et al., 2013, 2015; Titschack et al., 2016; Wang et al., 2019; Wienberg, 2019). However, due to the lack of cores encompassing longer periods, most of the research has focussed on the coral mound development since the Last Glacial Maximum (Fink et al., 2013; Stalder et al., 2018; Wang et al., 2019). In this study we are able to expand that time frame by >390 kyr, bringing unprecedented insights into the evolution of CWC mounds in the Alboran Sea.

One of the main findings of this study is the large age difference in mound formation intervals between the south and north CMP cores (i.e. MD13-3469G and MD13-3470G), with the former encompassing from >390 until 9.3 ka BP and the latter from 14.4 to 0.3 ka BP (Figs. 3.4A, 3.6A). Furthermore, the cores present overlapping mound growth periods from the B/A until

the Early Holocene, allowing for a continuous tracking of CMP evolution since the middle Pleistocene. Considering that the gravity cores retrieved 10.4 and 8.4 m of coral-bearing sediments in areas where the coral mounds were up to 50–60 m in height, only the most recent developmental stages of the mound could be elucidated in this study. The modern age of the uppermost corals dated in the northern CMP and the concurrent stagnation of its southern counterpart reflect the current state of the habitats observed on the coral mounds summit, which display living CWCs reefs on the northernmost sector and dead CWC frameworks on the southernmost mound (Corbera et al., 2019).

3.6.1. Coral mound development during the Middle and Late Pleistocene

Throughout the Middle and Late Pleistocene (773–14.7 ka BP; Core MD13-3469G Units A, B, C, D, E), mound growth periods in the CMP generally occurred during temperate interstadials (i.e. MIS 9c, 7a and 5c), but with quite low ARs (4–23 cm kyr^{-1}; Fig. 3.4A). No mound formation is observed during glacial periods, with the exception of MIS 6 glacial, which presents the lowest ARs observed in this study (3.5 cm kyr^{-1}; Fig. 3.4A). The absence of growth during MIS 8 and MIS 2–4 glacials is represented in the core record as hiatuses in coral mound development, that lasted up to ~98 kyr.

During the Middle Pleistocene (773–126 ka BP; Core MD13-3469G Units A, B, C, D), the first coral ages (Unit A-B: 588–373 ka BP) and the CPPs in which they are found, suggest an extremely slow mound formation stage and could be the result of either particularly limited coral growth and/or erosional processes that altered part of the mound development stratigraphic record. This would match with what has been observed in the CT-scans, which display sediments with mostly unidentifiable scattered bioclasts, coral rubble deposits (CPP D1, C1) and an unconformity (Fig. 3.2B).

The following mound growth stage (Unit B: 352–306 ka BP; Fig. 3.4A) started after a period of stagnation corresponding to MIS 10 glacial and displays an average AR of 4 cm kyr^{-1}. The older and less preserved coral deposits of this mound development period (CPP D2, D3, D4 and CPP C2, C3), which are separated by unconformities, indicate an intermittent mound formation stage marked by a gradual change in the taxonomic composition of the coral clasts, from facies formed by *D. pertusum*, *M. oculata* and *D. dianthus* to a *D. cornigera* dominated one (Figs. 3.2B, 3.3B). Although no relevant changes in terms of SWTs or Ba/Ca are observed during this period, the change in the dominating species could be related to the presence of unfavourable environmental conditions for the growth of *D. pertusum* and *M. oculata* during MIS 9. Dendrophyllid corals are known to withstand a wider range of environmental conditions, including higher temperatures and turbidity values (Naumann et al., 2013; Gori et al., 2014, 2015; Castellan et al., 2019). Furthermore, these corals used to dominate the Mediterranean coral communities before the Plio-Pleistocene transition, when less marked glacial-interglacial cycles occurred and the temperatures were higher (Vertino et al., 2019). Currently, dendrophyllid corals form assemblages in the warm and oligotrophic Eastern Mediterranean Basin (Orejas et al., 2019 and references therein), where the high temperature and salinity values of Levantine waters (i.e. 13.9–17.3°C and 38.8–39.1) prevent *D. pertusum* and *M. oculata* from proliferating. It is important to remark that the presence of a mound formation unit dominated by dendrophyllids has never been observed before on a submerged coral mound. However, the available data is not enough to completely describe the environmental setting in which this 110 cm long section formed. In the younger period of this mound formation stage (741–680 cm core depth), the species composi-

tion changes back to a *D. pertusum* dominated facies, which represents the main constituent of the Cabliers coral framework. This remains generally constant for the rest of the mound's evolution, although variations are observed in the accompanying taxa (e.g. *M. oculata* and *D. dianthus*; Fig. 3.2). This mound formation phase is followed by a coral mound stagnation period of ~98 kyr that encompasses the MIS 9a-b, MIS 8 and MIS 7d-e (Figs. 3.2B, 3.4A).

The absence of coral growth throughout MIS 7d stadial (Fig. 3.4A) might be related to a drastic sea-level and temperature decrease, that could have promoted variations in the surface circulation of the Alboran Sea (Vargas-Yáñez et al., 2002; Lo Iacono et al., 2014), probably affecting upwelling processes and thus primary productivity. Towards the second half of MIS 7, when the temperatures and sea-level rose again, coral mound formation occurred (Unit C: 207–192 ka BP). Yet, it was characterised by the presence of scattered corals fragments within the matrix sediments (CPP D5), coral rubble deposits (CPP C5) and two unconformities, which indicates this was not a thriving mound formation period, as confirmed by its low AR of 5 cm kyr^{-1} (Figs. 3.2B, 3.4A).

After a short stagnation stage of ~24 kyr matching with the start of MIS 6 glacial, the last mound growth period of the Middle Pleistocene started (Unit D: 168–127 ka BP; Fig. 3.4A). However most of the ages cluster towards the end of the MIS 6, between 150–127 ka BP. The low SWTs observed during this period (<6.5°C; Fig. 3.4C) confirm these samples grew during a cold interval. Although observing coral growth in a glacial setting does not fit with the general pattern of this mound's development, coral deposits corresponding to this period are only formed by *D. pertusum* (Fig. 3.2), demonstrating the higher capability of this species to cope with temperatures <7°C (Nauman et al., 2014). In addition, the presence of coral rubble (CPP C5), Fe-Mn coated corals and one unconformity suggests that the southern CMP mound did not develop under flourishing conditions during MIS 6 (Fig. 3.2B). Instead, the low AR (3.5 cm kyr^{-1}) indicates sporadic coral growth events, but without enough reef growth to promote significant mound formation. The unconformity observed during this period (561–551 cm, 143–129 ka BP; Figs. 3.2B, 3.3C) is defined by the occurrence of abundant and closely-packed parallel bivalve shells, some of them still displaying both of the valves, which indicates an in-situ ecological aggregation undergoing limited transport by moderate bottom currents (Kidwell and Holland, 1991; Hauser et al., 2008). The presence of thriving bivalve populations within CWC reefs has been described in many Atlantic coral mound provinces, which display, among other species, abundant individuals of the genus *Acesta* (Hovland & Mortensen 1999; Buhl Mortensen et al., 2016). The unidentified bivalve facies observed here is placed between coral ages ranging from 143 to 129 ka BP, thus indicating that it could correspond to an interval of cold conditions related to the end of MIS 6. Bivalve assemblages are known to thrive in the Mediterranean during glacial periods (Colantoni, 1973; Taviani and Colantoni, 1979; Bouchet and Taviani 1992; López-Correa et al., 2006), thus they might have replaced coral assemblages during this colder phase of MIS 6.

During the Late Pleistocene (126–14.7 ka BP), coral mound growth only occurred during MIS 5c (Unit E: 99–87 ka BP) and it was preceded by a 29 kyr long mound stagnation period (Fig. 3.4A). Excluding MIS 5e, when the sea-level was significantly higher, the absence of corals during the rest of MIS 5 cannot be attributed to this factor. The only exception would occur during MIS 5a, as some evidences in the Mediterranean Sea indicate the presence of a sea-level highstand characterised by rapid changes, which raised 1 m above the current sea-level (Dorale et al., 2010). Throughout MIS 5b-d, other environmental variables (e.g. primary productivity, dissolved oxygen, water mass circulation) might have played a relevant role limiting coral

mound formation. The mound formation phase that occurred during MIS 5c is characterised by the presence of slightly collapsed coral framework deposits (CPP B2), followed by coral framework in living position (CPP A1), and corresponds with higher ARs (25 cm kyr^{-1}) than those observed during the Middle Pleistocene (<5 cm kyr^{-1}). The SWTs and the Ba_{SW} values registered by corals during this time span do not show significant differences from those observed in previous mound formation phases (Fig. 3.4C, D), which means that other environmental variables might have had a greater effect on promoting a higher pace of mound growth. One of them could be food supply related to surface productivity, which has previously been regarded as a key variable affecting the development of several coral mounds, including the WMM and EMM provinces, located a few kilometres south of the CMP (Fink et al., 2013; Wang et al., 2019).

3.6.2. Coral mound development from the Bølling-Allerød to the present-day

Both MD13-3469G (Unit F) and MD13-3470G (Unit A, B) cores, collected respectively from the southern and northern sectors of the CMP, exhibit pronounced coral mound formation during the B/A interstadial and the Early Holocene (Figs. 3.4B, 3.6A), as observed in the Melilla coral mound provinces (Fink et al., 2013; Wang et al., 2019). Mound formation started just after the Melt Water Pulse-1A (MWP-1A), which supposed a sea-level increase of 20 m in ~500 years. With the continuous sea-level increase, growth on the southern mound stopped at 9.3 ka BP, while the shallower mound located at the northernmost region of the CMP is still growing in the present day (Corbera et al., 2019). Similar to what has been observed in the Pleistocene and given the uncertainty of the U-Th solution ages, if we assume a continuous stratigraphic record, our data suggests that mound formation did not occur during the cold stadial interval of the YD (12.8–11.8 ka BP). This fits again with what has been observed in other Alboran Sea coral mounds (Fink et al., 2015; Wang et al., 2019). In Fink et al. (2015) the authors speculate that the absence of coral growth during the YD could be the result of a change in the Alboran Sea water mass circulation, affecting the stability of the WAG and EAG, thus limiting the formation of upwelling regions and ultimately surface productivity. Nonetheless, the Ba/Al increase observed in sediment cores from other studies point to an enhanced productivity during this period (Jiménez-Espejo et al., 2015; Martinez-Ruiz et al., 2015), which is also reported in the diatom record from the Alboran Sea (Barcena et al., 2001). Jiménez-Espejo et al. (2015) and Martinez-Ruiz et al. (2015) also reported lower oxygenation throughout the YD, a factor that might have also affected coral growth during this cold period. The absence of growth during the YD also matches with a drastic grain size increase registered in core MD13-3470G (i.e. from fine silt to very fine sand; Fig. 3.5B). Fink et al. (2013) and Wang et al. (2019), also described increased sediment grain size related to intense hydrodynamic conditions during this cold stadial, yet with considerably lower values (~15–27 mm) than the ones observed in the northern CMP (105 mm). Although we measured total sediment instead of just measuring the siliciclastic fraction, the temporal correspondence of the grain size peak observed in this study with the one observed in Fink et al. (2013) and Wang et al. (2019) suggests that it could be related to an overall intensification of the currents associated to the upper layer of the LIW.

Following the YD period, mound development restarted simultaneously in both CMP regions with the onset of the Early Holocene. At the southern sector, this last mound formation period (i.e. Unit F: 12.1–9.3 ka BP) exhibited an AR of 24 cm kyr^{-1}, which occurred before the mound entered in a stagnation stage until the present day (Fig. 3.4B). This AR value is considerably lower than the rates observed at the WMM (75–107 cm kyr^{-1}) and EMM (140–291 cm kyr^{-1}) during the Early Holocene (Fink et al., 2013; Stalder et al., 2015; Wang et al., 2019). Yet, the low

AR during the most recent development of the southern CMP matches with the prevalence of *M. oculata* over *D. pertusum* in the coral deposits, which presumably has a lower capability to form mounds due to it thinly branched and more fragile skeleton (Fig. 3.2A; Wienberg, 2019). During the same period, the northernmost region of the CMP presents a flourishing growth phase from the onset of the Early Holocene (i.e. 11.8 ka BP) until 10.7 ka BP (Unit B), with an AR of 203 cm kyr^{-1} and a 280 cm thick coral deposit, formed by *D. pertusum* framework preserved in living position (CPP A2; Figs. 3.5, 3.6A). This high AR is within the values observed in the EMM and is comparable to the rates observed in the thriving Northeast Atlantic mounds (Titschack et al., 2015).

After 10.7 ka BP the coral deposits in the northern CMP mound gradually changed from *D. pertusum* to *M. oculata* dominated facies, which also translated into a continuous decrease of the ARs until the present-day (Figs. 3.5A, 3.6A). From 10.7 to 3.9 ka BP (Unit C-D) the AR decreased to 56 cm kyr^{-1}, which is within the range of ARs observed on the WMM during this period (12–107 cm kyr^{-1}) (Wang et al., 2019). Furthermore, whereas no mound growth is observed on the WMM or EMM from 3.8 ka BP to the present-day, the northern region of the CMP continued to develop at a very slow pace (Unit D: 22 cm kyr^{-1}), almost exclusively sustained by the growth of *M. oculata*. Such change in species composition throughout the Holocene has been observed in other Alboran Sea coral mounds (Stalder et al., 2015; Wienberg, 2019) and is apparent in the current living CWC assemblages found in the Mediterranean Sea, which are dominated by *M. oculata* interspersed with some colonies of *D. pertusum* (Orejas et al., 2009; Taviani et al., 2017; Corbera et al., 2019). It is hard to exactly determine the environmental trigger of this change in species dominance throughout the Holocene, yet it is likely that rising SWTs towards the Mid Holocene combined with lower food supply, coinciding with the end of Organic Rich Layer 1 (ORL1; western Mediterranean equivalent of sapropels), might have had detrimental effects for the proliferation of *D. pertusum* (Martrat et al., 2004; Fink et al., 2013; Wang et al., 2019). In contrast, *M. oculata*, which is known to withstand higher temperatures and unstable conditions (Naumann et al., 2014), might have been able to cope with these drastic environmental changes.

Besides coral growth, persistent sediment sources are needed for coral mound development, since it stabilises the coral framework, preventing it from collapsing and thus promoting a fast mound formation (Wienberg and Titschack, 2017). Hence, besides the lower capability of *M. oculata* to form mounds (Wienberg, 2019), the decreased ARs observed during the Mid and Late Holocene could also be caused by a decreased sediment supply after the end of the sea-level rise (Church et al., 2008; Vacchi et al., 2016). This hypothesis is consistent with decreasing regional Ba_{SW} values at our site since the end of the last deglaciation (Fig. 3.6C), a pattern that might have been driven by either a reduction of riverine run-off in the Alboran Sea or by a reduced amount of suspended particles being transported by intermediate waters.

While the Pleistocene stages of any Mediterranean coral mound have not been described so far, the development of the CMP during deglacials and temperate interstadials seems to occur before that of the Irish and Norwegian coral mounds. The latter solely develop during interglacials (Roberts et al., 2006; Kano et al., 2007; Frank et al., 2011; de Haas et al., 2009; Thierens et al., 2010), when the ice-sheets retreat and the polar front moves northwards, enhancing the flow of cold nutrient-rich waters onto the continental shelves (Frank et al., 2011; Titschack et al., 2015). In contrast, the coral mounds of the adjacent Gulf of Cadiz, the closest mound region to the Alboran Sea, show an opposite evolution pattern during the Pleistocene, with

mound growth occurring almost exclusively during glacial periods (Wienberg et al., 2010; Vandorpe et al., 2017). This is due to the oceanographic configuration of the Gulf of Cadiz, which promotes enhanced surface productivity during glacial periods owed to a strengthened upwelling along the Azores front and intensified eolian dust transport, providing a sufficient food supply for the development of the mounds (Bertrand et al., 1996; Volkov and Fu, 2010; Wienberg et al., 2010).

On the other hand, the contrasting mound formation rates observed during the Holocene and the present-day differences in living coral abundance between northern and southern CMP (Corbera et al., 2019) suggest that the latter has generally been exposed to less suitable environmental conditions for coral mound formation. This also applies when comparing the southern CMP mound development (417 m water depth) to that of the WMM and EMM (251–379 m water depth; Fink et al., 2013; Stalder et al., 2015; Wang et al., 2019). The distinct paleo-evolution of the mounds within the CMP and the fact that its northernmost mound still manages to thrive while all coral mounds in the Alboran Sea are in a stage of decline, reflects the paramount role of this coral mound province within the Mediterranean Basin.

3.6.3. Local environmental variables and regional paleo-climatic events controlling the development of the Cabliers Coral Mound Province

The fastest ARs of the CMP occurred during periods when the SWTs ranged between ~7–11°C (Figs. 3.4, 3.6), fitting within the known temperature range tolerated by *D. pertusum* and *M. oculata* (4–13°C; Roberts et al., 2006). Ba/Ca values observed in this study (7.7–16.9 mmols mol^{-1}; Table S3.5) match with the ones observed in Norwegian coral mounds, generally ranging between 8 and 20 mmols mol^{-1} (Raddatz et al., 2016). The high Ba_{SW} values associated to mound growth during deglacials (>70 nmol kg^{-1}; Fig. 3.4D) could be explained by a combination of increased LIW influence at the site and enhanced riverine input derived from the Atlas glaciers melting into the Moulouya river (Hughes et al., 2011). The latter ends directly south of the CMP, most probably increasing particulate and thus dissolved Ba in the region. This would match with what has been observed in previous studies, where increased Ba_{SW} has been suspected to be associated with enhanced riverine input (Raddatz et al., 2016). On the other hand, Ba_{SW} observed during mound formation occurring in temperate interstadials (~35–55 nmol kg^{-1}; Fig. 3.4D) correspond with present-day values closer to those of the AW (Jacquet et al., 2016; Jullion et al., 2017; Roy-Barman et al., 2019). Despite the mound's summit is too deep to be bathed by the former water mass vertical mixing processes, such as downwelling and/or internal waves (Oguz et al., 2014; Van Haren et al., 2014), may have brought shallower waters down to the mound during the examined interstadial periods, thus reducing the amount of Ba_{SW} around the growing corals.

The most pronounced mound formation stages of the CMP occurred during deglacials and temperate interstadials, but not during glacials (Figs. 3.4, 3.6). During warm periods, a larger amount of AW flows into the Mediterranean basin through the Strait of Gibraltar due to high sea-levels (Sierro et al., 2005). The higher inflow of AW together with enhanced freshwater input derived from continental melt-waters causes a reduction of the surface water salinity, thus promoting stratification of the water column and a far less evident formation of WMDW in the Gulf of Lion (Rogerson et al., 2008; Toucanne et al., 2012). This leads to a slowdown of the Mediterranean thermohaline circulation (Rogerson et al., 2008; Toucanne et al., 2012; Stumpf et al., 2010) and a simultaneous reduction of LIW formation in the Eastern Mediterranean basin (Toucanne et al., 2012; Jiménez-Espejo et al., 2015). Nonetheless, the high values of our

Ba_{sw} data towards the transition into warmer periods (Fig. 3.4D) is indicative of an increased influence of the LIW at the coral site, most likely driven by the sea-level rise. These findings coincide with observations of Taviani et al. (2017), who suggested an evident positive impact of the LIW on Mediterranean CWC communities, since currently all thriving CWC assemblages are found within the depths bathed by this water mass (Orejas et al., 2009; Fabri et al., 2017; Taviani et al., 2017; Corbera et al., 2019; Lo Iacono et al., 2019). Furthermore, the structure of the water column in the Alboran Sea displays a water mass interface between AW and LIW at an average depth of 200 m. Water mass interfaces are known to accumulate particulate matter, mainly consisting of plankton (McManus et al., 2003; Mienis et al., 2007). The interaction between two water masses might promote the creation of internal waves, which propagate along the interface, increasing sediment resuspension and vertical mixing, which could promote increased transfer of organic matter to deeper regions (Davies et al., 2009; White and Dorschel, 2010; Van Haren, 2014). Internal waves have been observed in the Alboran Sea at 250 m water depth with an amplitude of up to 90 m, reaching down to 300 m water depth (Van Haren, 2014). During deglacials and temperate interstadials the AW-LIW interface was closer to the southern CMP mound summit, which combined with the potential presence of internal waves might have contributed to provide enough food supply to promote mound formation.

Although LIW influence on the mounds increases during warm periods, Toucanne et al. (2012) reported that its flow intensity fluctuates following Milankovitch cycles. During insolation maxima, North African monsoons migrate northwards, which results in higher precipitation over the Nile watershed and the North African fossil drainage system (Rohling et al., 2002, 2004; Osborne et al., 2010). This causes an increase in nutrient-rich freshwater inflow, particularly to the Eastern Mediterranean Basin, that promotes a strong stratification of the water column, enhanced primary productivity and reduced deep-water ventilation, which in turn trigger the deposition of sapropels (i.e. bands of organic-rich sediments; Capotondi et al., 2011; Grant et al., 2016; Wu et al., 2018). The water column stratification in the Eastern Mediterranean basin caused during sapropel events triggers a collapse in the LIW's formation (Filippidi et al., 2016), which translates into a reduced circulation of this water mass in the West Mediterranean Basin and ultimately in the Strait of Gibraltar (Toucanne et al 2012; Bahr et al., 2015). Additionally, the water mass bathing the mounds would present lower oxygen levels due to the reduced ventilation characteristic of sapropel events in the Eastern Mediterranean Basin (Grant et al., 2016), and this could have had detrimental effects for coral growth. Indeed, these events are remarkably concurrent with periods of coral demise in the CMP, at least since the age of Sapropel 7 (Fig. 3.4A). The decreased flow of LIW in the Alboran Sea during sapropel depositions might have also altered somehow the structure of the interface between Atlantic and Mediterranean water masses, affecting the accumulation of organic matter and thus the food delivery to the mounds. Sapropel deposition has already been reported to have detrimental effects on CWC growth in the Eastern Mediterranean (Fink et al., 2015; Taviani et al., 2019), but clear evidence here supports a negative impact of these paleo-climatic events on coral mound formation in the westernmost Mediterranean as well, thousands of km away from the main region where they occur. Nevertheless, to formulate robust hypotheses on the effects of cyclic regional climatic changes on the development of coral mounds in the Mediterranean Sea, more coral-bearing cores of Pleistocene age from different regions of the basin should be acquired.

The differences in mound formation patterns between the northern (313 m water depth) and the southern (417 m water depth) CMP during the Holocene might be related to the vertical distance of the mounds' summits to the AW-LIW interface. With the last sea-level rise, a shal-

lower AW-LIW interface might have prevented the southern mound from receiving enough food supply for coral sustainment. The shoaling of the interface (currently at ~200 m), together with the onset of the S1 deposition, which supposed a decrease in LIW formation, might have contributed to the demise of the southern CMP at ~ 9.3 ka BP (Fig. 4B). In contrast, the northern CMP underwent a particularly flourishing period during the Early Holocene, after which it continued to grow until the present day, albeit at a slower pace (Fig. 3.6A). The combination of suitable environmental conditions making this region unique in the entire Mediterranean during the Early Holocene, most likely included appropriate depth of the AW-LIW interface caused by sea-level changes, intensified productivity throughout the ORL1 deposition and high sediment input during deglaciation (Cacho et al., 2002; Lo Iacono et al., 2014; Fink et al., 2013; Wang et al., 2019). Overall, the present-day local oceanographic conditions, involving the jet of highly productive Atlantic waters, the action of internal waves and the presence of a downwelling region directly above the CMP (Oguz et al., 2014; Van Haren, 2014), which might have been present since the end of the sea-level rise around 7 ka BP, have most likely been crucial to sustain the CWC communities of its northernmost sector, after the rest of the Alboran Sea coral mounds entered in a stage of stagnation (Fink et al., 2013; Stalder et al., 2015; Wang et al., 2019).

3.7. Conclusions

In this study, we acquired 110 U-Th coral ages encompassing a period from the Middle Pleistocene to the present-day, which contributed to describe the development of two coral mounds located on opposite ends of the CMP (Alboran Sea-Western Mediterranean) and to expand our knowledge of coral mound development in the Mediterranean Sea beyond 50 ka BP back to the Calabrian stage. We conclude that:

The fastest mound growth of the CMP occurred during deglacials and temperate interstadials, when sea-level changes placed the AW-LIW interface close enough to the mound's summit, probably enhancing food supply to the corals.

Our data support a detrimental influence of Sapropel derived events, such as an interruption in LIW formation, on coral mound development in the Western Mediterranean Sea.

The change from *D. pertusum* to *M. oculata* dominated coral deposits during the Holocene seems to have occurred at increasing seawater temperatures, and preceding periods of decreased food supply caused by the sea-level rise that placed the AW-LIW interface further away from the mounds.

The high ARs and present flourishing state of the northern CMP mound makes it the most thriving CWC mound currently known in the Mediterranean Sea.

Overall, the lower ARs and higher number of hiatuses observed in the southern CMP indicate that this sector is subjected to less favourable environmental conditions for mound formation than its northernmost counterpart. This is probably caused by the greater distance of this mound's summit to the AW-LIW interface.

Contrasting mound development patterns between north and south CMP yield important insights on how local changes in oceanographic conditions can have crucial implications on coral mound formation.

3.8. Acknowledgements

Guillem Corbera is funded by the Graduate School of the National Oceanography Centre Southampton (GSNOCS), with the collaboration of the NGO OCEANA. We are grateful for the ship time provided by IPEV on the R/V Marion Dufresne within the framework of the EuroFLEETS GATEWAY project (Grant Agreement 228344) and we acknowledge all the participants and crew of the GATEWAY Cruise for their professional work during the expedition. We appreciate the help provided by Suzanne MacLachlan and the British Ocean Sediment Core Research Facility (BOSCORF) team during sampling. We acknowledge Andy Milton and Mathew Cooper for their analytical help. We are grateful to Laura Robinson for supplying the VS001/1-A aragonite standard. We are also grateful for the help provided by Heather Goring-Harford.

Chapter 4

Glacial-aged development of the Tunisian Coral Mound Province controlled by glacio-eustatic oscillations and changes in surface productivity

This chapter is a reproduction of the text submitted to the journal *Marine Geology* as **Corbera, G.**, Lo Iacono, C., Standish, C.D., Gràcia, E., Ranero, C., Huvenne, V.A.I., Anagnostou, E., Foster, G.L. Glacial-aged development of the Tunisian Coral Mound Province controlled by glacio-eustatic oscillations and changes in surface productivity.

Author contributions: Corbera, G., Lo Iacono, C., Huvenne, V.A.I., Foster, G.L. and Anagnostou, E. conceptualised the chapter. Lo Iacono, C., Gràcia, E. and Ranero, C. collected the gravity cores. Corbera, G., Standish, C.D. and Anagnostou, E. acquired and analysed the data. Corbera, G. wrote the manuscript and all authors reviewed and commented on it.

4.1. Abstract

Cold-water corals (CWC) are key species of benthic ecosystems, sensitive to changes in climate and capable of recording them in the chemical composition of their skeletons. The study of CWC mound development in relation to palaeoceanographic variations during the Pleistocene and Holocene stages in the Mediterranean Sea has mainly been focussed in the Alboran Sea (Western Mediterranean). The present study describes the coral deposits and corresponding ages of 3 gravity cores, acquired from the newly discovered Tunisian Coral Mound Province (Central Mediterranean), which comprises several ridge-like mounds. All the cores acquired displayed dense coral deposits, dominated by *Desmophyllum pertusum* fragments embedded within a muddy sediment matrix. Overall, 64 coral samples have been dated through U-Th laser ablation MC-ICP-MS, revealing mostly Pleistocene corals with mound formation phases ranging from ~424 ka BP to ~8.4 ka BP. The main coral mound development stages occurred during the last glacial period, an opposite pattern to what has been observed so far in the rest of the Mediterranean Sea. Coral mound formation during the last glacial was most likely caused by a colder sea water temperature than the one observed in the present-day and an increased surface productivity combined with an appropriate depth of the interface between Atlantic Waters and Levantine Intermediate Waters. The combination of the data acquired here with that of previous mound formation studies from the Alboran Sea also suggests that CWC mounds located at greater depths develop at slower rates than those found in shallower settings.

4.2. Introduction

Scleractinian cold-water corals (hereafter referred as CWCs) form complex and fragile three-dimensional habitats that enhance the spatial heterogeneity of the seafloor and provide ecological niches for a wide range of species (Henry and Roberts, 2007; Lo Iacono et al., 2018; Price et al., 2019). These biological assemblages are generally found in areas of the continental margins characterised by moderate to strong hydrodynamic regimes, such as submarine canyons, seamounts and ridges (Davies and Guinotte, 2011; Du Preez et al., 2020; Pearman et al., 2020). The strong bottom currents found in these areas provide hard surfaces and enhanced food supply that promote CWC settlement and growth (Fosså et al., 2005; Wheeler et al., 2007). In addition, the physicochemical conditions of the bathing water-mass (e.g. temperature, pH, dissolved oxygen) play a relevant role in controlling CWC survival and growth (Dodds et al., 2007; Maier et al., 2009; Duineveld et al., 2012; Brooke et al., 2013), even though the environmental range tolerated by the corals still needs to be refined.

On geological timescales (i.e. thousands of years) CWC assemblages can develop into large geomorphological build-ups, known as coral mounds (Roberts et al., 2006; Wienberg and Titschack, 2017; Lo Iacono et al., 2018). These features are formed through the combination of intermittent coral growth and sediment supply (Roberts et al., 2006). Under suitable environmental conditions, coral frameworks reduce the bottom current speed, thus stimulating sediment deposition within the reef (Huvenne et al., 2009), which has a critical role in stabilising and allowing mound formation (Hebbeln et al., 2016). Although coral mound development can last from thousands to several millions of years (Kano et al., 2007; Victorero et al., 2016), their formation is not continuous and instead the mound stratigraphic records commonly display hiatuses that correspond to periods of stagnation and/or erosion (Wienberg et al., 2018; Wang et al., 2019; Corbera et al., 2021). In addition, coral skeletons can be dated and their chemical and isotopic composition record the physicochemical changes of the bathing water-masses, making

coral mounds useful archives of paleoclimatic changes (Titschack et al., 2009; Thierens et al., 2013; Thiagarajan et al., 2014; Studer et al., 2018). The combination of U-series to absolutely date corals and the acquisition of geochemical proxies can, therefore, help to highlight the environmental factors driving coral mound formation (Raddatz et al., 2016; Dubois-Dauphin et al., 2019; Wang et al., 2019; Corbera et al., 2021).

In the Mediterranean Sea, scleractinian CWCs are currently close to their ecological limits, regarding water temperature (Brooke et al., 2013). As a consequence, they generally occur in small assemblages, mainly distributed within submarine canyons and on seamounts (Fabri et al., 2014; Taviani et al., 2017; De la Torriente et al., 2018; Lo Iacono et al., 2019). Only a few coral mounds currently host living CWC assemblages: the coral-topped mounds of Santa Maria di Leuca offshore Calabria, Italy (Savini and Corselli 2010), the Corsica Coral Mound Province located in the Corsica Channel (Angeletti et al., 2020), and the exceptionally thriving coral reefs found on the Cabliers Coral Mound Province, in the eastern Alboran Sea (Lo Iacono et al., 2016; Corbera et al., 2019). Nonetheless, the presence of further coral mound clusters in the Alboran Sea (i.e. West and East Melilla Mounds; Comas and Pinheiro, 2010; Fink et al., 2013; Lo Iacono et al., 2014; Hebbeln , 2019) and, to a lesser extent, in the Tyrrhenian (Remia and Taviani, 2005; Angeletti et al., 2020) and the Ionian Seas (Taviani et al., 2005; Martorelli et al., 2011), suggests that at some points in the past, persistent favourable environmental conditions allowed cold-water corals to form large and thriving reefs and mounds in this basin (Fink et al., 2013; Stalder et al., 2018; Wang et al., 2019; Corbera et al., 2021).

Globally, coral mound development generally follows glacial-interglacial cycles, with mound formation occurring either in interglacial (e.g. Irish, Scottish and Norwegian mounds; Kano et al., 2007; Thierens et al., 2010; Frank et al., 2011) or glacial periods (Gulf of Cadiz, Mauritanian and Argentinian mounds; Wienberg et al., 2010; Eisele et al., 2011; Steinmann et al., 2020), depending on the environmental setting of their location. So far, in the Mediterranean Sea coral mound formation has been reported to mainly occur during temperate interstadials and interglacials (Fink et al., 2013, 2015; Stalder et al., 2018; Wang et al., 2019; Corbera et al., 2021). However, available studies in this basin have only described past coral mound development in the Alboran Sea (Westernmost Mediterranean; Fink et al., 2013; Wang et al., 2019; Corbera et al., 2021). According to the latest findings, coral mound formation in this sub-basin has been related to the depth of the interface between the entering Atlantic Water (AW) and the outflowing Levantine Intermediate Water (LIW), currently located at ~200 m water depth (Wang et al 2019; Corbera et al., 2021), where the interaction between different water-masses likely generates internal waves that increase vertical mixing, and thus enhance food supply to deeper areas (Davies et al., 2009; Van Haren, 2014).

The present study describes, by means of U-Th and trace element analyses, the development of three CWC mounds belonging to a recently discovered coral mound province located along the Tunisian continental margin (the Tunisian Coral Mound Province, hereafter referred as TMP; Fig. 4.1; Camafort et al., 2020). The TMP is located off the northern Tunisian coast and west of the Strait of Sicily, the intersection between the Western and Eastern Mediterranean basins (Fig. 4.1). In order to expand our knowledge of the environments role in determining coral mound development in the Mediterranean Sea, we aim to: (1) describe part of the temporal evolution of this coral mound province, (2) relate the development of the studied mounds to changes in the local environmental setting and (3) compare the temporal patterns of mound development observed in this province with those reported in coral mound provinces of the Alboran Sea.

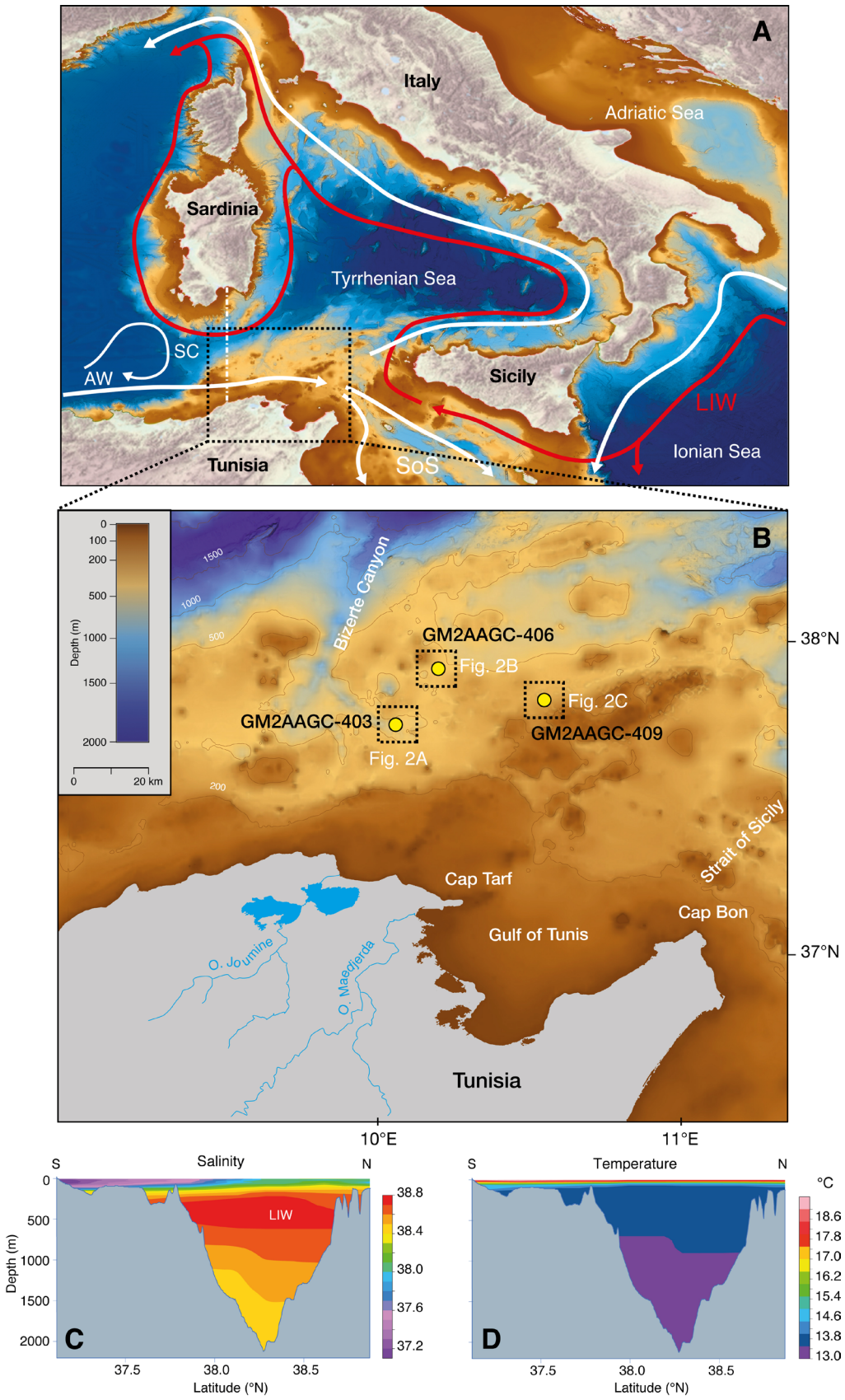

Figure 4.1. Bathymetric map of the Central Mediterranean Sea (A), with the black dotted rectangle and the dotted white line indicating the location of the TMP (B) and the vertical hydrographic profiles (C, D) respectively. White and red arrows indicate the circulation patterns of surface (AW) and intermediate (LIW) water masses (Dubois-Dauphin et al., 2017). AW: Atlantic Water, LIW: Levantine Intermediate Water, SoS: Strait of Sicily. (B) Location of GM2AAGC-403, GM2AAGC-406, GM2AAGC-409 gravity cores (yellow dotes) on a bathymetric map of the northern Tunisian shelf. Salinity (C) and temperature (D) profiles acquired from the World Ocean Atlas 2018 at 0.25° horizontal resolution (Locarnini et al., 2018; Zweng et al., 2019). The Digital Terrain Model at 115 m horizontal resolution has been derived from the EMODnet Bathymetry portal - http://www.emodnet-bathymetry.eu.

4.3. Geological and oceanographic setting

The TMP is situated on a plateau cut by the Bizerte Canyon on the northern Tunisian continental slope (South Tyrrhenian Sea; Fig. 4.1A, B). The plateau is characterised by a complex morphology that consists of a close ridge alignment of parallel ridges and basins that relate to NE-SW trending anticlines and synclines respectively (Mascle et al., 2001). All these features are displaced by NW-SE trending faults, with the Bizerte Canyon being the only landmark that follows a major fault running NE-SW (Fig. 4.1B; Mascle et al., 2001). The Tunisian Plateau also displays several contourite deposits, mainly reported to the west of the Bizerte Canyon (Camafort et al., 2020). This sector of the Tunisian slope becomes shorter and steeper towards the west and shapes the southern margin of the Sardinian Channel (Fig. 4.1B). To the southeast, the plateau is bound by the Strait of Sicily (Fig. 4.1B), which is characterised by a sill of 400 m water depth.

In terms of ocean circulation, the Sardinia-Sicily passage represents an area of key importance within the Mediterranean Sea, as it controls the exchange of water-masses between the Eastern and the Western Basins (Astraldi et al., 2002). The Algerian Current, which flows on the sea surface parallel to the Algerian coast and towards the Tyrrhenian Sea, advects Atlantic nutrient-rich waters all the way from the Alboran Sea at a speed between 10 and 30 cm s^{-1} (Fig. 4.1A, Millot, 1999; Onken et al., 2003; Jouini et al., 2016). Baroclinic instabilities throughout the entire course of the Algerian Current generate anticyclonic eddies, often involving both surface and intermediate waters (Obaton et al., 2000). At the entrance of the Strait of Sicily, the AW splits into two branches, the first flowing along the northern coast of Sicily and the second crossing the strait towards the Eastern Mediterranean Basin (Manzella et al., 1990; Sorgente et al., 2011). In the studied region, the AW occupies the first ~200 m of the water column, displaying a salinity core lying around 37.6 psu and a temperature around ~14–15°C (Fig. 4.1C, D; Gana et al., 2015; Taviani et al., 2017). Below ~200 m, where the AW-LIW interface occurs, and down to ~1000 m the LIW flows in opposite direction at a speed around 5–15 cm s^{-1}, from the Strait of Sicily into the Tyrrhenian Sea and through the Sardinian Channel into the Algero-Provençal Basin (Fig. 4.1A, C; Onken et al., 2003). This water mass is characterised by a salinity core of 38.7 psu and a temperature of ~13.75°C (Fig. 4.1C, D; Gana et al., 2015; Taviani et al., 2017).

D'Ortenzio and Ribera d'Alcalà (2009) categorised this region as an oligotrophic area with a well-defined seasonal productivity, characterised by low biomass during spring-summer and higher productivity throughout autumn and winter. Lastly, Dinarès-Turell et al. (2003) defined an almost constant sedimentation pattern of 2.77 cm kyr^{-1} on the Tunisian Plateau (Core LC07) during the last 400 kyr. Throughout the same period of time, Camafort et al. (2020) described maximum sedimentation rates of 2 cm kyr^{-1}, mainly derived from the depositional sequences closer to the coast.

4.4. Material and methods

4.4.1. Core acquisition

Three gravity cores (GM2AA-GC403, GM2AA-GC406, GM2AA-GC409) were collected in December 2013 from the summit of different coral mounds located in contrasting regions of the TMP (Table 4.1, Figs. 4.1B, 4.2). This survey was carried out on board of the Research Vessel Ra-

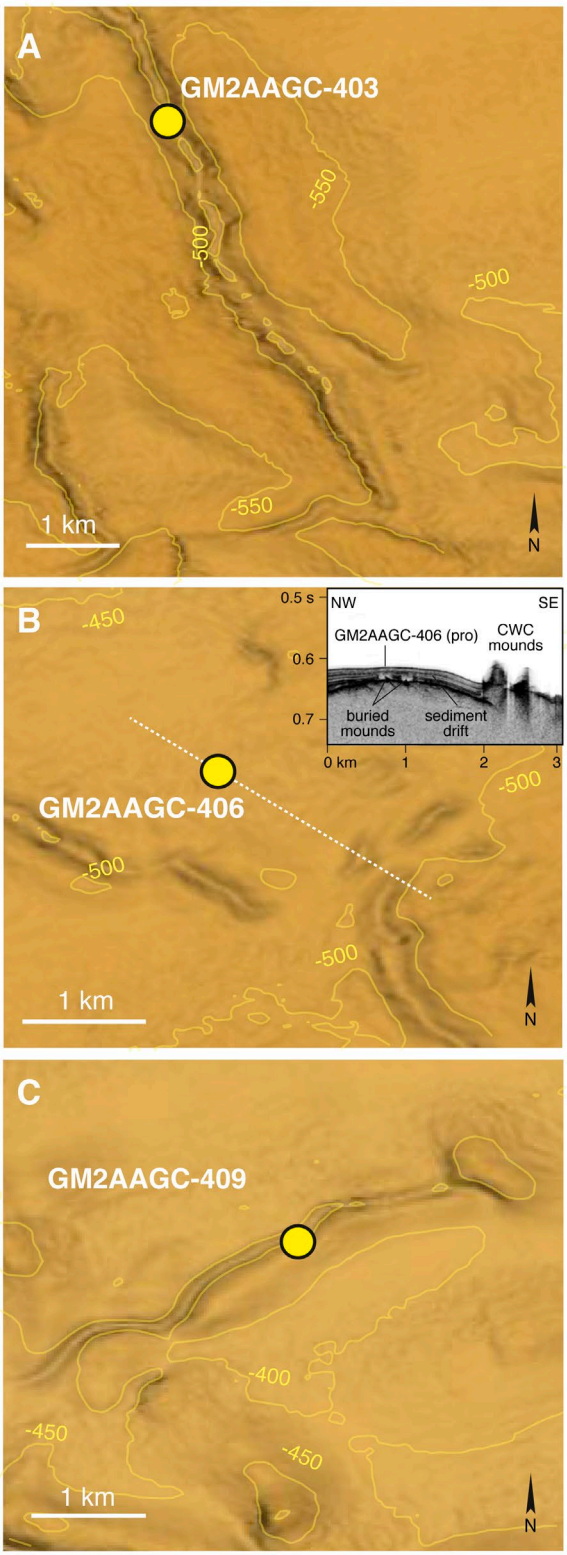

Figure 4.2. Close-up bathymetric maps of the coral mounds from which the gravity cores GM2AAGC-403 (A), GM2AAGC-406 (B), GM2AAGC-409 (C) were acquired. The white dotted line in (B) indicates the location of the TOPAS multiparametric echo-sounder profile showed in the inset.

Table 4.1. Location, water depth and recovery of the three gravity cores analysed in this study. The U-Th and trace element samples acquired from each core together with the youngest and oldest ages are also indicated.

Core	Lat (°N)	Long (°E)	Water depth (m)	Recovery (cm)	U-Th samples	Li/Mg and Ba/Ca samples	Age (ka BP)	
							Min.	Max.
GM2AAGC403	37.7694070	10.0654777	505	234	22	7	8.39	423.96
GM2AAGC406	37.9496727	10.1927011	475	421	32	6	15.26	85.47
GM2AAGC409	37.8577622	10.5746398	383	78	10	1	14.39	20.86

mon Margalef from the Instituto Español de Oceanografia (IEO), chartered within the frame of the Geomargen-2 Project by the Institute of Marine Sciences (ICM-CSIC) in collaboration with REPSOL. Core GM2AAGC-403, 234 cm long, was extracted from a ridge-like mound located at the head of one of the branches of the Bizerte Canyon (505 m water depth). The mound extends for 6.4 km in length, rises up to 90 m from the surrounding seafloor, displays flanks with up to 26° of inclination and is accompanied by a series of smaller ridge-like mounds located to the west (Figs. 4.1B, 4.2A). Core GM2AAGC-406, 421 cm long, was collected from a coral mound located at 475 m water depth and buried by a thin layer of sediment up to 6 m thick (Figs. 4.1B, 4.2B). This mound is found several hundreds of meters to the north of a series of ridge-like mounds that occur in a depth range of 450–500 m (Fig. 4.2B). Core GM2AAGC-409, 78 cm long, was acquired from a ridge-like mound located at 383 m water depth that extends for 3.7 km in length, rises up to 50 m from the surrounding seafloor and presents steep flanks of up to 28° of inclination (Figs. 4.1B, 4.2C). GM2AA-GC403, GM2AA-GC406 and GM2AA-GC409 predominantly consist of coral fragments embedded in hemipelagic sediments (Fig. 4.3). The cores were cut into 1 m sections and frozen prior to being split with a diamond rock saw, which minimises coral fragmentation during the cutting process. After splitting, the sections were defrosted, HD photographed by means of a Geotek MSCL-Core Imaging System in the British Ocean Sediment Core Research Facility (BOSCORF). All cores were subsequently visually logged to characterise changes in coral density and species composition.

4.4.2. Laser ablation U-Th dating

Uranium series techniques were used to date a total of 21, 32 and 10 coral samples acquired from cores GM2AA-GC403, GM2AA-GC406 and GM2AA-GC409, respectively (Table 4.1), following the methodology outlined in Corbera et al. (2021). Prior to analyses by laser ablation multi-collector inductively coupled plasma mass spectrometry (LA-MC-ICP-MS), samples and standards were mounted in 2.5 cm diameter epoxy resin disks and polished until the surface of the resin was flat and the samples exposed. Analyses were performed using an Elemental Scientific Lasers (Bozeman, MT, USA) NWR193 excimer laser ablation system with a TwoVol2 ablation chamber coupled to a Thermo Scientific Neptune Plus MC-ICP mass spectrometer (Thermo Fisher Scientific, Waltham, MA, USA) equipped with nine Faraday cup detectors and an energy filter (Retarding Potential Quadrupole lens) on the central ion counter the University of Southampton.

A peak hopping approach was employed, with ^{230}Th and ^{234}U intensities measured on the central ion counter and ^{238}U intensities measured using Faraday cups (Corbera et al., 2021). Integration and idle times of 4.194 s and 1 s were used respectively for both sub-configurations, amounting to a total cycle time of 10.388 s. Since measuring ^{232}Th for correction of initial Th is generally not necessary when analysing CWCs (Spooner et al., 2016), measurements of ^{232}Th were not included in the approach employed here. This decision is further validated by the accuracy of the internal standards discussed below. Typical operating conditions for the laser ablating procedure are detailed in Corbera et al. (2021). Prior to the analyses, coral samples were pre-ablated in order to remove any surface contamination. Laser ablation was performed along a straight line on the sample surface moving at a rate of 10 μm s^{-1}.

Data were collected over 40 analytical cycles. An on-peak gas blank was analysed before and after ablation (both 10 cycles), with 5 cycles allowed for sample washout prior to the latter. Blank corrections were applied to all intensities based on the mean of the preceding and suc-

ceeding blank measurements. A fragment of inorganically precipitated aragonite vein, VS001/1-A (Kampman et al., 2012), which was shown to be homogenous on a centimetre scale by Spooner et al. (2016), was analysed bracketing every two samples and used to correct for isotopic and elemental fractionation. Resulting ratios for each coral sample were screened and cycles falling outside the 3σ of the mean were removed. Lastly, the following decay constants were used for the calculation of activity ratios: λ_{230} = (9.1577±0.028)·10^{-6} a^{-1} (Cheng et al., 2000), λ_{234} = (2.826±0.0056)·10^{-6} a^{-1} (Cheng et al., 2000), and λ_{238} = (1.55125±0.0017)·10^{-10} a^{-1} (Jaffey et al., 1971). Ages were computed iteratively from the activity ratios and employing these half-lives. Coral samples that were dated multiple times are reported as the mean value of the different ages with an error of 2σ.

Accuracy of the laser ablation MC-ICP-MS approach was demonstrated on a set of CWC fragments also analysed by solution MC-ICP-MS (Corbera et al., 2021). Following Spooner et al. (2016), age uncertainties were determined based on the relationship between the external reproducibility of CWC samples analysed ≥3 times and their ($^{230}Th/^{238}U$; Corbera et al., 2021). Calculated age uncertainties (at 95% confidence) give values of ~0.7 ka for ages of 0–10 ka, ~0.9 ka for ages of ~15 ka, ~5 ka for ages of 100 ka, and ~19 ka for ages of ~350 ka. These are comparable to other studies that have used laser ablation MC-ICP-MS (Eggins et al., 2005; McGregor et al., 2011; Spooner et al., 2016). The uncertainty of samples >400 ka could not be characterised following this approach and thus, such ages were not considered in detail here. Potential open system behaviour of the samples is assessed through their $\delta^{234}U_i$. Nonetheless, due to the uncertainty associated with the $\delta^{234}U_i$ (7‰ on seawater and 25‰ on LA values), only those samples with values >178.5‰ or <114.5‰ are identified as being beyond the acceptable range and not considered in the discussion (see Corbera et al., 2021 for further details).

4.4.3. Trace elements analyses

A total of 7, 6 and 1 additional fragments from the dated corals in cores GM2AA-GC403, GM2AA-GC406 and GM2AA-GC409 were also analysed to acquire Li/Mg and Ba/Ca ratios. The former ratio is used in CWCs as a proxy for seawater temperature (SWT; Case et al., 2010; Montagna et al., 2014), while Ba/Ca ratios are linked to seawater Ba concentrations (Ba_{SW}; Anagnostou et al., 2011; Spooner et al., 2018), which provide information about changes in terrigenous input and can be used to trace different water masses (Roy-Barman et al., 2019). With the aim of removing any Fe-Mn crust and visible borings, the coral fragments were mechanically cleaned using a circular saw and ultra-sonicated to detach any loose sediments trapped within the coral skeleton. The samples were then subjected to oxidative and reductive cleaning, to eliminate the remaining organic and crustal material (Corbera et al., 2021).

A Thermo Scientific Element XR at the University of Southampton, with a long-term precision (2s) of consistency standards of 2% for Ba/Ca, and 4% for Li/Mg, was used to measure the elemental ratios following established protocols (Stewart et al., 2016). The multispecies calibration of Montagna et al. (2014) was used to convert Li/Mg ratios into SWT, while the multispecies calibration of Spooner et al. (2018) was employed for Ba_{SW} reconstructions. Due to the long residence time of Li and Mg in the ocean, the changes in the Li/Mg ratio of seawater during the last million years are negligible (Huh et al., 1998) and thus, it can be assumed that seawater Li/Mg ratios did not vary significantly during the timespan encompassed by this study (i.e. ~400 kyrs). SWT and Ba_{SW} reconstructions and uncertainties were calculated through the propa-

gation of both the analytical uncertainty of our elemental data and the uncertainty associated to the regression fit of each calibration, refitted here using York (2004), with a Monte Carlo approach (n=1000; Corbera et al., 2021). The means and standard deviations of the SWT and Ba_{SW} Monte Carlo permutations for each sample are the values used in the subsequent discussion (Table 4.3).

4.5. Results

4.5.1. Tunisian Coral Mound Province

The recently discovered TMP consists of up to 160 exposed mounds located within a water depth of 200–670 m. Seismic profiles acquired during the research survey also indicate the presence of contourites and several buried mounds, increasing even more the number of coral build-ups present in the area. Although some conical mounds are present, most of the coral mounds in this province display a ridge-like morphology that in some cases extends for up to 7 km, with the presence of considerable moats in either one or both sides of the coral mounds' base. The average height of the mounds is 39 m, yet some of them can rise up to 100 m from the surrounding seafloor. Most of the mounds (i.e. 80%) are located on the slope east of the Bizerte Canyon in a 1700 km^2 sector. This sector displays the highest concentration of rocky outcrops and fault scarps, which longitudinal direction coincides with the NNW-SSE and NNE-SSW orientation of the mounds. Nonetheless, several mounds are also present inside the Bizerte Canyon branches and along them.

4.5.2. Core description

4.5.2.1. *Core GM2AAGC-403*

This core was acquired from the top of a coral mound at 505 m water depth (Fig. 4.2A), and consists of 234 cm of CWC fragments embedded in an olive grey muddy sediment matrix (Fig. 4.3). Besides corals, other invertebrates such as bivalves and echinoids are also found within the sediment matrix. The first 11 cm of matrix sediment present a brownish tone, which denotes that oxidative processes have occurred. Below this point, the colour of the sediment changes to olive grey and keeps relatively constant, with only one light grey band at around 126–133 cm core depth (Fig. 4.3).

Qualitative visual logging of the core allowed determination of the density of coral fragments along the core and identification of the main species conforming the coral deposits. 71% of the core length is characterised by the presence of highly dense coral deposits, 14% contains dispersed but still abundant fragments and 13% displays low coral density (Fig. 4.3). In contrast, only 2% of the core length is characterised by the absence of coral fragments. Most coral fragments throughout the core display a high degree of bio-erosion, and corals with Fe-Mn crusts are observed between 150 and 140 cm core depth (Fig. 4.3). Cold-water corals are mainly represented by framework-building species. Although *Desmophyllum pertusum* (synonym= *Lophelia pertusa;* Addamo et al., 2016) is the main species observed among the coral fragments, the deepest part of the core (i.e. below 220 cm) consists of a layer formed by a mix of *D. pertusum* and *Madrepora oculata* accompanied by some bivalve shells (Fig. 4.3). Similarly, several *Desmophyllum dianthus* individuals are observed between 160 and 75 cm core depth. Lastly, *M. oculata* and the solitary coral *D. dianthus* also occur in the uppermost 16 cm of the core (Fig. 4.3).

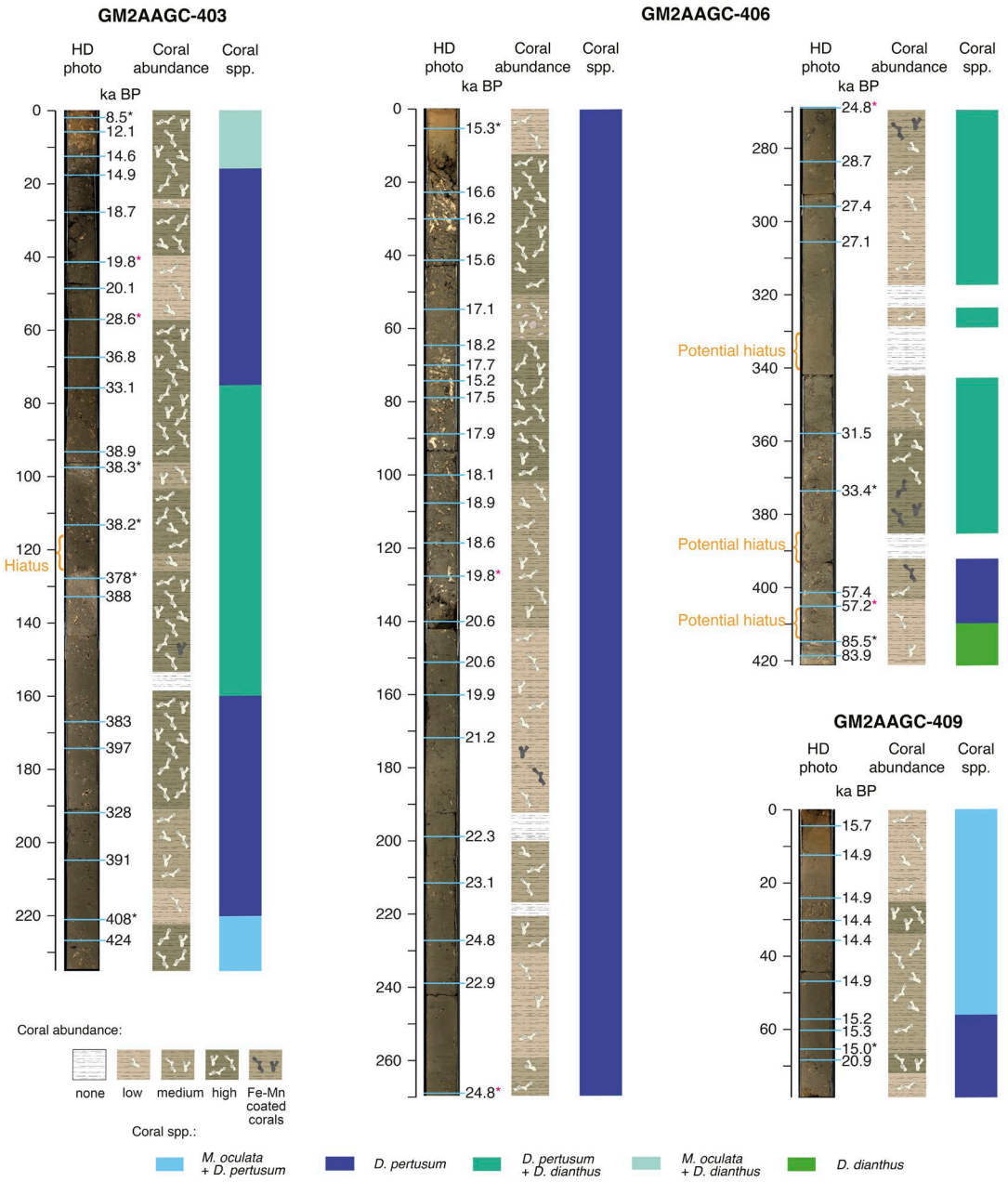

Figure 4.3. Stratigraphic logs of cores GM2AAGC-403, GM2AAGC-406 and GM2AAGC-409. From left to right: Core HD photo, with location of the coral samples obtained for U-Th dating (blue lines) and their corresponding ages; stratigraphic representation of coral abundance and preservation state; dominant coral species. The asterisk next to some of the coral ages indicate which of the coral samples were also used for trace element analyses, with the red ones denoting trace element data with unrealistic values that are beyond calibration.

4.5.2.2. *Core GM2AAGC-406*

This core was collected from the top of a CWC mound buried by a thin sediment layer up to 6 m thick, at a depth of 475 m (Fig. 4.2B). It consists of 421 cm of CWC and other invertebrates' fragments fixed in an olive grey muddy sediment matrix (Fig. 4.3). Similarly to core GM2AAGC-403, the first 15 cm of sediment matrix present a brownish colour that corresponds to oxidative processes and which gradually changes towards grey coloured mud that characterises the rest of the core (Fig. 4.3).

Coral fragments present a varying density throughout the core; 25% of its length presents a high coral density, mainly concentrated in the upper 100 cm (Fig. 4.3). Below this point, the coral de-

posits generally display medium (32%) and low (34%) density of coral fragments; only 9% of the core length is depleted of coral fragments. In comparison with core GM2AAGC-403, the CWC fragments in this core are in a considerably better state of preservation, with almost no bio-erosion observed in the corals. Nonetheless, several sections of the core contain corals covered with a Fe-Mn crust (400–370 cm, 280–270 cm, 190–174 cm). As for the previous core, most of the coral fragments observed here belong to framework-building species, with *D. pertusum* being the main species observed (Fig. 4.3). Some individuals of the solitary coral *D. dianthus* are also observed in the lower half of the core (385 cm and 270 cm), and they become especially abundant in the last 15 cm of the core. Although several bivalve shells are observed throughout the core, a considerable accumulation of these invertebrates can be observed between 65 and 55 cm core depth (Fig. 4.3).

4.5.2.3. *Core GM2AAGC-409*

This core was acquired from the top of a coral mound at 383 m water depth (Fig. 4.2C) and consists of 78 cm of CWC fragments embedded in a muddy sediment matrix, which displays a brownish colour until 12 cm core depth and then gradually changes to olive grey (Fig. 4.3).

In comparison with GM2AAGC-403 and GM2AAGC-406, CWC fragment density is relatively low in this core, with only two high density intervals in between 25–34 cm and 66–72 cm core depth, equivalent to 19% of the core length (Fig. 4.3). The rest of the core is characterised by one section of medium coral density and two sections of low coral density, amounting to 41% and 40% of the core length respectively. Coral preservation is not optimal, as many remineralised fragments are present, especially in the last 10 cm of the core. Most of the coral fragments belong to the framework-building species *D. pertusum*. Nonetheless, several *M. oculata* fragments are observed in the upper 55 cm of the core (Fig. 4.3).

4.5.3. Coral mound development

4.5.3.1. *Core GM2AAGC-403*

The age-depth model of this core is based on 21 coral samples dated through U-series and ranges from 423.96 ± 18.04 to 8.39 ± 0.79 ka BP (Figs. 4.4, 4.5, Table 4.2). Most of these samples (i.e. 48%) correspond to the Marine Isotopic Stage (MIS) 3–2 of the last glacial period, 14% coincide with the MIS 1 interglacial and 38% could not be categorised within any period due to their analytical uncertainty (Fig. 4.4A). Two clear mound development stages are observed in this core, covering periods of ~46 kyr and 30 kyr, and separated by a large coral mound stagnation interval that lasted ~344 kyr. The first mound formation period stretches from ~424 to ~383 ka BP (Fig. 4.4A). The $\delta^{234}U_i$ values of all analysed samples from this period of mound growth indicate that most have likely experienced open system behaviour. This, along with the high uncertainty associated with these older ages, means calculating the Aggradation Rate (AR) would not be reliable. After ~344 kyr of coral mound stagnation, the second mound formation stage extends from ~38.9 to ~8.4 ka BP, i.e. largely within the last glacial. Although this mound formation stage seems to be continuous, changes in the ARs occur at ~36.8 ka BP, ~20.1 ka BP and 18.7 ka BP. From ~38.9 to ~36.8 ka BP the mound forms at a rate of 22.1 cm kyr^{-1} (Fig. 4.5). After this period, mound development stops (AR= 1.1 cm kyr^{-1}) until ~20.1 ka BP, when mound aggradation starts again with an AR of 15.3 cm kyr^{-1} (Fig. 4.5). The most recent mound formation stage is characterised by a reduced aggradation of 2.5 cm kyr^{-1} and coincides with the Early Holocene and the start of a coral mound stagnation period that lasts until the present day (Fig. 4.5).

Table 4.2. Laser ablation MC-ICP-MS U-Th results from the Tunisian Mound Province coral samples. Ratios within parentheses are activity ratios. i = initial. See section 4.4.3. for explanation of the age uncertainties. $(^{230}Th/^{238}U)_A = 1 - e^{-\lambda_{230}T} + (\delta^{234}U\text{measured}/1000)\,[\lambda_{230}/(\lambda_{230} - \lambda_{234})]\,(1 - e^{-(\lambda_{230}-\lambda_{234})T})$, where T is the age. $\delta^{234}U = ((^{234}U/^{238}U)_A - 1) \times 1000$. Ages in years before present (2019) with propagated uncertainties (2σ). Ages are uncorrected for initial Th. Samples in italics are characterised by $\delta^{234}U_i$ outside the acceptable range for closed-system behaviour and thus, they were not included in the calculation of mean ages or used for coral mound development interpretation.

Core	Depth (cm)	$(^{230}Th/^{238}U)$	2 SE	$(^{234}U/^{238}U)$	2 SE	Age (ka BP)	2σ	$\delta^{234}U_i$
GM2AAGC403	2	0.085	0.010	1.148	0.016	8.39	0.79	151
GM2AAGC403	6	0.122	0.013	1.151	0.017	12.16	0.89	156
GM2AAGC403	13	0.144	0.018	1.143	0.021	14.63	0.96	149
GM2AAGC403	18	0.147	0.028	1.148	0.013	14.86	0.97	154
GM2AAGC403	28	0.181	0.018	1.139	0.016	18.75	1.09	147
GM2AAGC403	41	0.192	0.018	1.145	0.017	19.83	1.13	154
GM2AAGC403	49	0.192	0.012	1.132	0.019	20.12	1.13	140
GM2AAGC403	57	0.264	0.013	1.139	0.015	28.56	1.43	150
GM2AAGC403	67	0.326	0.025	1.128	0.019	36.85	1.76	143
GM2AAGC403	76	0.298	0.016	1.128	0.017	33.14	1.60	141
GM2AAGC403	93	0.348	0.027	1.148	0.050	38.93	1.89	166
GM2AAGC403	98	0.340	0.030	1.138	0.030	38.29	1.84	154
GM2AAGC403	113	0.337	0.046	1.131	0.022	38.23	1.82	146
GM2AAGC403	128	1.027	0.032	1.039	0.011	404.76	17.89	122
GM2AAGC403	*128*	*1.017*	*0.069*	*1.040*	*0.018*	*363.03*	*17.28*	*113*
GM2AAGC403	*128*	*1.005*	*0.051*	*1.036*	*0.024*	*345.36*	*16.60*	*97*
GM2AAGC403	128	1.023	0.047	1.040	0.017	384.34	17.64	118
GM2AAGC403	128	1.032	0.057	1.044	0.022	394.51	18.13	134
GM2AAGC403	*133*	*1.018*	*0.067*	*1.035*	*0.017*	*388.09*	*17.33*	*104*
GM2AAGC403	*167*	*1.079*	*0.142*	*1.082*	*0.055*	*382.75*	*21.22*	*244*
GM2AAGC403	*174*	*1.012*	*0.067*	*1.029*	*0.019*	*397.68*	*17.00*	*88*
GM2AAGC403	*192*	*0.996*	*0.080*	*1.035*	*0.029*	*327.78*	*16.09*	*89*
GM2AAGC403	*205*	*1.015*	*0.097*	*1.032*	*0.031*	*391.11*	*17.18*	*98*
GM2AAGC403	221	1.024	0.044	1.036	0.016	408.12	17.71	*114*
GM2AAGC403	*221*	*0.995*	*0.083*	*1.039*	*0.013*	*317.98*	*16.08*	*96*
GM2AAGC403	227	1.030	0.062	1.037	0.019	423.96	18.04	124
GM2AAGC406	5	0.152	0.013	1.156	0.013	15.26	0.99	163
GM2AAGC406	22	0.167	0.015	1.158	0.016	16.93	1.04	165
GM2AAGC406	30	0.159	0.017	1.147	0.019	16.19	1.01	154
GM2AAGC406	42	0.156	0.021	1.148	0.025	15.80	1.00	154
GM2AAGC406	55	0.169	0.015	1.157	0.026	17.14	1.05	165
GM2AAGC406	65	0.179	0.021	1.153	0.031	18.23	1.08	161
GM2AAGC406	70	0.171	0.021	1.143	0.035	17.60	1.05	151
GM2AAGC406	74	0.150	0.013	1.148	0.011	15.23	0.98	154
GM2AAGC406	79	0.171	0.018	1.146	0.020	17.48	1.05	153
GM2AAGC406	89	0.173	0.018	1.140	0.020	17.87	1.06	147
GM2AAGC406	100	0.175	0.027	1.133	0.019	18.14	1.06	140
GM2AAGC406	108	0.185	0.014	1.148	0.015	18.99	1.10	156
GM2AAGC406	119	0.181	0.014	1.148	0.016	18.57	1.09	156
GM2AAGC406	128	0.192	0.012	1.145	0.014	19.83	1.13	154
GM2AAGC406	140	0.197	0.019	1.135	0.016	20.64	1.14	143
GM2AAGC406	151	0.198	0.014	1.144	0.016	20.61	1.15	153
GM2AAGC406	160	0.190	0.024	1.131	0.018	19.89	1.12	139
GM2AAGC406	172	0.202	0.014	1.137	0.015	21.23	1.17	145
GM2AAGC406	199	0.212	0.015	1.137	0.022	22.28	1.20	146
GM2AAGC406	211	0.221	0.019	1.147	0.015	23.15	1.24	157
GM2AAGC406	227	0.233	0.018	1.134	0.016	24.85	1.29	144
GM2AAGC406	239	0.219	0.022	1.147	0.028	22.92	1.23	157
GM2AAGC406	269	0.234	0.017	1.146	0.013	24.76	1.30	156
GM2AAGC406	283	0.264	0.015	1.131	0.013	28.74	1.43	143
GM2AAGC406	296	0.253	0.018	1.129	0.023	27.41	1.38	140
GM2AAGC406	306	0.258	0.073	1.165	0.070	27.07	1.40	178
GM2AAGC406	358	0.286	0.020	1.131	0.020	31.54	1.54	144
GM2AAGC406	374	0.303	0.023	1.141	0.031	33.37	1.63	156
GM2AAGC406	401	0.465	0.027	1.124	0.024	57.39	2.78	146
GM2AAGC406	405	0.466	0.032	1.129	0.024	57.24	2.79	152
GM2AAGC406	415	0.616	0.039	1.118	0.016	85.47	4.58	151
GM2AAGC406	419	0.613	0.034	1.125	0.016	83.93	4.53	159
GM2AAGC409	4	0.153	0.014	1.137	0.035	15.68	0.99	143
GM2AAGC409	12	0.147	0.016	1.145	0.023	14.90	0.97	152
GM2AAGC409	24	0.146	0.016	1.140	0.026	14.89	0.97	146
GM2AAGC409	30	0.143	0.019	1.149	0.023	14.39	0.96	155
GM2AAGC409	*36*	*0.136*	*0.018*	*1.094*	*0.021*	*14.40*	*0.94*	*98*
GM2AAGC409	47	0.148	0.011	1.151	0.023	14.94	0.97	158
GM2AAGC409	57	0.150	0.024	1.149	0.022	15.18	0.98	155
GM2AAGC409	60	0.151	0.015	1.148	0.018	15.25	0.98	154
GM2AAGC409	66	0.148	0.024	1.148	0.025	15.01	0.98	154
GM2AAGC409	68	0.199	0.020	1.135	0.022	20.86	1.15	143

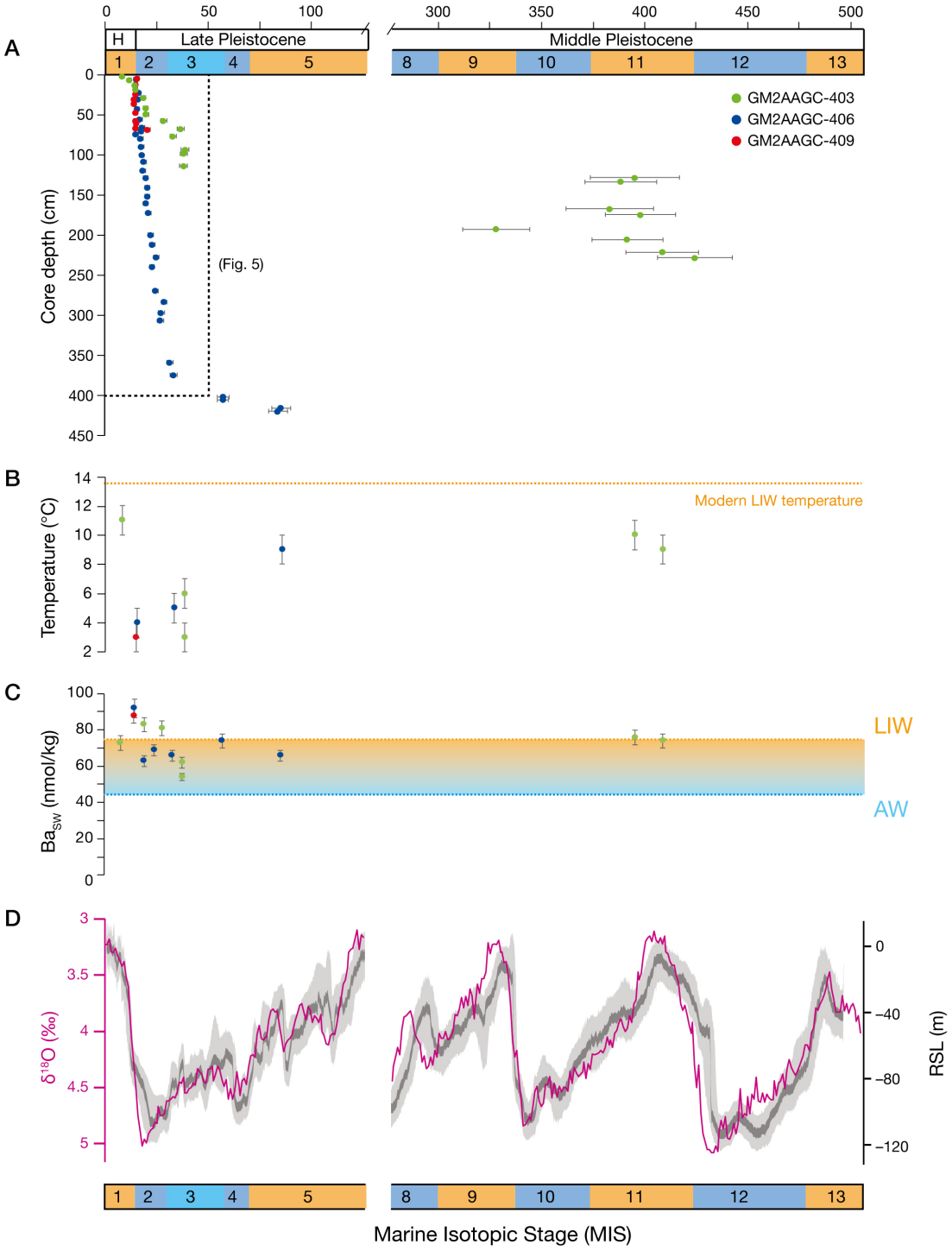

Figure 4.4. U-Th coral ages (green dots: GM2AAGC-403, blue dots: GM2AAGC-406, red dots: GM2AAGC-409) with associated 2s uncertainties against core depth (A); Sea Water Temperature (SWT) derived from Li/Mg ratios (B); Ba_{SW} values derived from Ba/Ca ratios (C); LR04 $\delta^{18}O$ (‰) stack data for the last 650 kyr (Lisiecki and Raymo, 2005) and Relative Sea-Level (RSL) dataset from Grant et al. (2014) (D). The orange and blue bars in A indicate interglacial and glacial Marine Isotopic Stages (MIS). The orange and blue dotted lines in (D) show the present-day Ba_{SW} values of the Levantine Intermediate Water (LIW) and the Atlantic Water (AW).

4.5.3.2. *Core GM2AAGC-406*

In this core, the age-depth model is based on 32 U-Th dated coral samples ranging from 85.47 ± 4.58 to 15.26 ± 0.99 ka BP (Figs. 4.4, 4.5, Table 4.2). Most of the coral ages lie within the last glacial period (i.e. MIS 4–MIS 2) and only the two oldest samples fall within the MIS 5 interglacial (Fig. 4.4A). Mound development seems to occur continuously, with the exception of the

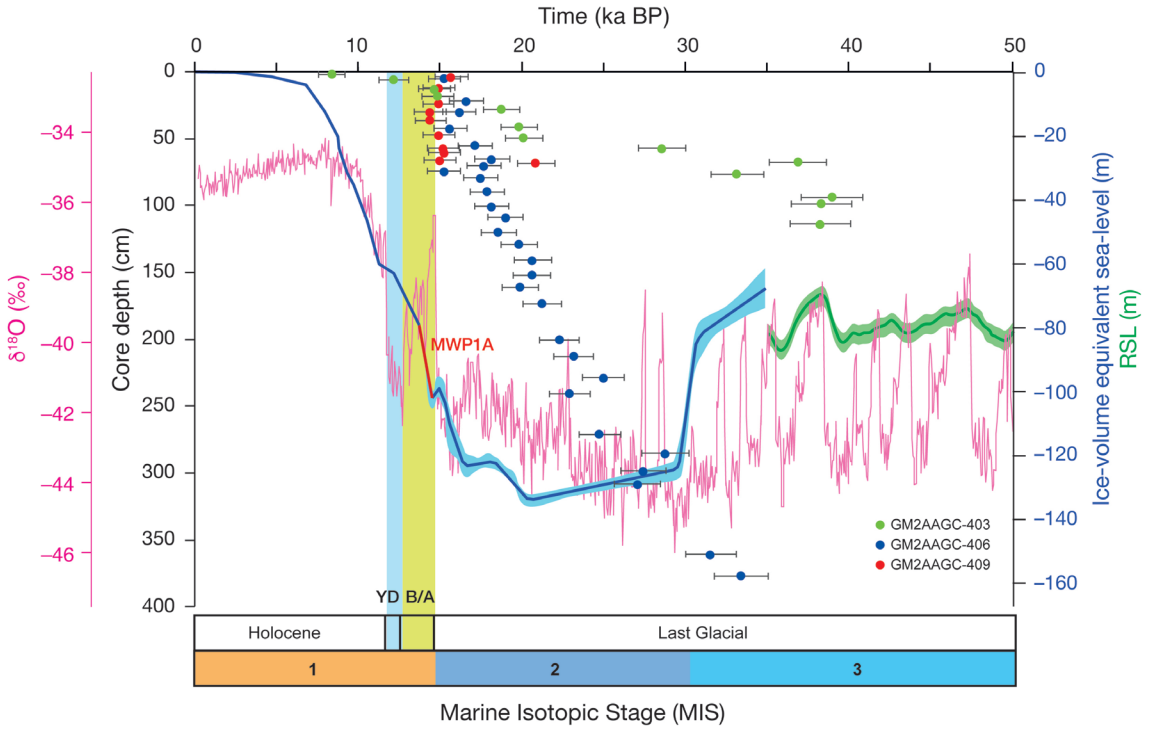

Figure 4.5. U-Th coral ages (green dots: GM2AAGC-403, blue dots: GM2AAGC-406, red dots: GM2AAGC-409) during the last glacial and Holocene against core depth. Ice-volume equivalent sea-level curve (blue line) from Lambeck et al. (2014), Relative Sea-Level data (green line) from Grant et al. (2014) and NGRIP $\delta^{18}O$ (‰) data (purple line) from North Greenland Ice Core Project members, 2004 are also plotted. B/A: Bølling-Allerød, YD: Younger Dryas

coral ages ranging from ~85.5 to ~33.4 ka BP, which represent either a period of near coral mound stagnation with a negligible AR of 0.9 cm kyr^{-1} or two extremely short periods of coral growth separated by potential hiatuses (Fig. 4.4A). After this period and coinciding with the end of the MIS 3 and the entire MIS 2, the coral mound starts developing at a faster pace (AR: 20.3 cm kyr^{-1}; Fig. 4.5). This mound formation stage continued until ~15.2 ka BP, when the mound entered a stagnation stage that is still ongoing (Fig. 4.5).

4.5.3.3. *Core GM2AAGC-409*

The age-depth model for this core comprises 10 coral samples dated through U-Th series, with ages that range from 20.86 ± 1.15 ka BP to 14.39 ± 0.96 ka BP (Fig. 4.5). The majority of the coral ages fall within the end of the last glacial period (i.e. MIS 2), with the exception of two ages that fall within the Bølling-Allerød (Fig. 4.5). A hiatus of ~5 kyr is observed in the coral ages of the deepest part of the core, after which a continuous mound formation stage can be observed (Fig. 4.5). This period extends from ~15.68 ka BP to ~14.4 ka BP. Nonetheless, its oldest age corresponds with the shallowest sample of the core and thus, caution should be taken when interpreting the calculated AR of 48 cm kyr^{-1}.

4.5.4. Paleo-environmental proxies

Li/Mg ratios from all the cores present values ranging from 3.2 to 4.5 µmol mol^{-1}, while the derived SWT present values below the present-day temperature (i.e. 13.7°C) that oscillate between 3 ± 1 and 11 ± 1°C (Fig. 4.4C; Table 4.3). From the 14 SWT values acquired through trace element analyses, 5 were discarded due to their unrealistic values (e.g. negative or close to 0°C). This is likely a consequence of diagenetic alteration, high Mn contents or Li con-

Table 4.3. Trace element data showing Li/Mg and Ba/Ca ratios together with reconstructed sea water temperatures (SWTs) and dissolved seawater Barium (Ba_{sw}), with their respective associated errors (σ). Samples in italics indicate unrealistic reconstructed values that are beyond calibration (Bc), probably caused by diagenetic alteration or contamination during sample preparation and/or analysis.

Core	Depth	Age		Species	Li/Mg		SWTs		Ba/Ca		Ba_{sw}	
	(cm)	(ka BP)	2σ		(μmol mol^{-1})	2σ	(°C)	2σ	(μmol mol^{-1})	2σ	(nmol kg^{-1})	2σ
403	2	8.39	0.8	*M. oculata*	3.2	0.3	11	1	13.4	1.3	73	4
403	*41*	*19.83*	1.1	*D. pertusum*	*5.2*	*0.5*	*<2*	*Bc*	*15.1*	*1.5*	*83*	*4*
403	*57*	*28.56*	1.4	*D. pertusum*	*6.1*	*0.6*	*<2*	*Bc*	*14.7*	*1.5*	*81*	*4*
403	98	38.29	1.8	*D. pertusum*	4.0	0.4	6	1	10.2	1	54	2
403	113	38.23	1.8	*D. pertusum*	4.5	0.5	3	1	11.5	1.2	62	3
403	128	394.54	20.4	*D. pertusum*	3.4	0.3	10	1	13.9	1.4	76	4
403	221	408.12	17.7	*M. oculata*	3.4	0.3	9	1	13.5	1.3	74	4
406	5	15.26	1.0	*D. pertusum*	4.4	0.4	4	1	16.6	1.7	92	5
406	*128*	*19.83*	1.1	*D. pertusum*	*6.0*	*0.6*	*<2*	*Bc*	*11.6*	*1.2*	*63*	*3*
406	*269*	*24.76*	1.3	*D. pertusum*	*5.4*	*0.5*	*<2*	*Bc*	*12.7*	*1.3*	*69*	*3*
406	374	33.37	1.6	*D. pertusum*	4.2	0.4	5	1	12.1	1.2	66	3
406	*405*	*57.39*	2.8	*D. dianthus*	*5.4*	*0.5*	*<2*	*Bc*	*13.5*	*1.4*	*74*	*4*
406	415	85.47	4.6	*D. dianthus*	3.5	0.4	9	1	12.1	1.2	66	3
409	66	15.01	1.0	*D. pertusum*	4.5	0.5	3	1	16.0	1.6	88	4

tamination during sample preparation (Table 4.3). The oldest samples (i.e. 394, 318 and 85 Ka BP), which correspond with periods of near coral mound stagnation, show a SWT ~9°C. In contrast, during the last glacial period, SWT shows a decreasing trend from 6 ± 1°C in MIS 3 (38.3 ka BP) to 3 ± 1°C in MIS 2 (15.0 ka BP; Fig. 4.4C). This colder period corresponds with the fastest mound formation stages observed in all the coral mounds studied in this region (Fig. 4.4A, C). The youngest sample (i.e. 8.4 ka BP), which lies within the Early Holocene exhibits a SWT of 11 ± 1°C, the highest temperature observed in this study (Fig. 4.4C).

Ba/Ca values from the extracted coral samples range from 10.2 ± 0.1 to 16.6 ± 0.2 μmol mol^{-1}, resulting in a Ba_{sw} range of 54.2 ± 2.5–92.1 ± 4.6 nmol kg^{-1} (Fig. 4.4D, Table 4.3). Almost half of the samples display Ba_{sw} values within the present-day range of the two Mediterranean Sea end-members (i.e. AW and LIW). Only four samples present higher Ba_{sw} values than those generally observed for the LIW (i.e. >70–75 nmol kg^{-1}; Jacquet et al., 2016). The highest Ba_{sw} values (i.e. 88 and 92 nmol kg^{-1}) correspond with the start of the last deglacial period.

4.6. Discussion

The main finding of the present study resides in the glacial-aged development of the TMP coral mounds, at least throughout the Late Pleistocene. However, as it generally occurs with most of the studies aiming to highlight the evolution of coral mounds (Fink et al., 2013; Eisele et al., 2011; Wang et al., 2019; Corbera et al., 2021), the recovery depth of the cores (i.e. 0.9–4.2 m) only allow to constrain the latest stages of mound formation. In addition, as it has been observed here, significant differences in the ARs among different mounds might occur within the same province (Corbera et al., 2021).

4.6.1. Coral mound development during the Middle and Late Pleistocene

Throughout the Middle Pleistocene (773–126 ka BP), mound formation in the TMP occurred during ~MIS 12–10 in core GM2AAGC-403, which corresponds to the westernmost and deepest mound presented here. Although the coral ages indicate that this mound development stage extends from ~424 to ~383 ka BP, the low $\delta^{234}U_i$ values (<115‰) indicate that most of the samples from this mound formation period have probably experienced open system behav-

iour (Table 2; Robinson et al., 2014; Spooner et al., 2016; Corbera et al., 2021). Therefore, the AR of this period was not calculated and coral ages are just an indication that mound formation occurred sometime between MIS 12 and 11. Following this period, a large hiatus of ~344 kyr is present in core GM2AAGC-403, stretching from MIS 10 to 4 and coinciding with a change in sediment colour and decrease in coral density (Figs. 4.3, 4.4A). Such a large hiatus, including both glacial and interglacial cycles, could be the result of erosional processes that could have reworked, and altered (e.g. removed) a section of the mound's development record. The other two cores did not recover enough material to determine if the same hiatus occurs in all the sampled mounds presented here.

According to available information, coral mound formation in the TMP did not start again until the Late Pleistocene (126–11.8 ka BP; Fig. 4.4A). During this period, sporadic coral growth characterised by a *D. dianthus* facies is first observed in the mound corresponding to core GM2AAGC-406 at ~85 ka BP (MIS 5), followed by a short hiatus of ~27 kyr and another episode of coral growth that dates ~57 ka BP (MIS 3; Figs. 4.3, 4.4). It is not until ~39 ka BP and ~33 ka BP that mound formation starts, as observed in cores GM2AAGC-403 and GM2AAGC-406 respectively (Figs. 4.3, 4.5). The beginning of this mound formation period is preceded in core GM2AAGC-406 by the occurrence of Fe-Mn coated corals, which most probably indicate that coral skeletons were exposed to seawater for a long time, coinciding either with a mound formation hiatus or extremely intermittent coral growth since ~57 ka BP (Fig. 4.3). Throughout the MIS 3 and 2 cold periods (~39–14.6 ka BP) the core GM2AAGC-403 displays a discontinuous mound formation, with the fastest ARs occurring between ~39–37 ka BP and ~20–19 (i.e. 22.1 and 15.3 cm kyr^{-1}; Fig. 4.5). The ages from core GM2AAGC-406 relate to a slightly different mound formation pattern to that of GM2AAGC-403, as the mound develops almost continuously with an AR of 20.3 cm kyr^{-1} from ~33 ka BP until ~15 ka BP. Due to the short length of core GM2AAGC-409, its coral mound formation record only starts at ~21 ka BP with an episode of coral growth, followed by a short hiatus of ~5 kyr (Fig. 4.5). Mound development starts again at ~15.6 ka BP and lasts until ~14.4 ka BP, displaying a continuous and allegedly faster formation period (AR: 48.0 cm kyr^{-1}) than those observed in cores GM2AAGC-403 and GM2AAGC-406. It is, however, important to remark that age reversals occur in all three cores (i.e. GM2AAGC-403: 33.1 ka BP at 76 cm core depth; GM2AAGC-406: 15.2 ka BP at 74 cm core depth; GM2AAGC-409: 15.7), indicating a potential collapse of the coral frameworks or the occurrence of a mass wasting event that might have altered the stratigraphic consistency of the mounds' developmental records. Therefore, and considering the lower precision of laser ablation compared to solution U-Th dating, the ARs calculated for these cores should be taken with caution and understood as an approximate indication of mound formation pace. Nonetheless, it is apparent that all three cores display high ARs during the second half of MIS 2. Lastly, the two youngest ages acquired in this study are found in the core GM2AAGC-403 corresponding to the Younger Dryas and the Early Holocene (~12.2 and ~8.4 ka BP) respectively (Fig. 4.5). The presence of sporadic coral growth in this mound after the last glacial termination could be the result of the enhanced hydrodynamic conditions generally found within submarine canyons (López-Fernández et al., 2013; Pearman et al., 2020). The intense hydrodynamics and the funnelling effect observed in canyons tends to translate into increased particle fluxes in comparison to nearby slope settings (DeGeest et al., 2008; López-Fernández et al., 2013).

Overall, the main mound formation periods of the TMP occur during the last glacial period and terminate with the onset of the Bølling Allerød (B/A), a pattern that is also observed in Atlantic

coral mound provinces such as the ones found in the Gulf of Cadiz and off Mauritania (Wienberg et al., 2010, 2018; Eisele et al., 2011). This is however an opposite pattern compared to what has been observed in the Alboran Sea (westernmost Mediterranean Sea), where mound formation occurs mainly during glacial terminations and temperate interstadial periods (Fink et al., 2013; Stalder et al., 2015; Wang et al., 2019; Corbera et al., 2021). Following a demise stage throughout the last glacial period, mound formation in the Alboran Sea starts soon after the onset of the B/A and lasts until the Early and Mid-Holocene in the case of the Southern Cabliers, the East Melilla and the West Melilla coral mound provinces (Fink et al., 2013; Stalder et al., 2015; Wang et al., 2019; Corbera et al., 2021). It is only on the summit of the mounds from the northern sector of the Cabliers Coral Mound Province, where coral reefs are still thriving in the present-day (Corbera et al., 2019, 2021).

As there are many factors that can affect coral mound formation, it is challenging to characterise the exact causes of the contrasting temporal patterns in coral mound development within the Mediterranean Sea and specifically between the Alboran Sea provinces and the TMP. Nonetheless, a potential scenario describing the main environmental variables that drive glacial coral mound formation in the TMP is proposed below.

4.6.2. Paleo-environmental controls on coral mound development

Mound formation in the TMP occurred mainly throughout the second half of the MIS 3 and all of MIS 2 cold periods (i.e. 38.9–14.4 ka BP), coinciding with some of the highest Ba_{SW} values recorded (~60–94 nmol kg^{-1}; Fig. 4.4C). The high Ba_{SW} values observed towards the end of the last glacial period (Termination I) agree with what has been observed in North Atlantic CWC records, which also show elevated Ba_{SW} values due to increased terrigenous input during the start of the deglaciation (Raddatz et al., 2016). Indeed, the Joumine and Medjerda rivers, which originate in the Tell Atlas, end directly south of the TMP and could be one of the causes promoting the increased Ba_{SW} values. These rivers are characterised by displaying enhanced fluvial activity during cold-arid stages (Zielhofer et al., 2008), typical of glacial periods in this region (Incarbona et al., 2008), which might have provided a sufficient sediment supply for coral mound formation. However, similarly to what has been observed in the Alboran Sea (Corbera et al., 2021), the Ba_{SW} values >70 nmol kg^{-1} acquired in the TMP towards the end of the MIS 2 glacial could also be the consequence of a higher influence of LIW in the region, caused by the sea-level rise (Jacquet et al., 2016).

Although coral growth is almost continuous during the last glacial, the mound corresponding to core GM2AAGC-403 displays the lowest ARs (1.1–22.1 cm kyr^{-1}) and most discontinuous mound formation observed in the province (Fig. 4.5). Therefore, at least during the last glacial period, it seems that this mound was exposed to less suitable environmental conditions for coral mound development than those experienced by the mounds corresponding to cores GM2AAGC-406 and GM2AAGC-409. GM2AAGC-403 was the deepest core recovered from the TMP (i.e. 505 m water depth) and thus it represents the development of a mound located further away from the AW-LIW interface than its counterparts (i.e. GM2AAGC-406: 476 m water depth; GM2AAGC-409: 382 m water depth). Water-mass interfaces tend to accumulate and transport organic particles that can be used as food supply by the corals (McManus et al., 2003) and thus, mounds that are located at a water depth closer to such interfaces can more easily access the organic matter that they contain. In fact, the main mound formation stages of the TMP occurred throughout periods of time when the sea level was lowest (–100 to – 140 m;

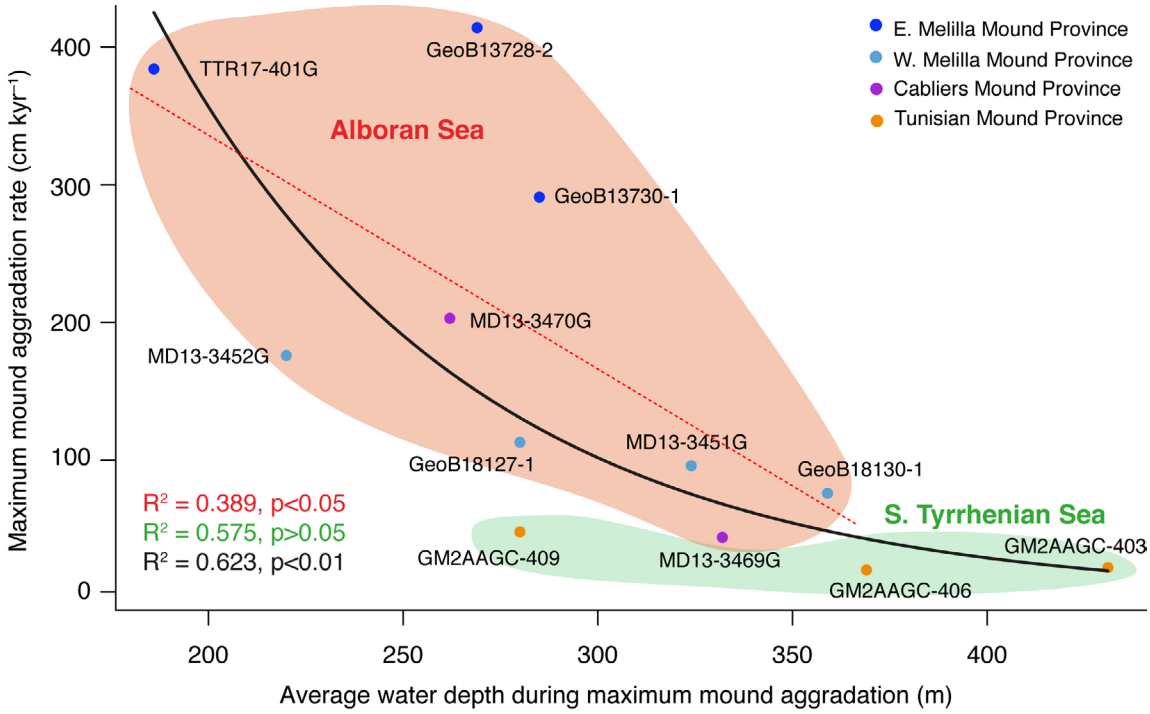

Figure 4.6. Linear regression models showing the correlation between maximum mound aggradation rates (ARs) and mounds' summit water depth in the Alboran Sea (red dotted line; East Melilla Mound Province, West Melilla Mound Province and Cabliers Mound Province), the South Tyrrhenian Sea and the Mediterranean Sea as a whole (black line). The ARs have been extracted from Fink et al. (2013), Stalder et al. (2015), Wang et al. (2019) and Corbera et al. (2021).

Figs. 4.4, 4.5) and thus, when the AW-LIW interface was the closest it could be to the mounds' summits. Although a couple of Holocene coral ages were obtained from the uppermost part of the core GM2AAGC-403, coral mound stagnation in the TMP seems to coincide with the fastest sea-level rise of the last deglaciation (i.e. Meltwater Pulse 1A event; Fig. 4.5), when an increase of 20 m in less than 500 years might have moved the AW-LIW interface too far away from the mounds (Lambeck et al., 2014). This argument fits with the results acquired by Wang et al. (2019) and Corbera et al. (2021) in the Alboran Sea, where glacio-eustatic oscillations of the AW-LIW interface were linked to regional coral mound development.

In addition to the contrasting temporal pattern of coral mound development observed between the Alboran Sea and the TMP mounds, the pace at which these features develop in the latter province is also considerably slower (Fig. 4.6). Tentatively, this might be also related to the depth of the mounds during mound formation. Data shown in Figure 4.6 indicate that, in the Mediterranean Sea, coral mounds located at greater depths develop at a significantly slower pace than those located on shallower areas (R^2=0.62, p<0.01). The most thriving mound formation periods of Northern Cabliers, East Melilla and West Melilla coral mounds (average water depth during mound aggradation (WDMA)= 186–359 m), which occurred during the B/A and the Early Holocene, present maximum ARs ranging between 75 and 414 cm kyr^{-1} (Fig. 4.6; Fink et al., 2013; Stalder et al., 2015; Wang et al., 2019; Corbera et al., 2021). In contrast, the fastest mound formation periods of the TMP (WDMA = 280–431 m) display ARs ranging from 20.3 to 48 cm kyr^{-1}, similar to those observed in Southern Cabliers (WDMA = 332 m), which displays a maximum AR of 44 cm kyr^{-1} (Figs. 4.5, 4.6; Corbera et al., 2021). The data from the different mounds follows a negative exponential curve, which means that the potential effect of the AW-LIW interface on mound ARs increases rapidly towards shallower depths, whereas mound summits located below 375 m water depth display minimal changes in ARs (Fig. 4.6).

Although the pattern of increasing ARs towards shallower depths is evident within each of the two regions, it is statistically significant only in the Alboran Sea (Fig. 4.6; Alboran Sea: R^2=0.39, $p<0.05$; TMP: R^2=0.57, $p>0.05$). The fact that no significant correlation was observed within the Tunisian mounds could be a consequence of the reduced number of mounds studied and the small differences in ARs between mounds (Fig. 4.6). Furthermore, it has to be considered that depth alone does not control mound formation pace, as it could be influenced by changes in other environmental variables. Nonetheless, it is relevant to remark that the Particulate Organic Carbon decay with depth also follows a negative exponential curve (Marsay et al., 2015), which supports our hypothesis on the relation between coral mound formation pace and mounds' water depth.

A further environmental factor with a relevant role in the TMP development during the last glacial could have been surface productivity. Indeed, studies on coccolithophores and foraminifera from the Sardinia Channel and the northern Tunisian Slope (Core LC07) described reduced productivity during interglacial periods (Incarbona et al., 2008; Di Stefano et al., 2015). In contrast, during glacial periods, floral and faunal records in the area indicate the presence of cold and highly productive surface waters (Incarbona et al., 2008; Di Stefano et al., 2015). Strong westerlies blowing along North Africa (Bout-Roumazeilles et al., 2007) probably caused a strengthening of the Algerian Current that lead to enhanced dynamics of oceanographic features such as eddies (Incarbona et al., 2008; Capotondi et al., 2016). This oceanographic pattern promoted vertical mixing that increased nutrient supply and thus productivity in the sea surface (Cardona and Bracco, 2012). Furthermore, in the Ionian Sea, Capotondi et al. (2016) described the last parts of glacial periods as being more productive than the start. Considering the proximity between the TMP and the Ionian Sea, similar changes in productivity might have occurred near the core sites presented in this study. Indeed, such increases in productivity towards the end of glacial periods coincide with the time when the most thriving stage for mound formation occurred in this province (Fig. 4.5).

Besides the high sea level and decreased productivity characteristic of interglacial periods in this region, SWT was also higher (Table 4.3, Fig. 4.4). During the last glacial period, coral mound formation in the TMP occurred when the reconstructed SWT ranged between 3 ± 1 and 6 ± 1°C and the reef assemblage was dominated by *D. pertusum* (Fig. 4.3, 4.4B). These main stages of mound formation finished with the onset of the B/A interstadial (Fig. 4.5). Nonetheless, the uppermost section of the core GM2AAGC-403, which is dominated by *M. oculata*, presents a couple of coral ages corresponding to the Early Holocene and to a SWT of 11°C (Figs. 4.3, 4.4). This change in coral facies with increasing temperatures has also been observed in the Alboran Sea (Stalder et al., 2015; Wienberg, 2019; Corbera et al., 2021), as *M. oculata* is known to withstand higher SWT than *D. pertusum* (Naumann et al., 2014). The modern SWT of the LIW in the study area is over 13.7°C (Taviani et al., 2017), a value close to the CWCs' physiological limit (i.e. 14°C; Davies and Guinotte, 2011; Brooke et al., 2013) and thus, it is possible that SWT typical of interglacial periods might have also contributed to limiting coral growth in this province.

Overall, our chronological and geochemical study suggests that coral mound stagnation in the TMP during interglacial periods was most likely caused by a combination of less productive and warmer waters together with an AW-LIW interface located further away from the mounds. Although the three gravity cores acquired suggest a glacial development of the coral mounds, some of the mounds discovered could still host scattered CWC colonies growing on their sum-

mits. Thus, in order to confirm the glacial-aged development of each of these three mounds, to determine the initial settlement of corals and to describe the current ecological state of the province, further studies involving additional cores that drill down to the base of the mounds and Remoted Operated Vehicle (ROV) video- or photo-transects should be performed. This would help to provide a more comprehensive description of the TMP development and the changes occurring in the environmental setting throughout mound formation and stagnation phases.

4.7. Conclusions

This study broadens the current knowledge on coral mound formation in the Mediterranean Sea through the description of mound development in the recently discovered Tunisian Coral Mound Province (TMP; South Tyrrhenian). We conclude that:

The TMP is the first Mediterranean coral mound province so far that displays the most thriving mound formation stages during glacial periods.

Coral mound formation during cold periods was most likely driven by enhanced surface water productivity combined with an appropriate depth of the AW-LIW interface and a cooler sea water temperature than the one observed in the present-day.

The increasing ARs from deeper to shallower mounds suggest that, as described in the Alboran Sea, the distance from the AW-LIW interface to the mounds might be key in determining their formation pace.

Additional cores drilling all the way to the base of the mounds and video-transect data are needed to assess the past mound formation patterns in this region and confirm the general demise of the mounds during the present-day.

4.8. Acknowledgements

Guillem Corbera is funded by the Graduate School of the National Oceanography Centre Southampton (GSNOCS). Veerle Huvenne is supported by the NERC-funded CLASS programme (Grant No. NE/R015953/1) and the EU H2020 programme iAtlantic (Grant No 818123). We are thankful to all the scientists and crew of the Geomargen-2 Cruise for their outstanding work. We are grateful to Andy Milton and Mathew Cooper for their help throughout the analytical processes and we acknowledge Heather Goring-Harford for her assistance in acquiring a subset of the trace element data. We appreciate the help provided by Suzanne MacLachlan and the British Ocean Sediment Core Research Facility (BOSCORF) team during sampling. We are also grateful to Laura Robinson for supplying the VS001/1-A standard. The regional Digital Terrain Model data products have been derived from the EMODnet Bathymetry portal - http://www.emodnet-bathymetry.eu.

Chapter 5
Synthesis

5.1. Thesis objectives

5.1.1. Overall thesis objective

The principal aim of this thesis was to: (1) quantify the cold-water corals (CWC) and main associated species present in a partly thriving Mediterranean coral mound province and describe their distribution along it; (2) explore the reef-building species dominance and the main environmental variables driving CWC distribution and mound formation in space and time.

Two contrasting regions of the Mediterranean Sea were chosen for the execution of this study: The Cabliers Coral Mound Province (CMP), located on the East Alboran Sea (Westernmost Mediterranean) and the Tunisian Coral Mound Province (TMP), situated off the Tunisian coast and between the Sardinian Channel and the Strait of Sicily.

The aim was achieved by means of: (1) ROV video-analysis, AUV high-resolution bathymetry and statistical analyses that helped to determine the most important seafloor variables controlling species distribution; and through (2) the comparison of data acquired from 5 gravity cores collected from the summit of CWC mounds, including U-series derived coral ages, computed tomography observations, grainsize analyses and trace element reconstructions of seawater temperature (SWT) and barium concentrations, with paleo-oceanographic data from previous studies.

The section below addressed these objectives by contextualising each of the chapters within the current paradigm of CWC research and by answering more specific questions that outline the main scientific findings.

5.1.2. Main scientific findings

5.1.2.1. *Chapter 2*

In comparison to the surrounding seafloor, CWC reefs, which are formed by a combination of living corals and dead coral framework, display a clear three-dimensional expression, which affects the local sedimentary and current dynamics and provides habitat for a wide range of benthic species (Lo Iacono et al., 2018a). The enhanced habitat complexity and heterogeneity of CWC reefs also provide a higher number of available ecological niches than those present in most benthic habitats (Jones et al., 1994; Buhl-Mortensen et al., 2010; Price et al., 2019). In addition, the habitat complexity provided by the coral frameworks promotes the creation of predator-free spaces that are used by many species as shelter or nursery grounds (Costello et al., 2005). CWC reefs are therefore considered to be biodiversity hotspots, with over 1300

species associated to *D. pertusum* reefs (Roberts et al., 2006). Furthermore, with the presence of persistent favourable environmental conditions and by baffling suspended sediments, coral reefs can develop into coral mounds that rise up to >250 m from the seafloor (Mienis et al., 2007; Wheeler et al., 2007). With the discovery of further CWC mounds in contrasting regions of the Atlantic, more species have been observed to be associated to these reefs (Henry and Roberts, 2007; Ross and Nizinski, 2007; Roberts et al., 2008, 2009b; Purser et al., 2013; Buhl-Mortensen et al., 2017). Nonetheless, in the Mediterranean Sea living CWC reefs are very scarce and thus, quantitative studies of the species inhabiting these habitats remain in their infancy (Mastrototaro et al., 2010; Vertino et al., 2010; Lo Iacono et al., 2018b; Angeletti et al., 2020a). In addition, a detailed characterisation of the distribution of CWCs on a Mediterranean coral mound in relation to seafloor variables is yet to be provided. Therefore, the performance of a quantitative and thorough description of Mediterranean CWC reefs would help towards acquiring a better knowledge of these sensitive ecosystems, which would result in the application of more appropriate conservation measures.

The study carried out for this chapter of the thesis provided a novel and comprehensive view on the structure of Mediterranean CWC reefs and their associated species.

- **Research questions:**

Q1: *What are the main reef-building and associated species occurring on the Cabliers Coral Mound Province? Are these assemblages impacted by fishing activities?*

Based on ROV observations, the flourishing CWC reefs found in the CMP were observed to be mostly constituted by *M. oculata* interspersed with *D. pertusum* colonies. Nonetheless, where the reefs were absent, gorgonian (i.e. *A. hirsuta*) and antipatharian (*P. larix*, *L. glaberrima* and *P. rigida*) assemblages covered the mounds, growing on dead coral framework and/or coral rubble. Among these benthic habitats, the most abundant species was the antipatharian *P. rigida* with 1532 colonies, followed by the gorgonian *A. hirsuta* with 1491 colonies, and *M. oculata* with 1160 colonies. Other abundant species growing along the mounds, were the sponges *A. setubalense* and *Pacastrella* sp., the antipatharian *P. larix*, squat lobsters and the echinoid *C. cidaris*. From these species it is important to note that *P. rigida* and *A. setubalense* are species of Atlantic origin (Opresko, 2009; Boury-Esnault et al., 2015), which adds a biogeographic value to these reefs. Indeed, the CMP is the first place in the Mediterranean Sea where *P. rigida* has been reported (Bo et al., 2018). Besides providing substratum and habitat for benthic species (Jones et al., 1994), these CWC reefs can also act as nursery areas and shelter for other taxa that use the coral framework to hide from predators (Costello et al., 2005). In this sense, juveniles of the fish *H. dactylopterus* were observed among the frameworks of the CMP reefs, confirming the use of CWC reefs as nursery areas by a commercially valuable species. Nonetheless, the exceptional ecological value of the CMP reefs is mainly reflected by the average densities of *M. oculata* and *D. pertusum* (0.81 and 0.14 col·m^{-2} respectively), which are considerably greater (one order of magnitude) than the ones observed on most of the CWC assemblages described so far in the Mediterranean Sea (Orejas et al., 2009; Savini and Corselli, 2010; Gori et al., 2013; Fabri et al., 2017; Taviani et al., 2017). Only the CWC reefs of Santa Maria di Leuca seem to be as thriving as the ones observed in the CMP, however no quantitative data is available in that region yet.

Lastly, this coral mound province seems to be in a practically pristine state, as only a single longline was observed during the video analysis carried out for the first chapter of this thesis.

As a matter of fact, the CMP is too far off-coast for its exploitation to be economically viable for artisanal fishermen from Spain, Morocco or Algeria. In addition, the complex geomorphology of the mounds might be too rough for industrial trawlers to operate in the area.

Q2: *What is the distribution of cold-water corals and associated megabenthic species on the Cabliers Coral Mound Province in relation to mound geomorphology?*

Although some coral colonies could be observed on the flanks of the mounds, the highest densities of CWCs were detected on the mounds' crest or summit. This agrees with previous observations in the Atlantic and potentially relates to the presence of more favourable environmental conditions (Huvenne et al., 2005; Davies et al., 2009; Lo Iacono et al., 2018a), such as enhanced hydrodynamics, food supply and structural stability. The top of the CMP mounds is characterised by the presence of successive ridge-like features with a morphology that resembles that of several mini mounds. Indeed, these ridge-like features were formed by living reefs that displayed the highest values of CWC density observed on the mounds' crest (Fig. 2.9). Such features are comparatively elevated to the rest of the crest, probably exposing the corals to more intense currents that might advect a larger amount of food particles towards them and prevent excessive sediment deposition that could be detrimental for the corals' growth. The fact that the summits of these reefs display the highest CWC densities seems to suggest that these features are the engine driving coral mound formation. Indeed, they could be the indication that Cabliers ridge-like mounds derive from the union of multiple smaller mounds (Buhl-Mortensen et al., 2017).

The distribution of some megabenthic species associated to these CWC reefs is also related to the morphology of the mounds, with the highest densities of *A. hirsuta*, *P. larix* and *A. setubalense* mostly occurring on the summits of the reefs found on the mounds' crests. Nonetheless their distribution along the reefs depends on coral density, for when corals are abundant these species are generally displaced to the flanks of these reefs, where there is a higher substrate availability in the form of dead coral framework (Fig. 2.9).

Q3: *Does the size of living cold-water coral patches vary among the different geo-morphic sectors of the mounds?*

Similarly to coral density, coral colony size also increases towards the crest of the mounds. This pattern is most likely caused by a higher substratum stability on the sub-horizontal mound crest that allows the coral colonies to grow larger than the ones on the flanks, which might be subjected to be buried or destroyed by structural collapses of coral framework from the upper sections of the mound.

Q4: *Are there differences in terms of species composition and abundances between northern and southern Cabliers mounds? What are the main seafloor variables driving species distribution?*

There are evident changes in species composition and relative abundance between the northern and southern Cabliers coral mounds. The northern mounds present a mixture of dense living coral and exposed dead coral framework, whereas the southern mounds are depleted of living coral and dominated by gorgonians and antipatharians. Besides framework-building corals, other species such as the antipatharians *P. rigida* and *L. glaberrima,* and the hexactinellid sponge *A. setubalense* also decrease in abundance or are completely absent in the southern

region of Cabliers. The gorgonian *A. hirsuta*, the antipatharian *P. larix* and squat lobsters are the only abundant species that can be found in both regions, with a higher abundance reported on the southern Cabliers mounds.

The observed patterns in taxonomic composition and relative abundance suggest a significant change in the environmental conditions between the northern and southern Cabliers mounds. Nevertheless, the physicochemical conditions of the water bathing the two sectors of the CMP should be almost identical as they are found within the same water mass (i.e. LIW) and thus, it must be the changes in other environmental factors what determines the patterns in taxonomic composition observed along the province. For instance, the potential presence of weaker currents in the southern mounds would bring less food to the organisms living there and could explain the greater amount of fine sediments observed on the mound's crest. Lower intensity currents would also produce less resuspension of organic material from the seafloor, preventing the corals and other species from exploiting the additional food source that these resuspended sediments represent. In addition, the crest of the coral mounds from the southern CMP is found at a greater water depth (~420–445 m) than the crest of the northern ones (~280–325 m), which could also be a relevant factor affecting the species distribution. This hypothesis coincides with the results of the Canonical Correspondence Analysis, as depth was found to be one of the main seafloor variables affecting species distribution, together with substratum type. Water depth has long been regarded to be linked to changes in several other environmental variables such as temperature, salinity, particulate organic carbon and dissolved oxygen. In this sense, the southern and probably less prolific part of the CMP is located considerably further away from the interface between Atlantic and Levantine Intermediate Waters (AW-LIW; ~200 m water depth) than its northern counterparts. Water mass interfaces are known to accumulate both organic and inorganic suspended particles and are able to make them oscillate vertically and to transport them laterally through the action of enhanced hydrodynamic processes such as internal waves (Dickson and McCave, 1986; Mienis et al., 2007). As a matter of fact, internal waves have been observed to form along the AW-LIW interface in the Alboran Sea (Van Haren et al., 2014; Ercilla et al., 2016). Hence, the observed ~100 m of difference in water depth between the N and S mounds might have placed the southern mounds too far from the AW-LIW interface to experience the enhanced hydrodynamics associated with these oceanographic features, ultimately reducing the food availability to the corals growing in this region. Furthermore, the difference in water depth between the two regions of the mound province could have also affected the past development of the coral mounds during the Quaternary glacio-eustatic oscillations and thus, this topic was investigated in Chapter 3.

Q5: *Are there differences between the fauna observed in this coral mound province in comparison to other Mediterranean and Atlantic coral mounds?*

Although the megafauna found in coral mound provinces from the Mediterranean Sea and the Atlantic Ocean belong to the same functional (i.e. mainly filter-, suspension-feeders) and broad taxonomic groups (e.g. gorgonians, hexactinellid sponges, demosponges, squat lobsters and sebastid fishes), the fauna associated with the CMP displays significant differences compared to that of other mounds, but especially to those mounds outside the Mediterranean Sea. Indeed, the dominating species accompanying the *M. oculata* and *D. pertusum* reefs of Cabliers (i.e. *L. glaberrima*, *A. hirsuta* and *Pachastrella* sp.) are also observed on the Santa

Maria di Leuca coral-topped mounds (Ionian Sea). The main difference is the presence in the CMP of P. rigida and A. setubalense, which as noted before are Atlantic species (Opresko, 2009; Boury-Snault et al., 2015) and thus, they only occur in the westernmost sector of the Mediterranean Sea. The main difference between Mediterranean and Atlantic coral mounds resides in the relative abundance and taxonomic composition of the reef-building corals. The former are dominated by *M. oculata* and complemented by *D. pertusum* and some colonies of *D. cornigera*, whereas the latter are generally composed of *D. pertusum* accompanied by *M. oculata* and in some cases by *Solenosmillia variabilis* and *Enallopsamia profunda* (Freiwald, 2002; Vertino et al., 2010; Buhl-mortensen et al., 2017; Hanz et al., 2019). Similarly to the CMP, gorgonians, antipatharians, demosponges and hexactinellid sponges can be found among the main species associated to Atlantic coral mounds. However, most of the species belonging to these groups are different to those found in the CMP. Overall, the taxonomic differences observed between Atlantic and Mediterranean coral mounds, in terms of megabenthic assemblages, indicate that globally, the number of species associated with CWC reefs is probably higher than previously thought.

5.1.2.2. *Chapter 3*

Coral mounds commonly occur in clusters, with most of them reported so far in the Northeast Atlantic (Wheeler et al., 2007; Roberts et al., 2009a; Lo Iacono et al., 2018a). Nonetheless, during the last decade several new coral mound provinces have been described on West-African (Eisele et al., 2011; Van Dorpe et al., 2017; Wienberg et al., 2018; Tamborrino et al., 2019) and East-American (Raddatz et al., 2020; Steinman et al., 2020) continental slopes, and in the Mediterranean Sea (Comas and Pinhero, 2010; Lo Iacono et al., 2014, 2016; Savini and Corselli, 2010; Corbera et al., 2019). The formation of these complex geomorphologic features can last for up to several millions of years (Kano et al., 2007), over which dramatic climatic fluctuations related to glacial-interglacial cycles occur. These fluctuations cause drastic changes in relative sea-level, SWT and water mass circulation (Martrat et al., 2004; Rogerson et al., 2008; Grant et al., 2014), among other variables, that considerably affect the development of the mounds (i.e. increasing, reducing or impeding mound formation). Although several studies have tried to relate coral mound formation in the Mediterranean Sea to changes in the paleo-climatic setting, due to gravity core length limitations they could only investigate the shallowest part (i.e. <6 m) of the coral mounds' development (i.e. since the last deglaciation ~15 ka BP; Fink et al., 2013; Wang et al., 2019). Nonetheless, the mounds studied so far are considerably taller than the length recovered by the cores and thus they might have started to form much earlier than the last deglaciation. It is important to take into consideration that throughout a recent oceanographic cruise, several coral mounds of the Alboran Sea have been drilled to their base using a MeBo operational system, which can perform core drillings of up to 200 m. However, the data related to this survey is yet to be published in the scientific literature. Fink et al. (2013) and Wang et al. (2019) linked coral mound formation in the Alboran Sea to a complex interplay between surface productivity and changes in sea-level during the last deglaciation and the Holocene.

This chapter described the coral deposits and formation periods of two coral mounds located at the northern and southern ends of the Cabliers Coral Mound Province during the Middle Pleistocene-Holocene. The conclusions reached in this chapter have major implications towards achieving a better understanding of the environmental constraints driving coral mound formation in the Mediterranean Sea.

- **Research questions:**

Q6: *When did the mounds in the Cabliers Coral Mound Province develop?*

Although the gravity cores extracted from each mound recovered a similar amount of material (i.e. 840 and 1038 cm), substantial differences in mound formation between the two ends of the province were observed. The core corresponding to the northernmost mound (i.e. MD13-3470G; 313 m water depth) covers a period of mound development that goes from ~15 to 0.3 ka BP, whereas the one collected from the southernmost mound (i.e. MD13-3469G; 417 m water depth) encompasses coral mound formation stages from >390 to 9.3 ka BP. Hence, this study contributes to expand the current knowledge of coral mound development in the Mediterranean Sea, which was so far limited to the Holocene (Marine Isotopic Stage 1 [MIS 1]) and the last deglaciation. Throughout the last ~390 kyr several glacial-interglacial cycles occurred, with the main periods of coral mound development taking place during deglaciations and temperate interstadials (3.5–4.1 $d^{18}O‰$). These mound formation periods were intercalated with mound stagnation periods that ranged between ~24 and ~98 kyr, and that mainly coincided with glacial periods. Coral mound formation during interglacial periods (<3.5 $d^{18}O‰$) was only observed throughout the Holocene in the northern and shallower mound, which displayed the fastest Aggradation Rates (ARs) of the CMP (i.e. 203 cm kyr^{-1}).

Q7: *What are the main environmental variables driving coral growth on the Cabliers Coral Mound Province?*

Although coral growth has been observed on the *CMP* during periods with a SWT range of 4.6–13.1°C, the highest mound formation rates occurred when the SWT ranged between 7 and 11°C. During these fast mound formation periods the coral deposits were almost entirely dominated by *D. pertusum*, a species with a higher capability to promote enhanced mound formation than *M. oculata* (Wienberg, 2019). As observed in Wang et al. (2019), our data also suggest that one of the main variables controlling coral mound formation in this province is the depth of the AW-LIW interface (i.e. currently at ~200 m water depth). As noted above, these oceanographic features tend to be associated with accumulations of particulate matter that can be transported to deeper areas through the action of internal waves, potentially acting as a food source for the corals. This hypothesis is further strengthened by the absence of coral growth in the southern and deeper mound during interglacial periods, when the sea-level was similar to the one observed in the present day, and the AW-LIW interface is assumed to have shoaled. Although the depth at which the AW-LIW interface is located has major implications for coral mound development, there are other crucial factors that need to be considered. For instance, the amplitude of the internal waves produced in this interface represents a key factor in bringing particulate organic matter closer to the mounds, as waves with larger amplitude can reach deeper areas. Van Haren et al. (2014) described internal waves with amplitudes of up to 90 m at around 250 m water depth, which with the current sea level would only affect the northern and shallower mounds of the CMP. Nonetheless, further investigation on how these internal waves form and how they interact with the local physiography is needed in order to have a better understanding of their effect on coral mounds formation. Regardless of all these oceanographic processes, for the AW-LIW interface to promote a higher food supply to the coral mounds, there has to be enough surface productivity in the first place. Indeed, the Alboran Sea seems to present enhanced surface productivity during temperate interstadials and interglacial periods, as the southward shift of westerly winds causes an increased inflow of AW

that points to an enhanced gyre-induced upwelling (Cacho et al., 2000; Moreno et al., 2005). This also demonstrates that, further to internal waves, other oceanographic processes can act as mechanisms for building a nutritional link to deep-sea ecosystems.

Even within interstadial periods that could have been suitable for coral mound development, the reduced flow of LIW in the Alboran Sea caused by a strong stratification in the Eastern Mediterranean Basin during sapropel events is associated with periods of coral mound stagnation in the CMP. The lack of mound formation during these periods could have been caused by an alteration of the AW-LIW interface structure as a consequence of the reduced LIW flow. This could have negatively affected the accumulation of particulate organic matter, otherwise typically observed at water mass interfaces, and as a consequence reduced the food delivery to the corals. Due to the strong water column stratification in the Eastern Mediterranean Basin, the water mass bathing the CMP could have also presented variations in its physicochemical variables, including potentially lower oxygen levels. Although Atlantic CWCs have been observed to grow in areas with extremely low dissolved oxygen thanks to the presence of an intense and periodic food supply (Mienis et al., 2012b; Hanz et al., 2019; Hebbeln et al., 2020), in the CMP the potentially lower oxygen concentration of the LIW during Sapropel events would have been added to the already limited food supply of this oligotrophic basin (i.e. Western Mediterranean), thus causing unsuitable conditions for coral growth.

Q8: *What environmental variables regulate the differences in mound formation patterns between the northern and southern mounds of this province?*

The slower coral mound development and current stagnation state of the southern Cabliers mound suggest that this sector of the province has been and is actually subjected to less favourable environmental conditions for coral mound formation. Among the wide range of environmental variables that affect coral mound development, and as discussed above, water depth is likely a key factor driving the contrasting mound formation patterns observed between the two ends of the CMP. It is likely that under equal surface productivity conditions, the shoaling of the AW-LIW interface during the last sea-level rise prevented the southern mound from receiving a sufficient food supply for coral survival. Nonetheless, as the northern mound is ~100 m shallower than the southern mound, it might have been close enough to the water mass interface to keep growing until the present-day.

Q9: *Do fluctuations in the paleoclimatic setting cause changes in the taxonomic composition of the coral deposits?*

There is an almost synchronous change in the taxonomic composition of the coral deposits forming the two coral mounds studied here at around 9–10 ka BP. Both deposits change from *D. pertusum* to *M. oculata* dominated facies. A pattern that has also been observed in the other Alboran Sea coral mounds (Stalder et al., 2015; Wienberg, 2019) and is apparent in the present-day CWC assemblages of the Mediterranean Sea, as they are generally dominated by colonies of *M. oculata* occasionally mixed with some *D. pertusum* and *D. cornigera* colonies (Orejas et al., 2009; Freiwald et al., 2009; Vertino et al., 2010; Gori et al., 2013; Taviani et al., 2017). Indeed, *M. oculata* is known to withstand higher SWT than *D. pertusum* (Nauman et al., 2014) and thus, this species might have been able to adapt better to the high SWT characteristic of interglacial periods. It is also important to note that the core extracted from the southern CMP (i.e. MD13-3469G) is the first one so far to present a reef facies entirely dominated by *D. cornigera*,

which occurred from ~352–312 ka BP (MIS 9). This species dominated the Mediterranean Sea coral communities before the Plio-Pleistocene transition when the global temperatures were generally higher (Sosdian and Rosenthal, 2009). Aquaria experiments have also demonstrated that *D. cornigera* thrives at warmer SWT than *D. pertusum* and *M. oculata* (Gori et al., 2014). In the present day, dendrophyllid corals form dense assemblages in the Eastern Mediterranean Basin, where *D. pertusum* and *M. oculata* are scarcer due to the dominance of oligotrophic and warm waters in these regions. Although no significant differences in SWT are observed here between the period dominated by *D. cornigera* and the rest of coral mound development, the presence of other unfavourable environmental conditions might have impeded the growth of *D. pertusum* and *M. oculata*.

Q10: *Is there a difference in mound formation patterns between the Cabliers Coral Mound Province and the rest of coral mound provinces found in the Alboran Sea?*

All the mounds in the Alboran Sea show similar mound development patterns, as they generally present thriving coral reefs during temperate periods marked by a benthic foraminiferal $d^{18}O$ range of 3.5–4.1‰ (i.e. deglaciations and temperate interstadials). Nonetheless, it is important to note that while the West and East Melilla Mounds entered in a stagnation state before 4 ka BP (Fink et al., 2013; Wang et al., 2019), the northern sector of the CMP kept growing until the present-day. Indeed, thriving *M. oculata* and *D. pertusum* reefs can still be observed growing on the crest of these mounds. This is most likely caused by the present-day oceanographic conditions of the Alboran Sea, which involve the jet of highly productive Atlantic waters, the presence of a downwelling region and the action of internal waves at the AW-LIW interface that advect nutrient-rich surface waters closer to the mound's crest.

5.1.2.3. *Chapter 4*

So far, in the Mediterranean Sea all coral mound development studies have been focused in the Alboran Sea (Fink et al., 2013; Wang et al., 2019; Stalder et al., 2015, 2018; Fentimen et al., 2020; Corbera et al., 2021), with the most recent studies relating mound formation in this sub-basin to surface productivity and the depth of the AW-LIW interface (Fink et al., 2013; Wang et al., 2019; Corbera et al., 2021). Additionally, mound formation in this region has been reported to occur mainly during temperate/warm periods (i.e. deglaciations and temperate interstadials; Fink et al., 2013; Wang et al., 2019; Corbera et al., 2021) resulting in the hypothesis that mound development in the Mediterranean Sea does not occur during glacial periods.

This chapter described the mound formation periods during the Middle-Late Pleistocene of three coral mounds located on the newly discovered Tunisian Coral Mound Province. By reporting the first occurrence of glacial-aged coral mound formation in the Mediterranean Sea, this chapter provides an unprecedented view on the development of coral mounds in this basin.

- **Research questions:**

Q11: *When did the mounds in the Tunisian Coral Mound Province develop?*

The cores collected from the TMP present coral mound development stages that encompass a period of time going from 424 to 8.4 ka BP. Opposite to what has been reported so far in the Mediterranean Sea, the fastest development of the TMP coral mounds (ARs up to 48 cm kyr^{-1})

occurred during the last glacial period (i.e. 39–15 ka BP; MIS 3, 2), which expands the current knowledge on coral mound development in this basin. In addition, the deepest mound studied in this province (i.e. GM2AAGC-403; 505 m water depth) displays a hiatus of ~340 kyr, with another mound formation period occurring between ~424 and ~383 ka BP.

Q12: *What are the main environmental drivers determining cold-water coral mound formation in the Tunisian Coral Mound Province?*

Mound formation in this province mainly occurred during the last glacial period, when surface productivity was enhanced in this region (Incarbona et al., 2008). In addition to the productivity being higher, the sea level was at its lowest values (–100 to –140 m), hence placing AW-LIW interface the closest it can be to the mounds' crests (currently at 380–505 m). The combination of these two environmental drivers probably provided a sufficient food supply for coral mound formation during the last glacial period. As identified in the preceding chapters, this finding supports the importance of the distance between coral mounds and AW-LIW interface for mound development in the Mediterranean Sea. Indeed, the TMP stopped growing with the onset of the Meltwater Pulse 1A (14.7–13.5 ka BO), which caused an increase in sea level of 20 m in less than 500 years, most probably moving the AW-LIW interface too far away from the mounds to act as an efficient food source for the corals. Apart from the sea level increase and the decreased productivity typical of interglacial periods in this region, SWT also increased during the last sea level rise (Essallami et al., 2007). In fact, the modern SWT values of the LIW are over 13.7°C in this region, which is close to the physiological limit of *D. pertusum and M. oculata* (i.e. 14°C), a factor that might have contributed also to limit coral growth during interglacial periods.

Q13: *Are there differences in mound formation patterns among the three different mounds studied in this region? If yes, what environmental variables regulate these spatio-temporal differences in mound formation?*

Although all the coral mounds studied in this province record periods of mound formation during the last glacial, there are considerable differences among them. These are particularly evident when comparing the development of the two shallowest mounds (GM2AAGC-409 and GM2AAGC-406) to that of the deepest one (GM2AAGC-403). While the former present a practically continuous mound formation during the MIS 3 and 2, the latter displays a discontinuous and slower development, which suggests that this mound was subjected to less favourable environmental conditions during the last glacial. Indeed, the mound corresponding to GM2AAGC-403 was the deepest one (505 m water depth) and thus, according to our hypotheses it might have experienced the lowest food supply.

Q14: *Do the mound formation periods of the Tunisian Coral Mound Province match with those of the Alboran Sea coral mound provinces?*

The Tunisian and the Alboran Sea coral mounds display almost complementary mound formation periods. The former mainly formed during the last glacial (MIS 3 and 2) and entered in stagnation with the onset of the Meltwater Pulse 1A (MWP-1A). In contrast, the latter commonly developed during deglacials and temperate interstadials. During the last glacial-interglacial cycle, the Alboran Sea mounds started to grow soon after the MWP-1A and stopped throughout the Early-Mid Holocene. The only coral mound that managed to keep growing

during the Late Holocene is the northernmost mound of the CMP, which still presents thriving CWC reefs in the present-day.

Besides the contrasting coral mound formation patterns observed between the Alboran Sea and the TMP, the latter also develop at a considerably slower rate than most of the Alboran Sea mounds. This could be related to the greater water depth of the Tunisian mounds throughout their formation periods, which is associated with a greater distance between the mounds' crests and the AW-LIW interface. Indeed, Figure 4.6 shows a clear negative exponential relationship between the maximum ARs of each mound and water depth, supporting the overall importance of this interface in controlling the growth rate of coral mounds in the Mediterranean Sea during periods of enhanced productivity. Nonetheless, it is important to consider that mound aggradation does not only depend on coral growth but also on the amount of sediment baffled by the coral frameworks. Even with a fast coral growth, if their frameworks do not trap enough sediments to stabilise their structure, these would eventually collapse, resulting in a slow AR.

5.2. Thesis contributions

5.2.1. Scientific contributions

Three different branches of science (i.e. biology, geology and geochemistry) were used to provide a more comprehensive view and understanding of the functioning of CWC reef assemblages and coral mound formation in the Mediterranean Sea. Indeed, this doctoral thesis presents studies that encompass both the modern ecological state of thriving CWC reefs and the development of Mediterranean coral mounds in space and time, using a transversal approach that combines knowledge from all these scientific disciplines.

This thesis described for the first time the present-day ecological state of the CMP, a new cluster of coral mounds discovered in 2015 (Lo Iacono et al., 2016). The northern sector of this mound province includes the most thriving and pristine coral reefs found so far in the Mediterranean Sea, with CWC densities that are considerably higher than the ones recorded in other regions of this basin (Orejas et al., 2009; Gori et al., 2013). This work also provided the first quantitative data (i.e. density and relative abundance) on the main megabenthic species occurring within the living and dead reefs of a Mediterranean coral mound. The latter were found to be mainly formed by *M. oculata* and to a lower extent *D. pertusum*, accompanied by the gorgonian *A. hirsuta*, the sponges *Pacastrella* sp. and *A. setubalense*, the antipatharians *P. larix*, *L. glaberrima* and *P. rigida* and the echinoid *C. cidaris*. Although the megafauna observed in the CMP belongs to the same broad taxonomic groups that can be observed in Atlantic coral mounds, there are considerable differences at the species level, thus expanding the number of species associated to CWC reefs.

The CMP displays both thriving CWC reefs and areas with dead coral framework, covered by octocoral and antipatharian aggregations, which could represent the different ecological succession states characteristic of flourishing and stagnation mound formation periods respectively. Although thriving reefs are typically observed on the crests and summits of coral mounds (Freiwald et al., 2004; Huvenne et al., 2005; Davies et al., 2009), this thesis has brought further insight into the distribution of these reefs on ridge-like coral mounds. Indeed, the thriving CWC assemblages observed on the Cabliers mounds' crests seem to be spatially organised along it, with the highest concentration of living corals occurring on the

summit of recurrent reefs (as presented in this thesis in Figure 2.9). Based on the density of thriving CWCs and the observation of minimal fishing pressure on the CMP, this province could be used as a baseline to assess the state of conservation of CWC assemblages of the Mediterranean, most of which undergo severe pressure related to human activities.

In the Mediterranean Sea several studies have tried to link coral mound formation to paleoclimatic oscillations, yet they have mainly described coral mound development occurring from the last deglacial until the present day (Fink et al., 2013; Stalder et al., 2015, 2018; Wang et al., 2019). This thesis expands that timeframe beyond the last glacial to ~400 ka BP, which contributes to cover the gap of knowledge in coral mound development that exists from the Calabrian period (Middle Pleistocene) until the last deglaciation, bringing unprecedented insights into the evolution of CWC mounds in the Mediterranean Sea. The findings of this thesis are consistent with those of Wang et al. (2019), where the author also suggested that a combination between surface productivity variations and glacio-eustatic fluctuations of the AW-LIW interface play a relevant role in controlling coral mound development in the Alboran Sea. This agrees well with the distribution of Atlantic Coral mounds, as they also tend to be located close to water mass interfaces (Matos et al., 2017; Lo Iacono et al., 2018a; Wienberg et al., 2020). Although previous studies have reported a negative effect of Sapropel events on the growth of CWCs (Fink et al., 2012, 2015; Taviani et al., 2019), this was thought to be limited to the hypoxic and anoxic conditions observed in Eastern Mediterranean Basin during sapropel deposition. Nonetheless, this thesis has provided evidence that beyond affecting the Eastern Mediterranean Basin, the indirect effects of Sapropel events (i.e. reduction in LIW formation) were also detrimental to the development of coral mounds in the westernmost Mediterranean Sea.

Generally, the study of coral mound development in the Mediterranean Sea has focused in the Alboran Sea, despite the presence of further coral mound provinces in both the Tyrrhenian Sea (Remia and Taviani, 2005; Angeletti et al., 2020a; Camafort et al., 2020) and the Strait of Sicily (Martorelli et al., 2011). Therefore, by describing the development of three coral mounds from the TMP, this thesis has increased the knowledge regarding mound formation in the Mediterranean Sea. In addition, coral mound development in this basin has always been reported to occur throughout warm periods (Fink et al., 2013, 2015; Stalder et al., 2015, 2018; Wang et al., 2019) and thus, the glacial-aged formation of the TMP reforms the view that researchers had so far regarding mound formation in the Mediterranean Sea. A complex interplay between surface productivity and the depth of the AW-LIW interface also seems to have had an important role in controlling mound development in the TMP. Indeed, this study suggests that a direct correlation exists between the distance from the mounds' crest to this interface and the pace of mound formation.

Significant changes in the species dominating the coral deposits of both coral mound provinces could be observed during certain periods of mound development. Such changes in the main framework-building species promoting mound formation (*D. pertusum*, *M. oculata* or *D. cornigera*) are most likely related to crucial variations in the environmental conditions. Therefore, the results acquired here suggest that a more detailed study of the species forming the coral mounds throughout different periods can provide additional information regarding past changes in the environmental setting. However, in order to be able to acquire this additional data, a better constrained description of the physiological limitations and requirements of each of these species is strictly needed.

Overall, with the discovery of these two coral mound provinces and the description of their past development, the present thesis expands the current knowledge on coral mound formation in the Mediterranean Sea both in space and time, and provides a robust description of the main environmental drivers controlling it.

5.2.2. Applied contributions

The data presented in Chapter 2 has been used towards the preparation of a Fisheries Restricted Area (FRA) proposal for the General Fisheries Commission for the Mediterranean (GFCM). This Proposal will be sumitted to the GFCM, belonging to United Nations, by the NGO OCEANA in collaboration with the Institute of Marine Sciences (ICM-CSIC). The main aim of this action is to prohibit any fishery activity and ship transiting over the coral mounds and immediate surroundings, with the aim of protecting the exceptional benthic assemblages observed growing on the CMP. These assemblages include the semi-pristine coral reefs observed on the crest of the northern mounds of the province, the octocoral and black coral aggregations found on the crest of the southern mounds and the dense and almost monospecific black coral meadows of the mounds' flanks, mainly formed by the Atlantic species *P. rigida*.

Overall, the core area proposed to be protected encompasses 546.6 km^2 found within a depth range of 227 and 1500 m water depth. The core area is surrounded by a buffer zone that expands the area protected and its depth range to 862.6 km^2 and 1850 m water depth, respectively.

5.3. Limitations of the work

This thesis was principally aimed at describing the species distribution in a thriving Mediterranean CWC mound and at determining the main environmental variables driving coral mound formation in the Mediterranean Sea. However, the study of the present-day assemblages along the province is limited by the low number of ROV dives performed and their location, as only three transects were recorded, two in the northernmost mounds and the third in the southernmost ones. Hence, although the benthic assemblages described here represent a first attempt to characterise the fauna found in a Mediterranean coral mound province, they do not cover all the different environments present in this region. In a similar way, a gravity core only corresponds to a single-location set of observations and thus attention should be paid when extrapolating the development patterns of an entire coral mound province from one core. Indeed, the third chapter of this thesis shows that significant differences in mound development patterns can occur between two gravity cores collected from the same coral mound province. Another limitation of coral mound development studies becomes apparent during periods of mound stagnation, as the coral fragments preserved in the mound record can only be used to unveil the environmental conditions throughout periods of coral growth. In this sense, the study of foraminifera from off-mound cores could provide valuable information to characterise the environmental setting of the mounds during stagnation periods, thus providing a more continuous and comprehensive paleo-scenario. The characterisation of the environmental setting could also benefit from the use of additional geochemical proxies (e.g. Nd, P/Ca and potentially $\delta^{15}N$; Van de Flierdt et al., 2010; Anagnostou et al., 2011; Wang et al., 2015) to those already used here (i.e. Li/Mg and Ba/Ca).

Besides the limitations associated to the methodologies and sampling design used in this type of studies, the lack of quantitative data from other CWC assemblages of the Mediterranean Sea

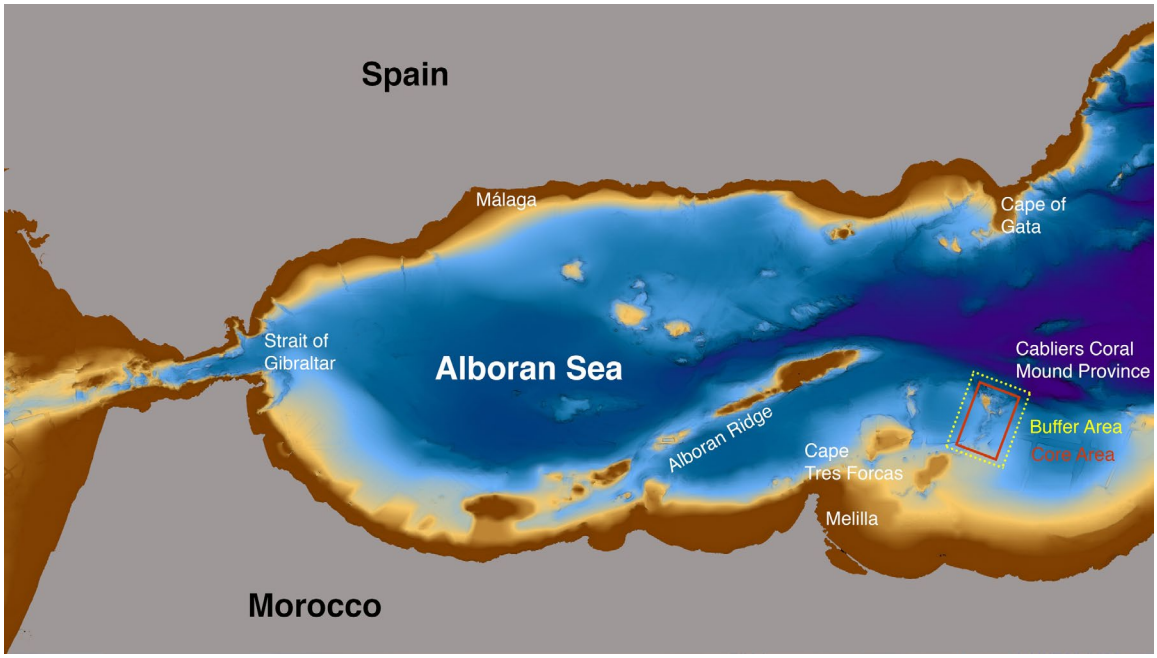

Fig. 5.1. Bathymetric map of the Alboran Sea including the Cabliers Coral Mound province with the core (red rectangle) and buffer areas (yellow dotted rectangle) proposed as a Fisheries Restricted Area. The Digital Terrain Model has been derived from the EMODnet Bathymetry portal – http://www.emodnet-bathymetry.eu.

(e.g. Vertino et al., 2010; Lastras et al., 2016; Taviani et al., 2017; Fabri et al., 2017; Angeletti et al., 2020a, b) limits the comparison between regions and the determination of the ecological state in which these assemblages are. In a similar way and depending on the area studied, the lack of background palaeoceanographic data can also restrict the interpretation of coral mound development in response to environmental fluctuations.

5.4. Future perspectives

5.4.1. Aims for the future study of the Cabliers and Tunisian Coral Mounds

The CMP represents a semi-pristine aggregation of coral mounds and thus, it could be used as a baseline to assess the ecological state of other mounds displaying thriving coral reefs on their summits (e.g. Corsica Coral Mounds; Angeletti et al., 2020a). Nonetheless, in order to do so, a detailed quantification of the actual extent of the thriving coral reefs covering the northern mounds and a more exhaustive description of the accompanying fauna (including mega-, macro- and meiofauna) occurring on both the living reefs and dead coral frameworks of the southern sector of the province, should be performed. This would also complement the initial study of the Santa Maria di Leuca coral-topped mounds carried out by Mastrototaro et al. (2010), thus providing a comprehensive description of the taxonomic composition and relative abundance of the fauna associated to Mediterranean CWC reefs. In addition, the contrasting abundances of living CWCs observed between the northern and southern Cabliers mounds must relate to sharp changes in the environmental conditions. Hence, a thorough characterisation of this coral mound province modern environmental setting, through the deployment of benthic landers or moorings, might help to unveil which are the most relevant physicochemical or biological variables driving present-day CWC distribution.

Although this thesis has already given the first insights into the formation of the CMP in relation to paleoclimatic changes, the core corresponding to the northernmost mound only

encompasses its development during the Holocene. Therefore, a longer core is needed to see how this sector of the province developed during the Pleistocene. The cores described here correspond to the two extremes of the province and thus, it would be of interest to collect additional gravity cores from the other mounds found along the CMP in order to acquire a more complete description of this province's coral mound development. This would also help to confirm the hypothesis that sea-level is a key variable driving coral mound development in the Mediterranean Sea (Wang et al., 2019; Corbera et al., 2021). A similar approach should be taken in the TMP (i.e. collection of additional and longer gravity cores), where coral mound development could only be described in detail for three different coral mounds and mainly throughout the last glacial. In addition to the acquisition of further on-mound gravity cores from each of these provinces, at least one off-mound core per region should be collected, which would help towards the characterisation of the environmental setting in periods of coral mound stagnation.

5.4.2. Overarching aims for the future of cold-water coral mound research

The recent discovery of the TMP suggests that further coral mounds should occur on the continental slopes of this basin. Particularly, as suggested both here and in Taviani et al. (2017) and Wang et al. (2019), research efforts should be focused on the exploration of continental slopes influenced by the highly productive AW and at a depth range bathed by the LIW. Although no coral mounds have been found yet east of the Strait of Sicily, it is possible that some other features developed along those margins during colder periods; hence, seafloor exploration using large-scale multibeam mapping and seismic profiles should be performed to investigate their potential occurrence. Together with the exploration for the discovery of new coral mound provinces, the past development of the Corsica Mounds (North Tyrrhenian Sea) and the Pantelleria Mounds (Strait of Sicily) should also be described. This would help towards acquiring a more comprehensive view of coral mound development in the Mediterranean Sea and to corroborate the environmental control hypotheses formulated so far in Fink et al. (2013), Wang et al. (2019) and this thesis. Another way of verifying this hypothesis would be to acquire a better characterisation of the surface productivity and water mass structure of the Mediterranean Sea shallow and intermediate waters (e.g. AW and LIW) over glacial-interglacial cycles. This could be used to model the changes in depth and strength of the AW-LIW and help towards having a better understanding of the influence of this oceanographic feature on CWC mound formation in this basin.

Although the precision of U-series acquired by Laser Ablation MC-ICP-MS is lower than that of solution MC-ICP-MS, the former method is more economical and can be used to rapidly produce age models of coral mound gravity cores (Spooner et al., 2016). Indeed, between 30 and 40 samples can be analysed in less than 24 hours, providing more complete and continuous age models than those produced only through solution MC-ICP-MS. Therefore, future production of coral mound age models should incorporate this methodology, ideally in order to complete the gaps between samples dated by means of solution methods.

Researchers tend to focus either on the current ecological state of the benthic assemblages living on coral mounds or on the environmental mechanisms that drove the past development of these geomorphological features. As demonstrated here, a combination of both types of study (ecological and geological) could help to better understand which are the main variables controlling coral mound development and the changes in species composition observed through-

out the different periods of mound formation. For instance, the contrasting environmental conditions found in coral reefs dominated by different species in the present day could be associated to sharp changes in the main species dominating the coral deposits of a gravity core. In addition, the study of accompanying calcareous species through time in coral mound research might give us additional information to that already provided by the corals (e.g. periods of mound development, environmental setting variations during mound aggradation). Throughout the past, variations in the accompanying fauna can be related to fluctuations in the environmental setting that might have affected coral mound development, whereas in the present-day the comparison of the reefs' associated fauna can offer information on the biogeography of intermediate depths.

While researchers have repeatedly studied the past development of coral mounds from different regions in relation to changes in the paleoenvironmental setting (Wienberg et al., 2010; Frank et al., 2011; Eisele et al., 2014; Tamborrino et al., 2019; Wang et al., 2019), robust and detailed models of how coral reefs and mounds form are lacking. In terms of reef formation, Mortensen et al. (2008) exposed that coral reefs subjected to a strong unidirectional current regime seem to grow against the prevailing current, while the lee side of the reef consists on dead coral framework and rubble. However, the exact hydrodynamic and physiological mechanisms that drive coral distribution on a reef exposed to a unidirectional current regime are not completely understood. Flume aquaria with small-scale artificial reefs and living coral nubbins could be used to recreate the current speed and turbulence conditions experienced by an actual reef and its consequences for nubbin growth and physiological state, which could help towards a better understanding of coral reef development. Nevertheless, many coral reefs are located in regions with a more complex hydrodynamic setting, involving a prevailing current flow that is combined with internal tides. The study of the formation of these reefs would proof to be more challenging, as it would be extremely complicated to recreate such hydrodynamic conditions.

5.5. Concluding remarks

The present study helped to increase our knowledge on the main species associated to Mediterranean CWC reefs and their relative abundance. The present-day megafaunal distribution on Mediterranean coral mounds was associated to their fine-scale geomorphology and to several seafloor factors, with substratum and depth being the most important ones. The taxa associated with CWC reefs in this basin displayed considerable variations compared to that of the different Atlantic coral mound provinces, thus suggesting that the number of species associated with these habitats is even larger than previously thought. On a different note, the results of this thesis also helped to define that coral mound development in this basin was most probably linked to a high surface productivity and a short distance between the mounds' crests and th AW-LIW interface, as these two factors combined would have been able to provide the mounds with a sufficient food supply for coral growth. Furthermore, on a regional scale, the oceanographic and physicochemical alterations triggered during Sapropel events seem to have been detrimental for the development of these complex geomorphic features. Overall, this thesis contributes towards a better understanding of the past development of coral mounds and the present-day distribution of species along these features in the Mediterranean Sea.

Appendix

Chapter 2 supplementary materials

Table S2.1. Results of the CCA analysis implemented at different sampling unit sizes.

SU size	SU N°	Total inertia	Constrained inertia	Unconstrained inertia	% Inertia explained by env. fact.	N° of assemblages
2	2159	8.6164	0.9363	7.6801	10.87	5
4	739	6.3787	0.8853	5.4934	13.88	5
10	349	4.0646	0.7633	3.3013	18.78	4
20	215	2.9713	0.6927	2.2786	23.31	3

Table S2.2. Abundance of the species identified in each ROV Dive and total abundance for the whole study area.

		Northern Cabliers		Southern Cabliers	
		Dive 1	Dive 2	Dive 3	Total
Cnidaria	*Phanopathes rigida*	816	716	0	1532
	Acanthogorgia hirsuta	345	228	918	1491
	Madrepora oculata	967	178	15	1160
	Leiopathes glaberrima	368	21	0	389
	Parantipathes larix	97	31	234	362
	Lophelia pertusa	84	27	2	113
	Dendrophyllia cornigera	59	25	2	86
	Antipathes dichotoma	30	29	0	59
	Cerianthus sp.	0	0	13	13
	Chyronephtia mediterranea	5	2	2	9
	Kophobelemnom sp.	1	1	6	8
	Callogorgia verticillata	1	0	0	1
Porifera	*Pacastrella* sp.	413	244	10	667
	Asconema setubalense	219	171	0	390
	Geodia sp.	0	30	8	38
	Axinella infundibulum	1	12	1	14
	Hamacantha falcula	0	13	0	13
	White encrusting sponge	0	8	0	8
	Yellow encrusting sponge	0	2	0	2
Echinodermata	*Cidaris cidaris*	186	116	68	370
	Echinus melo	7	5	0	12
	Asteroidea 1	1	1	9	11
	Echinus acutus	5	1	0	6
	Holothuroidea 1	3	2	1	6
	Asteroidea 2	0	0	4	4
	Holothuroidea 2	0	0	2	2
Arthropoda	Galatheoidea	25	27	348	400
	Bathynectes sp.	0	4	22	26
	Decapoda	5	0	9	14
Mollusca	Ostreida	0	12	0	12

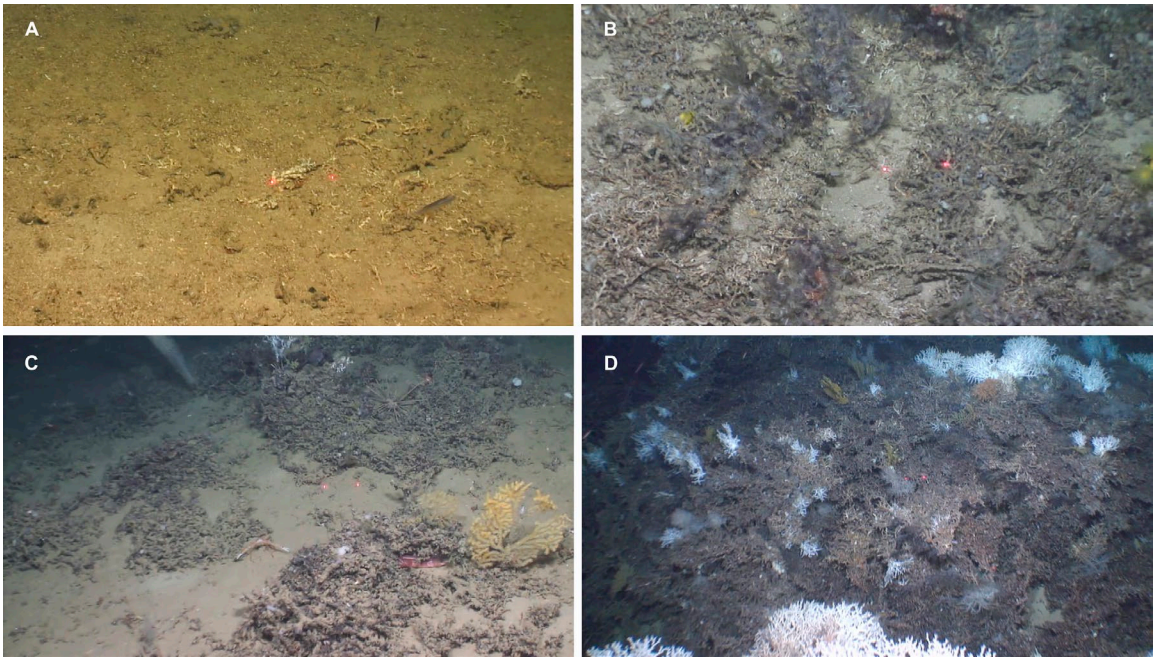

Figure S2.1. Substrate types observed on the Cabliers Coral Mound. Fine sands with coral rubble (A), coral rubble (B), coral framework with fine sands (C) and coral framework (D).

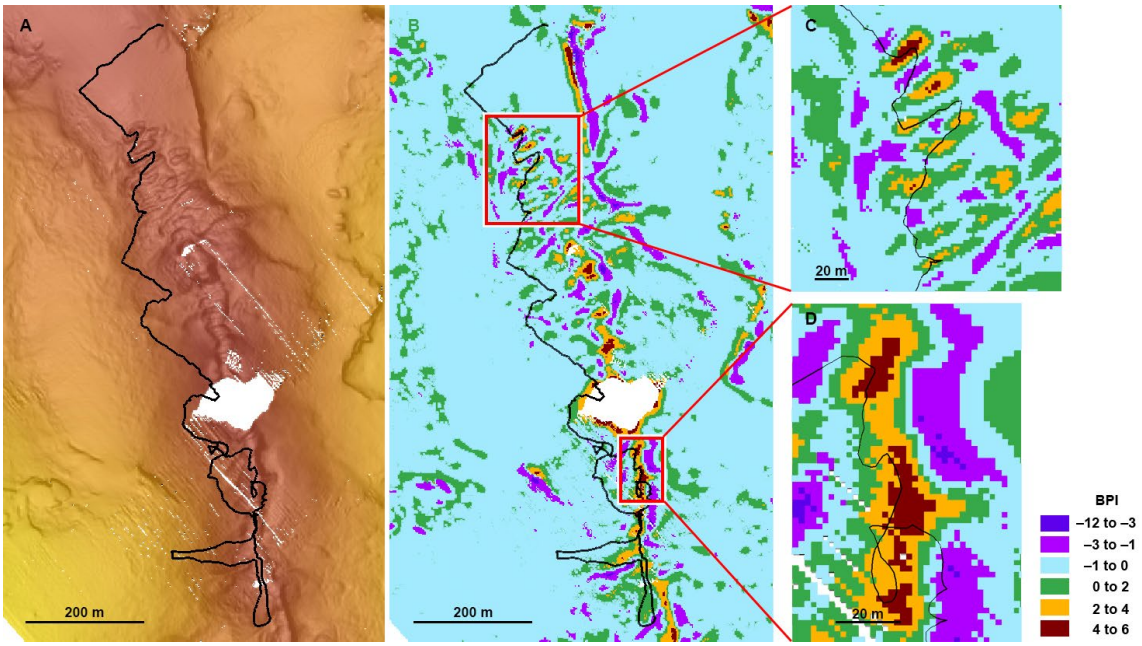

Figure S2.2. Map showing the Dive 1 ROV path (black line) on the AUV bathymetry (A) and the fine scale bathymetric position index (BPI; inner radius: 5 m, outer radius: 10 m) (B) used to identify the mini-mound like features located on the crest of the mound. Zooms from the red dashed boxes (C, D) show the areas where the ROV travelled over the crest of the mound. Dark and light purple represent negative elevation features (i.e. valleys, troughs); light blue and green indicate flat and gentle slopes; orange and brown denote positive elevation features (i.e. mini-mounds). Here the spearman rank correlation was used to assess the correlation between coral density and mini-mound occurrence.

Chapter 3 supplementary materials

Uranium series absolute dating

Equilibrium standard, uraninite URAN 84.5

The analyses of this secular equilibrium standard gave the following activity ratios ($^{230}Th/^{238}U$) = 1.0031 ± 0.0007 and ($^{234}U/^{238}U$) = 1.0001 ± 0.0002 (2s standard errors of the mean, n = 62), which are comparable to the values acquired in previous studies (Hoffman et al., 2007, 2018). A pristine speleothem sample, which serves as an internal reference material, is also routinely analysed as a further demonstration of external reproducibility (see Hoffmann et al., 2018). Analyses gave the following: ($^{230}Th/^{238}U$) = 0.4342 ± 0.0081, ($^{234}U/^{238}U$) = 1.0461 ± 0.0058, age = 58.26 ± 1.38 ka (errors are given as 2σ standard deviations of the mean, n = 18 over a 4 year period).

Laser ablation procedure and VS001/1-A standard

Data were collected over 40 analytical cycles. An on-peak gas blank was analysed before and after ablation (both 10 cycles), with 5 cycles allowed for sample washout prior to the latter. Blank corrections were applied to all intensities based on the mean of the preceding and succeeding blank measurements.

VS001/1-A, a fragment of inorganically precipitated aragonite vein from the Salt Wash Graben, Green River, Utah (Kampman et al., 2012) that was shown to be homogenous on a centimetre scale by Spooner et al. (2016), was analysed bracketing every two samples and used to correct for isotopic and elemental fractionation. Although in other studies researchers have used corals, calcite and NIST glass as standards to correct for machine induced fractionation, in the present study, aragonite VS001/1-A was preferred in accordance to Spooner et al. (2016) who observed that it provided the best internal precision on ($^{230}Th/^{238}U$). Prior to being used, it was analysed three times by solution MC-ICP-MS to confirm both its isotopic composition and homogeneity. Mean activity ratios for this aragonite vein were ($^{230}Th/^{238}U$) = 2.5891 ± 0.0084 and ($^{234}U/^{238}U$) = 3.8323 ± 0.0135, giving an age of 103.93 ± 0.06 ka (errors are given as 2σ standard deviations of the mean). These values are comparable to those reported by Spooner et al. (2016), confirming VS001/1-A as an appropriate standard to use in the laser ablation analyses. Resulting ratios were screened and cycles falling outside the 3 SD of the mean were removed.

Assessment of initial Th and open system behaviour

U-Th dating is frequently used to date both modern and fossil CWCs (Cheng et al., 2000; Robinson et al., 2014; Chutcharavan et al., 2018). Two key conditions that need to be demonstrated when assessing the reliability of such dates are: 1) that the ages are not affected by the presence of initial ^{230}Th in the sample, i.e. Th that is not the product of in situ radioactive decay, and 2) that the samples have not been altered by diagenetic processes (Cheng et al., 2000;

Robinson et al., 2014). The former is typically assessed by looking at the abundance of ^{232}Th, an indicator that initial Th is present in the sample, whilst the latter is assessed through the U concentration and a comparison between the age corrected ($^{234}U/^{238}U$), typically displayed in delta notation as $\delta^{234}U$ (defined in Table C3)$_i$, and that of modern seawater.

Here, assessment of these key criteria is based on the higher-precision solution MC-ICP-MS data in the first instance. Coral ($^{230}Th/^{232}Th$) are typically >1000, except for the samples acquired at 7 cm and 38 cm core depth from MD13-3469G and MD13-3470G respectively, which have ratios of 851 and 47 (Table S3.1). With these ratios, corrections for initial Th have a negligible effect on the calculated ages and in all cases are smaller than the calculated age uncertainties. U concentrations of ~3 – 4 ppm (Table S3.1) are consistent with modern day corals, and results from previous studies (Cheng et al., 2000; McCulloch et al., 2010; Robinson et al., 2014). It is believed that the $\delta^{234}U$ of seawater has essentially remained constant over hundreds of thousands of years, and corals that have remained a closed-system, will have a $\delta^{234}U_i$ close to this value (Cheng et al. 2000; Robinson et al. 2014). Studies therefore typically screen samples based on their $\delta^{234}U_i$, with those falling outside a predetermined range from seawater considered unreliable. Here we follow Robinson et al. (2005; 2014) and consider values within 7 ‰ of the closed system value of 146.5 ‰ as acceptable. Of the eight samples analysed by solution MC-ICP-MS, five fall within this range whilst three are elevated above it ($\delta^{234}U_i$ 166 – 170; Table S3.1). The three that are not consistent with closed-system behaviour (MD13-3469G-452, MD13-3469G-745, MD13-3469G-1048) all have U-Th ages ≥130 ka BP. Coral samples of this age therefore may have been subjected to diagenetic alteration (e.g. Scholz et al. 2004; Yehudai et al., 2017). Whilst little is known about the $\delta^{234}U$ of the Mediterranean Sea during this period (although see Sivan et al. 2016 who recorded $\delta^{234}U_i$ of ~157 at ~110 ka BP based on analyses of *Strombus bubonius* shells from the region), and there is some evidence to suggest distinct $\delta^{234}U$ signatures do exist between some deep water masses (Chutcharavan et al., 2018), we therefore restrict our interpretations when considering these older dates and accept them as approximate guides to coral growth and mound formation.

U-Th laser ablation MC-ICP-MS ages demonstrate excellent stratigraphic consistency overall. Initial Th corrections were not built into the analytical protocol because such corrections on CWCs are typically on the order of ~400 years; well within the age uncertainty for most of the corals dated by the laser ablation approach (Robinson et al., 2014). This is demonstrated further by the solution dates produced here which show negligible initial Th age corrections, whilst the chronological consistency of all the U-Th ages analysed through both techniques suggests that initial Th does not pose an issue here (see also, e.g., McCulloch et al., 2010). Screening for diagenetically altered corals is also possible with the laser ablation data. However, due to the large uncertainty associated with the $\delta^{234}U_i$ (7 ‰ on the seawater value and 25 ‰ on the laser ablation value), only those analyses characterised by values >178.5 ‰ or <114.5 ‰ would be identifiable as being outside the acceptable range (12 of the 183 laser ablation analyses are outside this range; Table S3.2). The higher precision solution MC-ICP-MS analyses therefore act as a better guide to possible open-system behaviour, and following that all three solution ages ≥130 ka BP are elevated above the acceptable $\delta^{234}U_i$ range, it is considered likely that this will also be the case for samples of a similar age analysed by laser ablation. Therefore, whilst the above screening is applied to all laser ablation samples, we consider all dates ≥130 ka BP as approximate guides to coral growth.

Chemical cleaning procedure for trace element analyses

Oxidative cleaning consisted of submerging the coral samples in a 500-1000 ml solution (depending on the size of the coral fragment), containing a 50:50 mixture of 30% H_2O_2 and 0.1M NH_4OH, in a hot water bath (80°C) for 20 minutes, with 15 seconds ultra-sonications every 5 minutes. The pH of the mixture was monitored to ensure it was consistently ≥7, ensuring minimal dissolution of the corals. The process was repeated with fresh oxidative mixture until there was no change in the colour of the coral pieces, and no further visible reactivity of the peroxide mixture with the corals. The reductive cleaning involved adding a mixture of 1200 ml hydrous hydrazine, 10 ml ~14M NH_4OH and 10 ml 0.3M citric acid in 14M NH_4OH enough to fully cover the samples. The vials were then placed in a hot water bath (80°C) for 30 minutes, and were ultra-sonicated briefly every two minutes. After rinsing with 18.2 MΩ cm (ultrapure) H_2O, the samples were subjected to a weak acid leach with $5{\cdot}10^{-4}$ M HNO_3 for 30 seconds, and to dissolution through a stepwise addition of 0.5M HNO_3.

Table S3.1. Solution MC-ICP-MS U-Th analysis of Cabliers coral samples and aragonite vein VS001/1-A. Ratios within parentheses are activity ratios. i = initial. Uncertainties are fully propagated, and all analytical errors are 2σ of the mean. $(^{230}Th/^{238}U)A = 1 - e^{-\lambda 230T} + (\delta^{234}U\text{measured}/1000)[\lambda 230/(\lambda 230 - \lambda 234)](1 - e^{-(\lambda 230 - \lambda 234)T})$, where T is the age. $\delta^{234}U = ((^{234}U/^{238}U)A - 1) \times 1000$. Ages in years before present (2019). Decay constants are 9.1577×10^{-6} a^{-1} for ^{230}Th, 2.826×10^{-6} a^{-1} for ^{234}U (Cheng et al. 2000), 1.55125×10^{-10} a^{-1} for ^{238}U (Jaffey et al. 1971), and 4.94752×10^{-11} a^{-1} for ^{232}Th (Holden 1990). The degree of initial Th contamination is indicated by the measured $(^{230}Th/^{232}Th)_A$; an initial $(^{238}U/^{232}Th)_A$ of 0.8 ± 0.4 is used to obtain a corrected U–Th age. Samples in italics are characterised by $\delta^{234}U_i$ outside the acceptable range for closed-system behaviour.

Description	Depth (cm)	^{238}U (ng/g)	^{232}Th (ng/g)	$(^{232}Th/^{238}U)_A$	$(^{230}Th/^{232}Th)_A$	$(^{230}Th/^{238}U)_A$
Core MD3469G	4	3383.15±40.26	0.36±0.03	0.000035±0.000003	2707.01±215.46	0.0940±0.0008
Core MD3469G	*441*	*2616.97±27.55*	*0.70±0.03*	*0.000088±0.000004*	*9046.74±324.11*	*0.7932±0.0061*
Core MD3469G	*731*	*2877.28±37.92*	*0.25±0.03*	*0.000029±0.000003*	*36113.84±4410.35*	*1.0330±0.0087*
Core MD3469G	*1032*	*3858.28±68.04*	*2.48±0.06*	*0.000210±0.000004*	*4952.43±73.07*	*1.0409±0.0243*
Core MD3470G	36	3261.27±55.02	6.07±0.12	0.000609±0.000005	47.00±0.77	0.0286±0.0005
Core MD3470G	256	3623.12±45.40	0.30±0.03	0.000027±0.000003	2346.44±245.89	0.0626±0.0006
Core MD3470G	662	2957.64±31.98	0.31±0.03	0.000035±0.000003	3386.75±286.69	0.1177±0.0010
Core MD3470G	831	3233.95±35.55	0.30±0.03	0.000030±0.000003	4450.69±461.08	0.1353±0.0012
Aragonite Vein VS001/1-A	-	4556.80±64.54	0.09±0.05	0.000006±0.000004	423573.24±232024.95	2.5864±0.0219
Aragonite Vein VS001/1-A	-	4354.83±63.27	0.05±0.06	0.000004±0.000005	738809.15±591047.32	2.5868±0.0222
Aragonite Vein VS001/1-A	-	4473.18±57.42	0.05±0.07	0.000004±0.000005	662805.10±743935.10	2.5939±0.0192

Description	Depth (cm)	$(^{234}U/^{238}U)_A$	Age Uncorrected (ka)	$(^{234}U/^{238}U)_{Ai}$	Age Corrected (ka)	$(^{234}U/^{238}U)_{Ai}$	$\delta^{234}U_i$
Core MD3469G	4	1.1487±0.0025	9.31+0.09–0.09	1.1526±0.0026	9.30+0.09–0.09	1.1526±0.0026	153
Core MD3469G	*441*	*1.1170±0.0020*	*130.74+1.92–1.98*	*1.1693±0.0027*	*130.73+1.94–1.94*	*1.1693±0.0027*	*169*
Core MD3469G	*731*	*1.0663±0.0033*	*325.66+19.19–16.10*	*1.1664±0.0030*	*325.66+19.53–16.73*	*1.1664±0.0030*	*166*
Core MD3469G	*1032*	*1.0322±0.0024*	*588.97+233.61–198.53*	*1.1701±0.0030*	*588.95+247.48–199.25*	*1.1702±0*	*170*
Core MD3470G	36	1.1492±0.0022	2.75+0.05–0.05	1.1504±0.0023	2.71+0.06–0.06	1.1505±0.0023	150
Core MD3470G	256	1.1486±0.0023	6.11+0.06–0.06	1.1512±0.0023	6.11+0.06–0.06	1.1512±0.0023	151
Core MD3470G	662	1.1457±0.0026	11.81+0.11–0.11	1.1507±0.0027	11.81+0.11–0.11	1.1507±0.0027	151
Core MD3470G	831	1.1457±0.0022	13.69+0.13–0.13	1.1514±0.0023	13.69+0.13–0.13	1.1514±0.0023	151
Aragonite Vein VS001/1-A	-	3.8282±0.0084	103.95+1.31–1.29	4.7940±0.0066	103.95+1.35–1.31	4.7940±0.0066	3794
Aragonite Vein VS001/1-A	-	3.8287±0.0082	103.95+1.41–1.29	4.7947±0.0064	103.95+1.37–1.33	4.7947±0.0064	3795
Aragonite Vein VS001/1-A	-	3.8401±0.0077	103.90+1.18–1.15	4.8094±0.0060	103.90+1.16–1.16	4.8095±0.0060	3809

Table S3.2. Laser Ablation MC-ICP-MS U-Th analysis of Cabliers coral samples. Ratios within parentheses are activity ratios. i = initial. See text for explanation of the age uncertainties. $(^{230}Th/^{238}U)_A = 1 - e^{-\lambda 230T} + (\delta^{234}Umeasured/1000)[\lambda 230/(\lambda 230 - \lambda 234)](1 - e^{-(\lambda 230 - \lambda 234)T})$, where T is the age. $\delta^{234}U = ((^{234}U/^{238}U)_A - 1) \times 1000$. Ages in years before present (2019). Decay constants are 9.1577×10^{-6} a^{-1} for ^{230}Th, 2.826×10^{-6} a^{-1} for ^{234}U (Cheng et al. 2000), 1.55125×10^{-10} a^{-1} for ^{238}U (Jaffey et al. 1971), and 4.94752×10^{-11} a^{-1} for 232Th (Holden 1990). Ages are uncorrected for initial Th. Samples in italics are characterised by $\delta^{234}Ui$ outside the acceptable range for closed-system behaviour and thus, they were not included in the calculation of mean ages or used for coral mound development interpretation.

Core	Depth (cm)	$(^{230}Th/^{238}U)$	$(^{234}U/^{238}U)$	Age (ka)	$\delta^{234}U_i$	Mean Age (ka)
MD13-3469G	4	0.0984 ± 0.0111	1.1497 ± 0.0148	9.71 ± 0.83	154	9.31 ± 0.68
MD13-3469G	4	0.0982 ± 0.0192	1.1610 ± 0.0291	9.59 ± 0.83	165	
MD13-3469G	4	0.0912 ± 0.0097	1.1524 ± 0.0139	8.96 ± 0.81	156	
MD13-3469G	4	0.0919 ± 0.0083	1.1561 ± 0.0164	8.99 ± 0.81	160	
MD13-3469G	17	0.0952 ± 0.0064	1.1503 ± 0.0125	9.37 ± 0.82	154	9.36 ± 0.6
MD13-3469G	17	0.0932 ± 0.0081	1.1476 ± 0.0094	9.19 ± 0.81	151	
MD13-3469G	17	0.0913 ± 0.0078	1.1490 ± 0.0101	8.99 ± 0.81	153	
MD13-3469G	17	0.0941 ± 0.0077	1.1497 ± 0.0100	9.27 ± 0.81	154	
MD13-3469G	17	0.1015 ± 0.0065	1.1583 ± 0.0180	9.96 ± 0.84	163	
MD13-3469G	17	0.0953 ± 0.0139	1.1480 ± 0.0180	9.41 ± 0.82	152	
MD13-3469G	34	0.0959 ± 0.0130	1.1564 ± 0.0166	9.40 ± 0.82	161	10.07 ± 0.83
MD13-3469G	34	0.1070 ± 0.0135	1.1455 ± 0.0156	10.64 ± 0.85	150	
MD13-3469G	34	0.1011 ± 0.0143	1.1481 ± 0.0136	10.00 ± 0.83	152	
MD13-3469G	34	0.1048 ± 0.0160	1.1547 ± 0.0138	10.33 ± 0.84	159	
MD13-3469G	34	0.1014 ± 0.0162	1.1539 ± 0.0153	9.98 ± 0.83	158	
MD13-3469G	43	0.1152 ± 0.0097	1.1382 ± 0.0148	11.58 ± 0.87	143	
MD13-3469G	55	0.1241 ± 0.0142	1.1506 ± 0.0163	12.38 ± 0.90	156	
MD13-3469G	71	0.1204 ± 0.0087	1.1439 ± 0.0192	12.07 ± 0.89	149	
MD13-3469G	71	0.1209 ± 0.0133	1.1484 ± 0.0218	12.07 ± 0.89	154	
MD13-3469G	108	0.1305 ± 0.0119	1.1402 ± 0.0173	13.19 ± 0.92	146	
MD13-3469G	117	0.1305 ± 0.0184	1.1500 ± 0.0251	13.06 ± 0.92	156	
MD13-3469G	130	0.1315 ± 0.0113	1.1527 ± 0.0229	13.14 ± 0.92	159	
MD13-3469G	137	0.1251 ± 0.0079	1.1467 ± 0.0252	12.54 ± 0.90	152	
MD13-3469G	153	0.1397 ± 0.0133	1.1412 ± 0.0245	14.16 ± 0.95	147	
MD13-3469G	160	0.1160 ± 0.0170	1.1352 ± 0.0256	11.69 ± 0.88	140	
MD13-3469G	168	0.1321 ± 0.0123	1.1360 ± 0.0176	13.41 ± 0.92	141	
MD13-3469G	172	0.1334 ± 0.0177	1.1422 ± 0.0212	13.47 ± 0.93	148	
MD13-3469G	175	0.6415 ± 0.0238	1.1076 ± 0.0184	92.38 ± 4.99	140	
MD13-3469G	180	0.6237 ± 0.0323	1.0928 ± 0.0183	90.51 ± 4.70	120	87.54 ± 3.54
MD13-3469G	180	0.6171 ± 0.1008	1.1073 ± 0.0319	87.12 ± 4.60	137	
MD13-3469G	180	0.6084 ± 0.0434	1.1023 ± 0.0284	85.92 ± 4.47	130	
MD13-3469G	180	0.6176 ± 0.0298	1.1120 ± 0.0147	86.61 ± 4.61	143	
MD13-3469G	192	0.6556 ± 0.0352	1.1146 ± 0.0209	94.52 ± 5.22	150	
MD13-3469G	204	0.6589 ± 0.0289	1.1048 ± 0.0203	96.77 ± 5.28	138	
MD13-3469G	218	0.6522 ± 0.0291	1.1161 ± 0.0175	93.55 ± 5.17	151	
MD13-3469G	230	0.6398 ± 0.0352	1.1015 ± 0.0250	92.87 ± 4.96	132	
MD13-3469G	249	0.6310 ± 0.0345	1.1118 ± 0.0201	89.50 ± 4.82	144	
MD13-3469G	266	0.6361 ± 0.0495	1.1121 ± 0.0196	90.56 ± 4.90	145	
MD13-3469G	285	0.6277 ± 0.0269	1.1082 ± 0.0202	89.25 ± 4.76	139	
MD13-3469G	303	0.6739 ± 0.0427	1.111 ± 0.0266	99.31 ± 5.55	147	
MD13-3469G	316	0.6464 ± 0.0349	1.1149 ± 0.0233	92.44 ± 5.07	149	
MD13-3469G	327	0.6557 ± 0.0323	1.1004 ± 0.0156	96.71 ± 5.23	132	
MD13-3469G	348	0.6756 ± 0.0267	1.1161 ± 0.0212	98.90 ± 5.58	154	
MD13-3469G	365	0.6527 ± 0.0386	1.1211 ± 0.0271	92.93 ± 5.17	158	
MD13-3469G	374	0.6441 ± 0.0452	1.1261 ± 0.0210	90.37 ± 5.03	163	
MD13-3469G	385	0.6562 ± 0.0315	1.1090 ± 0.0206	95.51 ± 5.24	143	92.88 ± 6.79
MD13-3469G	385	0.6406 ± 0.0289	1.1133 ± 0.0162	91.38 ± 4.97	147	
MD13-3469G	385	0.6268 ± 0.0235	1.1114 ± 0.0171	88.64 ± 4.75	143	
MD13-3469G	385	0.6335 ± 0.0316	1.1061 ± 0.0171	90.83 ± 4.86	137	
MD13-3469G	385	0.6684 ± 0.0597	1.1111 ± 0.0157	98.01 ± 5.45	147	
MD13-3469G	397	0.6572 ± 0.0443	1.1239 ± 0.0219	93.55 ± 5.25	162	
MD13-3469G	*418*	0.6445 ± 0.0362	1.0865 ± 0.0179	96.25 ± 5.04	114	98.47 ± 5.38
MD13-3469G	418	0.6564 ± 0.0353	1.0924 ± 0.0197	98.13 ± 5.24	122	
MD13-3469G	418	0.6681 ± 0.0448	1.0990 ± 0.0227	99.86 ± 5.45	131	
MD13-3469G	418	0.6749 ± 0.0453	1.0987 ± 0.0236	101.58 ± 5.57	132	
MD13-3469G	418	0.6541 ± 0.0492	1.1137 ± 0.0220	94.32 ± 5.20	149	
MD13-3469G	441	0.7934 ± 0.0352	1.1139 ± 0.0150	131.06 ± 8.24	165	131.4 ± 8.03
MD13-3469G	441	0.7783 ± 0.0368	1.1095 ± 0.0188	127.48 ± 7.84	157	
MD13-3469G	441	0.7863 ± 0.0525	1.0935 ± 0.0273	134.15 ± 8.05	137	
MD13-3469G	441	0.7727 ± 0.036	1.1132 ± 0.0141	124.92 ± 7.70	161	
MD13-3469G	441	0.8032 ± 0.0416	1.1099 ± 0.0144	135.19 ± 8.51	161	
MD13-3469G	441	0.803 ± 0.0396	1.1083 ± 0.0408	135.57 ± 8.51	159	
MD13-3469G	443	0.7786 ± 0.0445	1.1045 ± 0.0105	128.82 ± 7.85	150	

Core	Depth (cm)	(^{230}Th/^{238}U)	(^{234}U/^{238}U)	Age (ka)	$\delta^{234}U_i$	Mean Age (ka)
MD13-3469G	455	0.8323 ± 0.0626	1.1079 ± 0.0209	145.69 ± 9.38	163	
MD13-3469G	455	0.8290 ± 0.0493	1.1078 ± 0.0123	144.55 ± 9.27	162	
MD13-3469G	469	0.8104 ± 0.0472	1.1184 ± 0.0162	135.24 ± 8.72	174	
MD13-3469G	469	0.8304 ± 0.0560	1.1086 ± 0.0193	144.79 ± 9.32	164	
MD13-3469G	*478*	*0.9179 ± 0.0991*	*1.1234 ± 0.0356*	*174.16 ± 12.45*	*202*	
MD13-3469G	478	0.8413 ± 0.0614	1.1112 ± 0.0119	147.87 ± 9.66	169	
MD13-3469G	500	0.7786 ± 0.0578	1.1127 ± 0.0175	126.81 ± 7.85	161	
MD13-3469G	507	0.7893 ± 0.0454	1.1066 ± 0.0145	131.62 ± 8.13	155	
MD13-3469G	521	0.8240 ± 0.0531	1.1195 ± 0.0300	139.39 ± 9.12	177	
MD13-3469G	*533*	*0.8614 ± 0.0504*	*1.1223 ± 0.0211*	*151.66 ± 10.33*	*188*	
MD13-3469G	550	0.7806 ± 0.0382	1.1065 ± 0.0251	128.94 ± 7.90	154	
MD13-3469G	563	0.8091 ± 0.0540	1.0914 ± 0.0365	142.54 ± 8.68	137	
MD13-3469G	583	0.8670 ± 0.0556	1.0851 ± 0.0253	167.84 ± 10.52	137	
MD13-3469G	599	0.9395 ± 0.0308	1.0907 ± 0.0139	202.46 ± 13.37	161	203.01 ± 12.02
MD13-3469G	599	0.9471 ± 0.0269	1.0973 ± 0.0144	202.87 ± 13.71	173	
MD13-3469G	599	0.9488 ± 0.0357	1.0854 ± 0.0131	211.84 ± 13.79	156	
MD13-3469G	599	0.9270 ± 0.0430	1.0912 ± 0.0217	194.87 ± 12.83	158	
MD13-3469G	615	0.9345 ± 0.0518	1.0882 ± 0.0207	201.00 ± 13.15	156	
MD13-3469G	*633*	*0.9684 ± 0.1452*	*1.1102 ± 0.0561*	*207.49 ± 14.71*	*198*	
MD13-3469G	652	0.9463 ± 0.1409	1.0923 ± 0.0266	205.55 ± 13.67	165	
MD13-3469G	675	0.9126 ± 0.0442	1.0814 ± 0.0114	192.46 ± 12.23	140	192.43 ± 7.19
MD13-3469G	675	0.9132 ± 0.0406	1.0873 ± 0.0171	189.47 ± 12.26	149	
MD13-3469G	675	0.9096 ± 0.0406	1.0840 ± 0.0158	189.35 ± 12.11	144	
MD13-3469G	675	0.9248 ± 0.0465	1.0947 ± 0.0102	191.67 ± 12.74	163	
MD13-3469G	675	0.9297 ± 0.0662	1.0865 ± 0.0205	199.19 ± 12.94	152	
MD13-3469G	719	1.0228 ± 0.0516	1.0632 ± 0.0158	313.30 ± 17.62	154	313.83 ± 27.89
MD13-3469G	719	1.0386 ± 0.0468	1.0700 ± 0.0136	326.00 ± 18.56	176	
MD13-3469G	*719*	*1.0409 ± 0.0469*	*1.0718 ± 0.0145*	*326.14 ± 18.70*	*181*	
MD13-3469G	719	1.0388 ± 0.1009	1.0707 ± 0.0251	324.77 ± 18.57	178	
MD13-3469G	719	1.0063 ± 0.0468	1.0615 ± 0.0227	291.25 ± 16.68	140	
MD13-3469G	777	1.0405 ± 0.0950	1.0630 ± 0.0151	348.24 ± 18.67	169	346.56 ± 5.04
MD13-3469G	777	1.0367 ± 0.0463	1.0619 ± 0.0164	343.00 ± 18.44	164	
MD13-3469G	*777*	*1.0477 ± 0.0334*	*1.0697 ± 0.0132*	*345.23 ± 19.13*	*185*	
MD13-3469G	777	1.0448 ± 0.0401	1.0663 ± 0.0116	348.45 ± 18.94	178	
MD13-3469G	*777*	*1.0537 ± 0.0402*	*1.0654 ± 0.0186*	*374.13 ± 19.51*	*189*	
MD13-3469G	798	1.0318 ± 0.0487	1.0708 ± 0.0241	312.43 ± 18.15	172	
MD13-3469G	812	1.0279 ± 0.0486	1.0620 ± 0.0168	325.04 ± 17.91	156	
MD13-3469G	*857*	*1.0537 ± 0.0463*	*1.0765 ± 0.0107*	*339.43 ± 19.51*	*200*	
MD13-3469G	874	1.0289 ± 0.0472	1.0720 ± 0.0119	305.50 ± 17.97	171	
MD13-3469G	900	1.0156 ± 0.0409	1.0588 ± 0.0123	310.42 ± 17.20	142	
MD13-3469G	971	1.0346 ± 0.0394	1.0512 ± 0.0124	372.66 ± 18.31	147	
MD13-3469G	*990*	*1.0657 ± 0.0283*	*1.0538 ± 0.0133*	*512.06 ± 20.30*	*230*	
MD13-3470G	0	0.0031 ± 0.0012	1.1649 ± 0.0107	0.29 ± 0.60	165	
MD13-3470G	14	0.0114 ± 0.0022	1.1657 ± 0.0103	1.07 ± 0.62	166	
MD13-3470G	23	0.0174 ± 0.0023	1.1732 ± 0.0106	1.62 ± 0.63	174	
MD13-3470G	36	0.0285 ± 0.0044	1.1443 ± 0.0113	2.74 ± 0.66	145	2.76 ± 0.46
MD13-3470G	36	0.0259 ± 0.0056	1.1442 ± 0.0182	2.49 ± 0.65	145	
MD13-3470G	36	0.0318 ± 0.0207	1.1501 ± 0.0152	3.05 ± 0.66	151	
MD13-3470G	51	0.0317 ± 0.0049	1.1696 ± 0.0120	2.98 ± 0.66	171	
MD13-3470G	76	0.0415 ± 0.0060	1.1744 ± 0.0194	3.91 ± 0.68	176	
MD13-3470G	92	0.0411 ± 0.0051	1.1707 ± 0.0132	3.89 ± 0.68	173	
MD13-3470G	100	0.0441 ± 0.0072	1.1520 ± 0.0217	4.24 ± 0.69	154	
MD13-3470G	*114*	*0.0452 ± 0.0076*	*1.1801 ± 0.0186*	*4.25 ± 0.69*	*182*	
MD13-3470G	148	0.0504 ± 0.0087	1.1533 ± 0.0177	4.85 ± 0.71	155	
MD13-3470G	158	0.0575 ± 0.0093	1.1605 ± 0.0243	5.52 ± 0.72	163	
MD13-3470G	168	0.0524 ± 0.0067	1.1540 ± 0.0206	5.04 ± 0.71	156	
MD13-3470G	184	0.0573 ± 0.0076	1.1602 ± 0.0189	5.51 ± 0.72	163	
MD13-3470G	*201*	*0.0614 ± 0.0267*	*1.1771 ± 0.053*	*5.82 ± 0.73*	*180*	
MD13-3470G	219	0.0647 ± 0.0169	1.1558 ± 0.0244	6.26 ± 0.74	159	
MD13-3470G	248	0.0582 ± 0.0126	1.1410 ± 0.0149	5.69 ± 0.72	143	
MD13-3470G	268	0.0682 ± 0.0104	1.1652 ± 0.0125	6.55 ± 0.75	168	
MD13-3470G	277	0.0686 ± 0.0093	1.1690 ± 0.0211	6.57 ± 0.75	172	
MD13-3470G	291	0.0740 ± 0.0083	1.1679 ± 0.0189	7.10 ± 0.76	171	
MD13-3470G	305	0.0690 ± 0.0073	1.1652 ± 0.0145	6.63 ± 0.75	168	
MD13-3470G	327	0.0841 ± 0.0085	1.1731 ± 0.0147	8.07 ± 0.79	177	
MD13-3470G	347	0.0842 ± 0.0094	1.1504 ± 0.0149	8.25 ± 0.79	154	
MD13-3470G	388	0.0874 ± 0.0096	1.1505 ± 0.0169	8.57 ± 0.80	154	
MD13-3470G	397	0.0984 ± 0.0122	1.1455 ± 0.0164	9.75 ± 0.83	150	
MD13-3470G	402	0.0881 ± 0.0094	1.1516 ± 0.0134	8.64 ± 0.80	155	
MD13-3470G	426	0.0988 ± 0.0157	1.1475 ± 0.0264	9.77 ± 0.83	152	
MD13-3470G	444	0.1074 ± 0.0119	1.1518 ± 0.0162	10.63 ± 0.85	156	

Core	Depth (cm)	(^{230}Th/^{238}U)	(^{234}U/^{238}U)	Age (ka)	$\delta^{234}U_i$	Mean Age (ka)
MD13-3470G	453	0.1081 ± 0.0157	1.1555 ± 0.0221	10.66 ± 0.85	160	
MD13-3470G	483	0.1137 ± 0.0319	1.1560 ± 0.0190	11.24 ± 0.87	161	
MD13-3470G	505	0.1127 ± 0.0208	1.1175 ± 0.0245	11.54 ± 0.87	121	
MD13-3470G	517	0.1184 ± 0.0152	1.1478 ± 0.0196	11.81 ± 0.88	153	
MD13-3470G	536	0.1145 ± 0.0165	1.1497 ± 0.0175	11.38 ± 0.87	155	
MD13-3470G	557	0.1114 ± 0.0127	1.1388 ± 0.0154	11.18 ± 0.86	143	
MD13-3470G	566	0.1184 ± 0.0332	1.1603 ± 0.0262	11.67 ± 0.88	166	
MD13-3470G	582	0.1072 ± 0.0105	1.1400 ± 0.0170	10.72 ± 0.85	144	
MD13-3470G	599	0.1150 ± 0.0140	1.1460 ± 0.0140	11.48 ± 0.87	151	
MD13-3470G	636	0.1176 ± 0.0133	1.1447 ± 0.0271	11.76 ± 0.88	150	
MD13-3470G	653	0.1073 ± 0.0133	1.1463 ± 0.0221	10.67 ± 0.85	151	
MD13-3470G	670	0.1131 ± 0.0142	1.1484 ± 0.0246	11.26 ± 0.87	153	
MD13-3470G	681	0.1199 ± 0.0154	1.1421 ± 0.0334	12.04 ± 0.89	147	11.39 ± 0.91
MD13-3470G	681	0.1137 ± 0.0124	1.1514 ± 0.0206	11.28 ± 0.87	156	
MD13-3470G	681	0.1130 ± 0.0134	1.1456 ± 0.0208	11.27 ± 0.87	150	
MD13-3470G	681	0.1052 ± 0.0114	1.1216 ± 0.0189	10.69 ± 0.85	125	
MD13-3470G	681	0.1173 ± 0.0120	1.1484 ± 0.0195	11.69 ± 0.88	153	
MD13-3470G	691	0.1095 ± 0.0115	1.1312 ± 0.0133	11.05 ± 0.86	135	
MD13-3470G	707	0.1191 ± 0.0176	1.1454 ± 0.0234	11.91 ± 0.89	150	11.24 ± 1.1
MD13-3470G	707	0.1021 ± 0.0136	1.1329 ± 0.0250	10.25 ± 0.84	137	
MD13-3470G	707	0.1149 ± 0.0209	1.1440 ± 0.0262	11.49 ± 0.87	149	
MD13-3470G	707	0.1128 ± 0.0157	1.1338 ± 0.0145	11.37 ± 0.87	138	
MD13-3470G	707	0.1113 ± 0.0130	1.1396 ± 0.0140	11.15 ± 0.86	144	
MD13-3470G	720	0.1271 ± 0.0112	1.1458 ± 0.0228	12.75 ± 0.91	151	11.64 ± 1.43
MD13-3470G	720	0.1204 ± 0.0144	1.1540 ± 0.0204	11.95 ± 0.89	159	
MD13-3470G	720	0.1146 ± 0.0228	1.1505 ± 0.0240	11.38 ± 0.87	155	
MD13-3470G	720	0.1083 ± 0.0289	1.1677 ± 0.0426	10.56 ± 0.85	173	
MD13-3470G	720	0.1164 ± 0.0153	1.1530 ± 0.0167	11.55 ± 0.88	158	
MD13-3470G	737	0.1219 ± 0.0197	1.1574 ± 0.0168	12.07 ± 0.89	163	
MD13-3470G	747	0.1282 ± 0.0169	1.1434 ± 0.0199	12.90 ± 0.91	149	
MD13-3470G	748	0.1160 ± 0.0190	1.1553 ± 0.0191	11.48 ± 0.88	160	
MD13-3470G	765	0.1275 ± 0.0125	1.1480 ± 0.0135	12.77 ± 0.91	153	
MD13-3470G	788	0.1343 ± 0.0172	1.1400 ± 0.0247	13.60 ± 0.93	146	
MD13-3470G	804	0.1375 ± 0.0932	1.1600 ± 0.0478	13.69 ± 0.94	166	
MD13-3470G	813	0.1296 ± 0.0161	1.1505 ± 0.0243	12.96 ± 0.92	156	
MD13-3470G	831	0.1460 ± 0.0128	1.1517 ± 0.0194	14.70 ± 0.97	158	14.61 ± 1.28
MD13-3470G	831	0.1442 ± 0.0106	1.1571 ± 0.0091	14.43 ± 0.96	164	
MD13-3470G	831	0.1583 ± 0.0180	1.1458 ± 0.0143	16.11 ± 1.01	153	
MD13-3470G	831	0.1445 ± 0.0125	1.1474 ± 0.0161	14.60 ± 0.96	154	
MD13-3470G	831	0.1431 ± 0.0148	1.1527 ± 0.0194	14.37 ± 0.96	159	
MD13-3470G	831	0.1481 ± 0.0128	1.1497 ± 0.0161	14.96 ± 0.97	156	
MD13-3470G	831	0.1506 ± 0.0111	1.1440 ± 0.0159	15.31 ± 0.98	150	
MD13-3470G	831	0.1476 ± 0.0126	1.1488 ± 0.0163	14.91 ± 0.97	155	
MD13-3470G	831	0.1346 ± 0.0140	1.1470 ± 0.0141	13.54 ± 0.93	153	
MD13-3470G	831	0.1391 ± 0.0124	1.1505 ± 0.0188	13.98 ± 0.95	157	
MD13-3470G	831	0.1399 ± 0.0113	1.1454 ± 0.0188	14.13 ± 0.95	151	
MD13-3470G	831	0.1478 ± 0.0167	1.1531 ± 0.0278	14.87 ± 0.97	160	
MD13-3470G	831	0.1401 ± 0.0158	1.1577 ± 0.0224	13.98 ± 0.95	164	

Table S3.3. Faraday Cup configuration for laser ablation MC-ICP-MS analyses.

Sub-configuration	SEM	H1	H2 ($10^{11}\Omega$ resistor)	H3	H4 ($10^{11}\Omega$ resistor)	Integration Time	Idle Time
1	^{230}Th	-	-	-	^{238}U	4.194 s	1 s
2	^{234}U	-	^{238}U	-	-	4.194 s	1 s

Table S3.4. Typical operating conditions for U-Th dating by laser ablation MC-ICP-MS.

Instrument		
Mass Spectrometer	Thermo Scientific Neptune Plus multi-collector inductively coupled plasma mass spectrometer	
Laser Ablation System	Elemental Scientific Lasers NWR193 excimer laser ablation system with a TwoVol2 ablation chamber	
RF Power	1400 W	
Cones	Nickel skimmer (X) and jet sample	
Gas Flows		
Cooling Gas (argon)	16 L min^{-1}	
Auxiliary Gas (argon)	0.7 L min^{-1}	
Make-up gas (argon)	0.9–1.0 L min^{-1}	
Ablation cell carrier gas (helium)	0.8–1.0 L min^{-1}	
Additional Gas (nitrogen)	0.006–0.008 L min^{-1}	
Ablation Conditions	**Pre-Ablation**	**Ablation**
Laser power density	~4 J cm^{-2}	~8 J cm^{-2}
Laser repetition rate	10 Hz	20 Hz
Laser spot size	150 µm	150 µm
Laser tracking speed	200 µm s	10 µm s
Ablation mode	Line	Line

Table S3.5. Trace element data showing Li/Mg and Ba/Ca ratios together with reconstructed sea water temperatures (SWTs) and dissolved seawater Barium (Ba_{SW}), with their respective associated errors (2s). Samples in italics indicate unrealistic reconstructed values, probably caused by diagenetic alteration or contamination during sample preparation and/or analysis. Species: D.c., *Dendrophylla cornigera*; D.d., *Desmophyllum dianthus*; D.p., *Desmophyllum pertusum*; M.o., *Madrepora oculata*.

Core	Depth	Age	Species	Li/Mg	–2s	+2s	SWTs	–2s	+2s	Ba/Ca	–2s	+2s	BaSW	–2s	+2s
+2s	(cm)	(ka BP)		(mmol mol^{-1})			C			(mmol mol^{-1})			(nmol kg^{-1})		
69	4	9.31	D.p..	2.88	0.08	0.09	13.13	0.69	0.68	11.26	0.18	0.18	55.93	1.29	1.32
69	71	12.07	D.p..	3.59	0.11	0.12	8.38	0.72	0.71	10.65	0.18	0.17	52.32	1.29	1.26
69	137	12.54	D.p..	3.72	0.12	0.12	7.65	0.69	0.72	14.35	0.24	0.25	74.44	1.68	1.67
69	172	13.47	D.p..	3.78	0.12	0.13	7.29	0.72	0.78	13.04	0.22	0.21	66.65	1.46	1.32
69	180	87.54	D.p..	3.63	0.12	0.14	8.15	0.80	0.72	10.08	0.16	0.17	48.89	1.34	1.44
69	303	99.31	D.d.	3.35	0.11	0.11	9.89	0.70	0.74	8.87	0.14	0.15	41.72	1.65	1.51
69	303	99.31	D.d.	3.47	0.11	0.12	9.12	0.76	0.71	9.87	0.16	0.16	47.62	1.38	1.30
69	418	98.47	D.p..	3.45	0.11	0.12	9.25	0.76	0.76	8.31	0.14	0.13	38.31	1.65	1.69
69	441	130.74	D.p..	4.27	0.13	0.14	4.61	0.73	0.71	14.03	0.23	0.24	72.52	1.48	1.55
69	441	130.74	D.p..	4.08	0.14	0.13	5.62	0.76	0.80	15.91	0.25	0.26	83.75	2.02	1.87
69	441	130.74	D.p..	4.12	0.13	0.14	5.42	0.78	0.71	16.86	0.27	0.26	89.41	2.17	2.20
69	500	126.81	D.p..	5.55	0.19	0.19	-1.05	0.83	0.88	16.70	0.25	0.28	88.49	2.16	2.36
69	550	128.94	D.d.	5.73	0.18	0.20	-1.75	0.78	0.81	14.46	0.26	0.21	75.02	1.68	1.76
69	550	128.94	D.d.	5.05	0.17	0.17	1.02	0.81	0.81	14.62	0.25	0.21	75.96	1.60	1.67
69	583	167.84	D.p..	3.75	0.13	0.13	7.47	0.75	0.82	9.61	0.16	0.17	46.08	1.45	1.46
69	599	203.01	D.d.	3.64	0.11	0.12	8.12	0.71	0.71	8.12	0.14	0.14	37.16	1.57	1.68
69	599	203.01	D.d.	3.55	0.12	0.12	8.66	0.71	0.75	8.31	0.13	0.13	38.39	1.59	1.57
69	675	192.43	D.p..	3.18	0.10	0.11	11.00	0.74	0.65	11.06	0.19	0.18	54.81	1.31	1.24
69	731	325.7	D.p..	3.52	0.11	0.12	8.80	0.77	0.72	8.92	0.16	0.15	41.98	1.45	1.53
69	798	312	D.c..	3.21	0.11	0.11	10.78	0.73	0.79	7.71	0.12	0.12	34.74	1.72	1.79
69	812	325.04	D.c..	3.74	0.12	0.13	7.50	0.74	0.72	9.22	0.15	0.16	43.77	1.51	1.50
69	812	325.04	D.c..	3.68	0.12	0.13	7.88	0.76	0.75	9.30	0.15	0.16	44.25	1.47	1.51
69	857	339.4	D.p..	3.44	0.11	0.12	9.34	0.76	0.72	10.41	0.17	0.17	50.85	1.39	1.43
69	1032	588.9	D.p..	3.51	0.11	0.13	8.89	0.76	0.77	11.73	0.20	0.18	58.73	1.38	1.25
70	0	0.29	M.o.	3.33	0.11	0.12	10.01	0.75	0.74	10.09	0.16	0.16	48.99	1.41	1.27
70	36	2.75	D.p..	3.10	0.10	0.11	11.59	0.76	0.71	9.10	0.15	0.15	43.08	1.46	1.44
70	100	4.24	D.p..	3.13	0.10	0.10	11.33	0.76	0.77	9.71	0.15	0.17	46.73	1.42	1.37
70	256	6.11	D.p..	2.85	0.10	0.10	13.38	0.75	0.77	11.72	0.19	0.19	58.72	1.37	1.30
70	347	8.25	D.p..	3.00	0.10	0.10	12.32	0.74	0.76	12.54	0.20	0.20	63.57	1.34	1.31
70	444	10.63	D.p..	3.21	0.10	0.11	10.79	0.69	0.75	11.75	0.19	0.19	58.84	1.31	1.36
70	557	11.18	D.p..	3.14	0.10	0.10	11.33	0.67	0.69	11.51	0.18	0.18	57.50	1.25	1.29
70	662	11.81	D.p..	3.62	0.12	0.12	8.23	0.74	0.80	12.19	0.19	0.20	61.50	1.30	1.29
70	765	12.77	D.p..	3.45	0.12	0.10	9.25	0.69	0.82	10.32	0.17	0.16	50.29	1.37	1.29
70	831	13.69	M.o.	3.79	0.12	0.13	7.24	0.74	0.72	11.71	0.19	0.19	58.62	1.33	1.27

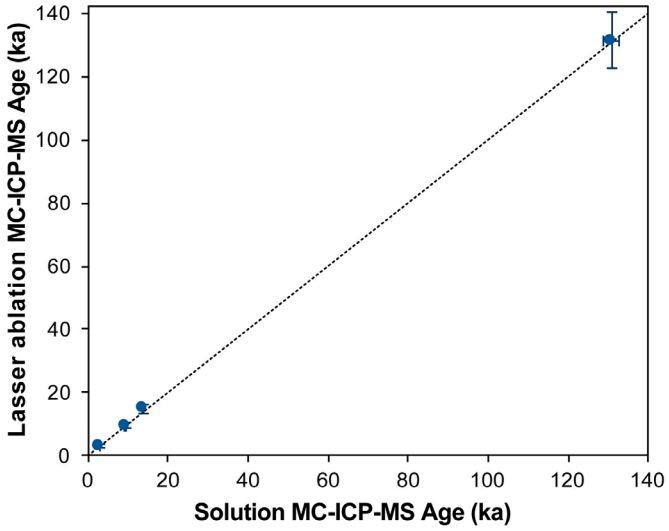

Figure S3.1. Accuracy of laser ablation MC-ICP-MS dating versus solution MC-ICP-MS with the respective 2σ uncertainties.

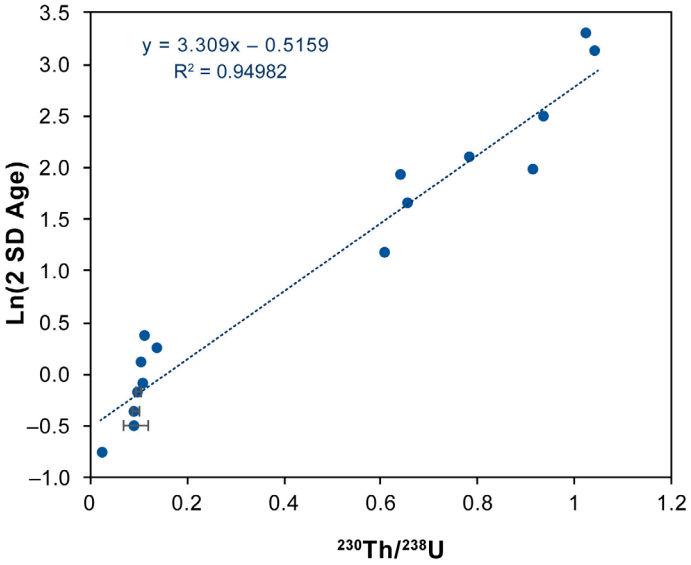

Figure S3.2. Relationship between the external reproducibility of those samples analysed multiple (≥3) times by laser ablation MC-ICP-MS and their ($^{230}Th/^{238}U$) with 2σ uncertainties.

Research papers coauthored during the course of this Ph.D.

Seafloor litter sorting in different domains of Cap de Creus continental shelf and submarine canyon (NW Mediterranean Sea)

Carlos Dominguez-Carrió[a,*], Anna Sanchez-Vidal[b], Claude Estournel[c], Guillem Corbera[a], Joan Lluís Riera[d], Covadonga Orejas[e], Miquel Canals[b], Josep-Maria Gili[a]

[a] Institut de Ciències del Mar, Consejo Superior de Investigaciones Científicas, Passeig Marítim de la Barceloneta 37-49, 08003 Barcelona, Spain
[b] GRC Geociències Marines, Departament de Dinàmica de la Terra i de l'Oceà, Facultat de Ciències de la Terra, Universitat de Barcelona, Martí i Franquès s/n, 08028 Barcelona, Spain
[c] Laboratoire d'Etudes en Géophysique et Océanographie Spatiales (LEGOS), CNRS/UPS/CNES/IRD, Avenue Edouard Belin 14, 31400 Toulouse, France
[d] Departament de Biologia Evolutiva, Ecologia i Ciències Ambientals, Universitat de Barcelona, Avinguda Diagonal 643, 08028 Barcelona, Spain
[e] Spanish Institute of Oceanography (IEO), Oceanographic Centre of the Balearics (COB), Ecosystem Oceanography Group (GRECO), Moll de Ponent s/n, 07015 Palma, Spain

We analyzed litter occurrence in 68 underwater video transects performed on the middle/outer continental shelf and submarine canyon off Cap de Creus (NW Mediterranean), an area recently declared Site of Community Importance (SCI). Low densities of urban litter were registered on the shelf (7.2 items ha1), increasing in abundance towards the deepest part of the submarine canyon, with 188 items ha^{-1} below 1000 m depth. We hypothesize that the strong bottom currents that recurrently affect this area efficiently move litter objects from the shelf towards the deep. Of all litter items, approximately 50% had a fishing-related origin, mostly longlines entangled on rocks in the canyon head and discarded trawl nets in deeper areas. Over 10% of cold-water colonies observed had longlines entangled, indicating the harmful effects of such practices over benthic habitats. These results should be considered when designing mitigation measures to reduce litter pollution in Cap de Creus SCI.

https://doi.org/10.1016/j.marpolbul.2020.111744

Evidences of human impact on megabenthic assemblages of bathyal sediments in the Alboran Sea (western Mediterranean)

Jordi Grinyó[a,b,*], Claudio Lo Iacono[a], Martina Pierdomenico[d], Suzanne Conlon[c], Guillem Corbera[c], Eulàlia Gràcia[a]

[a] Institut de Ciències del Mar (CSIC), Pg. Marítim de la Barceloneta 37-49, 08003, Barcelona, Spain
[b] Sorbonne Université, Laboratoire d'Ecogeochimie des Environnements Benthiques, LECOB, Banyuls-sur-Mer, France
[c] National Oceanography Centre, University of Southampton Waterfront Campus, European Way, Southampton, SO14 3ZH, UK
[d] Istituto per lo studio degli impatti Antropici e Sostenibilità in ambiente marino (CNR-IAS), Roma, Via della Vasca Navale 79, 00146, Rome, Italy

Megabenthic assemblages in deep-sea sedimentary environments receive far less attention than those occurring on rocky environments, despite they have been widely impacted by destructive trawling activities, mainly due to their association with important commercial species. ROV dives conducted on bathyal muds of the Alboran Sea continental slope (western Mediterranean) were used to characterize megabenthic assemblages, as well as assess their response to trawling and benthic litter. We identified a multispecific assemblage, dominated by the isidid *Isidella elongata*, and two monospecific assemblages composed by the sea-pens *Funiculina quadrangularis* and *Kophobelemnon stelliferum*. These assemblages are defined as vulnerable marine ecosystems by international institutions. Trawled areas exhibit significant low densities of habitat-forming species and a striking impoverishment of habitat complexity and diversity. Plastic debris and lost fishing gears were the most abundant components of the marine litter. This study highlights the destructive effects of human activities on bathyal muds, emphasizing the need for urgent conservation measures.

https://doi.org/10.1016/j.dsr.2020.103369

Reference list

2008/56/EC, 2008. Directive of the European Parliament and of the Council of 17 June 2008 establishing a framework for community action in the field of marine environmental policy (Marine Strategy Framework Directive), European Commission: Brussels.

92/43/EEC, 1992. Council Directive 92/43/EEC of 21 May on the conservation of natural habitats and of wild fauna and flora. OJ L206, 22.07.92. p.7.

Addamo, A.M., Vertino, A., Stolarski, J., García-Jiménez, R., Taviani, M., Machordom, A., 2016. Merging scleractinian genera: The overwhelming genetic similarity between solitary *Desmophyllum* and colonial *Lophelia*. BMC Evol. Biol. 16, 1–17. doi:10.1186/s12862-016-0654-8

Aguilar, R., Marín, P., Gerovasileiou, V., Bakran-Petricioli, T., Ballesteros, E., Bazairi, H., Bianchi, C.N., Bussotti, S., Canese, S., Chevaldonné, P., Evans, D., Fourt, M., Grinyó, J., Harmelin, J.-G., Jeudy de Grissac, A., Mačić, V., Orejas, C., Otero, M. d. M., Pergent, G., Petricioli, D., Ramos-Esplá, A.A., Rosso, A., Sanfilippo, R., Taviani, M., Tunesi, L., Würtz, M., 2017. Draft Guidelines for Inventoring and Monitoring of Dark Habitats.

Althaus, F., Williams, A., Schlacher, T.A., Kloser, R.J., Green, M.A., Barker, B.A., Bax, N.J., Brodie, P., Schlacher-Hoenlinger, M.A., 2009. Impacts of bottom trawling on deep-coral ecosystems of seamounts are long-lasting. Mar. Ecol. Prog. Ser. 397, 279–294.

Ambroso, S., Gori, A., Dominguez-Carrió, C., Gili, J.M., Berganzo, E., Teixidó, N., Greenacre, M., Rossi, S., 2013. Spatial distribution patterns of the soft corals *Alcyonium acaule* and *Alcyonium palmatum* in coastal bottoms (Cap de Creus, northwestern Mediterranean Sea). Mar. Biol. 160, 3059–3070. doi:10.1007/s00227-013-2295-4

Anagnostou, E., Sherrell, R.M., Gagnon, A., LaVigne, M., Field, M.P., McDonough, W.F., 2011. Seawater nutrient and carbonate ion concentrations recorded as P/Ca, Ba/Ca, and U/Ca in the deep-sea coral *Desmophyllum dianthus*. Geochim. Cosmochim. Acta 75, 2529–2543. doi:10.1016/j.gca.2011.02.019

Anagnostou, E., Huang, K.F., You, C.F., Sikes, E.L., Sherrell, R.M., 2012. Evaluation of boron isotope ratio as a pH proxy in the deep sea coral *Desmophyllum dianthus*: Evidence of physiological pH adjustment. Earth Planet. Sci. Lett. 349–350, 251–260. doi:10.1016/j.epsl.2012.07.006

Angeletti, L., Taviani, M., Canese, S., Foglini, F., Mastrototaro, F., Argnani, A., Trincardi, F., Bakran-Petricioli, T., Ceregato, A., Chimienti, G., Mačić, V., Poliseno, A., 2014. New deep-water cnidarian sites in the southern Adriatic Sea. Mediterr. Mar. Sci. 15, 263–273. doi:10.12681/mms.558

Angeletti, L., Castellan, G., Montagna, P., Remia, A., Taviani, M., 2020a. The "Corsica Channel Cold-Water Coral Province" (Mediterranean Sea). Front. Mar. Sci. 7, 661. doi:10.3389/fmars.2020.00661

Angeletti, L., Prampolini, M., Foglini, F., Grande, V., Taviani, M., 2020b. Cold-water coral habitat in the Bari Canyon System, Southern Adriatic Sea (Mediterranean Sea), in: Seafloor Geomorphology as Benthic Habitat. Elsevier, pp. 811–824. doi:10.1016/b978-0-12-814960-7.00049-x

Anscombe, F.J., Glynn, W.J., 1983. Distribution of the kurtosis statistic b 2 for normal samples. Biometrika 70, 227–234.

Armstrong, C.W., Foley, N.S., Kahui, V., Grehan, A., 2014. Cold water coral reef management from an ecosystem service perspective. Mar. Policy 50, 126–134.

Arnaud-Haond, S., Van den Beld, I.M.J., Becheler, R., Orejas, C., Menot, L., Frank, N., Grehan, A., Bourillet, J.F., 2017. Two "pillars" of cold-water coral reefs along Atlantic European margins: Prevalent association of *Madrepora oculata* with *Lophelia pertusa,* from reef to colony scale. Deep. Res. Part II Top. Stud. Oceanogr. 145, 110–119. doi:10.1016/j.dsr2.2015.07.013

Astraldi, M., Gasparini, G.P., Vetrano, A., Vignudelli, S., 2002. Hydrographic characteristics and interannual variability of water masses in the central Mediterranean: A sensitivity test for long-term changes in the Mediterranean Sea. Deep. Res. Part I Oceanogr. Res. Pap. 49, 661–680. doi:10.1016/S0967-0637(01)00059-0

Auster, P.J., Gjerde, K., Heupel, E., Watling, L., Grehan, A., Rogers, A.D., 2011. Definition and detection of vulnerable marine ecosystems on the high seas: problems with the "move-on" rule. ICES J. Mar. Sci. 68, 254–264. doi:10.1093/icesjms/fsq074

Bahr, A., Kaboth, S., Jiménez-Espejo, F.J., Sierro, F.J., Voelker, A.H.L., Lourens, L., Röhl, U., Reichart, G.J., Escutia, C., Hernández-Molina, F.J., Pross, J., Friedrich, O., 2015. Persistent monsoonal forcing of mediterranean outflow water dynamics during the late Pleistocene. Geology 43, 951–954. doi:10.1130/G37013.1

Bárcena, M.A., Cacho, I., Abrantes, F., Sierro, F.J., Grimalt, J.O., Flores, J.A., 2001. Paleoproductivity variations related to climatic conditions in the Alboran Sea (western Mediterranean) during the last glacial-interglacial transition: The diatom record. Palaeogeogr. Palaeoclimatol. Palaeoecol. 167, 337–357. doi:10.1016/S0031-0182(00)00246-7

Bargain, A., Marchese, F., Savini, A., Taviani, M., Fabri, M.-C., 2017. Santa Maria di Leuca Province (Mediterranean Sea): Identification of Suitable Mounds for Cold-Water Coral Settlement Using Geomorphometric Proxies and Maxent Methods. Front. Mar. Sci. 4, 338. doi:10.3389/fmars.2017.00338

Bertrand, P., Shimmield, G., Martinez, P., Grousset, F., Jorissen, F., Paterne, M., Pujol, C., Bouloubassi, I., Buat Menard, P., Peypouquet, J.P., Beaufort, L., Sicre, M.A., Lallier-Verges, E., Foster, J.M., Ternois, Y., 1996. The glacial ocean productivity hypothesis: The importance of regional temporal and spatial studies. Mar. Geol. 130, 1–9. doi:10.1016/0025-3227(95)00166-2

Bett, B.J., Billett, D.S.M., Masson, D.G., Tyler, P.A., 2001. RRS Discovery Cruise 248, 07 Jul-10 Aug 2000. A multidisciplinary study of the environment and ecology of deep-water coral ecosystems and associated seabed facies and features (The Darwin Mounds, Porcupine Bank and Porcupine Seabight). Southampton Oceanography Centre, Southampton.

Bo, M., Canese, S., Bavestrello, G., 2014a. Discovering Mediterranean black coral forests: *Parantipathes larix* (Anthozoa: Hexacorallia) in the Tuscan Archipelago, Italy. Ital. J. Zool. 81, 112–125. doi:10.1080/11250003.2013.859750

Bo, M., Cerrano, C., Canese, S., Salvati, E., Angiolillo, M., Santangelo, G., Bavestrello, G., 2014b. The coral assemblages of an off-shore deep Mediterranean rocky bank (NW Sicily, Italy). Mar. Ecol. 35, 332–342. doi:10.1111/maec.12089

Bo, M., Bavestrello, G., Angiolillo, M., Calcagnile, L., Canese, S., Cannas, R., Cau, A., D'Elia, M., D'Oriano, F., Follesa, M.C., others, 2015. Persistence of pristine deep-sea coral gardens in the Mediterranean Sea (SW Sardinia). PLoS One 10, e0119393.

Bo, M., Barucca, M., Biscotti, M.A., Brugler, M.R., Canapa, A., Canese, S., Lo Iacono, C., Bavestrello, G., 2018. Phylogenetic relationships of Mediterranean black corals (Cnidaria : Anthozoa : Hexacorallia) and implications for classification within the order Antipatharia. Invertebr. Syst. 32, 1102. doi:10.1071/IS17043

Bonneau, L., Colin, C., Pons-Branchu, E., Mienis, F., Tisnérat-Laborde, N., Blamart, D., Elliot, M., Collart, T., Frank, N., Foliot, L., Douville, E., 2018. Imprint of Holocene Climate Variability on Cold-Water Coral Reef Growth at the SW Rockall Trough Margin, NE Atlantic. Geochemistry, Geophys. Geosystems 19, 2437–2452. doi:10.1029/2018GC007502

Bosc, E., Bricaud, A., Antoine, D., 2004. Seasonal and interannual variability in algal biomass and primary production in the Mediterranean Sea, as derived from 4 years of SeaWiFS observations. Global Biogeochem. Cycles 18, GB1005. doi:10.1029/2003gb002034

Bouchet, P., Taviani, M., 1992. The Mediterranean deep-sea fauna: pseudopopulations of Atlantic species? Deep Sea Res. Part A, Oceanogr. Res. Pap. 39, 169–184. doi:10.1016/0198-0149(92)90103-Z

Bouillin, J.-P., Durand-Delga, M., Olivier, P., 1986. Betic-Rifian and Tyrrhenian Arcs : Distinctive Features, Genesis and Development Stages. Dev. Geotecton. 21, 281–304. doi:10.1016/B978-0-444-42688-8.50017-5

Boury-Esnault, N., Vacelet, J., Reiswig, H.M., Fourt, M., Aguilar, R., Chevaldonné, P., 2015. Mediterranean hexactinellid sponges, with the description of a new *Sympagella* species (Porifera, Hexactinellida). J. Mar. Biol.

Assoc. United Kingdom 95, 1353–1364. doi:10.1017/S0025315414001891

Bout-Roumazeilles, V., Combourieu Nebout, N., Peyron, O., Cortijo, E., Landais, A., Masson-Delmotte, V., 2007. Connection between South Mediterranean climate and North African atmospheric circulation during the last 50,000 yr BP North Atlantic cold events. Quat. Sci. Rev. 26, 3197–3215. doi:10.1016/j.quascirev.2007.07.015

Brooke, S., Schroeder, W.W., 2007. State of deep coral ecosystems in the Gulf of Mexico region: Texas to the Florida Straits. In: S.E. Lumsden, Hourigan, T.F., Bruckner, A.W., Dorr, G. (Eds.) The State of Deep Coral Ecosystems of the United States, 271-306. NOAA Technical Memorandum CRCP-3. Silver Spring MD 365 pp.

Brooke, S., Young, C.M., 2005. Embryogenesis and larval biology of the ahermatypic scleractinian *Oculina varicosa*. Mar. Biol. 146, 665–675. doi:10.1007/s00227-004-1481-9

Brooke, S.D., Holmes, M.W., Young, C.M., 2009. Sediment tolerance of two different morphotypes of the deep-sea coral *Lophelia pertusa* from the Gulf of Mexico. Mar. Ecol. Prog. Ser. 390, 137–144.

Brooke, S., Ross, S.W., Bane, J.M., Seim, H.E., Young, C.M., 2013. Temperature tolerance of the deep-sea coral *Lophelia pertusa* from the southeastern United States. Deep Sea Res. Part II Top. Stud. Oceanogr. 92, 240–248.

Buhl-Mortensen, P., Fosså, J.H., 2006. Species diversity and spatial distribution of invertebrates on deep-water *Lophelia* reefs in Norway, in: Suzuki, Y. et al. (Ed.), Proceedings of the 10th International Coral Reef Symposium. pp. 1849–1860.

Buhl-Mortensen, L., Vanreusel, A., Gooday, A.J., Levin, L.A., Priede, I.G., Buhl-Mortensen, P., Gheerardyn, H., King, N.J., Raes, M., 2010. Biological structures as a source of habitat heterogeneity and biodiversity on the deep ocean margins. Mar. Ecol. 31, 21–50.

Buhl-Mortensen, P., Buhl-Mortensen, L., Purser, A., 2016. Trophic Ecology and Habitat Provision in Cold-Water Coral Ecosystems, in: Marine Animal Forests. Springer International Publishing, pp. 919–944. doi:10.1007/978-3-319-17001-5_20-1

Buhl-Mortensen, L., Serigstad, B., Buhl-Mortensen, P., Olsen, M.N., Ostrowski, M., Błażewicz-Paszkowycz, M., Appoh, E., 2017. First observations of the structure and megafaunal community of a large *Lophelia* reef on the Ghanaian shelf (the Gulf of Guinea). Deep Sea Res. Part II Top. Stud. Oceanogr. 137, 148–156.

Bullimore, R.D., Foster, N.L., Howell, K.L., 2013. Coral-characterized benthic assemblages of the deep Northeast Atlantic: defining ``Coral Gardens'' to support future habitat mapping efforts. ICES J. Mar. Sci. 70, 511–522.

Cacho, I., Grimalt, J.O., Sierro, F.J., Shackleton, N., Canals, M., 2000. Evidence for enhanced Mediterranean thermohaline circulation during rapid climatic coolings. Earth Planet. Sci. Lett. 183, 417–429. doi:10.1016/S0012-821X(00)00296-X

Cacho, I., Grimalt, J.O., Canals, M., 2002. Response of the Western Mediterranean Sea to rapid climatic variability during the last 50,000 years: A molecular biomarker approach. J. Mar. Syst. 33–34, 253–272. doi:10.1016/S0924-7963(02)00061-1

Cairns, S.D., 2007. Deep-water corals: an overview with special reference to diversity and distribution of deep-water scleractinian corals. Butlletin Mar. Sci. 81, 311–322.

Caldeira, K., Wickett, M.E., 2003. Anthropogenic carbon and ocean pH. Nature 425, 365. doi:10.1038/425365a

Camafort, M., Gràcia, E., Ranero, C.R., 2020. Quaternary Seismostratigraphy and Tectonosedimentary Evolution of the North Tunisian Continental Margin. Tectonics 39. doi:10.1029/2020TC006243

Capotondi, L., Vigliotti, L., Bergami, C., Sangiorgi, F., 2011. The Dark Side of the Mediterranean Geological Record: the sapropel layers and a case study from the Ionian Sea, in: Marine Research at CNR. Dipartimento Terra e Ambiente—CNR, Roma, pp. 658–669.

Capotondi, L., Girone, A., Lirer, F., Bergami, C., Verducci, M., Vallefuoco, M., Afferri, A., Ferraro, L., Pelosi, N., De Lange, G.J., 2016. Central Mediterranean Mid-Pleistocene paleoclimatic variability and its association with global climate. Palaeogeogr. Palaeoclimatol. Palaeoecol. 442, 72–83. doi:10.1016/j.palaeo.2015.11.009

Cardona, Y., Bracco, A., 2012. Enhanced vertical mixing within mesoscale eddies due to high frequency winds in the South China Sea. Ocean Model. 42, 1–15. doi:10.1016/j.ocemod.2011.11.004

Carlier, A., Le Guilloux, E., Olu, K., Sarrazin, J., Mastrototaro, F., Taviani, M., Clavier, J., 2009. Trophic relationships in a deep Mediterranean cold-water coral bank (Santa Maria di Leuca, Ionian Sea). Mar. Ecol. Prog. Ser. 397, 125–137. doi:10.3354/meps08361

Case, D.H., Robinson, L.F., Auro, M.E., Gagnon, A.C., 2010. Environmental and biological controls on Mg and Li in deep-sea scleractinian corals. Earth Planet. Sci. Lett. 300, 215–225. doi:10.1016/j.epsl.2010.09.029

Castellan, G., Angeletti, L., Taviani, M., Montagna, P., 2019. The Yellow Coral *Dendrophyllia cornigera* in a Warming Ocean. Front. Mar. Sci. 6, 692. doi:10.3389/fmars.2019.00692

Cau, A., Follesa, M.C., Moccia, D., Alvito, A., Bo, M., Angiolillo, M., Canese, S., Paliaga, E.M., Orrù, P.E., Sacco, F., others, 2015. Deepwater corals biodiversity along roche du large ecosystems with different habitat complexity along the south Sardinia continental margin (CW Mediterranean Sea). Mar. Biol. 162, 1865–1878.

Chambers, J.M., Hastie, T.J., others, 1992. Statistical models in S. Wadsworth & Brooks/Cole Advanced Books & Software Pacific Grove, CA.

Cheng, H., Adkins, J., Edwards, R.L., Boyle, E.A., 2000. U-Th dating of deep-sea corals. Geochim. Cosmochim. Acta 64, 2401–2416. doi:10.1016/S0016-7037(99)00422-6

Chutcharavan, P.M., Dutton, A., Ellwood, M.J., 2018. Seawater $^{234}U/^{238}U$ recorded by modern and fossil corals. Geochim. Cosmochim. Acta 224, 1–17. doi:10.1016/j.gca.2017.12.017

Church, J.A., White, N.J., Aarup, T., Wilson, W.S., Woodworth, P.L., Domingues, C.M., Hunter, J.R., Lambeck, K., 2008. Understanding global sea levels: Past, present and future. Sustain. Sci. 3, 9–22. doi:10.1007/s11625-008-0042-4

Coiras, E., Lo Iacono, C., Gracia, E., Danobeitia, J., Sanz, J.L., 2011. Automatic segmentation of multi-beam data for predictive mapping of benthic habitats on the Chella Seamount (North-Eastern Alboran Sea, Western Mediterranean). IEEE J. Sel. Top. Appl. Earth Obs. Remote Sens. 4, 809–813.

Colantoni, P., 1973. A glacial mollusc fauna from Baronie Seamount (off eastern Sardinia). Rapp. Comm. int. Mer Médit. 21, 896–900.

Colin, C., Frank, N., Copard, K., Douville, E., 2010. Neodymium isotopic composition of deep-sea corals from the NE Atlantic: Implications for past hydrological changes during the Holocene. Quat. Sci. Rev. 29, 2509–2517. doi:10.1016/j.quascirev.2010.05.012

Comas, M., Pinheiro, L.M., 2010. The Melilla carbonate mounds: do deep-water coral mounds count on seeping fluids in the Alboran Sea? Rapp. Comm. int. Mer Médit. 39.

Corbera, G., Lo Iacono, C., Gracia, E., Grinyó, J., Pierdomenico, M., Huvenne, V.A.I., Aguilar, R., Gili, J.-M., 2017. Cold-water coral assemblages on the Cabliers Mound (Alboran Sea, Western Mediterranean): Diversity and structure, in: European Coral Reef Symposium. Oxford.

Corbera, G., Lo Iacono, C., Gràcia, E., Grinyó, J., Pierdomenico, M., Huvenne, V.A.I., Aguilar, R., Gili, J.M., 2019. Ecological characterisation of a Mediterranean cold-water coral reef: Cabliers Coral Mound Province (Alboran Sea, western Mediterranean). Prog. Oceanogr. 175, 245–262. doi:10.1016/j.pocean.2019.04.010

Corbera, G., Lo Iacono, C., Standish, C.D., Anagnostou, E., Titschack, J., Katsamenis, O., Cacho, I., Van Rooij, D., Huvenne, V.A.I., Foster, G.L., 2021. Glacio-eustatic variations and Sapropel events as main controls on the Middle Pleistocene-Holocene evolution of the Cabliers Coral Mound Province (W Mediterranean). Quat. Sci. Rev. 253, 106783. doi:10.1016/j.quascirev.2020.106783

Costello, M.J., McCrea, M., Freiwald, A., Lundälv, T., Jonsson, L., Bett, B.J., van Weering, T.C.E., de Haas, H., Roberts, J.M., Allen, D., 2005. Role of cold-water *Lophelia pertusa* coral reefs as fish habitat in the NE Atlantic, in: Cold-Water Corals and Ecosystems. Springer, pp. 771–805.

Cortés, J.N., Risk, M.J., 1985. A reef under siltation stress: Cahuita, Costa Rica. Butlletin Mar. Sci. 36, 339–356.

Cyr, F., Haren, H., Mienis, F., Duineveld, G., Bourgault, D., 2016. On the influence of cold-water coral mound size on flow hydrodynamics, and vice versa. Geophys. Res. Lett. 43, 775–783.

D'Onghia, G., Maiorano, P., Sion, L., Giove, A., Capezzuto, F., Carlucci, R., Tursi, A., 2010. Effects of deep-water coral banks on the abundance and size structure of the megafauna in the Mediterranean Sea. Deep Sea Res.

Part II Top. Stud. Oceanogr. 57, 397–411.

D'Onghia, G., Indennidate, A., Giove, A., Savini, A., Capezzuto, F., Sion, L., Vertino, A., Maiorano, P., 2011. Distribution and behaviour of deep-sea benthopelagic fauna observed using towed cameras in the Santa Maria di Leuca cold-water coral province. Mar. Ecol. Prog. Ser. 443, 95–110. doi:10.3354/meps09432

D'Onghia, G., Maiorano, P., Carlucci, R., Capezzuto, F., Carluccio, A., Tursi, A., Sion, L., 2012. Comparing Deep-Sea Fish Fauna between Coral and Non-Coral "Megahabitats" in the Santa Maria di Leuca Cold-Water Coral Province (Mediterranean Sea). PLoS One 7, e44509. doi:10.1371/journal.pone.0044509

D'Onghia, G., Capezzuto, F., Cardone, F., Carlucci, R., Carluccio, A., Chimienti, G., Corriero, G., Longo, C., Maiorano, P., Mastrototaro, F., Panetta, P., Rosso, A., Sanfilippo, R., Sion, L., Tursi, A., 2015. Macro- and megafauna recorded in the submarine Bari Canyon (southern Adriatic, Mediterranean Sea) using different tools. Mediterr. Mar. Sci. 16, 180–196. doi:10.12681/mms.1082

D'Onghia, G., Sion, L., Capezzuto, F., 2019. Cold-water coral habitats benefit adjacent fisheries along the Apulian margin (central Mediterranean). Fish. Res. 213, 172–179. doi:10.1016/j.fishres.2019.01.021

D'Ortenzio, F., Ribera d'Alcalà, M., 2009. On the trophic regimes of the Mediterranean Sea: a satellite analysis. Biogeosciences 6, 139–148.

Davies, A.J., Wisshak, M., Orr, J.C., Murray Roberts, J., 2008. Predicting suitable habitat for the cold-water coral *Lophelia pertusa* (Scleractinia). Deep. Res. Part I Oceanogr. Res. Pap. 55, 1048–1062. doi:10.1016/j.dsr.2008.04.010

Davies, A.J., Duineveld, G.C.A., Lavaleye, M.S.S., Bergman, M.J.N., van Haren, H., Roberts, J.M., 2009. Downwelling and deep-water bottom currents as food supply mechanisms to the cold-water coral *Lophelia pertusa* (Scleractinia) at the Mingulay Reef Complex. Limnol. Oceanogr. 54, 620–629.

Davies, A.J., Duineveld, G.C.A., van Weering, T.C.E., Mienis, F., Quattrini, A.M., Seim, H.E., Bane, J.M., Ross, S.W., 2010. Short-term environmental variability in cold-water coral habitat at Viosca Knoll, Gulf of Mexico. Deep. Res. Part I Oceanogr. Res. Pap. 57, 199–212. doi:10.1016/j.dsr.2009.10.012

Davies, A.J., Guinotte, J.M., 2011. Global Habitat Suitability for Framework-Forming Cold-Water Corals. PLoS One 6, e18483. doi:10.1371/journal.pone.0018483

Davies, J.S., Guillaumont, B., Tempera, F., Vertino, A., Beuck, L., Ólafsdóttir, S.H., Smith, C.J., Fosså, J.H., van den Beld, I.M.J., Savini, A., Rengstorf, A., Bayle, C., Bourillet, J.F., Arnaud-Haond, S., Grehan, A., 2017. A new classification scheme of European cold-water coral habitats: Implications for ecosystem-based management of the deep sea. Deep. Res. Part II Top. Stud. Oceanogr. 145, 102–109. doi:10.1016/j.dsr2.2017.04.014

De Clippele, L.H., Huvenne, V.A.I., Orejas, C., Lundälv, T., Fox, A., Hennige, S.J., Roberts, J.M., 2018. The effect of local hydrodynamics on the spatial extent and morphology of cold-water coral habitats at Tisler Reef, Norway. Coral Reefs 37, 253–266.

De Clippele, L.H., Huvenne, V.A.I., Molodtsova, T.N., Roberts, J.M., 2019. The diversity and ecological role of non-scleractinian corals (Antipatharia and Alcyonacea) on scleractinian cold-water coral mounds. Front. Mar. Sci. 6, 184. doi:10.3389/fmars.2019.00184

De Haas, H., Mienis, F., Frank, N., Richter, T.O., Steinacher, R., De Stigter, H., der Land, C., Van Weering, T.C.E., 2009. Morphology and sedimentology of (clustered) cold-water coral mounds at the south Rockall Trough margins, NE Atlantic Ocean. Facies 55, 1–26.

De la Torriente, A., Serrano, A., Fernández-Salas, L.M., García, M., Aguilar, R., 2018. Identifying epibenthic habitats on the Seco de los Olivos Seamount: Species assemblages and environmental characteristics. Deep. Res. Part I Oceanogr. Res. Pap. 135, 9–22. doi:10.1016/j.dsr.2018.03.015

De la Torriente, A., Aguilar, R., González-Irusta, J.M., Blanco, M., Serrano, A., 2020. Habitat forming species explain taxonomic and functional diversities in a Mediterranean seamount. Ecol. Indic. 118, 106747. doi:10.1016/j.ecolind.2020.106747

De Leo, F., Puig, P., Lo Iacono, C., Durán, R., Palanques, A., Paradis, S., Arjona, M., Guillén, J., ABIDES Cruise Team. 2019. First observations of living Cold Water Corals surrounded by fishing grounds in Blanes Canyon (NW Mediterranean). 7th International Symposium on Deep-Sea Corals. Cartagena de Indias, Colombia, 29 de

Julio - 2 de Agosto de 2019. Póster.

De Mol, B., Van Rensbergen, P., Pillen, S., Van Herreweghe, K., Van Rooij, D., McDonnell, A., Huvenne, V., Ivanov, M., Swennen, R., Henriet, J.P., 2002. Large deep-water coral banks in the Porcupine Basin, southwest of Ireland. Mar. Geol. 188, 193–231. doi:10.1016/S0025-3227(02)00281-5

De Mol, B., Henriet, J.-P., Canals, M., 2005. Development of coral banks in Porcupine Seabight: do they have Mediterranean ancestors?, in: Cold-Water Corals and Ecosystems. Springer Berlin Heidelberg, pp. 515–533. doi:10.1007/3-540-27673-4_26

De Mol, B., Kozachenko, M., Wheeler, A., Alvares, H., Henriet, J.P., Olu-Le Roy, K., 2007. Thérèse Mound: A case study of coral bank development in the Belgica Mound Province, Porcupine Seabight. Int. J. Earth Sci. 96, 103–120. doi:10.1007/s00531-005-0496-x

De Mol, L., Van Rooij, D., Pirlet, H., Greinert, J., Frank, N., Quemmerais, F., Henriet, J.-P., 2011. Cold-water coral habitats in the Penmarc'h and Guilvinec Canyons (Bay of Biscay): Deep-water versus shallow-water settings. Mar. Geol. 282, 40–52.

De Mol, B., Amblas, D., Calafat, A., Canals, M., Duran, R., Lavoie, C., Muñoz, A., Rivera, J., 2012. Cold-water Coral Colonization of Alboran Sea Knolls, Western Mediterranean Sea, in: Seafloor Geomorphology as Benthic Habitat. Elsevier Inc., pp. 819–829. doi:10.1016/B978-0-12-385140-6.00060-8

DeGeest, A.L., Mullenbach, B.L., Puig, P., Nittrouer, C.A., Drexler, T.M., Durrieu de Madron, X., Orange, D.L., 2008. Sediment accumulation in the western Gulf of Lions, France: The role of Cap de Creus Canyon in linking shelf and slope sediment dispersal systems. Cont. Shelf Res. 28, 2031–2047. doi:10.1016/j.csr.2008.02.008

Deval, M.C., Kebapçıoğlu, T., Güven, O., Olguner, M.T., 2018. Population pattern and dynamics of the Bluemouth *Helicolenus dactylopterus* (Delaroche, 1809) in the eastern Mediterranean Sea. J. Appl. Ichthyol. 34, 568–580. doi:10.1111/jai.13613

Di Stefano, A., Foresi, L.M., Incarbona, A., Sprovieri, M., Vallefuoco, M., Iorio, M., Pelosi, N., Di Stefano, E., Sangiorgi, P., Budillon, F., 2015. Mediterranean coccolith ecobiostratigraphy since the penultimate Glacial (the last 145,000 years) and ecobioevent traceability. Mar. Micropaleontol. 115, 24–38. doi:10.1016/j.marmicro.2014.12.002

Dickson, R.R., McCave, I.N., 1986. Nepheloid layers on the continental slope west of Porcupine Bank. Deep Sea Res. Part A, Oceanogr. Res. Pap. 33, 791–818. doi:10.1016/0198-0149(86)90089-0

Dinarès-Turell, J., Hoogakker, B.A.A., Roberts, A.P., Rohling, E.J., Sagnotti, L., 2003. Quaternary climatic control of biogenic magnetite production and eolian dust input in cores from the Mediterranean Sea. Palaeogeogr. Palaeoclimatol. Palaeoecol. 190, 195–209. doi:10.1016/S0031-0182(02)00605-3

Dodds, L.A., Roberts, J.M., Taylor, A.C., Marubini, F., 2007. Metabolic tolerance of the cold-water coral *Lophelia pertusa* (Scleractinia) to temperature and dissolved oxygen change. J. Exp. Mar. Bio. Ecol. 349, 205–214.

Dodds, L., Black, K., Orr, H., Roberts, J., 2009. Lipid biomarkers reveal geographical differences in food supply to the cold-water coral *Lophelia pertusa* (Scleractinia). Mar. Ecol. Prog. Ser. 397, 113–124. doi:10.3354/meps08143

Domínguez-Carrió, C., 2018. ROV-based ecological study and management proposals for the offshore marine protected area of Cap de Creus (NW Mediterranean). University of Barcelona.

Dorale, J.A., Onac, B.P., Fornós, J.J., Ginés, J., Ginés, A., Tuccimei, P., Peate, D.W., 2010. Sea-Level Highstand 81,000 Years Ago in Mallorca. Science0 327, 860–863. doi:10.1126/science.1181725

Dorschel, B., Hebbeln, D., Rüggeberg, A., Dullo, W.C., Freiwald, A., 2005. Growth and erosion of a cold-water coral covered carbonate mound in the Northeast Atlantic during the Late Pleistocene and Holocene. Earth Planet. Sci. Lett. 233, 33–44. doi:10.1016/j.epsl.2005.01.035

Dorschel, B., Hebbeln, D., Foubert, A., White, M., Wheeler, A.J., 2007. Hydrodynamics and cold-water coral facies distribution related to recent sedimentary processes at Galway Mound west of Ireland. Mar. Geol. 244, 184–195. doi:10.1016/j.margeo.2007.06.010

Douarin, M., Elliot, M., Noble, S.R., Sinclair, D., Henry, L.A., Long, D., Moreton, S.G., Murray Roberts, J., 2013. Growth of north-east Atlantic cold-water coral reefs and mounds during the Holocene: A high resolution U-series and ^{14}C chronology. Earth Planet. Sci. Lett. 375, 176–187. doi:10.1016/j.epsl.2013.05.023

Du Preez, C., Swan, K.D., Curtis, J.M.R., 2020. Cold-Water Corals and Other Vulnerable Biological Structures on a North Pacific Seamount After Half a Century of Fishing. Front. Mar. Sci. 7, 17. doi:10.3389/fmars.2020.00017

Dubois-Dauphin, Q., Colin, C., Elliot, M., Dapoigny, A., Douville, E., 2019. Holocene shifts in sub-surface water circulation of the North-East Atlantic inferred from Nd isotopic composition in cold-water corals. Mar. Geol. 410, 135–145. doi:10.1016/j.margeo.2019.01.004

Duggen, S., Hoernle, K., van den Bogaard, P., Harris, C., 2004. Magmatic evolution of the Alboran region: the role of subduction in forming the western Mediterranean and causing the Messinian Salinity Crisis. Earth Planet. Sci. Lett. 218, 91–108.

Duineveld, G., Lavaleye, M., Berghuis, E., 2004. Particle flux and food supply to a seamount cold-water coral community (Galicia Bank, NW Spain). Mar. Ecol. Prog. Ser. 277, 13–23. doi:10.3354/meps277013

Duineveld, G.C.A., Jeffreys, R.M., Lavaleye, M.S.S., Davies, A.J., Bergman, M.J.N., Watmough, T., Witbaard, R., 2012. Spatial and tidal variation in food supply to shallow cold-water coral reefs of the Mingulay Reef complex (Outer Hebrides, Scotland). Mar. Ecol. Prog. Ser. 444, 97–115.

Dullo, W.-C., Flögel, S., Rüggeberg, A., 2008. Cold-water coral growth in relation to the hydrography of the Celtic and Nordic European continental margin. Mar. Ecol. Prog. Ser. 371, 165–176.

Eggins, S.M., Grün, R., McCulloch, M.T., Pike, A.W.G., Chappell, J., Kinsley, L., Mortimer, G., Shelley, M., Murray-Wallace, C. V., Spötl, C., Taylor, L., 2005. In situ U-series dating by laser-ablation multi-collector ICPMS: New prospects for Quaternary geochronology. Quat. Sci. Rev. 24, 2523–2538. doi:10.1016/j.quascirev.2005.07.006

Eisele, M., Frank, N., Wienberg, C., Hebbeln, D., López Correa, M., Douville, E., Freiwald, A., 2011. Productivity controlled cold-water coral growth periods during the last glacial off Mauritania. Mar. Geol. 280, 143–149. doi:10.1016/j.margeo.2010.12.007

Eisele, M., Frank, N., Wienberg, C., Titschack, J., Mienis, F., Beuck, L., Tisnerat-Laborde, N., Hebbeln, D., 2014. Sedimentation patterns on a cold-water coral mound off Mauritania. Deep. Res. Part II Top. Stud. Oceanogr. 99, 307–315. doi:10.1016/j.dsr2.2013.07.004

Ercilla, G., Juan, C., Hernández-Molina, F.J., Bruno, M., Estrada, F., Alonso, B., Casas, D., Farran, M., Llave, E., García, M., Vázquez, J.T., D'Acremont, E., Gorini, C., Palomino, D., Valencia, J., El Moumni, B., Ammar, A., 2016. Significance of bottom currents in deep-sea morphodynamics: An example from the Alboran Sea. Mar. Geol. 378, 157–170. doi:10.1016/j.margeo.2015.09.007

Essallami, L., Sicre, M.A., Kallel, N., Labeyrie, L., Siani, G., 2007. Hydrological changes in the Mediterranean Sea over the last 30,000 years. Geochemistry, Geophys. Geosystems 8, n/a-n/a. doi:10.1029/2007GC001587

Fabri, M.-C., Pedel, L., 2012. Biocénoses des fonds durs du bathyal et de l'abyssal/SRM MO.

Fabri, M.-C., Pedel, L., Beuck, L., Galgani, F., Hebbeln, D., Freiwald, A., 2014. Megafauna of vulnerable marine ecosystems in French Mediterranean submarine canyons: Spatial distribution and anthropogenic impacts. Deep Sea Res. Part II Top. Stud. Oceanogr. 104, 184–207.

Fabri, M.-C., Bargain, A., Pairaud, I., Pedel, L., Taupier-Letage, I., 2017. Cold-water coral ecosystems in Cassidaigne Canyon: An assessment of their environmental living conditions. Deep Sea Res. Part II Top. Stud. Oceanogr. 137, 436–453.

Fanelli, E., Delbono, I., Ivaldi, R., Pratellesi, M., Cocito, S., Peirano, A., 2017. Cold-water coral *Madrepora oculata* in the eastern Ligurian Sea (NW Mediterranean): Historical and recent findings. Aquat. Conserv. Mar. Freshw. Ecosyst. 27, 965–975.

FAO, 2009. International guidelines for the management of deep-sea fisheries in the high seas. Rome.

Fentimen, R., Feenstra, E., Rüggeberg, A., Vennemann, T., Hajdas, I., Adatte, T., Van Rooij, D., Foubert, A., 2020. Cold-Water Coral Mound Archive Provides Unique Insights Into Intermediate Water Mass Dynamics in the Alboran Sea During the Last Deglaciation. Front. Mar. Sci. 7. doi:10.3389/fmars.2020.00354

Filippidi, A., Triantaphyllou, M. V., De Lange, G.J., 2016. Eastern-Mediterranean ventilation variability during sapropel S1 formation, evaluated at two sites influenced by deep-water formation from Adriatic and Aegean Seas. Quat. Sci. Rev. 144, 95–106. doi:10.1016/j.quascirev.2016.05.024

Fink, H.G., Wienberg, C., Hebbeln, D., McGregor, H. V., Schmiedl, G., Taviani, M., Freiwald, A., 2012. Oxygen control on Holocene cold-water coral development in the eastern Mediterranean Sea. Deep. Res. Part I Oceanogr. Res. Pap. 62, 89–96. doi:10.1016/j.dsr.2011.12.013

Fink, H.G., Wienberg, C., De Pol-Holz, R., Wintersteller, P., Hebbeln, D., 2013. Cold-water coral growth in the Alboran Sea related to high productivity during the Late Pleistocene and Holocene. Mar. Geol. 339, 71–82.

Fink, H.G., Wienberg, C., De Pol-Holz, R., Hebbeln, D., 2015. Spatio-temporal distribution patterns of Mediterranean cold-water corals (*Lophelia pertusa* and *Madrepora oculata*) during the past 14,000 years. Deep. Res. Part I Oceanogr. Res. Pap. 103, 37–48. doi:10.1016/j.dsr.2015.05.006

Fontanier, C., Metzger, E., Waelbroeck, C., Jouffreau, M., Lefloch, N., Jorissen, F., Etcheber, H., Bichon, S., Chabaud, G., Poirier, D., Grémare, A., Deflandre, B., 2013. Live (stained) benthic foraminifera off walvis bay, namibia: A deep-sea ecosystem under the influence of bottom nepheloid layers. J. Foraminifer. Res. 43, 55–71. doi:10.2113/gsjfr.43.1.55

Fosså, J.H., Mortensen, P.B., Furevik, D.M., 2002. The deep-water coral *Lophelia pertusa* in Norwegian waters: distribution and fishery impacts. Hydrobiologia 471, 1–12.

Fosså, J.H., Lindberg, B., Christensen, O., Lundälv, T., Svellingen, I., Mortensen, P.B., Alvsvåg, J., 2005. Mapping of Lophelia reefs in Norway: experiences and survey methods, in: Cold-Water Corals and Ecosystems. Springer-Verlag, pp. 359–391. doi:10.1007/3-540-27673-4_18

Foubert, A., Huvenne, V.A.I., Wheeler, A., Kozachenko, M., Opderbecke, J., Henriet, J.P., 2011. The Moira Mounds, small cold-water coral mounds in the Porcupine Seabight, NE Atlantic: Part B-Evaluating the impact of sediment dynamics through high-resolution ROV-borne bathymetric mapping. Mar. Geol. 282, 65–78. doi:10.1016/j.margeo.2011.02.008

Fox, A.D., Henry, L.-A., Corne, D.W., Roberts, J.M., 2016. Sensitivity of marine protected area network connectivity to atmospheric variability. R. Soc. Open Sci. 3, 160494. doi:10.1098/rsos.160494

Frank, N., Ricard, E., Lutringer-Paquet, A., van der Land, C., Colin, C., Blamart, D., Foubert, A., Van Rooij, D., Henriet, J.P., de Haas, H., van Weering, T., 2009. The Holocene occurrence of cold water corals in the NE Atlantic: Implications for coral carbonate mound evolution. Mar. Geol. 266, 129–142. doi:10.1016/j.margeo.2009.08.007

Frank, N., Freiwald, A., López Correa, M., Wienberg, C., Eisele, M., Hebbeln, D., Van Rooij, D., Henriet, J.P., Colin, C., van Weering, T., de Haas, H., Buhl-Mortensen, P., Roberts, J.M., De Mol, B., Douville, E., Blamart, D., Hatté, C., 2011. Northeastern Atlantic cold-water coral reefs and climate. Geology 39, 743–746. doi:10.1130/G31825.1

Frederiksen, R., Jensen, A., Westerberg, H., 1992. The distribution of the scleractinian coral lophelia pertu sa around the faroe Islands and the relation to internal tidal mixing. Sarsia 77, 157–171. doi:10.1080/00364827.1992.10413502

Freiwald, A., Henrich, R., Pätzold, J., 1997. Anatomy of a Deep-Water Coral Reef Mound from Stjernsund, West Finnmark, Northern Norway, in: Cool-Water Carbonates. Special Publications of SEPM, 56, pp 141–161.

Freiwald, A., Wilson, J.B., Henrich, R., 1999. Grounding pleistocene icebergs shape recent deep-water coral reefs. Sediment. Geol. 125, 1–8. doi:10.1016/S0037-0738(98)00142-0

Freiwald, A., Huehnerbach, V., Lindberg, B., Wilson, J.B., Campbell, J., 2002. The Sula Reef Complex, Norwegian Shelf. Facies 47, 179–200.

Freiwald, A., Fosså, J.H., Grehan, A., Koslow, T., Roberts, J.M., 2004. Cold-water coral reefs. UNEP-WCMC, Cambridge, UK.

Freiwald, A., Beuck, L., Rüggeberg, A., Taviani, M., Hebbeln, D., R/V Meteor Cruise M70-1 participants, 2009. The white coral community in the central Mediterranean Sea revealed by ROV surveys. Oceanography 22, 58–74.

Gana, S., Iudicone, D., Ghenim, L., Mortier, L., Testor, P., Tintore, J., Olita, A., 2015. Monitoring water masses properties by Glider in Sardinia Channel during summer 2014. Geophys. Res. Abstr. 17.

García Lafuente, J., Cano, N., Vargas, M., Rubín, J.P., Hernández-Guerra, A., 1998. Evolution of the Alboran Sea hydrographic structures during July 1993. Deep Sea Res. Part I Oceanogr. Res. Pap. 45, 39–65.

Georgian, S.E., Deleo, D., Durkin, A., Gomez, C.E., Kurman, M., Lunden, J.J., Cordes, E.E., 2016. Oceanographic patterns and carbonate chemistry in the vicinity of cold-water coral reefs in the Gulf of Mexico: Implications for resilience in a changing ocean. Limnol. Oceanogr. 61, 648–665. doi:10.1002/lno.10242

GFCM, 2009. Criteria for the Identification of Sensitive Habitats of Relevance for the Management of Priority Species (General Fisheries Commission for the Mediterranean), Malaga, pp. 3.

Glogowski, S., Dullo, W.C., Feldens, P., Liebetrau, V., von Reumont, J., Hühnerbach, V., Krastel, S., Wynn, R.B., Flögel, S., 2015. The Eugen Seibold coral mounds offshore western Morocco: oceanographic and bathymetric boundary conditions of a newly discovered cold-water coral province. Geo-Marine Lett. 35, 257–269. doi:10.1007/s00367-015-0405-7

Gómez de la Peña, L., Ranero, C.R., Gràcia, E., 2018. The Crustal Domains of the Alboran Basin (Western Mediterranean). Tectonics 37, 3352–3377. doi:10.1029/2017TC004946

Gori, A., Bavestrello, G., Grinyó, J., Dominguez-Carrió, C., Ambroso, S., Bo, M., 2017. Animal Forests in Deep Coastal Bottoms and Continental Shelf of the Mediterranean Sea, in: Marine Animal Forests: The Ecology of Benthic Biodiversity Hotspots. Springer, pp. 1–27.

Gori, A., Rossi, S., Berganzo, E., Pretus, J.L., Dale, M.R.T., Gili, J.-M., 2011. Spatial distribution patterns of the gorgonians *Eunicella singularis, Paramuricea clavata*, and *Leptogorgia sarmentosa* (Cape of Creus, Northwestern Mediterranean Sea). Mar. Biol. 158, 143–158.

Gori, A., Orejas, C., Madurell, T., Bramanti, L., Martins, M., Quintanilla, E., Marti-Puig, P., Lo Iacono, C., Puig, P., Requena, S., others, 2013. Bathymetrical distribution and size structure of cold-water coral populations in the Cap de Creus and Lacaze-Duthiers canyons (northwestern Mediterranean). Biogeosciences 10, 2049–2060.

Gori, A., Reynaud, S., Orejas, C., Gili, J.M., Ferrier-Pagès, C., 2014. Physiological performance of the cold-water coral *Dendrophyllia cornigera* reveals its preference for temperate environments. Coral Reefs 33, 665–674. doi:10.1007/s00338-014-1167-9

Gori, A., Reynaud, S., Orejas, C., Ferrier-Pagès, C., 2015. The influence of flow velocity and temperature on zooplankton capture rates by the cold-water coral *Dendrophyllia cornigera*. J. Exp. Mar. Bio. Ecol. 466, 92–97.

Gràcia, E., Pallàs, R., Soto, J.I., Comas, M., Moreno, X., Masana, E., Santanach, P., Diez, S., García, M., Dañobeitia, J., Bartolomé, R., Farrán, M., Gómez, M., Alpiste, M.J.R., Lastras, G., Wilmott, V., Perea, H., Blondel, P., Gómez, O., Bullock, L., Jacobs, C., Rouse, I., White, D., Whittle, S., Terrinha, P., Gafeira, J., Roque, C., 2006. Active faulting offshore SE Spain (Alboran Sea): Implications for earthquake hazard assessment in the Southern Iberian Margin. Earth Planet. Sci. Lett. 241, 734–749. doi:10.1016/j.epsl.2005.11.009

Gràcia, E., Bartolome, R., Lo Iacono, C., Moreno, X., Stich, D., Martínez-Diaz, J.J., Bozzano, G., Martínez-Loriente, S., Perea, H., Diez, S., Masana, E., Dañobeitia, J.J., Tello, O., Sanz, J.L., Carreño, E., 2012. Acoustic and seismic imaging of the Adra Fault (NE Alboran Sea): in search of the source of the 1910 Adra earthquake. Nat. Hazards Earth Syst. Sci. 12, 3255–3267. doi:10.5194/nhess-12-3255-2012

Grant, K.M., Rohling, E.J., Bronk Ramsey, C., Cheng, H., Edwards, R.L., Florindo, F., Heslop, D., Marra, F., Roberts, A.P., Tamisiea, M.E., Williams, F., 2014. Sea-level variability over five glacial cycles. Nat. Commun. 5, 1–9. doi:10.1038/ncomms6076

Grant, K.M., Grimm, R., Mikolajewicz, U., Marino, G., Ziegler, M., Rohling, E.J., 2016. The timing of Mediterranean sapropel deposition relative to insolation, sea-level and African monsoon changes. Quat. Sci. Rev. 140, 125–141. doi:10.1016/j.quascirev.2016.03.026

Grasmueck, M., Eberli, G.P., Viggiano, D.A., Correa, T., Rathwell, G., Luo, J., 2006. Autonomous underwater vehicle (AUV) mapping reveals coral mound distribution, morphology, and oceanography in deep water of the Straits of Florida. Geophys. Res. Lett. 33, L23616. doi:10.1029/2006GL027734

Greenacre, M., Primicerio, R., 2013. Measures of distance between samples: noneuclidean. Multivar. Anal. Ecol. data 1–5.

Grevemeyer, I., Gràcia, E., Villaseñor, A., Leuchters, W., Watts, A.B., 2015. Seismicity and active tectonics in the Alboran Sea, Western Mediterranean: Constraints from an offshore-onshore seismological network and swath bathymetry data. J. Geophys. Res. Solid Earth 120, 8348–8365. doi:10.1002/2015JB012073

Grinyó, J., Gori, A., Ambroso, S., Purroy, A., Calatayud, C., Dominguez-Carrió, C., Coppari, M., Lo Iacono, C. , López-González, P.J., Gili, J.-M., 2016. Diversity, distribution and population size structure of deep Mediterranean gorgonian assemblages (Menorca Channel, Western Mediterranean Sea). Prog. Oceanogr. 145, 42–56.

Grinyó, J., Gori, A., Greenacre, M., Requena, S., Canepa, A., Lo Iacono, C. , Ambroso, S., Purroy, A., Gili, J.-M., 2018. Megabenthic assemblages in the continental shelf edge and upper slope of the Menorca Channel, Western Mediterranean Sea. Prog. Oceanogr. 162, 40–51.

Guinotte, J.M., Orr, J., Cairns, S., Freiwald, A., Morgan, L., George, R., 2006. Will human-induced changes in seawater chemistry alter the distribution of deep-sea scleractinian corals? Front. Ecol. Environ. doi:10.1890/1540-9295(2006)004[0141:WHCISC]2.0.CO;2

Hanz, U., Wienberg, C., Hebbeln, D., Duineveld, G., Lavaleye, M., Juva, K., Dullo, W.C., Freiwald, A., Tamborrino, L., Reichart, G.J., Flögel, S., Mienis, F., 2019. Environmental factors influencing benthic communities in the oxygen minimum zones on the Angolan and Namibian margins. Biogeosciences 16, 4337–4356. doi:10.5194/bg-16-4337-2019

Hauser, I., Oschmann, W., Gischler, E., 2008. Taphonomic Signatures On Modern Caribbean Bivalve Shells As Indicators Of Environmental Conditions (Belize, Central America). Palaios 23, 586–600. doi:10.2110/palo.2007.p07-075r

Hebbeln, D., 2009. Report and preliminary results of R/V POSEIDON Cruise 385 [POS385]" Cold-water corals of the Alboran Sea (western Mediterranean Sea)", Faro-Toulon, 29.5.-16.6. 2009.

Hebbeln, D., 2019. Highly Variable Submarine Landscapes in the Alborán Sea Created by Cold-Water Corals, in: Orejas, C., Jiménez, C. (Eds.), Mediterranean Cold-Water Corals: Past, Present and Future. Springer, Cham, pp. 61–65. doi:10.1007/978-3-319-91608-8_8

Hebbeln, D., Wienberg, C., 2016. The east Melilla cold-water coral province in the Alboran Sea. Rapp. Comm. int. Mer Médit. 41, 25.

Hebbeln, D., Wienberg, C., Beuck, L., Freiwald, A., Wintersteller, P., Cruise participants, 2009. Report and preliminary results of RV POSEIDON Cruise POS 385 "Cold-Water Corals of the Alboran Sea (western Mediterranean Sea)". Faro–Toulon, May 29–June 16, 2009.

Hebbeln, D., Wienberg, C., Wintersteller, P., Freiwald, A., Becker, M., Beuck, L., Dullo, C., Eberli, G.P., Glogowski, S., Matos, L., Forster, N., Reyes-Bonilla, H., Taviani, M., 2014. Environmental forcing of the Campeche cold-water coral province, southern Gulf of Mexico. Biogeosciences 11, 1799–1815. doi:10.5194/bg-11-1799-2014

Hebbeln, D., Van Rooij, D., Wienberg, C., 2016. Good neighbours shaped by vigorous currents: Cold-water coral mounds and contourites in the North Atlantic. Mar. Geol. 378, 171–185. doi:10.1016/j.margeo.2016.01.014

Hebbeln, D., Bender, M., Gaide, S., Titschack, J., Vandorpe, T., Van Rooij, D., Wintersteller, P., Wienberg, C., 2019a. Thousands of cold-water coral mounds along the Moroccan Atlantic continental margin: Distribution and morphometry. Mar. Geol. 411, 51–61. doi:10.1016/j.margeo.2019.02.001

Hebbeln, D., Portilho-Ramos, R. da C., Wienberg, C., Titschack, J., 2019b. The Fate of Cold-Water Corals in a Changing World: A Geological Perspective. Front. Mar. Sci. 6, 119. doi:10.3389/fmars.2019.00119

Henriet, J.P., De Mol, B., Pillen, S., Vanneste, M., Van Rooij, D., Versteeg, W., Croker, P.F., Shannon, P.M., Unnithan, V., Bouriak, S., Chachkine, P., 1998. Gas hydrate crystals may help build reefs. Nature. doi:10.1038/35530

Henry, L.-A., Roberts, J.M., 2007. Biodiversity and ecological composition of macrobenthos on cold-water coral mounds and adjacent off-mound habitat in the bathyal Porcupine Seabight, NE Atlantic. Deep Sea Res. Part I Oceanogr. Res. Pap. 54, 654–672.

Henry, L.A., Roberts, J.M., 2017. Global biodiversity in cold-water coral reef ecosystems, in: Rossi, S., Bramanti, L., Gori, A., Orejas, C. (Eds.), Marine Animal Forests. Springer International Publishing. doi:10.1007/978-3-319-17001-5_6-1

Henry, L.A., Nizinski, M.S., Ross, S.W., 2008. Occurrence and biogeography of hydroids (Cnidaria: Hydrozoa) from deep-water coral habitats off the southeastern United States. Deep. Res. Part I Oceanogr. Res. Pap. 55, 788–800. doi:10.1016/j.dsr.2008.03.002

Henry, L.-A., Moreno Navas, J., Roberts, J.M., 2013. Multi-scale interactions between local hydrography, seabed topography, and community assembly on cold-water coral reefs. Biogeosciences 10, 2737–2746. doi:10.5194/bg-10-2737-2013

Hoffmann, D.L., Prytulak, J., Richards, D.A., Elliott, T., Coath, C.D., Smart, P.L., Scholz, D., 2007. Procedures for accurate U and Th isotope measurements by high precision MC-ICPMS. Int. J. Mass Spectrom. 264, 97–109. doi:10.1016/j.ijms.2007.03.020

Hoffmann, J., Bahr, A., Voigt, S., Schönfeld, J., Nürnberg, D., Rethemeyer, J., 2014. Disentangling abrupt deglacial hydrological changes in northern South America: Insolation versus oceanic forcing. Geology 42, 579–582. doi:10.1130/G35562.1

Hoffmann, D.L., Standish, C.D., García-Diez, M., Pettitt, P.B., Milton, J.A., Zilhão, J., Alcolea-González, J.J., Cantalejo-Duarte, P., Collado, H., De Balbín, R., Lorblanchet, M., Ramos-Muñoz, J., Weniger, G.C., Pike, A.W.G., 2018. U-Th dating of carbonate crusts reveals Neandertal origin of Iberian cave art. Science 359, 912–915. doi:10.1126/science.aap7778

Holden, N.E., 1990. Total half-lives for selected nuclides. Pure Appl. Chem. 62, 941–958. doi:10.1351/pac199062050941

Horwitz, E.P., Dietz, M.L., Chiarizia, R., 1992. The application of novel extraction chromatographic materials to the characterization of radioactive waste solutions. J. Radioanal. Nucl. Chem. 161, 575–583. doi:10.1007/BF02040504

Hovland, M., Mortensen, P.B., 1999. Norske Korallrev Og Prosessor i Havbunnen.(Deep-water Coral-reefs and Processes on the Sea Floor). John Grieg Forlag.

Hovland, M., Risk, M., 2003. Do Norwegian deep-water coral reefs rely on seeping fluids? Mar. Geol. 198, 83–96.

Hovland, M., Croker, P.F., Martin, M., 1994. Fault-associated seabed mounds (carbonate knolls?) off western Ireland and north-west. Mar. Pet. Geol. 11, 234–246.

Hughes, P.D., Fenton, C.R., Gibbard, P.L., 2011. Quaternary Glaciations of the Atlas Mountains, North Africa, in: Developments in Quaternary Science. Elsevier, pp. 1065–1074. doi:10.1016/B978-0-444-53447-7.00076-3

Huh, Y., Chan, L.H., Zhang, L., Edmond, J.M., 1998. Lithium and its isotopes in major world rivers: implications for weathering and the oceanic budget. Geochim. Cosmochim. Acta 62, 2039–2051. doi:10.1016/S0016-7037(98)00126-4

Husebø, Nøttestad, L., Fosså, J.H., Furevik, D.M., Jørgensen, S.B., 2002. Distribution and abundance of fish in deep-sea coral habitats. Hydrobiologia 471, 91–99. doi:10.1023/A:1016549203368

Huvenne, V.A.I., De Mol, B., Henriet, J.P., 2003. A 3D seismic study of the morphology and spatial distribution of buried coral banks in the Porcupine Basin, SW of Ireland. Mar. Geol. 198, 5–25. doi:10.1016/S0025-3227(03)00092-6

Huvenne, V.A.I., Beyer, A., de Haas, H., Dekindt, K., Henriet, J.-P., Kozachenko, M., Olu-Le Roy, K., Wheeler, A.J., 2005. The seabed appearance of different coral bank provinces in the Porcupine Seabight, NE Atlantic: results from sidescan sonar and ROV seabed mapping, in: Cold-Water Corals and Ecosystems. Springer Berlin Heidelberg, pp. 535–569. doi:10.1007/3-540-27673-4_27

Huvenne, V.A.I., Van Rooij, D., De Mol, B., Thierens, M., O'Donnell, R., Foubert, A., 2009. Sediment dynamics and palaeo-environmental context at key stages in the Challenger cold-water coral mound formation: Clues from sediment deposits at the mound base. Deep. Res. Part I Oceanogr. Res. Pap. 56, 2263–2280. doi:10.1016/j.dsr.2009.08.003

Huvenne, V.A.I., Tyler, P.A., Masson, D.G., Fisher, E.H., Hauton, C., Hühnerbach, V., Le Bas, T.P., Wolff, G.A., 2011. A picture on the wall: innovative mapping reveals cold-water coral refuge in submarine canyon. PLoS One 6, e28755.

Huvenne, V.A.I., Bett, B.J., Masson, D.G., Le Bas, T.P., Wheeler, A.J., 2016. Effectiveness of a deep-sea cold-water coral Marine Protected Area, following eight years of fisheries closure. Biol. Conserv. 200, 60–69. doi:10.1016/j.biocon.2016.05.030

Incarbona, A., Di Stefano, E., Parti, B., Pelosi, N., Bonomo, S., Mazzola, S., Sprovieri, R., Tranchida, G., Zgozi, S.,

Bonanno, A., 2008. Holocene millennial-scale productivity variations in the Sicily Channel (Mediterranean Sea). Paleoceanography 23. doi:10.1029/2007PA001581

Ingrassia, M., Macelloni, L., Bosman, A., Chiocci, F.L., Cerrano, C., Martorelli, E., 2016. Black coral (Anthozoa, Antipatharia) forest near the western Pontine Islands (Tyrrhenian Sea). Mar. Biodivers. 46, 285–290.

Jacquet, S.H.M., Monnin, C., Riou, V., Jullion, L., Tanhua, T., 2016. A high resolution and quasi-zonal transect of dissolved Ba in the Mediterranean Sea. Mar. Chem. 178, 1–7. doi:10.1016/j.marchem.2015.12.001

Jaffey, A.H., Flynn, K.F., Glendenin, L.E., Bentley, W.C., Essling, A.M., 1971. Precision measurement of half-lives and specific activities of U235 and U238. Phys. Rev. C 4, 1889–1906. doi:10.1103/PhysRevC.4.1889

Jiménez-Espejo, F.J., Pardos-Gené, M., Martínez-Ruiz, F., García-Alix, A., van de Flierdt, T., Toyofuku, T., Bahr, A., Kreissig, K., 2015. Geochemical evidence for intermediate water circulation in the westernmost Mediterranean over the last 20kyrBP and its impact on the Mediterranean Outflow. Glob. Planet. Change 135, 38–46. doi:10.1016/j.gloplacha.2015.10.001

Jones, C.G., Lawton, J.H., Shachak, M., 1994. Organisms as ecosystem engineers. Oikos 69, 373–386.

Joubin, M.L., 1922. Les coraux de mer profonde nuisibles aux chalutiers. Office Scientifique et Technique des Pêches Maritimes, Notes et Mémoires, 18. Blondel la Rougery, Paris, 16 pp.

Jouini, M., Béranger, K., Arsouze, T., Beuvier, J., Thiria, S., Crépon, M., Taupier-Letage, I., 2016. The Sicily Channel surface circulation revisited using a neural clustering analysis of a high-resolution simulation. J. Geophys. Res. Ocean. 121, 4545–4567. doi:10.1002/2015JC011472

Jullion, L., Jacquet, S.H.M., Tanhua, T., 2017. Untangling biogeochemical processes from the impact of ocean circulation: First insight on the Mediterranean dissolved barium dynamics. Global Biogeochem. Cycles 31, 1256–1270. doi:10.1002/2016GB005489

Kampman, N., Burnside, N.M., Shipton, Z.K., Chapman, H.J., Nicholl, J.A., Ellam, R.M., Bickle, M.J., 2012. Pulses of carbon dioxide emissions from intracrustal faults following climatic warming. Nat. Geosci. 5, 352–358. doi:10.1038/ngeo1451

Kano, A., Ferdelman, T.G., Williams, T., Henriet, J.-P., Ishikawa, T., Kawagoe, N., Takashima, C., Kakizaki, Y., Abe, K., Sakai, S., others, 2007. Age constraints on the origin and growth history of a deep-water coral mound in the northeast Atlantic drilled during Integrated Ocean Drilling Program Expedition 307. Geology 35, 1051–1054.

Kelmo, F., Attrill, M.J., Jones, M.B., 2003. Effects of the 1997-1998 El Niño on the cnidarian community of a high turbidity coral reef system (northern Bahia, Brazil). Coral Reefs 22, 541–550. doi:10.1007/s00338-003-0343-0

Kenyon, N.H., Akhmetzhanov, A.M., Wheeler, A.J., Van Weering, T.C.E., De Haas, H., Ivanov, M.K., 2003. Giant carbonate mud mounds in the southern Rockall Trough. Mar. Geol. 195, 5–30. doi:10.1016/S0025-3227(02)00680-1

Khripounoff, A., Caprais, J.C., Decker, C., Le Bruchec, J., Noel, P., Husson, B., 2017. Respiration of bivalves from three different deep-sea areas: Cold seeps, hydrothermal vents and organic carbon-rich sediments. Deep. Res. Part II Top. Stud. Oceanogr. 142, 233–243. doi:10.1016/j.dsr2.2016.05.023

Kidwell, S.M., Holland, S.M., 1991. Field Description of Coarse Bioclastic Fabrics. Palaios 6, 426. doi:10.2307/3514967

Kiriakoulakis, K., Freiwald, A., Fisher, E., Wolff, G.A., 2007. Organic matter quality and supply to deep-water coral/mound systems of the NW European Continental Margin. Int. J. Earth Sci. 96, 159–170. doi:10.1007/s00531-006-0078-6

Komsta, L., Novomestky, F., 2012. Moments: Moments, cumulants, skewness, kurtosis and related tests [Computer Software]. R package version 0.13.

Konijnendijk, T.Y.M., Ziegler, M., Lourens, L.J., 2014. Chronological constraints on Pleistocene sapropel depositions from high-resolution geochemicalrecords of ODP Sites 967 and 968. Newsletters Stratigr. 47, 263–282.

Koslow, J., Gowlett-Holmes, K., Lowry, J., O'Hara, T., Poore, G., Williams, A., 2001. Seamount benthic macrofauna off southern Tasmania: community structure and impacts of trawling. Mar. Ecol. Prog. Ser. 213, 111–125.

doi:10.3354/meps213111

Lambeck, K., Rouby, H., Purcell, A., Sun, Y., Sambridge, M., 2014. Sea level and global ice volumes from the Last Glacial Maximum to the Holocene. Proc. Natl. Acad. Sci. U. S. A. 111, 15296–15303. doi:10.1073/pnas.1411762111

Larsson, A.I., Järnegren, J., Strömberg, S.M., Dahl, M.P., Lundälv, T., Brooke, S., 2014. Embryogenesis and larval biology of the cold-water coral *Lophelia pertusa*. PLoS One 9, e102222.

Lastras, G., Canals, M., Ballesteros, E., Gili, J.-M., Sanchez-Vidal, A., 2016. Cold-water corals and anthropogenic impacts in La Fonera submarine canyon head, Northwestern Mediterranean Sea. PLoS One 11, e0155729.

Le Bas, T.P., 2016. RSOBIA - A new OBIA Toolbar and Toolbox in ArcMap 10.x for Segmentation and Classification., in: GEOBIA 2016 : Solutions and Synergies. University of Twente Faculty of Geo-Information and Earth Observation (ITC). doi:https://doi.org/10.3990/2.448

Le Danois, E. 1948. Les profondeurs de la mer. Trente ans de recherches sur la faune sou-marine au large des côtes de France. Payot, Paris. 301 pp.

Le Guilloux, E., Olu, K., Bourillet, J.F., Savoye, B., Iglésias, S.P., Sibuet, M., 2009. First observations of deep-sea coral reefs along the Angola margin. Deep. Res. Part II Top. Stud. Oceanogr. 56, 2394–2403. doi:10.1016/j.dsr2.2009.04.014

Lim, A., Wheeler, A.J., Arnaubec, A., 2017. High-resolution facies zonation within a cold-water coral mound: The case of the Piddington Mound, Porcupine Seabight, NE Atlantic. Mar. Geol. 390, 120–130. doi:10.1016/j.margeo.2017.06.009

Lindberg, B., 2004. Cold-water coral reefs on the norwegian shelf—acoustic signature, geological, geomorphological and environmental setting. Ph.D. thesis. Department of Geology, University of Tromsø

Lisiecki, L.E., Raymo, M.E., 2005. A Pliocene-Pleistocene stack of 57 globally distributed benthic $\delta^{18}O$ records. Paleoceanography 20, 1–17. doi:10.1029/2004PA001071

Lo Iacono, C., Gràcia, E., Diez, S., Bozzano, G., Moreno, X., Dañobeitia, J., Alonso, B., 2008. Seafloor characterization and backscatter variability of the Almería Margin (Alboran Sea, SW Mediterranean) based on high-resolution acoustic data. Mar. Geol. 250, 1–18. doi:10.1016/j.margeo.2007.11.004

Lo Iacono, C., Gràcia, E., Bartolomé, R., Coiras, E., Dañobeitia, J.J., Acosta, J., 2012. Habitats of the Chella Bank, Eastern Alboran Sea (Western Mediterranean), in: Seafloor Geomorphology as Benthic Habitat. Elsevier, pp. 681–690.

Lo Iacono, C., Gràcia, E., Ranero, C.R., Emelianov, M., Huvenne, V.A.I., Bartolomé, R., Booth-Rea, G., Prades, J., Ambroso, S., Dominguez, C., others, 2014. The West Melilla cold water coral mounds, Eastern Alboran Sea: Morphological characterization and environmental context. Deep Sea Res. Part II Top. Stud. Oceanogr. 99, 316–326.

Lo Iacono, C., Gracia, E., Agnastounou, E., Emelianov, M., Foster, G.L., Garcia-Ladona, E., Gili, J.M., Grinyo, J., Huvenne, V.A.I., Kastamemis, O.L., Mavrogordato, M.N., Perea, H., Pierdomenico, M., Vertino, A., Victorero-Gonzalez, L., Van Rooij, D., 2016. Living reefs and DWC mounds in the Alboran Sea (Western Mediterranean): Holocene evolution and present-day conditions, in: 6 International Symposium on Deep-Sea Corals, 11.09.-16.09.2016. Boston, USA.

Lo Iacono, C., Savini, A., Basso, D., 2018a. Cold-water carbonate bioconstructions, in: Submarine Geomorphology. Springer, pp. 425–455.

Lo Iacono, C., Robert, K., Gonzalez-Villanueva, R., Gori, A., Gili, J.M., Orejas, C., 2018b. Predicting cold-water coral distribution in the Cap de Creus Canyon (NW Mediterranean): Implications for marine conservation planning. Prog. Oceanogr. 169, 169–180. doi:10.1016/j.pocean.2018.02.012

Lo Iacono, C., Savini, A., Huvenne, V.A.I., Gràcia, E., 2019. Habitat Mapping of Cold-Water Corals in the Mediterranean Sea, in: Orejas, C., Jiménez, C. (Eds.), Mediterranean Cold-Water Corals: Past, Present and Future. Springer, Cham, pp. 157–171. doi:10.1007/978-3-319-91608-8_15

Locarnini, M., Mishonov, A., Baranova, O., Boyer, T., Zweng, M., Garcia, H., Reagan, J., Seidov, D., Weathers, K., Paver, C., Smolyar, I., 2018. World Ocean Atlas 2018, Volume 1: Temperature.

Lomolino, M. V., Riddle, B.R., Brown, J.H. (Eds.), 2006. Biogeography. Sinauer Associates, Sunderland, MA.

Lopes, D.A., Hajdu, E., 2014. Carnivorous sponges from deep-sea coral mounds in the Campos Basin (SW Atlantic), with the description of six new species (Cladorhizidae, Poecilosclerida, Demospongiae). Mar. Biol. Res. 10, 329–356. doi:10.1080/17451000.2013.797587

López Correa, M., Freiwald, A., Hall-Spencer, J., Taviani, M., 2006. Distribution and habitats of Acesta excavata (Bivalvia: Limidae) with new data on its shell ultrastructure, in: Cold-Water Corals and Ecosystems. Springer-Verlag, pp. 173–205. doi:10.1007/3-540-27673-4_9

López Correa, M., Montagna, P., Joseph, N., Rüggeberg, A., Fietzke, J., Flögel, S., Dorschel, B., Goldstein, S.L., Wheeler, A., Freiwald, A., 2012. Preboreal onset of cold-water coral growth beyond the Arctic Circle revealed by coupled radiocarbon and U-series dating and neodymium isotopes. Quat. Sci. Rev. 34, 24–43. doi:10.1016/j.quascirev.2011.12.005

Lopez-Fernandez, P., Calafat, A., Sanchez-Vidal, A., Canals, M., Mar Flexas, M., Cateura, J., Company, J.B., 2013. Multiple drivers of particle fluxes in the Blanes submarine canyon and southern open slope: Results of a year round experiment. Prog. Oceanogr. 118, 95–107. doi:10.1016/j.pocean.2013.07.029

Macías, D., Bruno, M., Echevarría, F., Vázquez, A., García, C.M., 2008. Meteorologically-induced mesoscale variability of the North-western Alboran Sea (southern Spain) and related biological patterns. Estuar. Coast. Shelf Sci. 78, 250–266. doi:10.1016/j.ecss.2007.12.008

Maier, C., Hegeman, J., Weinbauer, M.G., Gattuso, J.-P., 2009. Calcification of the cold-water coral *Lophelia pertusa*, under ambient and reduced pH. Biogeosciences 6, 1671–1680.

Malinverno, E., Taviani, M., Rosso, A., Violanti, D., Villa, I., Savini, A., Vertino, A., Remia, A., Corselli, C., 2010. Stratigraphic framework of the Apulian deep-water coral province, Ionian Sea. Deep Sea Res. Part II Top. Stud. Oceanogr. 57, 345–359.

Manzella, G.M.R., Hopkins, T.S., Minnett, P.J., Nacini, E., 1990. Atlantic water in the strait of Sicily. J. Geophys. Res. Ocean. 95, 1569–1575. doi:10.1029/JC095IC02P01569

Marsay, C.M., Sanders, R.J., Henson, S.A., Pabortsava, K., Achterberg, E.P., Lampitt, R.S., 2015. Attenuation of sinking particulate organic carbon flux through the mesopelagic ocean. Proc. Natl. Acad. Sci. U. S. A. 112, 1089–1094. doi:10.1073/pnas.1415311112

Marsh, L., Copley, J.T., Huvenne, V.A.I., Linse, K., Reid, W.D.K., Rogers, A.D., Sweeting, C.J., Tyler, P.A., 2012. Microdistribution of Faunal Assemblages at Deep-Sea Hydrothermal Vents in the Southern Ocean. PLoS One 7, e48348. doi:10.1371/journal.pone.0048348

Martinez-Ruiz, F., Kastner, M., Gallego-Torres, D., Rodrigo-Gámiz, M., Nieto-Moreno, V., Ortega-Huertas, M., 2015. Paleoclimate and paleoceanography over the past 20,000yr in the Mediterranean Sea Basins as indicated by sediment elemental proxies. Quat. Sci. Rev. doi:10.1016/j.quascirev.2014.09.018

Martorelli, E., Petroni, G., Chiocci, F.L., others, 2011. Contourites offshore Pantelleria Island (Sicily Channel, Mediterranean Sea): depositional, erosional and biogenic elements. Geo-Marine Lett. 31, 481–493.

Martrat, B., Grimalt, J.O., Lopez-Martinez, C., Cacho, I., Sierro, F.J., Flores, J.A., Zahn, R., Canals, M., Curtis, J.H., Hodell, D.A., 2004. Abrupt temperature changes in the Western Mediterranean over the past 250,000 years. Science 306, 1762–1765. doi:10.1126/science.1101706

Mascle, G.H., Tricart, P., Torelli, L., Bouillin, J.P., Rolfo, F., Lapierre, H., Monié, P., Depardon, S., Mascle, J., Peis, D., 2001. Evolution of the Sardinia Channel (Western Mediterranean): New constraints from a diving survey on Cornacya seamount off SE Sardinia. Mar. Geol. 179, 179–201. doi:10.1016/S0025-3227(01)00220-1

Masson, D.G., Bett, B.J., Billett, D.S.M., Jacobs, C.L., Wheeler, A.J., Wynn, R.B., 2003. The origin of deep-water, coral-topped mounds in the northern Rockall Trough, Northeast Atlantic. Mar. Geol. 194, 159–180. doi:10.1016/S0025-3227(02)00704-1

Mastrototaro, F., D'Onghia, G., Corriero, G., Matarrese, A., Maiorano, P., Panetta, P., Gherardi, M., Longo, C., Rosso, A., Sciuto, F., others, 2010. Biodiversity of the white coral bank off Cape Santa Maria di Leuca (Mediterranean Sea): An update. Deep Sea Res. Part II Top. Stud. Oceanogr. 57, 412–430.

Matos, L., Wienberg, C., Titschack, J., Schmiedl, G., Frank, N., Abrantes, F., Cunha, M.R., Hebbeln, D., 2017. Coral

mound development at the Campeche cold-water coral province, southern Gulf of Mexico: Implications of Antarctic Intermediate Water increased influence during interglacials. Mar. Geol. 392, 53–65. doi:10.1016/j.margeo.2017.08.012

Mazzini, A., Akhmetzhanov, A., Monteys, X., Ivanov, M., 2012. The Porcupine Bank Canyon coral mounds: oceanographic and topographic steering of deep-water carbonate mound development and associated phosphatic deposition. Geo-Marine Lett. 32, 205–225.

McCulloch, M., Taviani, M., Montagna, P., López Correa, M., Remia, A., Mortimer, G., 2010. Proliferation and demise of deep-sea corals in the Mediterranean during the Younger Dryas. Earth Planet. Sci. Lett. 298, 143–152. doi:10.1016/j.epsl.2010.07.036

McGregor, H. V., Hellstrom, J., Fink, D., Hua, Q., Woodroffe, C.D., 2011. Rapid U-series dating of young fossil corals by laser ablation MC-ICPMS. Quat. Geochronol. 6, 195–206. doi:10.1016/j.quageo.2010.10.002

McManus, M., Alldredge, A., Barnard, A., Boss, E., Case, J., Cowles, T., Donaghay, P., Eisner, L., Gifford, D., Greenlaw, C., Herren, C., Holliday, D., Johnson, D., MacIntyre, S., McGehee, D., Osborn, T., Perry, M., Pieper, R., Rines, J., Smith, D., Sullivan, J., Talbot, M., Twardowski, M., Weidemann, A., Zaneveld, J., 2003. Characteristics, distribution and persistence of thin layers over a 48 hour period. Mar. Ecol. Prog. Ser. 261, 1–19. doi:10.3354/meps261001

Meibom, A., Cuif, J.P., Houlbreque, F., Mostefaoui, S., Dauphin, Y., Meibom, K.L., Dunbar, R., 2008. Compositional variations at ultra-structure length scales in coral skeleton. Geochim. Cosmochim. Acta 72, 1555–1569. doi:10.1016/j.gca.2008.01.009

Mienis, F., van Weering, T., de Haas, H., de Stigter, H., Huvenne, V., Wheeler, A., 2006. Carbonate mound development at the SW Rockall Trough margin based on high resolution TOBI and seismic recording. Mar. Geol. 233, 1–19. doi:10.1016/j.margeo.2006.08.003

Mienis, F., de Stigter, H.C., White, M., Duineveld, G., de Haas, H., van Weering, T.C.E., 2007. Hydrodynamic controls on cold-water coral growth and carbonate-mound development at the SW and SE Rockall Trough Margin, NE Atlantic Ocean. Deep. Res. Part I Oceanogr. Res. Pap. 54, 1655–1674. doi:10.1016/j.dsr.2007.05.013

Mienis, F., De Stigter, H.C., De Haas, H., Van Weering, T.C.E., 2009. Near-bed particle deposition and resuspension in a cold-water coral mound area at the Southwest Rockall Trough margin, NE Atlantic. Deep Sea Res. Part I Oceanogr. Res. Pap. 56, 1026–1038.

Mienis, F., De Stigter, H.C., De Haas, H., der Land, C., Van Weering, T.C.E., 2012a. Hydrodynamic conditions in a cold-water coral mound area on the Renard Ridge, southern Gulf of Cadiz. J. Mar. Syst. 96, 61–71.

Mienis, F., Duineveld, G.C.A., Davies, A.J., Ross, S.W., Seim, H., Bane, J., Van Weering, T.C.E., 2012b. The influence of near-bed hydrodynamic conditions on cold-water corals in the Viosca Knoll area, Gulf of Mexico. Deep Sea Res. Part I Oceanogr. Res. Pap. 60, 32–45.

Mienis, F., Duineveld, G.C.A., Davies, A.J., Lavaleye, M.M.S., Ross, S.W., Seim, H., Bane, J., van Haren, H., Bergman, M.J.N., de Haas, H., Brooke, S., van Weering, T.C.E., 2014. Cold-water coral growth under extreme environmental conditions, the Cape Lookout area, NW Atlantic. Biogeosciences 11, 2543–2560. doi:10.5194/bg-11-2543-2014

Millot, C., 1999. Circulation in the Western Mediterranean Sea. J. Mar. Syst. 20, 423–442. doi:10.1016/S0924-7963(98)00078-5

Millot, C., 2009. Another description of the Mediterranean Sea outflow. Prog. Oceanogr. 82, 101–124. doi:10.1016/j.pocean.2009.04.016

Mohn, C., Rengstorf, A., White, M., Duineveld, G., Mienis, F., Soetaert, K., Grehan, A., 2014. Linking benthic hydrodynamics and cold-water coral occurrences: A high-resolution model study at three cold-water coral provinces in the NE Atlantic. Prog. Oceanogr. 122, 92–104.

Montagna, P., Taviani, M., 2019. Mediterranean Cold-Water Corals as Paleoclimate Archives, in: Orejas, C., Jiménez, C. (Eds.), Mediterranean Cold-Water Corals: Past, Present and Future. Springer, Cham, pp. 95–108. doi:10.1007/978-3-319-91608-8_11

Montagna, P., McCulloch, M., Douville, E., López Correa, M., Trotter, J., Rodolfo-Metalpa, R., Dissard, D., Ferrier-

Pagès, C., Frank, N., Freiwald, A., Goldstein, S., Mazzoli, C., Reynaud, S., Rüggeberg, A., Russo, S., Taviani, M., 2014. Li/Mg systematics in scleractinian corals: Calibration of the thermometer. Geochim. Cosmochim. Acta 132, 288–310. doi:10.1016/j.gca.2014.02.005

Moreno, A., Cacho, I., Canals, M., Grimalt, J.O., Sánchez-Goñi, M.F., Shackleton, N., Sierro, F.J., 2005. Links between marine and atmospheric processes oscillating on a millennial time-scale. A multi-proxy study of the last 50,000 yr from the Alboran Sea (Western Mediterranean Sea). Quat. Sci. Rev. 24, 1623–1636. doi:10.1016/j.quascirev.2004.06.018

Moreno, X., Gràcia, E., Bartolomé, R., Martínez-Loriente, S., Perea, H., de la Peña, L.G., Lo Iacono, C., Piñero, E., Pallàs, R., Masana, E., Dañobeitia, J.J., 2016. Seismostratigraphy and tectonic architecture of the Carboneras Fault offshore based on multiscale seismic imaging: Implications for the Neogene evolution of the NE Alboran Sea. Tectonophysics 689, 115–132. doi:10.1016/j.tecto.2016.02.018

Mortensen, P.B., Fosså, J.H., 2006. Species diversity and spatial distribution of invertebrates on deep-water *Lophelia* reefs in Norway, in: Proceedings of 10th International Coral Reef Symposium. pp. 1849–1868.

Mortensen, P.B., Hovland, M., Brattegard, T., Farestveit, R., 1995. Deep water bioherms of the scleractinian coral *Lophelia pertusa* (L.) at 64° n on the norwegian shelf: Structure and associated megafauna. Sarsia 80, 145–158. doi:10.1080/00364827.1995.10413586

Mortensen, P.B., Hovland, T., Fosså, J.H., Furevik, D.M., 2001. Distribution, abundance and size of *Lophelia pertusa* coral reefs in mid-Norway in relation to seabed characteristics. J. Mar. Biol. Assoc. United Kingdom 81, 581–597. doi:10.1017/S002531540100426X

Mueller, C.E., Larsson, A.I., Veuger, B., Middelburg, J.J., Van Oevelen, D., 2014. Opportunistic feeding on various organic food sources by the cold-water coral *Lophelia pertusa*. Biogeosciences 11, 123–133. doi:10.5194/bg-11-123-2014

Naumann, M.S., Orejas, C., Ferrier-Pagès, C., 2013. High thermal tolerance of two Mediterranean cold-water coral species maintained in aquaria. Coral Reefs 32, 749–754. doi:10.1007/s00338-013-1011-7

Naumann, M.S., Orejas, C., Ferrier-Pagès, C., 2014. Species-specific physiological response by the cold-water corals *Lophelia pertusa* and *Madrepora oculata* to variations within their natural temperature range. Deep. Res. Part II Top. Stud. Oceanogr. 99, 36–41. doi:10.1016/j.dsr2.2013.05.025

Navarro, G., Vázquez, Á., Macías, D., Bruno, M., Ruiz, J., 2011. Understanding the patterns of biological response to physical forcing in the Alborán Sea (western Mediterranean). Geophys. Res. Lett. 38, L23606. doi:10.1029/2011GL049708

Neumann, A.C., Kofoed, J.W., Keller, G.H., 1977. Lithoherms in the Straits of Florida. Geology 5, 4–10. doi:10.1130/0091-7613(1977)5<4:LITSOF>2.0.CO;2

Neves, B.M., Du Preez, C., Edinger, E., 2014. Mapping coral and sponge habitats on a shelf-depth environment using multibeam sonar and ROV video observations: Learmonth Bank, northern British Columbia, Canada. Deep Sea Res. Part II Top. Stud. Oceanogr. 99, 169–183.

Obaton, D., Millot, C., Chabert D'Hières, G., Taupier-Letage, I., 2000. The algerian current: Comparisons between in situ and laboratory data sets. Deep. Res. Part I Oceanogr. Res. Pap. 47, 2159–2190. doi:10.1016/S0967-0637(00)00014-5

Oceana, 2015. Expedition 2014 Balearic Islands Cabrera National Park and Mallorca Channel Seamounts.

Oguz, T., Macias, D., Garcia-Lafuente, J., Pascual, A., Tintore, J., 2014. Fueling plankton production by a meandering frontal jet: a case study for the Alboran Sea (Western Mediterranean). PLoS One 9, e111482.

Oksanen, J., Blanchet, F.G., Friendly, M., Kindt, R., Legendre, P., McGlinn, D., Minchin, P.R., O'Hara, R.B., Simpson, G.L., Solymos, P., Stevens, M.H.H., Szoecs, E., Wagner, H., 2018. vegan: Community Ecology Package. R package version 2.5-2 [WWW Document].

Oliver, W.A., 1968. Some aspects of colony development in corals. J. Paleontol. 42, 16–34. doi:10.1017/s002233600006162x

Olu-Le Roy, K., J. Galéron & the Caracole Cruise Scientific Team. 2002. CARACOLE cruise report. Vol. 1&2.

Onken, R., Robinson, A.R., Lermusiaux, P.F.J., Haley, P.J., Anderson, L.A., 2003. Data-driven simulations of synoptic circulation and transports in the Tunisia-Sardinia-Sicily region. J. Geophys. Res. Ocean. 108. doi:10.1029/2002JC001348

Opresko, D.M., 2009. Antipatharia (Cnidaria) of the Gulf of Mexico, in: Gulf of Mexico Origin, Waters, and Biota. pp. 359–363.

Orejas, C., Gori, A., Lo Iacono, C., Puig, P., Gili, J.-M., Dale, M.R.T., others, 2009. Cold-water corals in the Cap de Creus canyon, northwestern Mediterranean: spatial distribution, density and anthropogenic impact. Mar. Ecol. Prog. Ser. 397, 37–51.

Orejas, C., Ferrier-Pagès, C., Reynaud, S., Gori, A., Beraud, E., Tsounis, G., Allemand, D., Gili, J., 2011. Long-term growth rates of four Mediterranean cold-water coral species maintained in aquaria. Mar. Ecol. Prog. Ser. 429, 57–65. doi:10.3354/meps09104

Orejas, C., Gori, A., Jiménez, C., Rivera, J., Lo Iacono, C., Hadjioannou, L., Andreou, V., Petrou, A., 2017. First in situ documentation of a population of the coral *Dendrophyllia ramea* off Cyprus (Levantine Sea) and evidence of human impacts. Galaxea, J. Coral Reef Stud. 19, 15–16.

Orejas, C., Gori, A., Jiménez, C., Rivera, J., Kamidis, N., Abu Alhaija, R., Lo Iacono, C., 2019. Occurrence and distribution of the coral *Dendrophyllia ramea* in Cyprus insular shelf: Environmental setting and anthropogenic impacts. Deep. Res. Part II Top. Stud. Oceanogr. 164, 190–205. doi:10.1016/j.dsr2.2019.04.006

Orr, J.C., Fabry, V.J., Aumont, O., Bopp, L., Doney, S.C., Feely, R.A., Gnanadesikan, A., Gruber, N., Ishida, A., Joos, F., Key, R.M., Lindsay, K., Maier-Reimer, E., Matear, R., Monfray, P., Mouchet, A., Najjar, R.G., Plattner, G.K., Rodgers, K.B., Sabine, C.L., Sarmiento, J.L., Schlitzer, R., Slater, R.D., Totterdell, I.J., Weirig, M.F., Yamanaka, Y., Yool, A., 2005. Anthropogenic ocean acidification over the twenty-first century and its impact on calcifying organisms. Nature 437, 681–686. doi:10.1038/nature04095

Osborne, A.H., Marino, G., Vance, D., Rohling, E.J., 2010. Eastern Mediterranean surface water Nd during Eemian sapropel S5: Monitoring northerly (mid-latitude) versus southerly (sub-tropical) freshwater contributions. Quat. Sci. Rev. 29, 2473–2483. doi:10.1016/j.quascirev.2010.05.015

OSPAR Commision, 2008. List of Threatened and/or Declining Species and Habitats [WWW Document]. URL https://www.ospar.org/work-areas/bdc/specieshabitats/%0Dlist-of-threatened-declining-species-habitats (accessed 5.21.18).

Ottesen, D., Dowdeswell, J.A., Rise, L., 2005. Submarine landforms and the reconstruction of fast-flowing ice streams within a large Quaternary ice sheet: The 2500-km-long Norwegian-Svalbard margin (57°-80°N). Bull. Geol. Soc. Am. 117, 1033–1050. doi:10.1130/B25577.1

Palomino, D., Alonso, B., Lo Iacono, C., Casas, D., D'Acremont, E., Ercilla, G., Gorini, C., Vazquez, J.T., 2015. Seamounts and Seamount-like Structures of the Alborán Sea, in: Wurz, M., Rovere, M. (Eds.), Atlas of the Mediterranean Seamounts and Seamount-like Structures. IUCN, International Union for Conservation of Nature, pp. 124–132.

Pearman, T.R.R., Robert, K., Callaway, A., Hall, R., Lo Iacono, C., Huvenne, V.A.I., 2020. Improving the predictive capability of benthic species distribution models by incorporating oceanographic data – Towards holistic ecological modelling of a submarine canyon. Prog. Oceanogr. 184, 102338. doi:10.1016/j.pocean.2020.102338

Perea, H., Gràcia, E., Martínez-Loriente, S., Bartolome, R., de la Peña, L.G., de Mol, B., Moreno, X., Lo Iacono, C., Diez, S., Tello, O., Gómez-Ballesteros, M., Dañobeitia, J.J., 2018. Kinematic analysis of secondary faults within a distributed shear-zone reveals fault linkage and increased seismic hazard. Mar. Geol. 399, 23–33. doi:10.1016/j.margeo.2018.02.002

Pierdomenico, M., Russo, T., Ambroso, S., Gori, A., Martorelli, E., D'Andrea, L., Gili, J.-M., Chiocci, F.L., 2018. Effects of trawling activity on the bamboo-coral *Isidella elongata* and the sea pen *Funiculina quadrangularis* along the Gioia Canyon (Western Mediterranean, southern Tyrrhenian Sea). Prog. Oceanogr.

Price, D.M., Robert, K., Callaway, A., Lo Iacono, C., Hall, R.A., Huvenne, V.A.I., 2019. Using 3D photogrammetry from ROV video to quantify cold-water coral reef structural complexity and investigate its influence on biodiversity and community assemblage. Coral Reefs 38, 1007–1021. doi:10.1007/s00338-019-01827-3

Purser, A., Orejas, C., Gori, A., Tong, R., Unnithan, V., Thomsen, L., 2013. Local variation in the distribution of

benthic megafauna species associated with cold-water coral reefs on the Norwegian margin. Cont. Shelf Res. 54, 37–51.

Quattrini, A.M., Partyka, M.L., Ross, S.W., 2009. Aspects of the Reproductive Biology of the Skate *Fenestraja plutonia* (Garman) off North Carolina. Southeast. Nat. 8, 55–70. doi:10.1656/058.008.0106

R Core Team, 2017. R: A language and environment for statistical computing. R Foundation for Statistical Computing, Vienna, Austria. 2016.

Raddatz, J., Liebetrau, V., Trotter, J., Rüggeberg, A., Flögel, S., Dullo, W.C., Eisenhauer, A., Voigt, S., McCulloch, M., 2016. Environmental constraints on Holocene cold-water coral reef growth off Norway: Insights from a multiproxy approach. Paleoceanogr. Paleoclimatology 31, 1350–1367. doi:10.1002/2016PA002974

Raddatz, J., Titschack, J., Frank, N., Freiwald, A., Conforti, A., Osborne, A., Skornitzke, S., Stiller, W., Rüggeberg, A., Voigt, S., Albuquerque, A.L.S., Vertino, A., Schröder-Ritzrau, A., Bahr, A., 2020. *Solenosmilia variabilis*-bearing cold-water coral mounds off Brazil. Coral Reefs 39, 69–83. doi:10.1007/s00338-019-01882-w

Rebesco, M., Taviani, M., 2019. A Turbulent Story: Mediterranean Contourites and Cold-Water Corals, in: Mediterranean Cold-Water Corals: Past, Present and Future. Springer, Cham, pp. 35–46.

Reed, J.K., 1980. Distribution and Structure of Deep-Water *Oculina varicosa* Coral Reefs off Central Eastern Florida. Bull. Mar. Sci. 30, 667–677.

Reed, J.K., 2002. Deep-water Oculina coral reefs of Florida: Biology, impacts, and management, in: Hydrobiologia. Springer, pp. 43–55. doi:10.1023/A:1016588901551

Reed, J.K., Shepard, A.N., Koenig, C.C., Scanlon, K.M., Gilmore, R.G., 2005. Mapping, habitat characterization, and fish surveys of the deep-water Oculina coral reef Marine Protected Area: a review of historical and current research, in: Cold-Water Corals and Ecosystems. Springer Berlin Heidelberg, pp. 443–465. doi:10.1007/3-540-27673-4_22

Remia, A., Taviani, M., 2005. Shallow-buried Pleistocene *Madrepora*-dominated coral mounds on a muddy continental slope, Tuscan Archipelago, NE Tyrrhenian Sea. Facies 50, 419–425.

Reyes, J., Santodomingo, N., Gracia, A., Borrero-Pérez, G., Navas, G., Mejía-Ladino, L.M., Bermúdez, A., Benavides, M., 2006. Southern Caribbean azooxanthellate coral communities off Colombia, in: Cold-Water Corals and Ecosystems. Springer-Verlag, pp. 309–330. doi:10.1007/3-540-27673-4_15

Rice, J., Gjerde, K.M., Ardron, J., Arico, S., Cresswell, I., Escobar, E., Grant, S., Vierros, M., 2011. Policy relevance of biogeographic classification for conservation and management of marine biodiversity beyond national jurisdiction, and the GOODS biogeographic classification. Ocean Coast. Manag. 54, 110–122. doi:10.1016/j.ocecoaman.2010.10.010

Roberts, J.M., Brown, C.J., Long, D., Bates, C.R., 2005. Acoustic mapping using a multibeam echosounder reveals cold-water coral reefs and surrounding habitats. Coral Reefs 24, 654–669. doi:10.1007/s00338-005-0049-6

Roberts, J.M., Wheeler, A.J., Freiwald, A., 2006. Reefs of the deep: the biology and geology of cold-water coral ecosystems. Science 312, 543–547.

Roberts, J.M., Henry, L.-A., Long, D., Hartley, J.P., 2008. Cold-water coral reef frameworks, megafaunal communities and evidence for coral carbonate mounds on the Hatton Bank, north east Atlantic. Facies 54, 297–316.

Roberts, J.M., Wheeler, A.J., Freiwald, A., Cairns, S.D., 2009a. Cold-water corals: The biology and geology of deep-sea coral habitats, Cold-Water Corals: The Biology and Geology of Deep-Sea Coral Habitats. Cambridge University Press. doi:10.1017/CBO9780511581588

Roberts, J., Davies, A., Henry, L., Dodds, L., Duineveld, G., Lavaleye, M., Maier, C., van Soest, R., Bergman, M., Hühnerbach, V., Huvenne, V., Sinclair, D., Watmough, T., Long, D., Green, S., van Haren, H., 2009b. Mingulay reef complex: an interdisciplinary study of cold-water coral habitat, hydrography and biodiversity. Mar. Ecol. Prog. Ser. 397, 139–151. doi:10.3354/meps08112

Robinson, A.R., Leslie, W.G., Theocharis, A., Lascaratos, A., 2001. Mediterranean Sea Circulation, in: Steele, J.H. (Ed.), Encyclopedia of Ocean Sciences. Academic Press, Oxford, pp. 1689–1705. doi:https://doi.org/10.1006/rwos.2001.0376

Robinson, L.F., Adkins, J.F., Keigwin, L.D., Southon, J., Fernandez, D.P., Wang, S.L., Scheirer, D.S., 2005. Ocean science: Radiocarbon variability in the western North Atlantic during the last deglaciation. Science 310, 1469–1473. doi:10.1126/science.1114832

Robinson, L.F., Adkins, J.F., Frank, N., Gagnon, A.C., Prouty, N.G., Brendan Roark, E., de Flierdt, T. van, 2014. The geochemistry of deep-sea coral skeletons: A review of vital effects and applications for palaeoceanography. Deep. Res. Part II Top. Stud. Oceanogr. 99, 184–198. doi:10.1016/j.dsr2.2013.06.005

Rogers, A.D., 1999. The biology of *Lophelia pertusa* (Linnaeus 1758) and other deep-water reef-forming corals and impacts from human activities. Int. Rev. Hydrobiol. 84, 315–406.

Rogerson, M., Cacho, I., Jimenez-Espejo, F., Reguera, M.I., Sierro, F.J., Martinez-Ruiz, F., Frigola, J., Canals, M., 2008. A dynamic explanation for the origin of the western Mediterranean organic-rich layers. Geochemistry, Geophys. Geosystems 9, 7. doi:10.1029/2007GC001936

Rohling, E.J., Cane, T.R., Cooke, S., Sprovieri, M., Bouloubassi, I., Emeis, K.C., Schiebel, R., Kroon, D., Jorissen, F.J., Lorre, A., Kemp, A.E.S., 2002. African monsoon variability during the previous interglacial maximum. Earth Planet. Sci. Lett. 202, 61–75. doi:10.1016/S0012-821X(02)00775-6

Rohling, E.J., Sprovieri, M., Cane, T., Casford, J.S.L., Cooke, S., Bouloubassi, I., Emeis, K.C., Schiebel, R., Rogerson, M., Hayes, A., Jorissen, F.J., Kroon, D., 2004. Reconstructing past planktic foraminiferal habitats using stable isotope data: A case history for Mediterranean sapropel S5. Mar. Micropaleontol. 50, 89–123. doi:10.1016/S0377-8398(03)00068-9

Rohling, E.J., Marino, G., Grant, K.M., 2015. Mediterranean climate and oceanography, and the periodic development of anoxic events (sapropels). Earth-Science Rev. 143, 62–97. doi:10.1016/j.earscirev.2015.01.008

Rona, P., Guida, V., Scranton, M., Gong, D., Macelloni, L., Pierdomenico, M., Diercks, A.-R., Asper, V., Haag, S., 2015. Hudson submarine canyon head offshore New York and New Jersey: A physical and geochemical investigation. Deep Sea Res. Part II Top. Stud. Oceanogr. 121, 213–232.

Ross, S.W., 2006. Review of distribution, habitats, and associated fauna of deep water coral reefs on the southeastern United States continental slope (North Carolina to Cape Canaveral, Fl). Charleston.

Ross, S.W., Nizinski, M.S., 2007. State of deep coral ecosystems in the US southeast region: Cape Hatteras to southeastern Florida., in: The State of Deep Coral Ecosystems of the United States. pp. 233–270.

Ross, S.W., Rhode, M., Brooke, S., 2017. Reprint of – Deep-sea coral and hardbottom habitats on the west Florida slope, eastern Gulf of Mexico. Deep Sea Res. Part I Oceanogr. Res. Pap. 127, 114–128. doi:10.1016/j.dsr.2017.08.008

Roy-Barman, M., Pons-Branchu, E., Levier, M., Bordier, L., Foliot, L., Gdaniec, S., Ayrault, S., Garcia-Orellana, J., Masque, P., Castrillejo, M., 2019. Barium during the GEOTRACES GA-04S MedSeA cruise: The Mediterranean Sea Ba budget revisited. Chem. Geol. 511, 431–440. doi:10.1016/j.chemgeo.2018.09.015

Rüggeberg, A., Dullo, C., Dorschel, B., Hebbeln, D., 2007. Environmental changes and growth history of a cold-water carbonate mound (Propeller Mound, Porcupine Seabight). Int. J. Earth Sci. 96, 57–72. doi:10.1007/s00531-005-0504-1

Rüggeberg, A., Flögel, S., Dullo, W.-C., Raddatz, J., Liebetrau, V., 2016. Paleoseawater density reconstruction and its implication for cold-water coral carbonate mounds in the northeast Atlantic through time. Paleoceanography 31, 365–379. doi:10.1002/2015PA002859

Santín, A., Grinyó, J., Ambroso, S., Uriz, M.J., Gori, A., Dominguez-Carrió, C., Gili, J.-M., 2017. Sponge assemblages on the deep Mediterranean continental shelf and slope (Menorca Channel, Western Mediterranean Sea). Deep Sea Res. Part I Oceanogr. Res. Pap.

Santín, A., Grinyó, J., Ambroso, S., Uriz, M.J., Dominguez-Carrió, C., Gili, J.M., 2019. Distribution patterns and demographic trends of demosponges at the Menorca Channel (Northwestern Mediterranean Sea). Prog. Oceanogr. 173, 9–25. doi:10.1016/j.pocean.2019.02.002

Santín, A., Grinyó, J., Bilan, M., Ambroso, S., Puig, P., 2020. First report of the carnivorous sponge *Lycopodina hypogea* (Cladorhizidae) associated with marine debris, and its possible implications on deep-sea connectivity. Mar. Pollut. Bull. 159, 111501. doi:10.1016/j.marpolbul.2020.111501

Sappington, J.M., Longshore, K.M., Thompson, D.B., 2007. Quantifying Landscape Ruggedness for Animal Habitat Analysis: A Case Study Using Bighorn Sheep in the Mojave Desert. J. Wildl. Manage. 71, 1419–1426. doi:10.2193/2005-723

Sartoretto, S., Zibrowius, H., 2018. Note on new records of living Scleractinia and Gorgonaria between 1700 and 2200 m depth in the western Mediterranean Sea. Mar. Biodivers. 48, 689–694. doi:10.1007/s12526-017-0829-6

Savini, A., Corselli, C., 2010. High-resolution bathymetry and acoustic geophysical data from Santa Maria di Leuca Cold Water Coral province (Northern Ionian Sea–Apulian continental slope). Deep Sea Res. Part II Top. Stud. Oceanogr. 57, 326–344.

Savini, A., Marchese, F., Verdicchio, G., Vertino, A., 2016. Submarine slide topography and the distribution of vulnerable marine ecosystems: a case study in the Ionian Sea (Eastern Mediterranean), in: Submarine Mass Movements and Their Consequences. Springer, pp. 163–170.

Schembri, P., Dimech, M., Camilleri, M., Page, R., 2007. Living deep-water *Lophelia* and *Madrepora* corals in Maltese waters (Strait of Sicily, Mediterranean Sea). Cah. Biol. Mar. 48, 77.

Scholz, D., Mangini, A., Felis, T., 2004. U-series dating of diagenetically altered fossil reef corals. Earth Planet. Sci. Lett. 218, 163–178. doi:10.1016/S0012-821X(03)00647-2

Sierro, F.J., Hodell, D.A., Curtis, J.H., Flores, J.A., Reguera, I., Colmenero-Hidalgo, E., Bárcena, M.A., Grimalt, J.O., Cacho, I., Frigola, J., Canals, M., 2005. Impact of iceberg melting on Mediterranean thermohaline circulation during Heinrich events. Paleoceanography 20, PA2019. doi:10.1029/2004PA001051

Sivan, D., Sisma-Ventura, G., Greenbaum, N., Bialik, O.M., Williams, F.H., Tamisiea, M.E., Rohling, E.J., Frumkin, A., Avnaim-Katav, S., Shtienberg, G., Stein, M., 2016. Eastern Mediterranean sea levels through the last interglacial from a coastal-marine sequence in northern Israel. Quat. Sci. Rev. 145, 204–225. doi:10.1016/j.quascirev.2016.06.001

Soetaert, K., Mohn, C., Rengstorf, A., Grehan, A., Van Oevelen, D., 2016. Ecosystem engineering creates a direct nutritional link between 600-m deep cold-water coral mounds and surface productivity. Sci. Rep. 6, 1–9. doi:10.1038/srep35057

Somoza, L., Ercilla, G., Urgorri, V., León, R., Medialdea, T., Paredes, M., Gonzalez, F.J., Nombela, M.A., 2014. Detection and mapping of cold-water coral mounds and living *Lophelia* reefs in the Galicia Bank, Atlantic NW Iberia margin. Mar. Geol. 349, 73–90. doi:10.1016/j.margeo.2013.12.017

Sorgente, R., Olita, A., Oddo, P., Fazioli, L., Ribotti, A., 2011. Numerical simulation and decomposition of kinetic energy in the Central Mediterranean: insight on mesoscale circulation and energy conversion. Ocean Sci. 7, 503–519. doi:10.5194/os-7-503-2011

Sosdian, S., Rosenthal, Y., 2009. Deep-sea temperature and ice volume changes across the pliocene-pleistocene climate transitions. Science 325, 306–310. doi:10.1126/science.1169938

Spakman, W., Chertova, M. V., Van Den Berg, A., Van Hinsbergen, D.J.J., 2018. Puzzling features of western Mediterranean tectonics explained by slab dragging. Nat. Geosci. 11, 211–216. doi:10.1038/s41561-018-0066-z

Spooner, P.T., Chen, T., Robinson, L.F., Coath, C.D., 2016. Rapid uranium-series age screening of carbonates by laser ablation mass spectrometry. Quat. Geochronol. 31, 28–39. doi:10.1016/j.quageo.2015.10.004

Spooner, P.T., Robinson, L.F., Hemsing, F., Morris, P., Stewart, J.A., 2018. Extended calibration of cold-water coral Ba/Ca using multiple genera and co-located measurements of dissolved barium concentration. Chem. Geol. 499, 100–110. doi:10.1016/j.chemgeo.2018.09.012

Stalder, C., Vertino, A., Rosso, A., Rüggeberg, A., Pirkenseer, C., Spangenberg, J.E., Spezzaferri, S., Camozzi, O., Rappo, S., Hajdas, I., 2015. Microfossils, a key to unravel cold-water carbonate mound evolution through time: Evidence from the Eastern Alboran Sea. PLoS One 10. doi:10.1371/journal.pone.0140223

Stalder, C., El Kateb, A., Vertino, A., Rüggeberg, A., Camozzi, O., Pirkenseer, C.M., Spangenberg, J.E., Hajdas, I., Van Rooij, D., Spezzaferri, S., 2018. Large-scale paleoceanographic variations in the western Mediterranean Sea during the last 34,000 years: From enhanced cold-water coral growth to declining mounds. Mar. Micropaleontol. 143, 46–62. doi:10.1016/j.marmicro.2018.07.007

Stalling, D., Westerhoff, M., Hege, H.-C., 2005. Amira: A highly interactive system for visual data analysis. Vis.

Handb. 38, 749–767.

Steinmann, L., Baques, M., Wenau, S., Schwenk, T., Spiess, V., Piola, A.R., Bozzano, G., Violante, R., Kasten, S., 2020. Discovery of a giant cold-water coral mound province along the northern Argentine margin and its link to the regional Contourite Depositional System and oceanographic setting. Mar. Geol. 427, 106223. doi:10.1016/j.margeo.2020.106223

Stevenson, A., Mitchell, F.J.G., Davies, J.S., 2015. Predation has no competition: factors influencing space and resource use by echinoids in deep-sea coral habitats, as evidenced by continuous video transects. Mar. Ecol. 36, 1454–1467. doi:10.1111/maec.12245

Stewart, H.A., Davies, J.S., Guinan, J., Howell, K.L., 2014. The Dangeard and Explorer canyons, South Western Approaches UK: Geology, sedimentology and newly discovered cold-water coral mini-mounds. Deep. Res. Part II Top. Stud. Oceanogr. 104, 230–244. doi:10.1016/j.dsr2.2013.08.018

Stewart, J.A., Anagnostou, E., Foster, G.L., 2016. An improved boron isotope pH proxy calibration for the deep-sea coral *Desmophyllum dianthus* through sub-sampling of fibrous aragonite. Chem. Geol. 447, 148–160. doi:10.1016/j.chemgeo.2016.10.029

Stewart, J.A., Robinson, L.F., Day, R.D., Strawson, I., Burke, A., Rae, J.W.B., Spooner, P.T., Samperiz, A., Etnoyer, P.J., Williams, B., Paytan, A., Leng, M.J., Häussermann, V., Wickes, L.N., Bratt, R., Pryer, H., 2020. Refining trace metal temperature proxies in cold-water scleractinian and stylasterid corals. Earth Planet. Sci. Lett. 545, 116412. doi:10.1016/j.epsl.2020.116412

Stolarski, J., 2003. Three-dimensional micro-and nanostructural characteristics of the scleractinian coral skeleton: a biocalcification proxy. Acta Palaeontol. Pol. 48, 497–530.

Strömberg, S.M., Larsson, A.I., 2017. Larval behavior and longevity in the cold-water coral *Lophelia pertusa* indicate potential for long distance dispersal. Front. Mar. Sci. 4, 411. doi:10.3389/fmars.2017.00411

Studer, A.S., Sigman, D.M., Martínez-García, A., Thöle, L.M., Michel, E., Jaccard, S.L., Lippold, J.A., Mazaud, A., Wang, X.T., Robinson, L.F., Adkins, J.F., Haug, G.H., 2018. Increased nutrient supply to the Southern Ocean during the Holocene and its implications for the pre-industrial atmospheric CO_2 rise. Nat. Geosci. 11, 756–760.

Stumpf, R., Frank, M., Schönfeld, J., Haley, B.A., 2010. Late Quaternary variability of Mediterranean Outflow Water from radiogenic Nd and Pb isotopes. Quat. Sci. Rev. 29, 2462–2472. doi:10.1016/j.quascirev.2010.06.021

Tamborrino, L., Wienberg, C., Titschack, J., Wintersteller, P., Mienis, F., Schroder-Ritzrau, A., Freiwald, A., Orejas, C., Dullo, W.C., Haberkern, J., Hebbeln, D., 2019. Mid-holocene extinction of cold-water corals on the namibian shelf steered by the benguela oxygen minimum zone. Geology 47, 1185–1188. doi:10.1130/G46672.1

Taviani, M., Colantoni, P., 1979. Thanatocoenoses Wurmiennes associees aux coraux blancs. Rapp. Comm. int. Mer Médit. 24/26.

Taviani, M., Remia, A., Corselli, C., Freiwald, A., Malinverno, E., Mastrototaro, F., Savini, A., Tursi, A., 2005. First geo-marine survey of living cold-water *Lophelia* reefs in the Ionian Sea (Mediterranean basin). Facies 50, 409–417. doi:10.1007/s10347-004-0039-0

Taviani, M., Vertino, A., López Correa, M., Savini, A., de Mol, B., Remia, A., Montagna, P., Angeletti, L., Zibrowius, H., Alves, T., Salomidi, M., Ritt, B., Henry, P., 2011. Pleistocene to Recent scleractinian deep-water corals and coral facies in the Eastern Mediterranean. Facies 57, 579–603. doi:10.1007/s10347-010-0247-8

Taviani, M., Angeletti, L., Canese, S., Cannas, R., Cardone, F., Cau, A., Cau, A.B., Follesa, M.C., Marchese, F., Montagna, P., others, 2017. The "Sardinian cold-water coral province"' in the context of the Mediterranean coral ecosystems." Deep Sea Res. Part II Top. Stud. Oceanogr. 145, 61–78.

Taviani, M., Angeletti, L., Foglini, F., Corselli, C., Nasto, I., Pons-Branchu, E., Montagna, P., 2019. U/Th dating records of cold-water coral colonization in submarine canyons and adjacent sectors of the southern Adriatic Sea since the Last Glacial Maximum. Prog. Oceanogr. 175, 300–308. doi:10.1016/j.pocean.2019.04.011

Thiagarajan, N., Subhas, A. V., Southon, J.R., Eiler, J.M., Adkins, J.F., 2014. Abrupt pre-Bølling-Allerød warming and circulation changes in the deep ocean. Nature 511, 75–78. doi:10.1038/nature13472

Thiem, Ø., Ravagnan, E., Fosså, J.H., Berntsen, J., 2006. Food supply mechanisms for cold-water corals along a continental shelf edge. J. Mar. Syst. 60, 207–219.

Thierens, M., Titschack, J., Dorschel, B., Huvenne, V.A.I., Wheeler, A.J., Stuut, J.B., O'Donnell, R., 2010. The 2.6 Ma depositional sequence from the Challenger cold-water coral carbonate mound (IODP Exp. 307): Sediment contributors and hydrodynamic palaeo-environments. Mar. Geol. 271, 260–277. doi:10.1016/j.margeo.2010.02.021

Thierens, M., Browning, E., Pirlet, H., Loutre, M.F., Dorschel, B., Huvenne, V.A.I., Titschack, J., Colin, C., Foubert, A., Wheeler, A.J., 2013. Cold-water coral carbonate mounds as unique palaeo-archives: The Plio-Pleistocene Challenger Mound record (NE Atlantic). Quat. Sci. Rev. 73, 14–30. doi:10.1016/j.quascirev.2013.05.006

Thomsen, L., Gust, G., 2000. Sediment erosion thresholds and characteristics of resuspended aggregates on the western European continental margin. Deep. Res. Part I Oceanogr. Res. Pap. 47, 1881–1897. doi:10.1016/S0967-0637(00)00003-0

Thresher, R., Althaus, F., Adkins, J., Gowlett-Holmes, K., Alderslade, P., Dowdney, J., Cho, W., Gagnon, A., Staples, D., McEnnulty, F., Williams, A., 2014. Strong Depth-Related Zonation of Megabenthos on a Rocky Continental Margin (~700–4000 m) off Southern Tasmania, Australia. PLoS One 9, e85872. doi:10.1371/journal.pone.0085872

Titschack, J., 2019. 10 Bathyal Corals Within the Aegean Sea and the Adjacent Hellenic Trench. Springer, Cham, pp. 85–94. doi:10.1007/978-3-319-91608-8_10

Titschack, J., Thierens, M., Dorschel, B., Schulbert, C., Freiwald, A., Kano, A., Takashima, C., Kawagoe, N., Li, X., 2009. Carbonate budget of a cold-water coral mound (Challenger Mound, IODP Exp. 307). Mar. Geol. 259, 36–46. doi:10.1016/j.margeo.2008.12.007

Titschack, J., Baum, D., De Pol-Holz, R., López Correa, M., Forster, N., Flögel, S., Hebbeln, D., Freiwald, A., 2015. Aggradation and carbonate accumulation of Holocene Norwegian cold-water coral reefs. Sedimentology 62, 1873–1898. doi:10.1111/sed.12206

Titschack, J., Fink, H.G., Baum, D., Wienberg, C., Hebbeln, D., Freiwald, A., 2016. Mediterranean cold-water corals - an important regional carbonate factory? Depos. Rec. 2, 74–96. doi:10.1002/dep2.14

Tong, R., Purser, A., Unnithan, V., Guinan, J., 2012. Multivariate statistical analysis of distribution of deep-water gorgonian corals in relation to seabed topography on the Norwegian margin. PLoS One 7, e43534.

Toucanne, S., Jouet, G., Ducassou, E., Bassetti, M.A., Dennielou, B., Angue Minto'o, C.M., Lahmi, M., Touyet, N., Charlier, K., Lericolais, G., Mulder, T., 2012. A 130,000-year record of Levantine Intermediate Water flow variability in the Corsica Trough, western Mediterranean Sea. Quat. Sci. Rev. 33, 55–73. doi:10.1016/j.quascirev.2011.11.020

UNEP-MAP-RAC/SPA, 2015. Action Plan for the conservation of habitats and species associated with seamounts, underwater caves and canyons, aphotic hard beds and chemo-synthetic phenomena in the Mediterranean Sea. DarkHabitats Action Plan. Ed. RAC/SPA, Tunis: 17 pp.

Vacchi, M., Marriner, N., Morhange, C., Spada, G., Fontana, A., Rovere, A., 2016. Multiproxy assessment of Holocene relative sea-level changes in the western Mediterranean: Sea-level variability and improvements in the definition of the isostatic signal. Earth-Science Rev. doi:10.1016/j.earscirev.2016.02.002

van de Flierdt, T., Robinson, L.F., Adkins, J.F., 2010. Deep-sea coral aragonite as a recorder for the neodymium isotopic composition of seawater. Geochim. Cosmochim. Acta 74, 6014–6032. doi:10.1016/j.gca.2010.08.001

van Haren, H., 2014. Internal wave–zooplankton interactions in the Alboran Sea (W-Mediterranean). J. Plankton Res. 36, 1124–1134. doi:https://doi.org/10.1093/plankt/fbu031

Van Oevelen, D., Duineveld, G., Lavaleye, M., Mienis, F., Soetaert, K., Heip, C.H.R., 2009. The cold-water coral community as a hot spot for carbon cycling on continental margins: A food-web analysis from rockall bank (northeast atlantic). Limnol. Oceanogr. 54, 1829–1844. doi:10.4319/lo.2009.54.6.1829

Van Rooij, D., Huvenne, V.A.I., Blamart, D., Henriet, J.P., Wheeler, A., de Haas, H., 2009. The Enya mounds: A lost mound-drift competition. Int. J. Earth Sci. 98, 849–863. doi:10.1007/s00531-007-0293-9

Van Rooij, D., Blamart, D., De Mol, L., Mienis, F., Pirlet, H., Wehrmann, L.M., Barbieri, R., Maignien, L., Templer, S.P., de Haas, H., Hebbeln, D., Frank, N., Larmagnat, S., Stadnitskaia, A., Stivaletta, N., van Weering, T., Zhang, Y., Hamoumi, N., Cnudde, V., Duyck, P., Henriet, J.P., 2011. Cold-water coral mounds on the Pen Duick

Escarpment, Gulf of Cadiz: The MiCROSYSTEMS project approach. Mar. Geol. 282, 102–117. doi:10.1016/j.margeo.2010.08.012

Van Soest, R.W.M., van Duyl, F.C., Maier, C., Lavaleye, M.S.S., Beglinger, E.J., Tabachnick, K.R., 2007. Mass occurrence of *Rossella nodastrella* Topsent on bathyal coral reefs of Rockall Bank, W of Ireland (Lyssacinosida, Hexactinellida), in: Custodio, M.R., Lôbo-Hajdu, G., Hajdu, E., Muriey, G. (Eds.), Porifera Research: Biodiversity, Innovationand SustainaBility. Museu National, Rio de Janeiro, pp. 645–652.

Van Soest, R.W.M., De Voogd, N.J., 2015. Sponge species composition of north-east Atlantic cold-water coral reefs compared in a bathyal to inshore gradient. J. Mar. Biol. Assoc. United Kingdom 95, 1461–1474. doi:10.1017/S0025315413001410

Vandorpe, T., Wienberg, C., Hebbeln, D., Van den Berghe, M., Gaide, S., Wintersteller, P., Van Rooij, D., 2017. Multiple generations of buried cold-water coral mounds since the Early-Middle Pleistocene Transition in the Atlantic Moroccan Coral Province, southern Gulf of Cádiz. Palaeogeogr. Palaeoclimatol. Palaeoecol. 485, 293–304. doi:10.1016/j.palaeo.2017.06.021

Vargas-Yáez, M., Plaza, F., García-Lafuente, J., Sarhan, T., Vargas, J.M., Vélez-Belchi, P., 2002. About the seasonal variability of the Alboran Sea circulation. J. Mar. Syst. 35, 229–248. doi:10.1016/S0924-7963(02)00128-8

Vargas-Yáñez, M., García-Martínez, M.C., Moya, F., Balbín, R., López-Jurado, J.L., Serra, M., Zunino, P., Pascual, J., Salat, J., 2017. Updating temperature and salinity mean values and trends in the Western Mediterranean: The RADMED project. Prog. Oceanogr. 157, 27–46. doi:10.1016/j.pocean.2017.09.004

Vertino, A., Savini, A., Rosso, A., Di Geronimo, I., Mastrototaro, F., Sanfilippo, R., Gay, G., Etiope, G., 2010. Benthic habitat characterization and distribution from two representative sites of the deep-water SML Coral Province (Mediterranean). Deep. Res. Part II Top. Stud. Oceanogr. 57, 380–396. doi:10.1016/j.dsr2.2009.08.023

Vertino, A., Taviani, M., Corselli, C., 2019. Spatio-Temporal Distribution of Mediterranean Cold-Water Corals, in: Orejas, C., Jiménez, C. (Eds.), Mediterranean Cold-Water Corals: Past, Present and Future. Springer, Cham, pp. 67–83. doi:10.1007/978-3-319-91608-8_9

Victorero, L., Blamart, D., Pons-Branchu, E., Mavrogordato, M.N., Huvenne, V.A.I., 2016. Reconstruction of the formation history of the Darwin Mounds, N Rockall Trough: How the dynamics of a sandy contourite affected cold-water coral growth. Mar. Geol. 378, 186–195. doi:10.1016/j.margeo.2015.12.001

Volkov, D.L., Fu, L.-L., 2010. On the Reasons for the Formation and Variability of the Azores Current. J. Phys. Oceanogr. 40, 2197–2220. doi:10.1175/2010JPO4326.1

Waelbroeck, C., Paul, A., Kucera, M., Rosell-Melé, A., Weinelt, M., Schneider, R., Mix, A.C., Abelmann, A., Armand, L., Bard, E., Barker, S., Barrows, T.T., Benway, H., Cacho, I., Chen, M.T., Cortijo, E., Crosta, X., De Vernal, A., Dokken, T., Duprat, J., Elderfield, H., Eynaud, F., Gersonde, R., Hayes, A., Henry, M., Hillaire-Marcel, C., Huang, C.C., Jansen, E., Juggins, S., Kallel, N., Kiefer, T., Kienast, M., Labeyrie, L., Leclaire, H., Londeix, L., Mangin, S., Matthiessen, J., Marret, F., Meland, M., Morey, A.E., Mulitza, S., Pflaumann, U., Pisias, N.G., Radi, T., Rochon, A., Rohling, E.J., Sbaffi, L., Schäfer-Neth, C., Solignac, S., Spero, H., Tachikawa, K., Turon, J.L., 2009. Constraints on the magnitude and patterns of ocean cooling at the Last Glacial Maximum. Nat. Geosci. 2, 127–132. doi:10.1038/ngeo411

Walbridge, S., Slocum, N., Pobuda, M., Wright, D.J., 2018. Unified Geomorphological Analysis Workflows with Benthic Terrain Modeler. Geosciences 8, 94. doi:10.3390/geosciences8030094

Wang, X.T., Sigman, D.M., Cohen, A.L., Sinclair, D.J., Sherrell, R.M., Weigand, M.A., Erler, D. V., Ren, H., 2015. Isotopic composition of skeleton-bound organic nitrogen in reef-building symbiotic corals: A new method and proxy evaluation at Bermuda. Geochim. Cosmochim. Acta 148, 179–190. doi:10.1016/j.gca.2014.09.017

Wang, H., Lo Iacono, C., Wienberg, C., Titschack, J., Hebbeln, D., 2019. Cold-water coral mounds in the southern Alboran Sea (western Mediterranean Sea): Internal waves as an important driver for mound formation since the last deglaciation. Mar. Geol. 412, 1–18. doi:10.1016/j.margeo.2019.02.007

Watling, L., Norse, E.A., 1998. Disturbance of the seabed by mobile fishing gear: a comparison to forest clearcutting. Conserv. Biol. 12, 1180–1197.

Wedepohl, K.H., 1995. The composition of the continental crust. Geochim. Cosmochim. Acta 59, 1217–1232. doi:10.1016/0016-7037(95)00038-2

Wesseling, I., Uychiaoco, A.J., Aliño, P.M., Aurin, T., Vermaat, J.E., 1999. Damage and recovery of four Philippine corals from short-term sediment burial. Mar. Ecol. Prog. Ser. 11–15.

Wheeler, A. J., Bett, B. J., Billett, D. S. M., Masson, D. G., Mayor, D. J., 2005. The impact of demersal trawling on northeast Atlantic deepwater coral habitats: The case of the Darwin mounds, United Kingdom. American Fisheries Society Symposium, 41, 807-818.

Wheeler, A.J., Beyer, A., Freiwald, A., de Haas, H., Huvenne, V.A.I., Kozachenko, M., Olu-Le Roy, K., Opderbecke, J., 2007. Morphology and environment of cold-water coral carbonate mounds on the NW European margin. Int. J. Earth Sci. 96, 37–56. doi:10.1007/s00531-006-0130-6

White, M., Dorschel, B., 2010. The importance of the permanent thermocline to the cold water coral carbonate mound distribution in the NE Atlantic. Earth Planet. Sci. Lett. 296, 395–402.

White, M., Mohn, C., de Stigter, H., Mottram, G., 2005. Deep-water coral development as a function of hydrodynamics and surface productivity around the submarine banks of the Rockall Trough, NE Atlantic, in: Cold-Water Corals and Ecosystems. Springer Berlin Heidelberg, pp. 503–514. doi:10.1007/3-540-27673-4_25

Wienberg, C., 2019. A Deglacial Cold-Water Coral Boom in the Alborán Sea: From Coral Mounds and Species Dominance, in: Orejas, C., Jiménez, C. (Eds.), Mediterranean Cold-Water Corals: Past, Present and Future. Springer, Cham, pp. 57–60. doi:10.1007/978-3-319-91608-8_7

Wienberg, C., Titschack, J., 2017. Framework-Forming Scleractinian Cold-Water Corals Through Space and Time: A Late Quaternary North Atlantic Perspective, in: Marine Animal Forests. Springer, Cham, pp. 1–34. doi:10.1007/978-3-319-17001-5_16-1

Wienberg, C., Beuck, L., Heidkamp, S., Hebbeln, D., Freiwald, A., Pfannkuche, O., Monteys, X., 2008. Franken Mound: Facies and biocoenoses on a newly-discovered "carbonate mound" on the western Rockall Bank, NE Atlantic. Facies 54, 1–24. doi:10.1007/s10347-007-0118-0

Wienberg, C., Frank, N., Mertens, K.N., Stuut, J.B., Marchant, M., Fietzke, J., Mienis, F., Hebbeln, D., 2010. Glacial cold-water coral growth in the Gulf of Cádiz: Implications of increased palaeo-productivity. Earth Planet. Sci. Lett. 298, 405–416. doi:10.1016/j.epsl.2010.08.017

Wienberg, C., Titschack, J., Freiwald, A., Frank, N., Lundälv, T., Taviani, M., Beuck, L., Schröder-Ritzrau, A., Krengel, T., Hebbeln, D., 2018. The giant Mauritanian cold-water coral mound province: Oxygen control on coral mound formation. Quat. Sci. Rev. 185, 135–152. doi:10.1016/j.quascirev.2018.02.012

Wienberg, C., Titschack, J., Frank, N., De Pol-Holz, R., Fietzke, J., Eisele, M., Kremer, A., Hebbeln, D., 2020. Deglacial upslope shift of NE Atlantic intermediate waters controlled slope erosion and cold-water coral mound formation (Porcupine Seabight, Irish margin). Quat. Sci. Rev. 237, 106310. doi:10.1016/j.quascirev.2020.106310

Wild, C., Wehrmann, L., Mayr, C., Schöttner, S., Allers, E., Lundälv, T., 2009. Microbial degradation of cold-water coral-derived organic matter: potential implication for organic C cycling in the water column above Tisler Reef. Aquat. Biol. 7, 71–80. doi:10.3354/ab00185

Wilson, J.B., 1979. Patch Development of the Deep-Water Coral *Lophelia pertusa* (L.) on Rockall Bank. J. Mar. Biol. Assoc. United Kingdom 59, 165–177. doi:10.1017/S0025315400046257

Wilson, M.F.J., O'Connell, B., Brown, C., Guinan, J.C., Grehan, A.J., 2007. Multiscale terrain analysis of multibeam bathymetry data for habitat mapping on the continental slope. Mar. Geod. 30, 3–35. doi:10.1080/01490410701295962

Wisshak, M., Freiwald, A., Lundälv, T., Gektidis, M., 2005. The physical niche of the bathyal *Lophelia pertusa* in a non-bathyal setting: environmental controls and palaeoecological implications, in: Freiwald, A., Roberts, J.M. (Eds.), Cold-Water Corals and Ecosystems. Springer, pp. 979–1001.

Whittaker, R.J., Araújo, M.B., Jepson, P., Ladle, R.J., Watson, J.E., Willis, K.J., 2005. Conservation biogeography: assessment and prospect. Divers. Distrib. 11 (1), 3–23.

Wu, J., Filippidi, A., Davies, G.R., de Lange, G.J., 2018. Riverine supply to the eastern Mediterranean during last interglacial sapropel S5 formation: A basin-wide perspective. Chem. Geol. 485, 74–89. doi:10.1016/j.chemgeo.2018.03.037

Würtz, M., Rovere, M. (Eds.), 2015. Atlas of the Mediterranean seamounts and seamount-like structures. IUCN International Union for Conservation of Nature, Gland and Málaga, 276 pp. doi:10.2305/iucn.ch.2015.07.en

Wynn, R.B., Huvenne, V.A.I., Le Bas, T.P., Murton, B.J., Connelly, D.P., Bett, B.J., Ruhl, H.A., Morris, K.J., Peakall, J., Parsons, D.R., Sumner, E.J., Darby, S.E., Dorrell, R.M., Hunt, J.E., 2014. Autonomous Underwater Vehicles (AUVs): Their past, present and future contributions to the advancement of marine geoscience. Mar. Geol. 352, 451–468. doi:10.1016/j.margeo.2014.03.012

Yehudai, M., Lazar, B., Bar, N., Kiro, Y., Agnon, A., Shaked, Y., Stein, M., 2017. U–Th dating of calcite corals from the Gulf of Aqaba. Geochim. Cosmochim. Acta 198, 285–298. doi:10.1016/j.gca.2016.11.005

York, D., Evensen, N.M., Martínez, M.L., De Basabe Delgado, J., 2004. Unified equations for the slope, intercept, and standard errors of the best straight line. Am. J. Phys. 72, 367–375. doi:10.1119/1.1632486

Zajac, R.N., Lewis, R.S., Poppe, L.J., Twichell, D.C., Vozarik, J., DiGiacomo-Cohen, M.L., 2000. Relationships among sea-floor structure and benthic communities in Long Island Sound at regional and benthoscape scales. J. Coast. Res. 16, 627–640.

Ziegler, M., Tuenter, E., Lourens, L.J., 2010. The precession phase of the boreal summer monsoon as viewed from the eastern Mediterranean (ODP Site 968). Quat. Sci. Rev. 29, 1481–1490. doi:10.1016/j.quascirev.2010.03.011

Zielhofer, C., Faust, D., Linstädter, J., 2008. Late Pleistocene and Holocene alluvial archives in the Southwestern Mediterranean: Changes in fluvial dynamics and past human response. Quat. Int. 181, 39–54. doi:10.1016/j.quaint.2007.09.016

Zweng, M., Reagan, J., Seidov, D., Boyer, T., Locarnini, M., Garcia, H., Mishonov, A., Baranova, O., Weathers, K., Paver, C., Smolyar, I., 2019. World ocean atlas 2018, volume 2: Salinity.